Universidade do Minho

I3Bs - Instituto de Investigação em Biomateriais, Biodegradáveis e Biomiméticos

Ana Cláudia Fernandes Lima

Nanoparticles for advanced treatments of arthritic diseases

Tese de Doutoramento

Doutoramento em Engenharia de Tecidos, Medicina Regenerativa e Células Estaminais

Trabalho efetuado sob a orientação do

Professor Doutor Nuno João Meleiro Alves das Neves

Outubro de 2019

ACKNOWLEDGMENTS

During this journey, I have been richly blessed by the support, love and kindness of some people that make this thesis possible. To them, I am and will always be grateful.

First, I would like to start by expressing my gratitude to my supervisor, Prof. Nuno Neves. No words can express how thankful I am for the patience, availability and inspiration during these last years. Thank you for accepting me as a PhD student and for all the conversations about science and life. You helped me on becoming a more independent researcher and taught me the power of imagination. This thesis would not be possible without all your knowledge and capability to supervise me. To the director of 3B's Research group, Prof. Rui L. Reis, I am forever grateful for the opportunity to join his group and to develop my PhD at this European Institute of Excellency. Thank you for being an inspiration on pursuing our dreams and ambitions.

It's also difficult to find words to describe how truly grateful I am to have Dr. Helena Ferreira in my life. She had a major contribution in this thesis, with all her help, motivation, support, inspiration, ideas and trust. Thank you, my dearest friend for always be there for me. I would like to acknowledge the co-authors in this thesis and everyone in the 3B's that helped me. To my friends in 3B's, we shared the good, the bad, frustrations and achievements, thank you all for the great memories. I have found really special people in this journey, special thanks to Gabriela and Catarina for all the love and friendship. Also mention my gratitude to all my close friends, because "friends are the family you choose".

Finally, I would like to thank all my family for all the unconditional love and support. I am so lucky to have this wonderful family, with all my uncles and cousins being always there for me. Special mention to my adored deceased grandparents and uncle that are always in my heart. This thesis is dedicated to the four most important people in my life: dad, mom, brother and fiancé. To my dad, my king and my hero. To my mom, my strength and my admiration. To my brother, my other half. I fell so blessed for having chosen you as my family. I own you the person that I am today, as you gave the opportunity to follow my dreams and transmitted me important principals. As you say "have courage and be kind". Last but not the least, to the love of my life, my everything, my fiancé Tiago. It's difficult to express how much I love and admire you. You are my safe harbor and my happy place. You are always there for me, making me see the brighter side of life. I am so deeply grateful to have found you my love. And I can say that the best is yet to come.

I would like to acknowledge the Foundation for Science and Technology (FCT) for my PhD scholarship (PD/BD/11384/2015).

STATEMENT OF INTEGRITY

I hereby declare having conducted this academic work with integrity. I confirm that I have not used plagiarism or any form of undue use of information or falsification of results along the process leading to its elaboration.

I further declare that I have fully acknowledged the Code of Ethical Conduct of the University of Minho.

ABSTRACT

Nanoparticles for advanced treatments of arthritic diseases

Arthritic diseases affect more than 350 million people worldwide. Their incidence, prevalence and global burden are increasing, mainly due to the aging of the population. The most common forms of arthritis, osteoarthritis (OA) and rheumatoid arthritis (RA), are chronic inflammatory diseases, which are characterized by synovial inflammation and cartilage and bone destruction. Despite the advances in the pharmaceutical field, there is currently no cure for arthritis. Moreover, current treatments are associated with low efficiency and severe side effects.

Recently, nanoparticles (NPs) have emerged as a powerful platform to overcome the present treatment limitations. The goal of this PhD work was to develop novel NPs to treat arthritic conditions. Taking into consideration their main drawbacks, we aimed to design NPs able to enhance the therapeutic index of relevant drugs. Therefore, biological agents were immobilized at the surface of biodegradable polymeric NPs and liposomes to protect, extend and enhance their therapeutic efficacy in OA and RA, respectively. While polymeric NPs were biofunctionalized with anti-IL-6 antibodies to selectively capture and neutralize this key pro-inflammatory cytokine, liposomes were biofunctionalized with anti-IL-23 antibodies in order to inhibit the differentiation of naive $CD4^+$ T cells into Th17 cells, by IL-23 neutralization. Furthermore, enzymatic- and redox-responsive polymeric micelles were developed for targeted and controlled drug delivery in arthritis. After accumulation in the inflammatory site, the dexamethasone encapsulated into the polymeric micelles undergo quick release triggered by both redox and glutathione reductase activity. For all NPs formulations, the size distribution, zeta potential and drug immobilization/encapsulation was assessed. Biological tests demonstrated their cytocompatibility in contact with human chondrocytes, macrophages and endothelial cells. Moreover, under inflammatory conditions the NPs were able to demonstrate their enhanced efficacy in comparison with the free drugs. A deeper characterization on the degree of NPs internalization and pathways was performed in a normal and inflammatory scenario by different cells affected by arthritic diseases. The results highlight the importance of considering the targeted cell type when designing functional NPs for specific diseases. Finally, *in vivo* studies demonstrated the safety and enhanced therapeutic efficacy of the biofunctionalized polymeric NPs immobilizing anti-TNF-α and anti-IL-6 antibodies. In conclusion, as these novel advanced NPs might overcome abovementioned drawbacks, they are promising strategies for radically improving the efficacy of arthritis treatments and severely limiting their side effects.

Keywords: Arthritic diseases, Nanoparticles, Antibodies immobilization, Controlled release.

RESUMO

Nanopartículas para o tratamento avançado de doenças artríticas

As doenças artríticas afetam mais de 350 milhões de pessoas em todo o mundo. A sua incidência, prevalência e encargos globais estão a aumentar sobretudo devido ao envelhecimento da população. A osteoartrite (OA) e a artrite reumatoide (AR) são as formas mais comuns destas doenças crónicas inflamatórias, que são caracterizadas pela inflamação sinovial e pela destruição da cartilagem e do osso. Apesar dos avanços na área farmacêutica, atualmente não existe cura para estas doenças. Além disso, os tratamentos disponíveis estão associados a uma baixa eficácia e a efeitos adversos graves.

Recentemente, as nanopartículas (NPs) emergiram como uma plataforma poderosa capaz de superar as limitações dos tratamentos atuais. Assim, o objetivo desta tese de doutoramento foi o desenvolvimento de novas NPs para o tratamento da artrite. Considerando as atuais limitações, diferentes NPs foram desenhadas de forma a aumentar o índice terapêutico de fármacos. Agentes biológicos foram imobilizados na superfície das NPs e lipossomas de forma a proteger, prolongar e aumentar as suas eficácias terapêuticas no tratamento da OA e AR, respetivamente. Enquanto as NPs foram biofuncionalizadas com anticorpos anti-IL-6 de forma a capturar e neutralizar seletivamente esta citoquina central, os lipossomas foram biofuncionalizados com anticorpos anti-IL-23 de forma a inibir a diferenciação das células T $CD4^+$ em células Th17. Além disso, micelas sensíveis à enzima glutationa redutase e a um ambiente redutor foram desenvolvidas para promover a libertação local e controlada do fármaco. De facto, depois de as NPs se acumularem na articulação inflamada, a dexametasona encapsulada dentro das micelas será facilmente libertada através daqueles mecanismos. Todas as formulações foram avaliadas em relação à homogeneidade do tamanho, ao potencial zeta e à quantidade dos fármacos imobilizada/encapsulada nas NPs. Os testes biológicos demonstraram a sua citocompatibilidade em contacto com condrócitos, macrófagos e células endoteliais humanas. Além disso, sob condições inflamatórias, as NPs revelaram uma maior eficácia em comparação com o fármaco livre. A percentagem e via de internalização das NPs foram avaliadas em condições normais e inflamatórias em diferentes tipos de células. Os resultados reforçam a importância de se considerar o tipo de célula alvo aquando do desenvolvimento das NPs. Finalmente, estudos *in vivo* demonstraram a segurança e o aumento da eficácia terapêutica das NPs biofuncionalizadas com anticorpos anti-TNF-α e anti-IL-6. Em conclusão, as novas NPs desenvolvidas são estratégias promissoras que podem mudar radicalmente a eficácia dos tratamentos e limitar significativamente os seus efeitos adversos.

Palavras-chave: Doenças artríticas, Nanopartículas, Imobilização de anticorpos, Libertação controlada.

TABLE OF CONTENTS

LIST OF ABBREVIATIONS

A

α - Alpha

7-AAD - 7-aminoactinomycin D

Ab - Antibody

AB - Alamar blue

AbIA - Anti-type II collagen antibody-induced arthritis

ABTS - 2,2'-azino-bis(3-ethylbenzothiazoline-6-sulphonic acid)

ADs - Autoimmune diseases

ADAMTSs - a disintegrin with thrombospondin motifs

AFM - Atomic Force Microscopy

AIA - Adjuvant-induced arthritis

APRIL - a proliferation-inducing ligand

ATR - Attenuated total reflectance

Au - Gold

AuNPs - Gold nanoparticles

B

β - Beta

BCA - Bicinchoninic acid

bDMARDs - Biologic disease-modified anti-rheumatic drugs

b-FGF - Basic fibroblast growth factor

BMPs - Bone morphogenetic proteins

BSA - Bovine serum albumin

C

C - Carbon

CAIA - Collagen antibody-induced arthritis

CC - Cholesteryl chloroformate

CCL - CC chemokine ligand

CD - Cluster of Differentiation

CDC - Centers for Disease Control and Prevention

cDNA - Complementary deoxyribonucleic acid

cfDNA - cell-free deoxyribonucleic acid

CFA - Complete Freund's adjuvant

CFSE - Carboxyfluorosuccinimide ester

Ch - Chitosan

CIA - Collagen-induced arthritis

cm - Centimeter

cm^{-1} - Reciprocal wavelength centimeter

CO_2 - Carbon dioxide

COOH - Carboxyl group

COX - Cyclooxygenase enzyme

CpG - deoxy-cytidylate-phosphate-deoxy-guanylate

Ctr - Control

Cu - Cupper

Cur - Curcumin

D

°C - Degree Celsius

D - Diffusion coefficient

DAMP - Damage-associated molecular patterns

DAPI - 4',6'-diamino-2-fenil-indol

DD - Degree of deacetylation

DDS - Drug delivery system

DEAE - Diethylethylamine

Dex - Dexamethasone

DGAV - Direcção Geral de Alimentação e Veterinária

DLS - Dynamic light scattering

DMARDs - Disease-modified anti-rheumatic drugs

DMEM - Dulbecco's modified Eagle's medium

DMSO - Dimethyl sulfoxide

DNA - Deoxyribonucleic acid

DPBS - Dulbecco's Phosphate-Buffered Saline

DPPC - Dipalmitoyl phosphatidylcholine

dsDNA - Double stranded Deoxyribonucleic acid

DS - Dextran sulfate

DSPE-PEG-Mal - 1,2-distearoyl-sn-glycero-3-phosphoethanolamineN-[maleimide(polyethyleneglycol)-2000]

E

EA (EA.hy926) - Human umbilical vein endothelial cell line

ECM - Extracellular matrix

ECAMs - Endothelial cell adhesion molecules

EDC - 1-ethyl-3-(3-(dimethylaminopropyl) carbodiimide

EDTA - Ethylenediamine tetraacetic

EE - Entrapment efficiency

EGCG - (−)-epigallocatechin gallate

ELISA - Enzyme-linked Immunosorbent Assay

EMA - European Medicines Agency

EPC - L-alfa-phosphatidylcholine from egg yolk

EPR - Enhanced permeability and retention

ER - Endoplasmic reticulum

EULAR - European League Against Rheumatism

F

FA - Folic acid

FBS - Fetal bovine serum

FCT - Foundation for Science and Technology

FDA - Food and Drug Administration

EGFR - Epidermal growth factor receptor

FITC - Fluorescein isothiocyanate

FLS - Fibroblast-like synoviocytes

FTIR - Fourier transform infrared spectroscopy

G

GA - Glucosamine

GAGs - Glycosaminoglycans

GC - Gas chromatography

GCs – Glucocorticoids

GDF - Growth differentiation factor

GM-CSF - Granulocyte-macrophage colony-stimulating factor

GR - Glutathione reductase

GSH - Glutathione

GSSG - Glutathione disulfide

H

h - Hour

H_2O_2 - Hydrogen peroxide

H&E - Hematoxylin and Eosin

HA - Hyaluronic acid

hACs - Human articular chondrocytes

HAP-1 - Synovial fibroblast-homing peptide

HEPES - 4-(2-hydroxyethyl)-1-piperazineethanesulfonic acid

HPLC - High performance liquid chromatography

HRP - Horseradish peroxidase

Hz - Hertz

I

2IT - 2-Iminothiolane

IA - Intra-articular

ICAM-1 - Intercellular cell-adhesion molecule-1

ICE - Interleukin-1 beta converting enzyme

i.e. - “in other words”, form latin *id est*

IFN-γ - Interferon-gamma

Ig - Immunoglobulin

IGF-1 - Insulin-like growth factor-1

IHC - Immunohistochemistry

Ihh - Indian Hedgehog

IL - Interleukin

IL1ra - Interleukin-1 receptor antagonist

IR – Infrared

ISO - International Organization for Standardization

J

JAK - Janus kinase

K

κ – Kappa

KBr - Potassium bromide

kDa - Kilodalton

kg - Kilogram

kV - Kilovolt

L

L - Liter

LPS - Lipopolysaccharide

LUVs - Unilamellar liposomes

LWT - Limb withdrawal threshold

M

μ - mu

μg - Microgram

μL - Microliter

μm - Micrometer

μM - Micromolar

m - Meter

M - Molar

MEM - Minimum Essential Medium

MES - 2-(N-morpholino)ethanesulfonic acid

mg - Milligram

min - minute

miRNA - micro ribonucleic acid

mL - Milliliter

MLVs - Multilamellar liposomes

mm - Millimeter

mM – Millimolar

mmol – Millimole

MMPs - Matrix metalloproteinases

mPEG - Methoxypolyethylene glycol amine

MRI - Magnetic resonance imaging

mRNA - messenger ribonucleic acid

mTNF-α - transmembrane tumor necrosis factor alfa

MTS - 3-(4,5-dimethylthiazol-2-yl)-5-(3-carboxymethoxyphenyl)-2-(4-sulfofenyl)-2H-tetrazolium

MTV - Multivesicular bodies

MTX - Methotrexate

mU - Milliunit

mV - Millivolt

MW - Molecular weight

MWCO - Molecular weight cut off

N

n - Number of independent samples

NaCl - Sodium chloride

NADH - Nicotinamide adenine dinucleotide

NADPH - Nicotinamide adenine dinucleotide phosphate

$NaHCO_3$ - Sodium bicarbonate

NaOH - Sodium hydroxide

NBD Cholesterol - 22-(N-(7-Nitrobenz-2-Oxa-1,3-Diazol-4-yl)Amino)-23,24-Bisnor-5-Cholen-3β-Ol

NF-κB - Nuclear factor kappa B

NH_2 - Amine group

NHS - N-hydroxysuccinimide

NIR - Near infrared

NLS - Nuclear localization signal

nm - Nanometers

nM - Nanomolar

NPC - Nuclear pore complex

NPs - Nanoparticles

NSAIDs - Non-steroidal anti-inflammatory drugs

O

O_2 - Oxygen

OA - Osteoarthritis

OARSI - Osteoarthritis Research Society International

OCH_3 - Methoxy group

OH - Hydroxyl group

P

p - Statistical level of significance

PA - Palmitic acid

PAM - Pressure application measurement

PAMAM - Poly(amidoamide)

PBMCs - Peripheral blood mononuclear cells

PBS - Phosphate buffered saline

PCL - Polycaprolactone

PDI - Polydispersity index

pDNA - Plasmid deoxyribonucleic acid

PDMA - Poly(2-(diethylamino)ethyl methacrylate)

PE - Phosphatidylethanolamine

PECs - Polyelectrolyte complexes

PEG - Polyethylene glycol

pH - Potential hydrogenionic

pKa - Negative log of the acid dissociation constant (Ka)

PLA - Polylactide

PLGA - Poly(lactic-co-glycolic acid)

PMA - Phorbol 12-myristate-13-acetate

PS - Pristine polystyrene

PsA - Psoriatic Arthritis

PSA - Polysialic acid

R

3Rs - Replacement, Reduction and Refinement

RA - Rheumatoid arthritis

RANKL - Receptor activator of the nuclear factor NF-κB ligand

RGD - Arginyl-Glycyl-L-Aspartic acid

RNA - Ribonucleic acid

ROS - Reactive oxygen species

Rpm - Rotations per minute

RPMI - Roswell Park Memorial Institute

RT - Room temperature

S

s - Seconds

SA - Sialic acid

SD - Standard deviation

SEM - Scanning Electron Microscopy

SH - Sulfhydryl group

siRNA - small interfering ribonucleic acid

SOX - Sry-related HMG box

SPIONs - Superparamagnetic iron oxide nanoparticles

T

2D - Two-dimensional

3D - Three-dimensional

TACE - Tumor necrosis factor-alpha converting enzyme

TBTU - 2-(1H-Benzotriazole-1-yl)-1,1,3,3-tetramethylaminium tetrafluoroborate

TCPS - Tissue culture polystyrene

TCZ - Tocilizumab

TE - Tris-EDTA

TEA - Triethylamine

TEM - Transmission Electron Microscopy

TGF - Transforming growth factor

Th - T helper cells

THF - Tetrahydrofuran

THP-1 - Human monocyte-like cell line

TLC - Thin layer chromatography

TLRs - Toll-like receptors

TMB - 3,3′,5,5′-Tetramethylbenzidine

TNF-α - Tumor necrosis factor-alpha

TPP - Triphenylphosphonium cation

TRAIL - Tumor necrosis factor-related apoptosis inducing ligand

Treg - Regulatory T cells

U

UV - Ultraviolet

UV-Vis - Ultraviolet-visible

V

VCAM - Vascular cell adhesion molecule

VECs - Vascular endothelial cells

VEGF - Vascular endothelial growth factor

VIP - Vasoactive intestinal peptide

(v/v) - Percentage of volume/volume

W

(w/v) – Percentage of weight/volume

(w/w) - Percentage of weight/weight

LIST OF FIGURES

LIST OF TABLES

SHORT *CURRICULUM VITAE*

Ana Cláudia Fernandes Lima was born in 1990 in Guimarães, Portugal. Nowadays, she works as a researcher in 3B's Research Group, I3Bs – Research Institute on Biomaterials, Biodegradables and Biomimetics, University of Minho, under the supervision of Prof. Nuno M. Neves.

She received her MSc degree in 2013 in Pharmaceutical Sciences at the Faculty of Pharmacy of the University of Porto, Portugal with a final grade of 15 (0-20). During the graduation she enrolled in research activities resulting in authorship of a paper entitled "Patulin assessment and fungi identification in organic and conventional fruits and derived products". In her last year, she had the opportunity to do a three-month internship at Strathclyde Institute of Pharmacy and Biomedical Sciences in Glasgow, United Kingdom. During that period she was enrolled in the project "Targeting Autophagy during Oncolytic Herpes Simplex Virus type 1 (HSV17+ wild type versus ICP34.5 null mutant HSV1716) cancer treatment".

In 2015, she joined 3B's Research Group, after being awarded with a grant under the scope of Foundation for Science and Technology (FCT) project Incentivo/SAU/LA0026/2014. In September of the same year, she was awarded with a FCT PhD scholarship (PD/BD/11384/2015), and started the PhD program in Tissue Engineering, Regenerative Medicine and Stem Cells (TERM&SC) in the University of Minho, being the main focus of her research the development of nanoparticles to treat arthritic diseases. During her PhD, she has been involved in the preparation of ICVS/3Bs and FCT project proposals. Additionally, she collaborated with her colleagues in different works, and also with different universities. During 3 months, she was a visiting student at the Faculty of Engineering in Chulalongkorn University, Bangkok, Thailand, studying the biological response of cells encapsulated into silk fibroin DMPG hydrogels.

As a result of her research work, she is author or co-author of 7 papers in international journals (2 published, 5 submitted), 2 issued patents, 3 oral presentations and 5 poster presentations. She attended several important international meetings in the field of tissue engineering and regenerative medicine.

LIST OF PUBLICATIONS

The work performed during the PhD period resulted in the publications listed below.

Papers in international scientific journals with referees (as first author)

1. **Lima A. C.**, Cunha C., Carvalho A., Ferreira H., Neves N. M. Interleukin-6 Neutralization by Antibodies Immobilized at the Surface of Polymeric Nanoparticles as a Therapeutic Strategy for Arthritic Diseases. *Acs Appl Mater Inter*. 2018, *10* (16): p. 13839-50.
2. **Lima A. C.**, Ferreira H., Reis R. L., Neves N. M. Biodegradable polymers: an update on drug delivery in bone and cartilage diseases. *Expert Opin Drug Deliv*. 2019, *16* (8): p. 795-813.
3. **Lima A. C.**, Amorim D., Laranjeira I., Almeida A., Reis R. L., Ferreira H., Pinto-Ribeiro F., Neves N. M. Nanoparticle-mediated neutralization of IL-6 and TNF-α for osteoarthritis treatment. *(Submitted)*. 2019.
4. **Lima A. C.**, Campos C. F., Cunha C., Carvalho A., Reis R. L., Ferreira H., Neves N. M. Interleukin-23 neutralization by biofunctionalized liposomes encapsulating gold nanoparticles for the treatment of rheumatoid arthritis. *(Submitted)*. 2019.
5. **Lima A. C.**, Ferreira H., Neves N. M. Enzymatic- and redox-responsive polymeric micelles for targeted and controlled drug delivery on arthritic diseases. *(Submitted).* 2019.
6. **Lima A. C.**, Ferreira H., Neves N. M. Cellular uptake of nanoparticles in an inflammatory arthritis scenario. *(Submitted).* 2019.

Papers in international scientific journals with referees (as co-author)

1. Ferreira H., Amorim D., **Lima A. C.**, Pirraco R., Costa Pinto A. R., Almeida R., Almeida A., Reis R. L., Pinto-Ribeiro F., Neves N. M. *In vitro* and *in vivo* compatibility of an injectable hydrogel for neurodegenerative diseases treatment. *(Submitted).* 2019.

Conference abstracts published in international scientific journals (as first author)

1. **Lima A. C.**, Cunha C., Carvalho A., Ferreira H., Neves N. M. Advanced treatment for arthritic diseases based on the capture and inactivation of interleukin-6 by biofunctionalized polymeric nanoparticles. *European cells and materials.* 2017, Vol. 33 Suppl. 2.

Conference oral presentations (as first author and speaker)

1. **Lima A. C.**, Cunha C., Carvalho A., Ferreira H., Neves N. M. Advanced treatment for arthritic diseases based on the capture and inactivation of interleukin-6 by biofunctionalized polymeric nanoparticles. TERMIS-EU 2017, Davos, Switzerland.
2. **Lima A. C.**, Cunha C., Carvalho A., Ferreira H., Neves N. M. Capture and neutralization of interleukin-6 by the intra-articular injection of biofunctionalized polymeric nanoparticles as advanced treatment for arthritic diseases. Chem2Nature 2017, Porto, Portugal.
3. **Lima A. C.**, Amorim D., Laranjeira I., Almeida A., Reis R. L., Ferreira H., Pinto-Ribeiro F., Neves N. M. Pro-inflammatory Cytokines neutralization by intra-articular injection of biofunctionalized nanoparticles as advanced treatment for osteoarthritis. TERMIS 2019, Rhodes, Greece.

Conference oral presentations (as co-author)

4. **Lima A. C.**, Campos C. F., Cunha C., Carvalho A., Reis R. L., Ferreira H., Neves N. M. IL-23 inactivation by targeted liposomes to mediate the regression of autoimmune diseases. TERMIS 2019, Rhodes, Greece.

Conference posters (as first author)

1. **Lima A. C.**, Cunha C., Carvalho A., Ferreira H., Neves N. M. Biofunctionalized polymeric nanoparticles for a prolonged and local capture of pro-inflammatory cytokines in arthritic joints. TERM STEM 2016, Guimarães, Portugal.
2. **Lima A. C.**, Amorim D., Almeida A., Reis R. L., Ferreira H., Pinto-Ribeiro F., Neves N. M. Interleukin-6 and Tumour Necrosis Factor-α neutralization by biofunctionalized nanoparticles after intra-articular injection for osteoarthritis treatment. TERM STEM 2017, Guimarães, Portugal.
3. **Lima A. C.**, Amorim D., Almeida A., Reis R. L., Ferreira H., Pinto-Ribeiro F., Neves N. M. Intra-articular injection of biofunctionalized nanoparticles to neutralize Interleukin-6 and Tumour Necrosis Factor-α to treat osteoarthritis. Chem2Nature 2018, Porto, Portugal.
4. **Lima A. C.**, Amorim D., Laranjeira I., Almeida A., Reis R. L., Ferreira H., Pinto-Ribeiro F., Neves N. M. Neutralization of Pro-inflammatory Cytokines by Intra-articular Injection of Biofunctionalized Nanoparticles as an Advanced Treatment for Osteoarthritis. Society for Biomaterials Annual Meeting and Exposition 2019, Seattle, USA.

5. **Lima A. C.**, Amorim D., Laranjeira I., Almeida A., Reis R. L., Ferreira H., Pinto-Ribeiro F., Neves N. M. A dual targeting strategy using antibodies immobilized at the surface of biodegradable nanoparticles for local osteoarthritis treatment. Achilles 2019, Porto, Portugal.

Patents

1. **Lima A. C**., Reis R.L., Ferreira H., Neves N. M. Phosphatidylcholine liposomes, methods and uses thereof. (*Filed*, 2019).
2. **Lima A. C**., Reis R.L., Ferreira H., Neves N. M. Polymeric micelle, methods of production and uses thereof. (*Filed*, 2019).

Awarded grants

1. Foundation for Science and Technology (FCT) PhD scholarship (PD/BD/11384/2015).

INTRODUCTION TO THE THESIS FORMAT

The present thesis is divided into six main sections (1 to 6) containing eight chapters (I to VIII). This structure was adopted to allow for a comprehensive organization of the data presented in the various chapters, preceded by a general introduction (Section 1, **Chapter I**), as well as an overall materials and methods section (Section 2, **Chapter II**). Section 3 (**Chapters III** to **V**) focuses on the development of the different nanoparticle (NP) formulations to treat arthritic diseases as well as their *in vitro* evaluation. Section 4 (**Chapter VI**) provides further evidence regarding the NPs internalization by relevant cells. Section 5 (**Chapter VII**) describes an *in vivo* study performed to assess the safety and therapeutic efficacy of the functionalized polymeric NPs. To finalize, Section 6 (**Chapter VIII**) completes this thesis with the concluding remarks and future perspectives.

The main body of the thesis is based on a series of manuscripts either published or submitted for publication in international journals. Each chapter is presented in a manuscript form, i.e., abstract, introduction, experimental section, results, discussion, conclusion and acknowledgements. A list of relevant references is also provided as a subsection within each chapter. The contents of each part and chapter are described below in more detail.

Section 1 – General introduction

Chapter I – Nanoparticles for arthritic diseases treatment: This chapter provides a general introduction on the pathogenesis and key molecular targets in arthritis, discussing the most successful and novel drugs in arthritis therapy, and also highlights recent trends in nanotechnology-based drug delivery approaches.

Section 2 – Experimental section

Chapter II – Materials and Methods: A list of the materials and methods used to obtain the results presented in this thesis is provided. The section is intended to provide additional details that are not included in the materials and methods section of published manuscripts.

Section 3 – Nanoparticles development and in vitro *evaluation*

In this section, we do report the design and production of novel nanocarriers to enhance the therapeutic efficacy of relevant drugs while reducing their adverse side effects. The experimental work involves the characterization of the developed NPs, the evaluation of the drug loading capacity, the assessment of their *in vitro* cytocompatibility and their biologic activity.

Chapter III - Interleukin-6 neutralization by antibodies immobilized at the surface of polymeric nanoparticles as a therapeutic strategy for arthritic diseases: This chapter describes the production of biodegradable polymeric NPs with anti-IL-6 antibodies immobilized at their surface. The biologic activity of the biofunctionalized NPs was assessed in chondrocytes stimulated with macrophage conditioned medium to model the exposure of the cells to inflammation.

Chapter IV - Interleukin-23 neutralization by biofunctionalized liposomes encapsulating gold nanoparticles for the treatment of rheumatoid arthritis: This chapter describes the production of liposomes encapsulating AuNPs and immobilizing anti-IL-23 antibodies. Peripheral blood mononuclear cells of healthy donors and RA patients were activated though Th17 differentiation, being assessed if the biofunctionalized liposomes were able to prevent the production of IL-17A.

Chapter V - Enzymatic- and redox-responsive polymeric micelles for targeted and controlled drug delivery on arthritic diseases: This chapter describes the development of polymeric micelles responsive to redox and glutathione reductase activity for targeted and controlled delivery of dexamethasone. The biologic efficacy of this strategy was assessed in a co-culture model of inflammatory arthritis.

Section 4 – Internalization studies

Chapter VIII – Cellular uptake of nanoparticles in an inflammatory arthritis scenario: This chapter aims to study the internalization degree and pathways of the NPs developed in Section 3 in a normal and inflammatory scenario by different cells, namely endothelial cells, chondrocytes and macrophages. Flow cytometry and confocal microscopy analyses were both used to evaluate the cellular NPs uptake.

Section 5 – In vivo *studies*

Chapter VII – Nanoparticle-mediated neutralization of IL-6 and TNF-α for osteoarthritis treatment: In this chapter the polymeric NPs developed in Chapter III, but functionalized with anti-TNF-αantibodies beyond anti-IL-6 antibodies, were studied in a co-culture model of inflammatory arthritis and in an experimental carrageenan-induced arthritis rat model. The objective was to confirm the *in vitro* results and to provide a more substantiated conclusion on their safety and therapeutic efficacy.

Section 6 – Concluding remarks

Chapter VIII – General conclusions and future perspectives: The final section of the thesis presents the general conclusions and implications, current limitations and potential of the work previously described for the treatment of arthritis. Furthermore, it is highlighted the future directions for the work developed in this thesis in order to move forwards into clinical studies.

"*Logic will get you from A to B. Imagination will take you everywhere.*"

Albert Einstein

SECTION 1

GENERAL INTRODUCTION

Chapter I

Nanoparticles for arthritic diseases treatment

Chapter I

Nanoparticles for arthritic diseases treatment[1]

ABSTRACT

Osteoarthritis (OA) and rheumatoid arthritis (RA), the most common types of arthritis, are chronic inflammatory diseases characterized by synovial joint inflammation and cartilage and bone tissue destruction. Despite the breakthroughs in the field of drug discovery, there is currently no cure for arthritis. Indeed, the unique physiology of the joint capsule protecting the cartilage and bone tissues makes the systemic delivery of free drugs to the joints very challenging. Consequently, effective and targeted delivery systems for arthritic diseases are of utmost importance. Among a wide variety of drug delivery devices, the unique properties of the nanoparticles (NPs) make them highly attractive for the design of carriers that enable a targeted and temporal controlled release of one or more drugs in concentrations within the therapeutic range. Moreover, the increased knowledge about biomaterials science and of the pathophysiology of diseases, biomarkers and targets as well as the development of innovative tools has led to the design of high value-added nanomedicines. However, some challenges persist and are mainly related with an appropriate residence time and a controlled and sustained release over a prolonged period of time of the therapeutic agents. This chapter focuses on the analysis of the pathogenesis and key molecular targets in arthritis, discussing the most successful and novel drugs in arthritis therapy, and also highlight recent trends in the nanotechnology-based drug delivery approaches. Herein, nanomedicines that showed great promise in improving arthritis treatment are reviewed, namely liposomes, polymeric NPs, polymeric micelles, dendrimers and metallic NPs.

[1]This chapter is based on the following publication:

A.C. Lima, H. Ferreira, R. L. Reis, N. M. Neves. Biodegradable polymers: an update on drug delivery in bone and cartilage diseases. *Expert Opin Drug Deliv.* 2019, *16* (8): p. 795-813.

I-1. INTRODUCTION

Inflammatory arthritis is an umbrella term that encompasses more than 150 different joint disorders characterized by joint and/or musculoskeletal system inflammation [1]. It affects more than 350 million people worldwide, and due to the increase of aging population, their incidence and prevalence are also increasing. As a result of their chronic, painful and debilitating features, arthritic diseases are one of the leading causes of work disability [2]. Moreover, in 2015 the overall costs of arthritis were estimated in more than $304 billion in the US [3].

The most common form of arthritis are osteoarthritis (OA) and rheumatoid arthritis (RA). OA, a local degenerative joint disease, is the leading cause of morbidity and disability in the elderly, affecting 9.6% of men and 18.0% of women aged over 60 years [4]. It is characterized by synovial inflammation and articular cartilage and subchondral bone degradation. The risk factors include genetic predisposition, aging, obesity, trauma and other systemic diseases. Conversely, RA is a systemic autoimmune disease that usually affects multiple joints [5]. It causes inflammation of joints, synovial hyperplasia, pannus formation, bone erosion and cartilage destruction. RA affects approximately 1% of the general population worldwide, being the incidence among women three times more than in men. Genetic factors, environmental factors and the adaptive immune response can trigger this chronic inflammatory disease.

Despite the significant occurrence of arthritic diseases, their effective treatments remains a challenge mainly due to the peculiar structure of cartilage [6]. This avascular and aneural tissue consists of collagen type II, proteoglycans (mainly aggrecan), hyaluronic acid (HA) and others glycosaminoglycans (GAGs) [7]. The highly organized network of collagen and GAGs fibrils surrounds the cell type characteristic of cartilage, the chondrocytes. Consequently, in response to injury, cartilage has a limited intrinsic ability to self-repair. Thus, in order to prevent irreversible or at least to minimize the extent of joint damage, rapid diagnosis and initiation of treatment is required.

Current treatments still present limited efficiency and severe side effects. To overcome these limitations, different strategies of drug delivery are currently used in the clinical practice. By definition, drug delivery system (DDS) refers to a method or process of administering a pharmaceutical compound to safely achieve its desired therapeutic effect [8]. These strategies are designed to alter the pharmacokinetic and/or biodistribution of their associated drug, to function as their reservoir, or both. Preclinical and clinical studies are exploring a variety of DDS within the nanosize range, also known as nanomedicines, including liposomes, polymeric nanoparticles (NPs), micelles, dendrimers and metallic

NPs (**Figure I-1**), which are slowly being translated into the clinical practice.

In the next sections, we will discuss the recent advances in the development of nanomedicines for treating arthritic diseases. First, arthritis pathogenesis and treatment are introduced and systematized. Then, recent advances including new therapeutic drugs, novel targeting approaches and innovative delivery vehicles are highlighted. Finally, to enable those systems to reach the clinical practice, a perspective of the challenges and future directions is given.

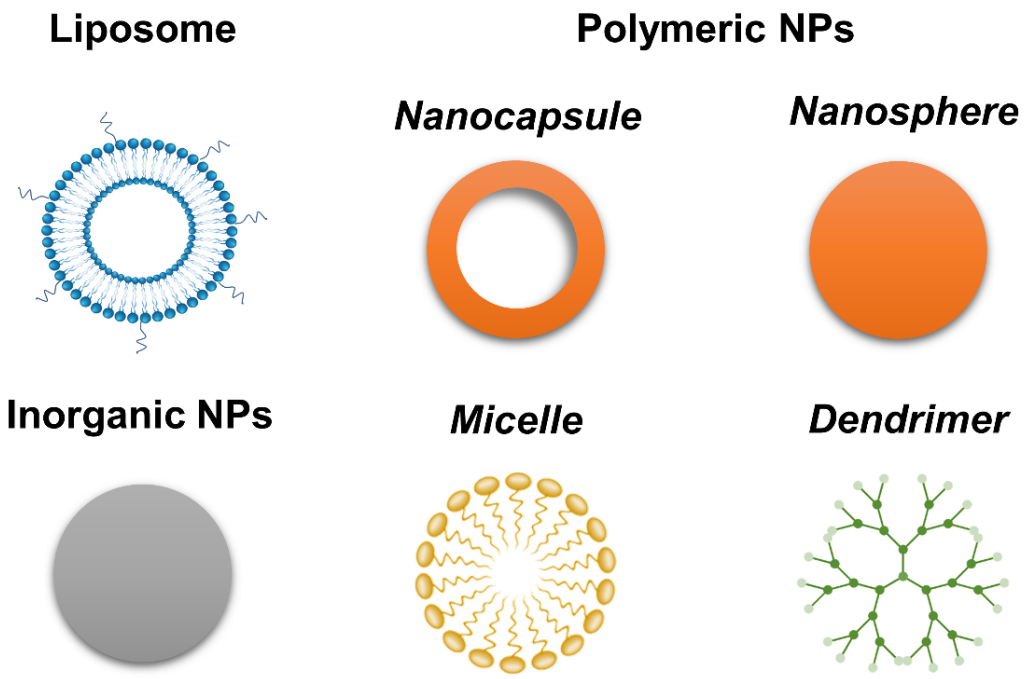

Figure I-1 - Schematic illustration of the various nanocarriers used in arthritis therapy.

I-2. ARTHRITIC DISEASES

Recent developments in the pathogenesis and molecular targets of arthritic diseases are revolutionizing the current therapeutic strategies, which are summarized in the following sub-sections.

I-2.1. Pathogenesis and molecular targets

Although joint damage in OA and RA involve different pathways, they share various mechanistic similarities (**Figure I-2**) [9]. In OA, as a result of cartilage damage and inflammatory process, the phenotype of chondrocytes is altered, becoming degenerated and hypertrophic. The chondrocytes start

to express matrix-degrading enzymes, and due to their increased sensitivity to inflammation, they stimulate the cycle of cartilage damage [10]. In RA, the immune system activation in combination with the release of extracellular matrix (ECM) products after cartilage damage activates the fibroblast-like synoviocytes (FLS) to develop into a stable, tumor-like phenotype. These activated FLS gradually invade and degrade the cartilage ECM and promote the activation and differentiation of adjacent cells, including the differentiation of monocytes and macrophages into osteoclasts. Therefore, cartilage damage in both diseases is associated with the increment of pro-inflammatory cytokines, such as tumor necrosis factor-α (TNF-α) and interleukins (IL, particularly IL-6 and IL-1β), which in its turn increase the production of catabolic factors and down-regulates anabolic mediators [5].

Even though the exact etiology and pathogenesis of arthritic diseases remains unknown, some key molecules were identified and are being used as therapeutic targets. Indeed, those targets include: *(i)* cytokines (pro-inflammatory and anti-inflammatory cytokines), *(ii)* enzymes (e.g. matrix metalloproteinases –MMPs, and a disintegrin with thrombospondin motifs –ADAMTSs), *(iii)* growth and differentiation factors (e.g. transforming growth factor –TGF, vascular endothelial growth factor –VEGF, Insulin-like growth factor-1 –IGF-1, granulocyte-macrophage colony-stimulating factor –GM-CSF, a proliferation-inducing ligand –APRIL, receptor activator of the nuclear factor kappa B ligand –RANKL), *(iv)* intracellular signaling molecules and transcription factors (e.g. janus kinase –JAK and NF-κB), and *(v)* inflammatory cells (e.g. macrophages, B and T lymphocytes, FLS and vascular endothelial cells –VECs) [11, 12].

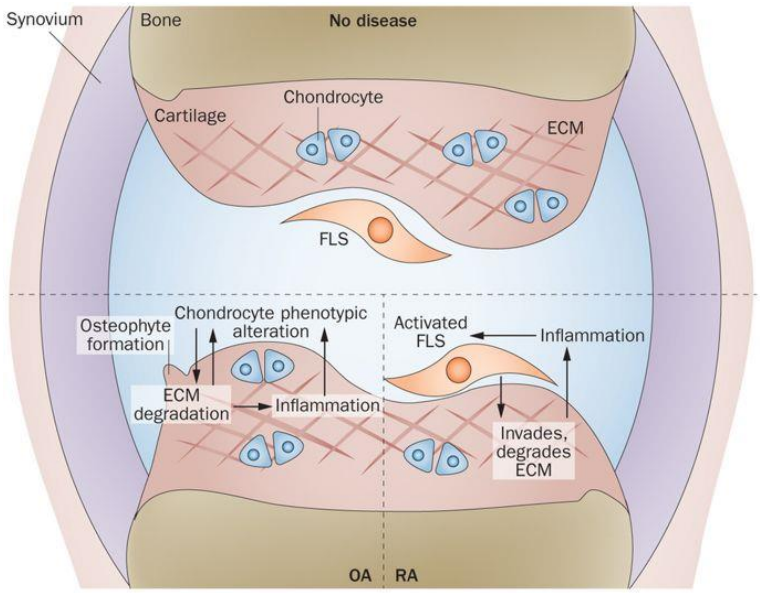

Figure I-2 – Comparison of joint damage in OA and RA (reprinted with permission [9]).

The participation of the group of inflammatory cytokines in the pathogenesis of arthritic diseases is by far the most widely and accurately documented in literature [9]. Cytokines act as local messengers in normal biological processes, such as cell growth, tissue repair, inflammation and immunity. Considering their role in the regulation of the inflammatory reactions, cytokines can be divided into pro-inflammatory cytokines and anti-inflammatory cytokines. The upregulated production of pro-inflammatory cytokines (especially TNF-α, IL-6, IL-1β, IL-23, IL-17 and IL-18) and/or the downregulated synthesis of anti-inflammatory cytokines (such as IL-4, IL-10 and IL-13) mediate the development and progression of arthritic diseases.

Pro-inflammatory cytokines promote the catabolic and destructive processes of arthritis. They affect the cells present in the joint through the impairment of intracellular pathways of signals transduction to produce cytokines, other inflammatory compounds and enzymes [13, 14]. The key role of pro-inflammatory cytokines in the pathogenesis of arthritic conditions is summarized in **Table I-1** [14, 15].

TNF-α is one of the 19 members of the TNF superfamily (**Figure I-3A**), which is originally formed as a homotrimeric transmembrane protein type II (mTNF-α) [16]. Its free form is cleaved by a metalloproteinase, TNF-α converting enzyme (TACE). Hence, the deregulation of either those enzymes or TNF receptors seems to be linked to its pro-inflammatory, cytotoxic and apoptotic responses [17]. TNF-α synthesis in the joint is governed by chondrocytes, osteoblasts, cells forming the synovial membrane, and mononuclear cells. In both diseases, TNF-α stimulates the production of other inflammatory mediators, including cytokines (especially IL-6 and IL-8), chemokines, adhesion molecules and enzymes, attracting

and activating immune and inflammatory cells into the joint (leukocytes, endothelial cells and FLS). In addition, this pro-inflammatory cytokine activates osteoclasts and, consequently, induces the resorption of bone (stimulation of osteoclastogenesis) [18]. Thus, as a regulatory cytokine that controls many other factors, TNF-α plays a key role in the pathogenesis of those conditions. Indeed, arthritic patients have an elevated level of TNF-α in both the synovial fluid, synovial membrane, cartilage and the subchondral bone layer [19, 20]. Therefore, in recent years, it has been also considered a biomarker of those diseases [21].

IL-6 belongs to the IL-6 superfamily (**Figure I-3B**), being mainly produced in the inflamed joints by chondrocytes, osteoblasts, FLS, macrophages, and adipocytes, usually in response of other pro-inflammatory cytokines (especially IL-1β and TNF-α) [22]. As IL-6 regulates a wide range of fundamental biological activities, including acute-phase responses, inflammation, and immune responses, it is also a key mediator in the pathophysiology of OA and RA [23]. IL-6 can promote synovitis and joint destruction by stimulating neutrophil migration and osteoclast maturation [24]. In RA, IL-6 may also contribute to the induction and maintenance of the autoimmune process through B-cell maturation, T helper type 17 (Th17) differentiation, and regulatory T cells (Treg) inhibition [23]. While Th17 cells are associated to autoimmune tissue inflammation through production of inflammatory cytokines [25], the role of Treg cells is to inhibit T-cell activation and suppress pro-inflammatory cytokine production. It is well established that the synovial fluid and serum of OA and RA patients present high concentrations of this pleiotropic cytokine [19, 20], being one of the most abundantly expressed cytokines in those diseases. Moreover, since IL-6 level correlate with the disease activity and joint destruction [26, 27], the development of biosensors to monitor IL-6 secretion *in vivo* are in progress [28].

IL-1β is one of the 11 representatives of the IL-1 family (**Figure I-3C**) [29]. It is originally synthesized as a cytosolic precursor protein and after the proteolysis by IL-1β converting enzyme (ICE), the active form is released into the extracellular space. IL-1β is secreted in the joint by the same cells that synthesize TNF-α, and its increased concentration is observed in the synovial fluid, synovial membrane, cartilage and subchondral bone layer, where increased levels of TNF-α and IL-6 are also detected [19, 30]. IL-1β is involved in the pathogenesis of arthritis by the activation of leukocytes, endothelial cells, chondrocytes and osteoclasts that stimulate the production of MMPs [31]. Moreover, it blocks the synthesis by chondrocytes of key ECM components, such as collagen type II and aggrecan. Hence, IL-1β not only induces cartilage degradation by enzymes, but it also inhibits its restoration process. In addition, it stimulates the synthesis of other cytokines, including TNF-α, IL-6, IL-8 and CCL5 chemokine.

IL-23 is a heterodimeric cytokine belonging to the IL-6/IL-12 family (**Figure I-3D**). It is composed of the p40 subunit in common with IL-12, and having a unique p19 subunit [25]. Despite sharing a strong structural relationship, IL-12 and IL-23 maintain different biological roles. While IL-12 drives Th1 cells differentiation that promote cellular immunity (protection against pathogens), IL-23 is responsible for Th17 cells differentiation that are usually associated to autoimmune tissue inflammation. Hence, IL-23 plays a central role in T cell-mediated responses and is considered a key promoter of immune-mediated conditions, including colitis, gastritis, psoriasis and arthritis [32, 33]. In the presence of other factors, such as IL-6 and TGF-β, IL-23 induces the differentiation of naive $CD4^+$ T cells into Th17 cells, which stimulates the production of other pro-inflammatory cytokines, including IL-17, IL-22, TNF-α and GM-CSF. IL-23 is mainly secreted by activated dendritic cells, macrophages or monocytes. Considering the high expression of IL-23 in the serum and synovial fluid of RA patients, it may also be a useful biomarker for the diagnosis of the different stages of RA progression [34, 35].

IL-17A is one of the six members of the IL-17 family (**Figure I-3E**). Stimulated $CD4^+$ T cells and mast cells that infiltrate the synovial membrane are the main source of IL-17A in both OA and RA. Indeed, IL-17A levels in the serum and synovial fluid of OA and RA patients is elevated, showing a positive correlation with the radiographic image of lesions [36, 37]. It stimulates the upregulation of pro-inflammatory cytokines (IL-6, IL-8, TNF-α), chemokines and metalloproteinases, being also crucial for the T cell-mediated activation of osteoclastogenesis [38]. Moreover, IL-17A and TNF-α act synergistically to promote increased expression of endothelial cell adhesion molecules, further increasing granulocyte recruitment to the sites of inflammation.

Table I-1 – Key pro-inflammatory cytokines, their function and production in arthritic diseases.

Cytokines	Function	Cell source
TNF-α	Activates immune and inflammatory cells (leukocytes, endothelial cells and synovial fibroblasts); Stimulates the production of cytokines, chemokines, adhesion molecules and enzymes; Suppress the regulatory T-cell function; Activates osteoclastogenesis.	Chondrocytes Osteoblasts Cells forming the synovial membrane Mononuclear cells
IL-6	Activates leukocytes and osteoclasts; Induces the differentiation of T cells in Th-1, Th-2 and Th-17 cells, and also B-cell maturation.	Chondrocytes Osteoblasts FLS Macrophages Adipocytes

IL-1β	Activate leukocytes, endothelial cells, chondrocytes, osteoclast and synovial fibroblasts; Induce MMPs that degrade the cartilage; Inhibits the synthesis of hyaline cartilage.	Chondrocytes Osteoblasts Cells forming the synovial membrane Mononuclear cells
IL-23	Induces Th17 differentiation.	Activated dendritic cells Macrophages Monocytes
IL-17A	Activation and expression of pro-inflammatory cytokines (IL-6, IL-8, TNF-α), chemokines and MMPs.	Stimulated $CD4^+$ T cells Mast cells

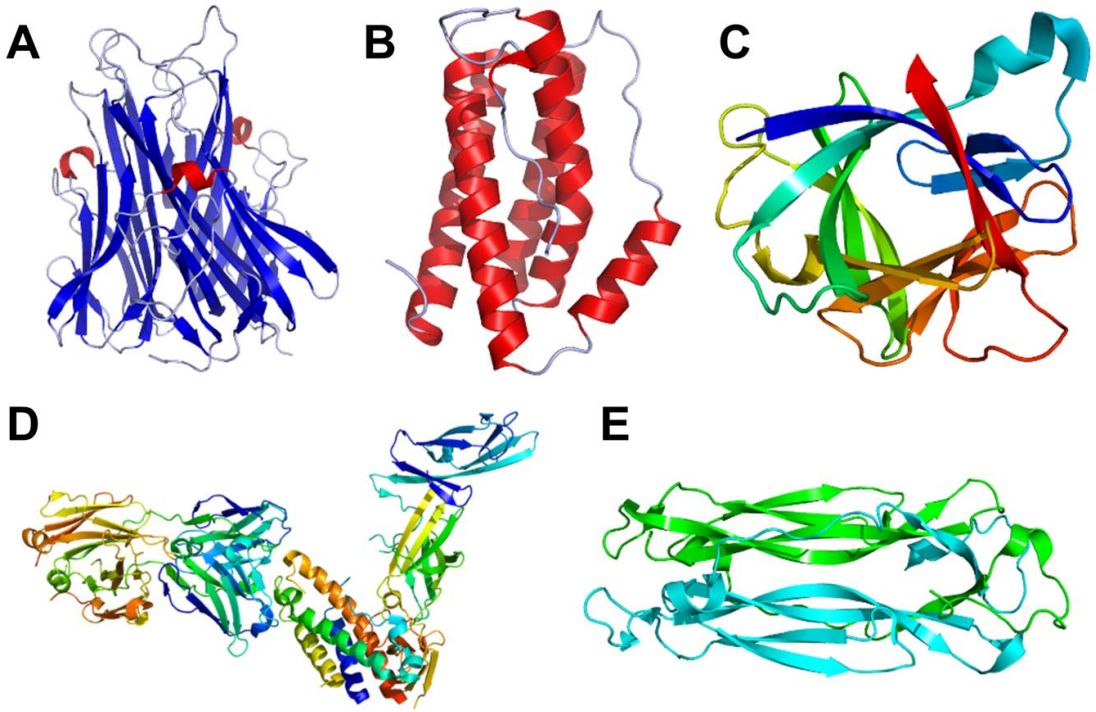

Figure I-3 – Protein structure of (A) TNF-α, (B) IL-6, (C) IL-1β, (D) IL-23 and (E) IL-17A.

I-2.2. Treatment

In the last years, the increased knowledge of the physiopathology of arthritic diseases led to a dramatic change in the available treatment modalities. Therefore, the term "drug" is not limited to the conventional therapeutic agents commonly used (e.g. anti-inflammatory drugs), including also recombinant proteins and genes. Recombinant proteins are used as highly effective medical treatments for a wide range of diseases in which a protein is either lacking or present in a deficient amount (e.g. anti-

inflammatory cytokines), or is abnormally highly expressed (e.g. antibodies to neutralize the excess of pro-inflammatory cytokines) [39]. Consequently, therapeutic proteins can include antibodies, hormones, growth factors, anticoagulants, blood factors, enzymes, Fc fusion proteins, interferons, interleukins and thrombolytic drugs, which are been produced by recombinant DNA technology.

As there is no current cure for OA and RA, the most commonly used therapeutic strategies include analgesics, non-steroidal anti-inflammatory drugs (NSAIDs) and glucocorticoids (GCs) [40]. Moreover, disease-modified anti-rheumatic drugs (DMARDs) and biological agents are the first line of treatment in RA in order to relieve joint damage and control the disease progression. However, despite all recent clinical trials, until date there is no DMARDs and biological agents approved for OA treatment [41]. Taking into consideration the mechanisms of initiation and progression of both diseases, in RA the systemic therapy is generally indicated and appropriated, while in OA the local therapy may offer particular advantages over systemic therapy [42, 43]. Nowadays, IA injections of HA and GCs are standard treatment options for the management of OA-related knee pain.

Despite the advances in developing new drugs to the key molecular targets of the disease onset and progression, their modest therapeutic effects are mainly attributed to their poor bioavailability at sites of disease. Indeed, many of these new therapeutic strategies are associated with short half-life, and poor pharmacokinetic distribution to the specific site of disease. Additionally, systemically administered agents with ubiquitous therapeutic targets are associated with severe side effects. In the following section, a brief description of the treatment modalities available for OA and RA will be provided. **Table I-2** summarizes the current options in the clinical practice.

Table I-2 – Summary of the available treatments for OA and RA.

Therapeutic Classification		Drugs/Agents	Mechanism of action	Side Effects	Disease	Ref
Analgesics		Acetominophen	Prostaglandin inhibitor	Hepatic	OA	[44]
	NSAIDs	Ibuprofen Indometacin Celecoxib Rofecoxib Valdecoxib	COXs inhibitors Immunomodulation	Gastrointestinal reaction Kidney and cardiac dysfunction	OA RA	[45]
	GCs	Dexamethasone Hydrocortisone Prednisone Betamethasone Methylprednisolone	Immunosuppression	Osteoporosis Hyperglycemia Insulin resistance Hypertension	OA RA	[46]
	Opioids	Hydrocodone Tramadol	Analgesia through acting in opioid receptors	Gastrointestinal reaction Abuse and addiction	OA RA	[47]
DMARs		Methotrexate Hydroxychloroquin Sulfasalazine Clodronate Leflunomide	Immunosuppression Disease-modifying activity	Myelosuppression Gastrointestinal reaction Liver and kidney dysfunction	RA	[48]
Biological agents	Anti-cytokines	Etanercept Infliximab Adalimumab Certolizumab pegol Golimumab	TNF-α inhibitor	Infection Tuberculosis	RA	[49]
		Tocilizumab Sarilumab	IL-6 receptor inhibitor	Infection Gastrointestinal perforation		
		Anakinra	IL-1 receptor inhibitor	Infection		
		Denosumab	RANKL inhibitor	Infection		
	Anti-T cell	Abatacept	T cell activation inhibitor (binding to CD80 and CD86 receptors)	Infection Malignancy		
	Anti-B cell	Rituximab	B-cell depletion (binding to CD20 receptor)	Infection Hypertension		
	Kinase inhibitors	Baricitinib Tofacitinib	JAK 1 and 2 inhibitors	Infection		

I-2.2.1. Analgesics and anti-inflammatory drugs

Analgesics are the most prescribed medicines in OA, mainly due to the lack of more effective treatments approved [50]. Regarding RA, they are no longer considered the first-line treatments, being only used as an adjunctive in symptomatic therapy or during the short phase until a diagnosis is established [51].

Acetaminophen, also known as paracetamol, is a simple analgesic that has both analgesic and antipyretic actions [44]. Due to its relative safety and effectiveness, most guidelines recommend acetaminophen as the first-line oral analgesic for mild-to-moderate OA [52]. For patients with severe symptoms or who do not respond to acetaminophen, more potent drugs should be considered, such as NSAIDs.

NSAIDs provide anti-inflammatory and analgesic effects, presenting better pain relief profiles than acetaminophen in moderate-to-severe OA [45]. They inhibit cyclooxygenase (COX) enzyme, which is involved in the conversion of arachidonic acid to prostaglandins. Traditional NSAIDs (e.g. ibuprofen and indometacin) are non-selective COX inhibitors, inhibiting both COX-1 and COX-2. Although the efficacy of NSAIDs for OA treatment has been well documented, the health concerns seriously restrict their extensive application. Indeed, ≈30% of the patients developed adverse effects, especially gastrointestinal complications [53]. In the last years, selective COX-2 inhibitors (e.g. celecoxib, rofecoxib and valdecoxib) appeared safer than traditional NSAIDs. Nevertheless, they are also associated with potential risk of serious adverse cardiovascular events. Therefore, there is a balance between the efficacy and safety of NSAIDs and, consequently, the benefit/risk ratio should be considered when prescribing these drugs. Osteoarthritis Research Society International (OARSI) guidelines recommend the use of NSAIDs at the minimum effective dose, avoiding their prolonged use.

GCs, such as dexamethasone (Dex) and prednisolone, have potent anti-inflammatory and immune-suppressive actions [54]. Despite the good therapeutic outcomes, their use is severely hampered, due to the risk of developing serious side effects, such as osteoporosis, hyperglycemia, insulin resistance and hypertension. Thus, GCs are usually limited in cases of moderate to severe OA, when NSAIDs are not effective [55]. Moreover, in order to minimize their systemic absorbance and avoid possible negative effects, they are frequently administered locally into the OA joint. In RA, the guidelines recommend the administration of low-dose GCs immediately after the diagnosis, followed by longer term modulation of inflammation using DMARDs (in I-2.2.2. section) [46].

When other pharmacological agents are either ineffective or contraindicated, opioids are considered for the treatment of refractory pain in patients with moderate-to-severe OA [52]. Despite the lack of information, it seems that a substantial number of patients with RA are also treated with opioids following the Centers for Disease Control and Prevention (CDC) guideline [56]. Indeed, opioids have outstanding efficacy regarding analgesia, however, they present frequent adverse effects, including nausea, vomiting, dizziness, constipation, sleepiness, tiredness and headache, which may outweigh the benefits in pain relief [57]. Moreover, there are other potential risks on increasing abuse and/or addiction, morbidity and mortality.

I-2.2.2. DMARDs

A DMARD is defined as a medicine that interferes with signs and symptoms of RA, improves physical function and inhibits progression of joint damage [58]. Traditional DMARDs include methotrexate (MTX), leflunomide, hydroxychloroquine, and sulfasalazine. MTX is currently the first-line therapy for RA, due to its efficacy in reducing the signs and symptoms and preserving cartilage function with relative safety. This drug presents a large dose-titratable range in oral or parenteral formulations and a good ratio benefit/cost [59]. While MTX monotherapy is recommended as an initial pharmacological strategy, it can also be used in combination with a wide variety of other drugs. Indeed, a combination of several DMARDs or a DMARD plus biological agents has been demonstrated to be favorable for the therapy outcome. Nevertheless, their adverse side effects can range from mild (rash, nausea, vomiting, stomatitis) to severe, including hepatotoxicity and bone marrow toxicity [48].

I-2.2.3. Biological agents

Biological therapy or immunotherapy is referred to the use of recombinant proteins intended to activate or suppress the activity of the immune system [60]. In inflammatory diseases, such as OA and RA, immunotherapies aim to suppress/reduce the immune system activity (e.g. by neutralizing pro-inflammatory cytokines and by binding and blocking receptors that trigger immune-cells activation) or to eliminate and regulate immune cells that contribute to tissue damage (e.g. effector lymphocytes). Recently, numerous biological agents have been approved for clinical practice, being even more under the development stage [61]. One of the highest selling class of biologicals since 2009 are the monoclonal antibodies [62]. Indeed, they gained significant attention due to their high specificity and potency [63].

Biological agents for the treatment of arthritic diseases can also be referred as biologic DMARDs (bDMARDs). They present a rapid improvement in clinical symptoms and delayed radiographic progression [64]. However, despite the success of these biological agents, up to 30% of patients with RA still may not respond adequately, and can present an increased risk of infections, along with other side effects, including malignancy, hypertension and administration reactions.

The first and most frequently used biological agents in RA are the TNFα inhibitors. Indeed, five different types of TNF-α inhibitors are currently licensed for clinical practice in RA treatment, namely infliximab, entarnecept, adalimumab, certalizumab pegol and golimumab [65]. Based on the currently available literature, TNF inhibitors became the first choice of bDMARDs therapy in RA patients that do not respond or are intolerant to the conventional DMARD treatment. For OA treatment, current evidence from the available studies with TNF-α blockers are still controversial, since while some clinical trials reported promising results, others failed to demonstrate a significant clinical improvement [66-68].

The first humanized anti-IL-6 receptor antibody, tocilizumab, is worldwide approved to treat RA, due to its outstanding clinical efficacy [69]. Recently, sarilumab was also approved, being many other IL-6 inhibitors in development or in clinical trials, including sirukumab and olokizumab. Additionally, IL-6 blocking is also in clinical trials to treat OA [70].

In contrast to the success of TNF-α blockade in arthritis, IL-1β inhibitors, such as anakinra (antagonist of the IL-1 receptor) have less efficiency in the suppression of joint inflammation in patients with RA [71]. Despite being abundantly expressed in RA, the paradox of this modest clinical outcome is not fully understood, but maybe reflects the redundancy of the IL-1 receptor signaling pathways.

IL-23 and IL-17A inhibitors are still in clinical trials for RA treatment [32]. For instance, the anti-IL-23 inhibitors ustekinumab and guselkumab were approved by the Food and Drug Administration (FDA) for Psoriatic Arthritis (PsA) treatment and moderate to severe plaque psoriasis, respectively [72]. Guselkumab is also in clinical trials for pustular psoriasis (phase III, NCT02343744), PsA (phase III, NCT0315828, NCT03162796), and RA (phase II, NCT01645280). Many other anti-IL-23 antibodies are under clinical evaluation for several immune-mediated conditions. Even though, in a phase II clinical trial, the signs and symptoms of RA were not significantly reduced by guselkumab and ustekinumab after subcutaneous administration [73], more clinical trials should investigate other therapeutic conditions (e.g. route of administration, doses, time of treatment and concomitant administration of other drugs) [74]. The IL-17A inhibitors, ixekizumab and secukinumab, were FDA approved for plaque psoriasis, ankylosing spondylitis and PsA [72]. Ixekizumab and secukinumab improved RA signs and symptoms in RA patients

that show an inadequate response to TNF inhibitors, in Phase II and III clinical trials, respectively [75, 76].

I-2.2.4. Gene therapies

Gene therapy is based on the intentional modulation of gene expression in specific cells by introducing exogenous nucleic acids to induce the production of proteins (plasmid deoxyribonucleic acid –pDNA, complementary DNA –cDNA, messenger ribonucleic acid –mRNA– and microRNA –miRNA), or to inhibit the transduction of harmful proteins (small interfering RNA –siRNA– or antisense oligonucleotides) [77, 78]. There are two different approaches to deliver nucleic acids to the targeted tissues: direct (using viral or non-viral vectors) or transduced cell-mediated (by *in vitro* genetic manipulation of cells). Even though in recent years, a vast number of therapeutic gene approaches have demonstrated effectiveness in preclinical models, only a few have moved forward into clinical trials [79]. Indeed, recent studies have demonstrated the efficacy and safety of an *ex vivo* gene therapy that contains non-transduced and transduced human allogeneic chondrocytes with the TGF-β1 gene [80, 81]. Due to the clinical effectiveness of TissueGene-C (Invossa™), it was recently approved in Korea for treatment of moderate knee OA, and it is currently in a Phase III clinical trial in the USA.

In arthritic diseases, gene therapy essentially focus on increase the expression of secreted proteins, such as growth factors (IGF-1, TGF-β, bone morphogenetic proteins –BMPs, basic fibroblast growth factor –bFGF, growth differentiation factor –GDF-5 and VEGF antagonist) and anti-inflammatory cytokines (IL10, IL-1 receptor antagonist –IL1ra, and anti-inflammatory mediators). More recently it also focus on intracellular and/or signaling components, such as transcription factors (SOX genes and ZNF145) and small, regulatory nucleic acids (miR-23b, miR-140, miR-181b, miR221, miR-145, miR-335) [82].

I-3. NANOMEDICINES

Two concepts introduced in the 19th and in the 20th centuries have been revolutionizing the medical field, namely the magic bullet and nanotechnology. The first concept was coined to Paul Ehrlich, in 1900, and is related with a limited effect of the drugs on the cellular target [83]. Therefore, the linking of a targeting moiety to a drug will increase its therapeutic index. Moreover, the assembling of this concept to nanotechnology has provided significant progresses in the diagnostic, treatment and prevention of human

diseases. The term nanotechnology has been assigned to Richard Feynman, in 1959 [84], but Norio Taniguchi was the first scientist to use that word at 1974 [85]. Nanotechnology embraces "The design, characterization, production and application of structures, devices, and systems ... at the nanometre scale" [86], "with at least one novel/superior characteristic or property" [87]. Although the International Organization for Standardization (ISO/TS 80004-1:2015) defines nanoscale as the "length range approximately from 1 to 100 nm", there is considerable controversy among the scientific community especially for the upper limit. Indeed, a straight relationship between size and novel effects or functions for different materials does not exist [88]. Therefore, despite the nanoscale definition, in the literature nanostructures frequently include sub-micron particles (1 nm to 1000 nm).

The drug delivery field has been advanced and reinforced mainly due to the development of novel and innovative technologies, and the remarkable increase of knowledge about materials science and pathophysiology, biomarkers and targets of the diseases [89]. Thus, the application of nanotechnology in the diagnosis, treatment and prevention of diseases is defined as nanomedicine. It includes NPs, both nanospheres and nanocapsules, liposomes, micelles and dendrimers. In addition, polymer-drug conjugates (including proteins and antibodies-conjugates) are also classified as nanomedicines. With an appropriate nanomedicine it is possible to circumvent important drawbacks of the conventional therapies, namely *(i)* to decrease the dose of drug administered (by avoiding its metabolism/degradation, clearance and distribution in non-target tissues), *(ii)* to abolish or drastically reduce the systemic side effects (by targeting delivery, which will enhance the pharmacokinetics and pharmacodynamics of the drug and, consequently, will increase its therapeutic index) and *(iii)* to reduce the frequency of administration (by the sustained release of therapeutic concentrations of the drug over time). Therefore, an appropriate delivery system can recover withdrawn drugs from the market by overcoming their side effects in non-target tissues/organs [90-92].

A rational design of a delivery system should consider the nature of the drug to be incorporated (e.g. hydrophobic, hydrophilic or amphipathic), the mechanisms that will control its release (e.g. diffusion, carrier degradation or dissolution, cleavage of chemical bonds, and external, physiological or pathological stimulus) and the disease (e.g. cell/tissue to target or tissue pH and vascularization). Ideally, the drug must be incorporated into the delivery device, being released only in the target cells or tissues in concentrations within the therapeutic range. Moreover, depending on the mechanism of action of the therapeutic agents (e.g. binding to a cell membrane receptor or to an intracellular or nuclear target), the design of delivery carriers should be carefully considered. The selection of the most adequate composition

is crucial to obtain a nanocarrier with the desirable drug release properties. Additionally, the preparation method as well as the physicochemical properties of the delivery device (e.g. size and degradation rate in the biological environment) will also influence the release of the drugs [93]. Efforts were also made to achieve a drug release in a pulsatile fashion, triggered by changes in the neighboring milieu (self-regulated delivery systems using different mechanisms, such as pH-sensitive polymers, enzymes, illness markers and pH-dependent drug solubility) or by an external stimulus (externally triggered systems by a magnetic, thermal, ultrasonic, electric or irradiation stimulus) [94-97].

I-3.1. Targeting strategies

The targeted delivery of a drug can be either passive or active. Passive targeting is widely investigated mainly in cancer and inflammatory conditions, due to the leaky vasculature or enhanced permeability and retention (EPR) effect [98]. For this and for many other features (e.g. drug release and interaction with cells [99]), the size as well as the surface and shape of the delivery systems are crucial. An active targeting is achieved by attaching to the drug or to the surface of the delivery devices a particular ligand that ideally will bind to a moiety specifically found in a specific organ, tissue or cell of interest (**Figure I-4**).

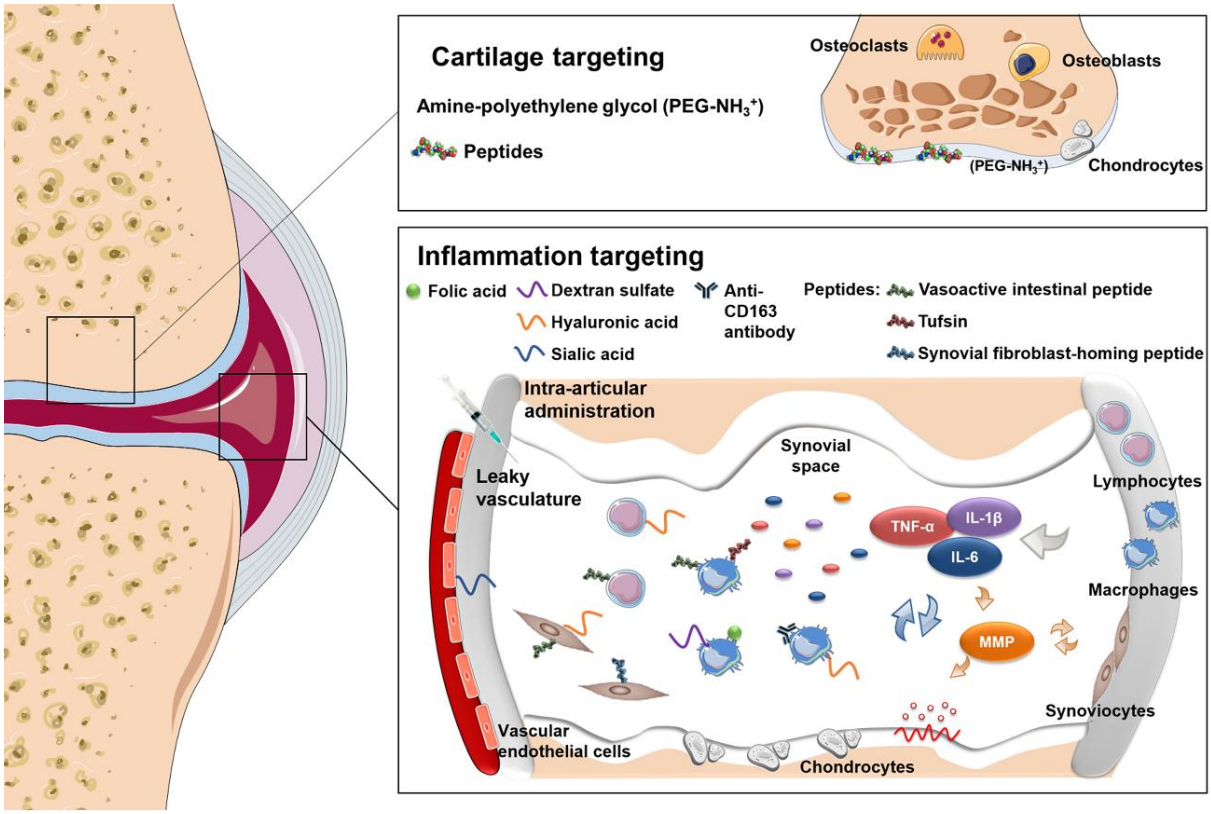

Figure I-4 – Examples of targeting moieties used to treat arthritic diseases.

I-3.1.1. Cartilage targeting

The peculiarity of cartilage structures difficult the attainment of drug concentrations required to elicit the desired biological response at the cell and matrix targets. Therefore, there is a huge interest in designing nanocarriers to selectively target cartilage in order to deliver the drug where its therapeutic action is required.

Cartilage is avascular what constitutes a major obstacle for drugs as well as for nanomedicines to diffuse and enter in its ECM. Therefore, local administration via intra articular (IA) injection in the joint space has been chosen in detriment of systemic administration to increase the drug bioavailability and to reduce drug dosage, systemic exposure and adverse events. Unfortunately, drugs injected into the joints are normally cleared very quickly (half-life of 0.1 to 6 h), which is even higher in the presence of inflammatory conditions, as in RA and OA. In addition, limited cartilage targeting also limits the therapeutic efficacy of the drugs [100]. To penetrate in the cartilage ECM, the design of a nanocarrier should consider its highly anionic charge and dense nature that leads to a 60 nm mesh size provided by the type II collagen [101] and the ≈ 3.2 and 4.4 nm of space between GAGs chains along fetal and mature aggrecan,

respectively [102]. It was already demonstrated that solutes with a diameter up to 10 nm can penetrate through diffusion or convective transport into the full thickness of an undamaged cartilage [103]. NPs presenting 15 nm of diameter can only access the superficial area of the healthy articular cartilage [103, 104]. However, they will be able to penetrate deeper if a damaged ECM is present [103, 104]. Indeed, three phenomena influence the penetration of large, positively charged molecules into the avascular negatively charged cartilage: *(i)* steric hindrance from the dense tissue ECM, *(ii)* binding to the intra-tissue sites, and *(iii)* electrostatic interactions. Nanocarriers with higher radius can also be useful if they have the ability to specifically bind to the cartilage surface. Therefore, their appropriate functionalization is of extreme importance. As previously referred cartilage presents a high negative charge that can be used to electrostatically bind, hold and accelerate the penetration of positively charged NPs [105]. Consequently, the functionalization of nanocarriers for cartilage target is usually performed with cationic moieties, including: *(i)* cell-penetrating peptides, such as the widely used TAT peptide for intracellular delivery [104, 106], *(ii)* amine-terminated polyethylene glycol (PEG) [103] and *(iii)* cationic peptides, such as collagen II α1 (COL2A1)-binding peptide (WYRGRL) [105], aggrecan-binding peptide (RLDPTSYLRTFW and HDSQLEALIKFM) [107] and heparin-binding peptide (KRKKKGKGLGKKRDPSLRKYK) [108].

I-3.1.2. Inflammation targeting

The leaky vasculature of the inflamed joints allows using the EPR effect (passive targeting). Nonetheless, active targeting have been taking advantage of the influx of various inflammatory cells including macrophages, FLS and lymphocytes into the synovial space [109]. Many receptors are upregulated on the activated macrophages, such as the folate receptor and the scavenger receptor. CD44 surface molecules are also overexpressed in macrophages, FLS and lymphocytes. The activation of epidermal growth factor receptor (EGFR) in FLS induces their proliferation and, consequently, RA pathogenesis [110]. In addition, the neovasculature composed by VECs have high expression of intercellular cell-adhesion molecule-1 (ICAM-1), E-selectin and integrins [111]. The upregulated expression of the receptors can be explored by the moieties summarized in the **Table I-3**.

Table I-3 – Examples of moieties explored for targeting delivery in inflammatory arthritis.

Moieties		Targeting	Cell	Ref
Folic acid (FA)		Folate receptor	Macrophages	[112]
Carbohydrates	Sialic acid (SA)	E-selectin receptor	VECs	[113]
	Dextran sulfate (DS)	Scavenger receptor	Activated macrophages	[114]
	Hyaluronic acid (HA)	CD44 surface molecules	Macrophages, FLS and lymphocytes	[115]
Antibodies	anti-CD163 antibody	Scavenger receptors	Activated macrophages	[116]
	Single-chain Fv A7	Microvasculature of human arthritic synovium	-	[117]
	Cetuximab monoclonal antibody	EGFR	FLS	[118]
Peptides	Arginyl-Glycyl-L-Aspartic acid (RGD)	αvβ3 integrin receptor	VECs	[119]
	Vasoactive intestinal peptide (VIP)	G protein-coupled receptors	T-lymphocytes, macrophages and FLS	[120]
	Tufsin	Fc and neuropilin-1 receptors	Macrophages	[121]
	Synovial fibroblast-homing peptide (HAP-1)	-	FLS	[122]
	GE11 (amino acid sequence YHWYGYTPQNV)	EGFR	FLS	[123]
	ART-1 (amino acid sequence CRNADKFPC)	-	Synovial endothelial cells	[124]

I-3.2. Nanomedicines in Arthritic Diseases

Several nanomedicines for arthritic diseases treatment will be explored in this section, being some examples summarized in **Table I-4**.

I-3.2.1. Liposomes

Liposomes were the first nanocarriers to be successfully translated into clinical applications, revolutionizing the pharmaceutical field [125, 126]. They are described as being biocompatible,

biodegradable, non-toxic and flexible. Liposomes are spherical vesicles characterized by a bilayer of lipids with an internal aqueous cavity. Thus, they can be used to encapsulate both hydrophobic and hydrophilic drugs within the bilayer and the aqueous core, respectively [127]. The bilayer is mostly composed of phospholipids, especially phosphatidylcholine, the most common phospholipid found in nature and cells, and other constituents, such as cholesterol and hydrophilic polymers [128]. The lipid composition critically impacts the vesicle size, surface charge and drug loading and, consequently, should be tuned based on the desired properties.

In the past few decades, liposomes has been widely explored as potential nanocarriers for arthritis therapy [129]. In order to improve the anti-inflammatory actions of GCs and enhance their site-specific distribution, PEGylated liposomes were extensively investigated in several preclinical and clinical studies. Dex-loaded liposomes were successfully developed for systemic administration using FDA approved excipients [130]. In an adjuvant-induced arthritis (AIA) rat model, the Dex-loaded liposomes showed prolonged retention time in the inflammatory joint tissues and a high suppression of the joint swelling and serum pro-inflammatory cytokines production, including TNF-α and IL-1β. Furthermore, the evaluation of safety suggested that they exhibited an improved alleviation of the hyperglycemia and hematological profiles in comparison with free Dex. PEG modified liposomes have also been used to improve the efficacy of other GCs (e.g. prednisolone [131, 132]), NSAIDs (e.g. indomethacin [133]), and DMARDs (e.g. MTX [134-136]).

Recently, targeting moieties are widely used to increase the targeted delivery into the arthritic joint. For instance, FA-liposomes demonstrated selective accumulation in arthritic rat paws to a greater extent than non-targeted liposomes [137]. In addition, the encapsulation of betamethasone in the FA-liposomes led to a lower level of paw swelling, lower arthritis scores and a reduction in bone erosion in an AIA rat model. RGD-targeted PEG liposomes to deliver Dex to arthritis affected sites proved their efficacy in an AIA rat model [138]. Indeed, the nanocarrier specifically binds to VECs *in vitro* and endothelium at sites of inflammation *in vivo*. Moreover, a synovium-specific targeted liposomal formulation was produced by conjugating the targeting peptide HAP-1 to the surface of long circulating PEGylated liposomes encapsulating prednisolone [139]. They displayed 10-fold increased accumulation in affected joints compared to heathy joints and improved drug therapeutic index in an AIA rat model. Despite all this works demonstrated a higher accumulation in arthritic joints after the functionalization with the targeting moieties, their value deeply relies on the drug side effects, which should decrease. Therefore, all these strategies need further *in vivo* studies in order to monitor the adverse side effects of the encapsulated

drug. As such, ART-1-coated liposomes were used to encapsulate IL-27 [140]. The peptide was able to direct the liposomes into the inflamed arthritic joints, enhancing the efficacy and reducing adverse effects of IL-27 treatment. The intravenous injection of ART-1-IL-27 liposomes to arthritic rats was more effective in suppressing disease progression and with better safety profile than control-IL-27 liposomes lacking ART-1 or free IL-27. In a recent work of the same authors, a novel peptide ligand (CKPFDRALC) named ART-2 was used to coat liposomes encapsulating Dex [141]. In an AIA rat model, ART-2-coated liposomes inhibited more effectively the arthritis progression in comparison with control-Dex liposomes or free Dex, however presented a comparable profile of adverse effects.

Cationic liposomes have also been exploited for the delivery of nucleic acids. siRNA against TNF-α, IL-1, IL-6 or IL-18 was encapsulated into a liposomal formulation to transport them to inflammatory sites [142]. The siRNA-liposome complexes significantly reduced the incidence and severity of arthritis in a collagen-induced arthritis (CIA) mice model. Moreover, RNAi to silence the *Indian Hedgehog (Ihh*) gene*,* which was previously associated with cartilage degeneration, was encapsulated into positive charged lipid NPs (Dlin-KC2-DMA/dipalmitoyl phosphatidylcholine (DPPC)/cholesterol/C16 ceramide-mPEG2000) to specifically target articular cartilage and increase the delivery of therapeutic genes to the chondrocytes [143]. *In vivo* results confirmed the specificity of the liposomes to cartilaginous tissue and in the rat model of OA, IA injection of LNP-*Ihh* siRNA demonstrated a chondroprotective effect that attenuated cartilage degeneration and OA progression.

I-3.2.2. Polymeric NPs

Polymeric NPs are defined as colloidal particles (1 to 1000 nm) that compromise the encapsulation or adsorption of the drug into a polymer. Considering the great potential of the polymeric NPs as nanocarriers, they are one of the most studied strategies in the nanomedicine field [144]. Among the wide variety of natural, semisynthetic or synthetic materials that can be used to produce polymeric NPs, biodegradable polymers (e.g. proteins, polysaccharides, poly(amino acids) and polyesters) have been preferred to produce innovative, effective and specialized release dosage forms, due to their advantages (e.g. avoiding body accumulation and predictable degradation) [34]. For instance, the synthetic polymers, poly(lactic-co-glycolic acid) (PLGA) and poly(ε-caprolactone) (PCL), and the natural polymers chitosan (Ch), HA, alginate and albumin are widely used for the preparation of NPs [35,36]. While nanospheres have a compact matrix structure and the drugs can be entrapped, dispersed, dissolved within the polymer

matrix or adsorbed at their surfaces [37], nanocapsules are vesicular systems with a hollow liquid core surrounded by a polymeric membrane, and besides the referred locations, the drugs can also be encapsulated in that core [37].

Several NPs produced with synthetic polymers were designed for arthritic treatment applications [12]. For instance, a novel twin-drug of diclofenac and Dex was formulated into polylactide (PLA) NPs to improve their solubility and to provide a sustained release system [145]. *In vitro* release studies showed the controlled conversion into its parent drugs by hydrolysis using an esterase enzyme. Moreover, NPs showed enhanced anti-inflammatory activity *in vivo*. Dex was also loaded into GE11-PLGA NPs to be specifically uptaken by EGFR-overexpressed FLS in RA [146]. Even though *in vitro* studies confirmed the active internalization of the NPs in EGFR-overexpressing cells [147], *in vivo* studies are required to validate this hypothesis. The intravenous administration of PLGA NPs encapsulating betamethasone demonstrated a marked reduction in the inflammatory response of arthritic rats and mice [148]. In addition, these polymers can also be modified with PEG segments, in order to increase its hydrophilicity and decrease the oposonization process. For instance, betamethasone was encapsulated in PLGA NPs formed from a blend of PLGA/PLA homopolymers and PEG-block-PLGA/PLA copolymers [149]. The administration in an AIA rat model and anti-type II collagen antibody-induced arthritis (AbIA) mice model showed enhanced therapeutic benefit of the copolymers, maybe due to prolonged blood circulation and targeting to the inflamed joint.

Polymeric NPs produced with natural polymers are also being widely explored for drug delivery in arthritis conditions. For instance, the positively charged polymer Ch has been mostly used as a gene delivery vehicle by using the electrostatic interaction with the negatively charged nucleic acids. A nanocomplex of polymerized siRNA (poly-siRNA) targeting TNF-α or notch1 with thiolated glycol Ch polymers was developed for RA treatment [150, 151]. Intravenous injection in a CIA mice model showed a high accumulation at the arthritic joint site, and a marked inhibition of tissue inflammation and bone erosion. Ch was also used in a nanocarrier, deploying folic acid, diethylethylamine (DEAE) and PEG (folate-PEG-CH-DEAE) for gene delivery of siRNA-TNFα [152]. In a collagen antibody-induced arthritis (CAIA) mouse model, the developed NPs were able to control inflammation as well as bone and cartilage destruction. Another study proposed Ch-HA-plasmid-DNA (pDNA) encoding IL-1 receptor antagonist gene (pIL-1Ra) for targeting the delivery into synoviocytes [153]. Even if the *in vitro* studies confirm the transfection efficacy of the gene, which could effectively reduce the inflammatory effects of IL-1β stimulation, *in vivo* studies are needed to confirm their therapeutic efficacy. Besides Ch, HA is also used

to produce nanocomplexes with PEG-derivatized TNF-related apoptosis inducing ligand (PEG-TRAIL) [154]. In a CIA mice model, nanocomplexes demonstrated significantly better therapeutic effects in clinical scores, histology and reduction of serum inflammatory cytokines. Another approach using tuftsin-decorated alginate NPs encapsulating the anti-inflammatory cytokine, IL-10, plasmid DNA shown enhanced localization in the inflamed paws of arthritic rats upon intraperitoneal administration [155]. Notably, targeted NPs treatment successfully re-polarized macrophages from M1 to M2 sub-type and significantly reduced joint damage. In order to improve the anti-arthritic activity of (–)-epigallocatechin gallate (EGCG) and glucosamine (GA), they were encapsulated into casein protein NPs (EGC-NPs) [156]. *In vivo* experiments in a CIA rat model demonstrated higher anti-arthritic effect of the EGC-NPs than the EGCG-GA mixture. Indeed, NPs were able to significantly improve the stability of EGCG during storage and in simulated gastrointestinal conditions, and a higher suppression of the expression of TNF-α, IL-1β, IL-6, and IL-8 was also observed. Thus, the EGC-NPs exhibit good potential as a food supplement for alleviating arthritis.

I-3.2.3. Micelles

Polymeric micelles are produced from amphiphilic copolymers that self-assemble in nanostructures with a hydrophobic core and a hydrophilic exterior in an aqueous solution (≈ 10-200 nm in size) [157, 158]. In the micelles, the hydrophobic cores are usually used to encapsulate hydrophobic drugs. Thus, most of the micelles applied in arthritis treatment incorporate poorly water-soluble DMARDs or GCs agents. Amphipathic polymer-drug conjugates (PEG-Dex) micelles, combined with a pH-responsive linker, exhibited preferential retention in targeted tissues in a rat model of AIA [159]. These micelles had targeted delivery to inflamed sites via the EPR effect, ensuring a higher release in the acidic arthritic joints and, consequently, enhanced therapeutic efficacy of the drug. Cholesteryl chloroformate - polysialic acid (CC-PSA) micelles were modified with folic acid to obtain targeted delivery of Dex in inflamed joints [160]. In an AIA model, the delivery of Dex by FA-CC-PSA micelles increased its half-life and bioavailability compared with commercial Dex. Moreover, micelles were retained longer in the joints, leading to reduced paw thickness and clinical arthritis index. For DMARDs delivery, dextran sulfate-graft-methotrexate conjugate (DS-g-MTX) micelles were developed, with excellent target ability to activated macrophages [161]. DS-g-MTX micelles showed significantly higher accumulation in the inflamed joints and stronger anti-inflammatory effect than the free MTX and the Dextran-g-MTX. In addition, DS-g-MTX efficiently inhibited the expression of pro-inflammatory cytokines, leading to significant relief of synovitis and protection of

articular cartilage in CIA mice model. Folate-modified dextran–MTX conjugate micelles (noted as Dex-g-MTX/FA) were developed for targeting delivery to macrophages [162]. The micelles shown higher cellular uptake mediated by the folate receptor and higher cytotoxicity toward lipopolysaccharide activated macrophages. Moreover, Dex-g-MTX/FA possessed improved biodistribution at the lesion site and stronger inhibition of pro-inflammatory cytokines, which significant suppressed the synovitis and effectively protected the articular cartilage. In another study, MTX loaded into sialic acid-dextran-octadecanoic acid (SA-Dex-OA/MTX) micelles considerably improved accumulation and transport to arthritic paws presenting a high expression of E-selectin [163]. In a CIA rat model, the micelles significantly inhibited the inflammatory response, diminished the adverse effects of MTX, and increased the bone mineral density.

Cationic micelles composed of the diblock copolymer of PLGA and poly(2-(diethylamino)ethyl methacrylate) (PDMA) self-assembled in 40 nm size structures. They scavenge cell-free DNA (cfDNA) derived from RA patients and inhibit the activation of primary synovial fluid monocytes and FLS [164]. As cfDNA exacerbates the pathogenesis of RA, the intravenous injection of the cationic micelles into a CpG-induced mouse or CIA rat mode relieved RA symptoms, including ankle and tissue swelling, and bone and cartilage damage. The positive therapeutic outcomes were also corroborated with the determination of intracellular trafficking, biodistribution, cfDNA levels in systemic circulation and inflamed joints, and cytokine levels in the joints. This innovative work suggests a new direction in treating inflammatory diseases though the effective and safe removal of pathogenic damage-associated molecular patterns (DAMP) molecules.

Natural polyphenols, such as curcumin (Cur), were extensively studied as therapeutic agents for various diseases, due to their remarkable anti-inflammatory, antioxidant, antitumor and antimicrobial activities. A novel anti-RA approach composed of HA/Cur micelles was able to overcome the poor bioavailability of Cur, being also able to exert a lubricating action in the joints [165]. When IA injected in a complete Freund's adjuvant (CFA) and Collagen II RA rat model, the micelles significantly decreased the degree of edema and the expression of pro-inflammatory cytokines (TNF-α and IL-1) and VEGF, which resulted in a marked inhibition of the inflammatory response. Moreover, the friction between the cartilage surfaces of the joints was reduced, protecting the cartilage from further degradation.

I-3.2.4. Dendrimers

Dendrimers (≈ 2-100 nm in diameter) are highly branched polymeric structures with enhanced functionality, due to the presence of several functional groups at their surface [166, 167]. The functional groups exhibit a high degree of molecular uniformity, which limits the molecular weight distribution and their size. Poly(amidoamide) (PAMAM) dendrimers of generation 5 were conjugated with MTX and FA to target inflammation-activated folate receptor overexpressing macrophages [168]. In an AIA rat model, G5-MTX and G5-FA-MTX had similar preventive effects on the development of arthritis as MTX. Importantly, G5-FA-MTX conjugates significantly decreased the spleen toxicity of MTX and, consequently, further studies are needed to determine whether other side effects of MTX are also attenuated. PAMAM dendrimers functionalized with PEG and conjugated with a growth factor, IGF-1, were designed for targeted delivery to chondrocytes and retention within the joint cartilage after IA injection [169]. The cationic nanoformulation was capable of enhancing drug therapeutic lifetime by 10-fold for up to 30 days and cartilage penetration to at least 1 mm within articular joints in 2 days. IGF-1 efficacy was enhanced by the dendrimer-IGF-1 formulation in protecting both cartilage and bone in a rat surgical model of OA, reducing the total area and width of medial tibial cartilage degeneration, as well as total volume of osteophytes in the joint.

Dendrimers can be functionalized with other NPs or polymers to combine the advantages and overcome the limitations of both systems. NanoGold-core multifunctional dendrimer were designed for pulsatile chemo-, photothermal- and photodynamic- therapy of RA [170]. The strategy of comprising gold (Au) NPs, MTX and IR780 into a dendrimer exhibited an important negative role in reactive oxygen species (ROS) generation *in vitro* and therefore may provide a synergistic opportunity to effectively treat RA. Cationic dendronized polymers (cDenpols) were designed and synthesized using PCL and different generations of cationic PAMAM dendrons to effectively eliminate cfDNA [171]. In a CIA rat model, cDenpols with longer backbones and higher charge densities were preferentially accumulated in the inflamed joint, resulting in the inhibition of joint swelling, synovial hyperplasia and bone destruction.

I-3.2.5. Inorganic NPs

Inorganic NPs include iron-oxide NPs, silica-Au nanoshells, AuNPs and quantum dots [172, 173]. They are widely applied in nanomedicine, due to their unique size and magnetic properties or enhanced

optical absorption. Indeed, theranostic systems (combining both therapeutic treatment and *in vivo* imaging) can be designed.

Hyaluronate/AuNP/Tocilizumab (HA-AuNP/TCZ) complex was developed to synergistically target the VEGF, since AuNPs have angiogenic effects, and the IL-6 receptor (TCZ is a humanized monoclonal antibody against IL-6 receptor) [174]. While *in vitro* results confirmed the simultaneous antiangiogenic and anti-inflammatory effects of the dual targeting, *in vivo* results using a CIA mouse model only showed anti-inflammatory therapeutic efficacy. Manganese ferrite and ceria NP-anchored mesoporous silica NPs (MFC-MSNs) were designed to efficiently generate O_2 and scavenge ROS for alleviating inflammation through M1 to M2 polarization of macrophages in RA [175]. IA injection of MFC-MSNs to an AIA rat model of RA alleviated hypoxia, inflammation and pathological features in the joint. Additionally, the encapsulation of MTX in the nanocarrier led to its sustained release and to the increment of the therapeutic effect of MFC-MSNs.

In imaging, iron oxide NPs, also termed superparamagnetic iron oxide NPs (SPIONs) coated with Dex and glucose were used for the detection and diagnosis of arthritis [176]. In addition, FA was conjugated to these SPIONs for better targeting to the activated macrophages in inflamed sites. The results demonstrated that this imaging system provides an enhanced contrast effect *in vivo*.

Table I-4 – Examples of nanomedicines for arthritic diseases.

Type	Formulation	Drug	Targeting rationale	Property/function	Condition	Ref.
Liposomes	Dex-loaded liposomes	Dex	Passive targeting through the EPR effect	Dex-loaded liposomes demonstrated superior therapeutic efficacy against arthritis and reduced side effects.	Arthritis	[130]
	FA-liposomes	Betamethasone	Folate receptor of macrophages via FA	Due to the selectively accumulation in arthritic rat paws, FA-liposomes encapsulating exhibited superior therapeutic efficacy.	RA	[137]
	PEGylated liposomes conjugate with HAP-1	Prednisolone	FLS via HAP-1	HAP-1 modified liposomes showed a 10 fold increase localization in affected joints compared to unaffected joints and enhanced therapeutic index in an AIA rat model.	Arthritis	[139]

Polymeric NPs	PEG-PLA NPs	Betamethasone	-	A single injection of the NPs system resulted in complete remission of the inflammatory response after 1 week in AbIA mice, exhibiting higher accumulation in inflamed joints.	Arthritis	[149]
	Poly-siRNA-thiolated glycol Ch NPs	siRNA targeting TNF-α	-	NPs showed high accumulation at the arthritic joint sites, with significantly inhibition of inflammation and bone erosion in CIA mice.	RA	[150]
	Tuftsin-decorated alginate NPs encapsulating IL-10 plasmid	IL-10 plasmid DNA	Activated macrophages of inflamed joints via tuftsin	Targeted formulation demonstrated higher transfection efficiency and reduced systemic and joint tissue pro-inflammatory cytokines, which prevented joint damage and delayed the onset of inflammation.	Arthritis	[155]
Micelles	PEG-Dex	Dex	Passive effect	PEG-Dex micelles, combined with a pH-responsive hydrazone linker, exhibit higher retention in the inflamed joints and enhanced therapeutic efficacy in an AIA rat model.	RA	[159]
	FA-Cholesteryl chloroformate - polysialic acid (FA-CC-PSA)	Dex	Folate receptor of macrophages via FA	*In vitro* and *in vivo* results demonstrated the suppression of key pro-inflammatory proteins, improvement of the drug pharmacokinetics and their safety profile.	RA	[160]
	Dextran sulfate-graft-methotrexate conjugate (DS-g-MTX) micelles	MTX	Scavenger receptor of activated macrophages via DS	DS-g-MTX micelles showed higher accumulation in the inflamed joints and stronger anti-inflammatory effect, leading to significant alleviation of synovitis and protection of articular cartilage.	RA	[161]
	Sialic acid-dextran-octadecanoic acid (SA-Dex-OA) micelles	MTX	E-selectin receptor of inflammatory vascular endothelial cells via SA	SA-Dex-OA/MTX micelles elicited excellent inhibition of inflammatory response and minor adverse effects on liver and kidneys. The synergistic effects between drug and carrier also enhanced bone repair.	RA	[163]
	Hyaluronic acid/Curcumin (HA/Cur) nanomicelles	Cur	IA injection	HA/Cur nanomicelles lowered the edema and cartilage degradation in RA rat models, with clear inhibition of the inflammatory response.	RA	[165]

Dendrimers	PAMAM-PEG-IGF-1	IGF-1	IA injection	The nanocarriers enhanced cartilage penetration and joint residence time up to 30 days. A single injection of dendrimer–IGF-1 rescued cartilage and bone more effectively than free IGF-1, in a surgical model of rat OA.	OA	[169]
	Cationic PCL-g-PAMAM dendrons (cDenpols)	-	-	cDenpols eliminates cfDNA and inhibits TLR recognition and nucleic acid-induced inflammation. In a CIA rat model, cDenpols inhibited joint swelling, synovial hyperplasia, and bone destruction.	RA	[171]
Inorganic NPs	Hyaluronate/ gold nanoparticle/Tocilizumab (HA-AuNP/TCZ) complex	TCZ	-	HA-AuNP/TCZ complex showed the dual targeting activity of the binding to VEGF and IL-6R *in vitro*. The therapeutic effect on a mouse RA model was verified by ELISA, histological, and Western blot analyses.	RA	[174]
	Manganese ferrite and ceria NP-anchored mesoporous silica NPs (MFC-MSNs)	MTX	IA injection	MFC-MSNs successfully induced polarization of M1 to M2 macrophages under hypoxic and inflammatory conditions both *in vitro* and *in vivo*. The IA injection successfully attenuated inflammation and pathological features in the joint, increasing their therapeutic effect.	RA	[175]

I-3.3. NPs internalization

In order to promote a targeted and controlled delivery of the encapsulated drugs from the NPs, it is fundamentally important to understand their uptake by different cells [177]. Indeed, many factors, including physicochemical properties of the NPs, protein-NPs and cell-NPs interactions as well as the cell type and cell's state affect the mechanism of NPs cellular internalization.

The pathway of cellular internalization of the nanomedicine is a key factor in determining their biomedical functions, biodistribution and toxicity [178]. To obtain a high therapeutic efficacy, the nanocarrier should enter into the cells without the induction of cytotoxicity, which deeply relies on the NPs entry pathway and intracellular localization [179]. In addition, since these carriers are usually aimed to

deliver the biomolecule to a specific sub-cellular compartment of the cell, intracellular trafficking and fate of NPs is a vital process for its success [180]. Indeed, although most of the nanocarriers can enter into cells via endocytosis, generally they are inevitably entrapped in endosomes, which subsequent merge with lysosomes. The lysosomes are acidic compartments (pH ranging from 4.5 to 5.5) that contain an array of hydrolytic enzymes capable to degrade macromolecules from the secretory, endocytic, autophagic and phagocytic membrane-trafficking pathways [181]. Consequently, the therapeutic molecules that are entrapped inside lysosomes undergo degradation, without providing their therapeutic action. Hence, when designing safe and efficient nanomedicines, it is crucial to understand their cellular uptake and intracellular trafficking.

I-3.3.1. Cellular Uptake Pathways of NPs

Endocytosis is the major route of cellular uptake of NPs, being an active transport that occurs against the concentration gradient by using energy [182]. It involves the generation of new intracellular membrane-enclosed vesicles from the plasma membrane with a concomitant internalization of lipids, proteins and extracellular fluid (**Figure I-5**). It is usually classified into two major categories: phagocytosis and pinocytosis.

Phagocytosis is an essential mechanism of the immune system defense, being predominantly used by phagocytes, such as macrophages, neutrophils and monocytes [183]. This pathway begins with the recognition of the NPs by the opsonins, such as immunoglobulin (IgG and IgM), complement component and blood serum proteins that attach to the cell surface through Fc receptors and complement receptors [184]. This trigger the polymerization of actin membrane protrusions at the site of ingestion and, consequently, engulfing and digesting larger particles and pathogens. After transporting the opsonized particle into the cell, the formed phagosome will undergo degradation by acidification and enzymolysis in the lysosomes.

Conversely to phagocytosis, pinocytosis is present in all types of cells and depending on the proteins involved in the pathways, it is classified to clathrin-mediated endocytosis, caveolae-mediated endocytosis, clathrin- and caveolae-independent endocytosis, and micropinocytosis.

Clathrin-mediated endocytosis comprises clathrin-coated vesicles formation in the presence of an adaptor protein, Epsin, and other accessory proteins such as dynamin (GTPase) [185]. Briefly, the NPs signaling on the cell surface aligns surface proteins to begin a clathrin-coating process on the inner

membrane of the cell [186]. With the assistance of dynamin, a clathrin-coated vesicle with a size of 100-150 nm is formed, that internally detaches from the donor membrane. The cell fate seems to be associated with the receptor at the cell surface to which the NPs attach (e.g. NPs could be transferred to lysosomes for degradation or released from the endocytosed vesicles).

Caveolae-mediated endocytosis is a pathway dependent on membrane cholesterol, dynamin and cell receptor mediation [187]. The binding of the NPs to the receptors of the plasma membrane, mainly caveolin -1, -2, -3, induce the formation of flask-shaped vesicles. The uncoated invagination initially assumes a flask shape with a body diameter of 60–80 nm and a neck diameter of 10–15 nm. The caveolae vesicles are afterwards cut off from the membrane by dynamin. Caveolae vesicles fuse with caveosomes or multivesicular bodies (MTV), which will move to the endoplasmic reticulum, cytosol or nucleus. Indeed, many pathogens including viruses and bacteria select this way to avoid lysosomal degradation. For the same reason, this pathway is believed to enhance the therapeutic effect of the drugs loaded into the NPs.

Clathrin- and caveolae-independent endocytosis occurs in cells that are deprived of clathrin and caveolin. The regulatory mechanisms of these pathways are still unknown, but cholesterol-rich microdomains on the plasma membrane, generally referred to as lipid rafts, are involved in this process [188]. Cell fate of the particles entering the cell through this pathway usually includes the delivery to the early endosomes, followed by the transfer to late endosomes and lysosomes. In addition, particles can be also directed to the trans-Golgi network or recycled back to the plasma membrane [189].

Macropinocytosis involves the uptake of large areas of the plasma and, consequently, allows the internalization of big NPs (> 1 μm) [190]. It is a clathrin-, caveolin- and dynamin-independent process. In this pathway, tyrosine kinases activate actin polymerization to form protrusions in the cell membrane. After the encapsulation of the particle, the protrusions fuses once again back with the cell membrane. The fate of macropinosomes will depend on the cell type.

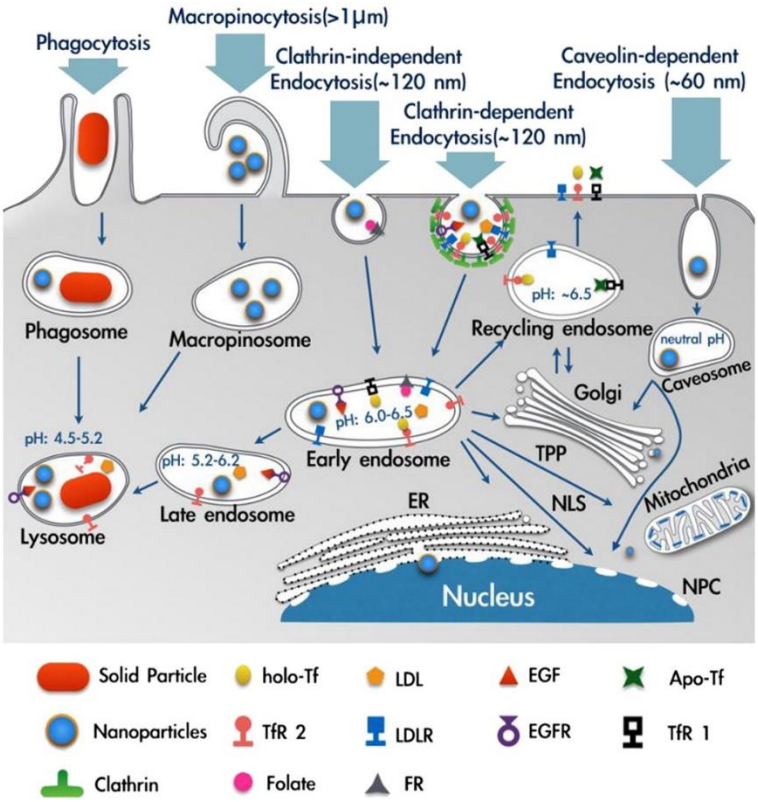

Figure I-5 – Schematic illustration of endocytic internalization pathways: phagocytosis, macropinocytosis, clathrin-dependent endocytosis, caveolae-dependent endocytosis and clathrin-independent endocytosis. Legend: endoplasmic reticulum (ER), nuclear localization signal (NLS), nuclear pore complex (NPC), triphenylphosphonium cation (TPP) (reprinted with permission [180]).

Although endocytosis is widely recognized to be the major processes by which NPs enter into cells, there are also other non-endocytic pathways, including passive diffusion, hole formation, direct microinjection and electroporation [177]. Moreover, recent studies have reported cell-penetrating peptides [191] and membrane fusion between liposomes and cells [192]. Even though those mechanisms are poorly understood, the direct cytosolic delivery of NPs payload via non-endocytic pathways also seems to be an optimal approach to minimize their degradation in the endosomes/lysosomes.

I-3.3.2. Effect of Physicochemical Properties of NPs on Cellular Uptake

The physicochemical properties of NPs, including size, shape, surface charge, surface hydrophobicity/hydrophilicity and surface functionalization are critical parameters on cellular uptake as it directly affect the uptake level, endocytotic route as well as cytotoxicity of NPs [178].

I-3.3.2.1 *Size*

Size of NPs is a key factor in determining their cellular uptake efficiency, potential toxicity, as well as uptake pathway [193]. Several studies have demonstrated that 50 nm NPs are internalized more efficiently and at a higher uptake rate than smaller particles (around 15–30 nm) or larger particles (around 70–240 nm) [194]. Considering the uptake pathways, the inconsistency of the results on the literature maybe rely on the complexity of controlling other parameters besides size during *in vitro* and *in vivo* studies (e.g. agglomeration and aggregation), and also the cell type under evaluation [195-197]. Nevertheless, it seems that small NPs (from a few to several hundred nanometers) enter the cells via pino- or macropinocytosis. NPs in the size range of 120-150 nm are mostly internalized via clathrin- or caveolin-mediated endocytosis (the maximum size reported to those pathways was 200 nm [195]), whereas NPs in the size range of 250 nm to 3 μm have been shown to have an optimal *in vitro* uptake through phagocytosis.

I-3.3.2.2 *Shape*

The shape of the NPs also seems to play a pivotal role in their uptake pathway and trafficking inside the cell, however the results are contradictory [178]. While some studies reported a higher uptake of spherical NPs when compared to rod-shaped NPs [194, 198], others describe the opposite [196, 199]. Moreover, there is no conclusion on the pathway selection of NPs considering their shape.

I-3.3.2.3 *Surface charge*

Surface charge is an important parameter in the characterization of NPs, as it determines the tendency for aggregation in storage and after administration in the blood and also the interaction with oppositely-charged compounds and the cell membrane. Indeed, highly charged positive or negative NPs present a higher stability, since the Coulombic repulsion forces can overcome the Van der Waals attractive forces between them and, consequently, preventing aggregation [200]. Even though some studies concluded that cationic particles have an increase rate and extent of internalization than negatively charged particles [201], due to the charge attraction between the positive NPs and negative cell membrane surface, the relationship between surface charge and cellular uptake is also contradictory. Indeed, many other studies have shown the successful internalization of negatively charged NPs [202].

Also the cellular pathways present inconsistent results, since a wide plethora of outcomes can be found, for example: *(i)* positively charged NPs are mainly internalized via macropinocytosis and negatively charged NPs by clathrin-/caveolae-independent endocytosis [203], *(ii)* both cationic and anionic NPs are internalized mainly by clathrin endocytic pathway [202], and *(iii)* the use of clathrin-mediated pathway by positively charged NPs and caveolae-mediated pathway by negatively charged NPs [204].

I-3.3.2.4 *Surface hydrophobicity/hydrophilicity*

The hydrophobicity/hydrophilicity of NPs is also important for the interaction with the cellular membrane [193]. The higher affinity for the cell membrane of the hydrophobic NPs improves their cellular uptake in comparison with hydrophilic NPs [205].

I-3.3.2.5 *Surface functionalization*

Surface chemical functionalization of the NPs is a tool that can be used to control distinct properties such as cytotoxicity, stability and cellular internalization [206]. Surface functionalization of NPs predominantly comprises PEG, the negative carboxyl group (-COOH), neutral functional groups like hydroxyl groups (-OH), and the positive amine group ($-NH_2$). Several studies have highlighting the key role of surface chemical functionalization in cellular interactions with NPs. As a representative example, pristine polystyrene (PS) NPs and amino-functionalized polystyrene NPs have demonstrated a higher uptake rate with the amino-functionalized NPs than PS-NPs, and while the former were internalized mainly via clathrin-mediated pathway, the latter was via clathrin-independent endocytosis [207]. In addition, several ligands and peptides were designed to increase the targeted delivery of the NPs into specific cells [208]. The strategy takes advantage of the up-regulation of receptors in diseased cells in order to increase their cellular uptake of the NPs. The method may facilitate the direct cell penetration or receptor-mediated endocytic pathways and, consequently, facilitate the delivery of NPs at the required cell compartment within a specific tissue.

I-3.3.3. Effect of Cell Properties over NPs Uptake

Cell types and their native environment (that can be altered, e.g., in diseased conditions) deeply affects the phenotype and, consequently, the endocytic pathway. For instance, under inflammatory

conditions endothelial cells become activated and express endothelial cell adhesion molecules (ECAMs, e.g. vascular cell adhesion molecule (VCAM), E-selectin, P-selectin and intercellular adhesion-1) [209]. Thus, NPs with targeted molecules for these receptors will have an enhanced uptake by those cells. Conversely, other cells do not express the proteins necessary for a specific endocytic pathway, which difficult the use of that particular mechanism. For example, HepG2 cells have no endogenous caveolin, so they are unable to uptake NPs by caveolae-mediated endocytosis [210].

Regarding inflammation, the current focus of investigation are the differences of internalization between M1 and M2 polarized macrophages. Indeed, depending on the local microenvironment and stimulation profile, macrophages differentiate into two different phenotypes, M1 and M2 [211]. M1 macrophages are defined as pro-inflammatory, whereas M2 macrophages are considered immuno-regulatory. Cellular uptake studies are very inconsistent, since while some studies reported higher NPs uptake after M2 polarization [212], others found higher phagocytic capacity of M1 macrophages [213]. Moreover, their internalization pathways seem to be tissue- and cell-state-specific. For arthritic diseases, current literature is limited to assess the NPs internalization after functionalization with a targeting moiety for FLS or macrophages.

Notably, there are distinct differences in the endocytic pathways between normal cells and tumor cells [214]. Despite those differences, most of the internalization studies are performed in carcinogenic cell lines, especially Hela cells [180, 215]. Moreover, most of the published research in this topic fail to focus in the connection between the cell origin and the endocytic pathways.

I-4. CONCLUSIONS AND FUTURE PERSPECTIVES

Nanomedicine holds the promise of contributing for more effective treatments. Indeed, the multidisciplinary expertise in nanotechnology, materials science, medicine and cell biology open new avenues and are revolutionizing the field of drug delivery. Ideally, NPs should improve the drugs therapeutic index by simultaneously: *(i)* promoting targeted delivery to the diseased/injured tissues, *(ii)* providing an optimal control and sustained release over the needed period of time, and *(iii)* reducing undesirable side effects and/or toxicity of the therapeutic agents. To accomplish a precise target delivery, many approaches were designed to increase the affinity of the NPs toward cartilage, bone and synovial tissues. On-demand drug release can be achieved by using stimuli-responsive polymers (e.g. pH, temperature, enzymes). Despite the progress achieved in the field, most of the existing delivery vehicles

present short term release caused by the kinetics of the drug release mechanisms, namely diffusion or hydrolysis and/or have limited loading capacity. Moreover, the residence time in circulation after systemic administration is limited and due to their off-target distribution, they are associated with severe side effects. Hence, a targeted, controlled and sustained release of the drug is an unmet need in order to enhance their efficacy and reduce systemic side effects.

The avascular, highly dense anionic ECM and small pore size of the cartilage makes drug delivery and diffusion very difficult. In recent years, local administration of NPs has attracted great interest to improve drug retention in the synovial cavity. However, due to the rapid turnover of the synovial fluid, improvements are still needed to ensure a long lasting therapeutic efficacy for cartilage diseases. Therefore, future direction involves the design of nanomedicines with higher capacity to attach and/or permeate through cartilaginous tissues. Albeit the advances in drug delivery for several arthritic diseases, there are many others that still need to be addressed in this field. Therefore, researchers should take into consideration recent discoveries regarding the targets and molecular mechanisms behind those diseases and design nanocarriers capable of increasing the efficacy of therapeutic agents and minimizing off-targeted delivery and the concomitant side effects.

Advanced *in vitro* studies, including bioreactors, co-cultures of different cells and microfluidics with microtissues are needed to increase the predictive power of the performance of the NPs *in vivo*. Despite the importance of rodents, due to the genotypic similarity, relatively inexpensive, easy to handle and an essential preliminary assessment, the confirmation of efficacy in large animal models is frequently required. Indeed, many clinical trials were suspended due to safety and/or efficacy issues that were not predicted in the pre-clinical tests. Therefore, animals presenting a high similarity to humans, such as humanized animal models or animals presenting biomechanics and anatomy similar to human are needed to provide a stronger perspective of the human scenario and a high chance of success in clinical trials. When designing nanoformulations, the researchers should make a compromise between innovative concepts (to achieve smart-responsive, controlled and highly efficient delivery) and simple and easy of use systems to have higher possibilities of clinical application.

In conclusion, considering the great progress in the development of nanomedicines in the preclinical stage, it is foreseeable that in the future an increase number of them will enter in clinical practice. This translation will alleviate the limitations in efficacy of currently available treatments and, more importantly, to radically improve the safety and efficacy of drugs when administrated in patients.

I-5. ACKNOWLEDGMENT

Authors acknowledge the financial support from FCT (Portuguese Foundation for Science and Technology) for the project PTDC/CTM-BIO/4388/2014 - SPARTAN, the Northern Portugal Regional Operational Programme (NORTE 2020), under the Portugal 2020 Partnership Agreement, through the European Regional Development Fund (FEDER) (NORTE-01-0145-FEDER-000023 - FROnTHERA) and the NORTE 2020 Structured Project, co funded by Norte2020 and Horizon 2020 by the contract number H2020-NMBP-PILOTS-2016 721062 Project Flexpol.

Authors would also like to acknowledge FCT/MCTES (Ministry of Science, Technology and Higher Education) and the FSE/ POCH (European Social Fund through the Operational Program of Human Capital), for the PhD scholarship PD/BD/11384/2015 of A. C. Lima (PD/59/2013).

I-6. REFERENCES

1. Brennan-Olsen, S. L., Cook, S., Leech, M. T.*, et al.*, Prevalence of arthritis according to age, sex and socioeconomic status in six low and middle income countries: analysis of data from the World Health Organization study on global AGEing and adult health (SAGE) Wave 1*. Bmc Musculoskel Dis*. 2017, *18* (1): p. 271-83.
2. Theis, K. A., Roblin, D. W., Helmick, C. G.*, et al.*, Prevalence and causes of work disability among working-age US adults, 2011-2013, NHIS*. Disabil Health J*. 2018, *11* (1): p. 108-15.
3. Murphy, L. B., Cisternas, M. G., Pasta, D. J.*, et al.*, Medical Expenditures and Earnings Losses Among US Adults With Arthritis in 2013*. Arthrit Care Res*. 2018, *70* (6): p. 869-76.
4. Eichaker, L. R., Cho, H. S., Duvall, C. L.*, et al.*, Future nanomedicine for the diagnosis and treatment of osteoarthritis*. Nanomedicine*. 2014, *9* (14): p. 2203-15.
5. Smolen, J. S., Aletaha, D. and McInnes, I. B., Rheumatoid arthritis*. Lancet*. 2016, *388* (10055): p. 2023-38.
6. Liu, M., Zeng, X., Ma, C.*, et al.*, Injectable hydrogels for cartilage and bone tissue engineering*. Bone research*. 2017, *5*: p. 17014-28.
7. Goldring, S. R. and Goldring, M. B., Changes in the osteochondral unit during osteoarthritis: structure, function and cartilage-bone crosstalk*. Nat Rev Rheumatol*. 2016, *12* (11): p. 632-44.
8. Allen, T. M. and Cullis, P. R., Drug delivery systems: Entering the mainstream*. Science*. 2004, *303* (5665): p. 1818-22.
9. Pap, T. and Korb-Pap, A., Cartilage damage in osteoarthritis and rheumatoid arthritis-two unequal siblings*. Nat Rev Rheumatol*. 2015, *11* (10): p. 606-15.
10. Glyn-Jones, S., Palmer, A. J., Agricola, R.*, et al.*, Osteoarthritis*. Lancet*. 2015, *386* (9991): p. 376-87.
11. McInnes, I. B. and Schett, G., The Pathogenesis of Rheumatoid Arthritis*. New Engl J Med*. 2011, *365* (23): p. 2205-19.
12. Roy, K., Kanwar, R. K. and Kanwar, J. R., Molecular targets in arthritis and recent trends in nanotherapy*. Int J Nanomed*. 2015, *10*: p. 5407-20.

13. Mateen, S., Zafar, A., Moin, S.*, et al.*, Understanding the role of cytokines in the pathogenesis of rheumatoid arthritis*. Clin Chim Acta*. **2016**, *455*: p. 161-71.
14. Wojdasiewicz, P., Poniatowski, L. A. and Szukiewicz, D., The role of inflammatory and anti-inflammatory cytokines in the pathogenesis of osteoarthritis*. Mediators Inflamm*. **2014**, *2014*: p. 561459-67.
15. McInnes, I. B. and Schett, G., Cytokines in the pathogenesis of rheumatoid arthritis*. Nat Rev Immunol*. **2007**, *7* (6): p. 429-42.
16. Bodmer, J. L., Schneider, P. and Tschopp, J., The molecular architecture of the TNF superfamily*. Trends Biochem Sci*. **2002**, *27* (1): p. 19-26.
17. Apostolaki, M., Armaka, M., Victoratos, P.*, et al.*, Cellular mechanisms of TNF function in models of inflammation and autoimmunity*. Curr Dir Autoimmun*. **2010**, *11*: p. 1-26.
18. Zhao, B. H., Grimes, S. N., Li, S. S.*, et al.*, TNF-induced osteoclastogenesis and inflammatory bone resorption are inhibited by transcription factor RBP-J*. J Exp Med*. **2012**, *209* (2): p. 319-34.
19. Savio, A. S., Diaz, A. C. M., Capote, A. C.*, et al.*, Differential expression of pro-inflammatory cytokines IL-15Ralpha, IL-15, IL-6 and TNFalpha in synovial fluid from Rheumatoid arthritis patients*. Bmc Musculoskel Dis*. **2015**, *16* (51): p. 1-8.
20. Farahat, M. N., Yanni, G., Poston, R.*, et al.*, Cytokine expression in synovial membranes of patients with rheumatoid arthritis and osteoarthritis*. Ann Rheum Dis*. **1993**, *52* (12): p. 870-5.
21. Mabey, T., Honsawek, S., Tanavalee, A.*, et al.*, Plasma and synovial fluid inflammatory cytokine profiles in primary knee osteoarthritis*. Biomarkers*. **2016**, *21* (7): p. 639-44.
22. Rose-John, S., Interleukin-6 Family Cytokines*. Cold Spring Harb Perspect Biol*. **2018**, *10* (2): p. 1-17.
23. Kimura, A. and Kishimoto, T., IL-6: regulator of Treg/Th17 balance*. Eur J Immunol*. **2010**, *40* (7): p. 1830-5.
24. Thiolat, A., Semerano, L., Pers, Y. M.*, et al.*, Interleukin-6 receptor blockade enhances CD39+ regulatory T cell development in rheumatoid arthritis and in experimental arthritis*. Arthritis Rheumatol*. **2014**, *66* (2): p. 273-83.
25. Paradowska-Gorycka, A., Grzybowska-Kowalczyk, A., Wojtecka-Lukasik, E.*, et al.*, IL-23 in the pathogenesis of rheumatoid arthritis*. Scand J Immunol*. **2010**, *71* (3): p. 134-45.
26. Livshits, G., Zhai, G., Hart, D. J.*, et al.*, Interleukin-6 Is a Significant Predictor of Radiographic Knee Osteoarthritis The Chingford Study*. Arthritis Rheum*. **2009**, *60* (7): p. 2037-45.
27. Madhok, R., Crilly, A., Watson, J.*, et al.*, Serum interleukin 6 levels in rheumatoid arthritis: correlations with clinical and laboratory indices of disease activity*. Ann Rheum Dis*. **1993**, *52* (3): p. 232-4.
28. Qi, M., Huang, J. W., Wei, H.*, et al.*, Graphene Oxide Thin Film with Dual Function Integrated into a Nanosandwich Device for in Vivo Monitoring of Interleukin-6*. Acs Appl Mater Inter*. **2017**, *9* (48): p. 41659-68.
29. Dinarello, C. A., Overview of the interleukin-1 family of ligands and receptors*. Semin Immunol*. **2013**, *25* (6): p. 389-93.
30. Farahat, M. N., Yanni, G., Poston, R.*, et al.*, Cytokine Expression in Synovial Membranes of Patients with Rheumatoid-Arthritis and Osteoarthritis*. Ann Rheum Dis*. **1993**, *52* (12): p. 870-75.
31. Kay, J. and Calabrese, L., The role of interleukin-1 in the pathogenesis of rheumatoid arthritis*. Rheumatology*. **2004**, *43*: p. 2-9.
32. Tang, C. L., Chen, S., Qian, H.*, et al.*, Interleukin-23: as a drug target for autoimmune inflammatory diseases*. Immunology*. **2012**, *135* (2): p. 112-24.

33. Frieder, J., Kivelevitch, D., Haugh, I., *et al.*, Anti-IL-23 and Anti-IL-17 Biologic Agents for the Treatment of Immune-Mediated Inflammatory Conditions. *Clin Pharmacol Ther*. 2018, *103* (1): p. 88-101.
34. Yago, T., Nanke, Y., Kawamoto, M., *et al.*, IL-23 and Th17 Disease in Inflammatory Arthritis. *J Clin Med*. 2017, *6* (9): p. 1-9.
35. Zaky, D. S. E. and El-Nahrery, E. M. A., Role of interleukin-23 as a biomarker in rheumatoid arthritis patients and its correlation with disease activity. *Int Immunopharmacol*. 2016, *31*: p. 105-8.
36. Chen, B., Deng, Y., Tan, Y., *et al.*, Association between severity of knee osteoarthritis and serum and synovial fluid interleukin 17 concentrations. *J Int Med Res*. 2014, *42* (1): p. 138-44.
37. Kellner, H., Targeting interleukin-17 in patients with active rheumatoid arthritis: rationale and clinical potential. *Ther Adv Musculoskelet Dis*. 2013, *5* (3): p. 141-52.
38. McKenzie, B. S., Kastelein, R. A. and Cua, D. J., Understanding the IL-23-IL-17 immune pathway. *Trends Immunol*. 2006, *27* (1): p. 17-23.
39. Lagasse, H. A., Alexaki, A., Simhadri, V. L., *et al.*, Recent advances in (therapeutic protein) drug development. *F1000Research*. 2017, *6*: p. 113-27.
40. Krishnan, Y. and Grodzinsky, A. J., Cartilage diseases. *Matrix Biol*. 2018, *71-72*: p. 51-69.
41. Persson, M. S. M., Sarmanova, A., Doherty, M., *et al.*, Conventional and biologic disease-modifying anti-rheumatic drugs for osteoarthritis: a meta-analysis of randomized controlled trials. *Rheumatology*. 2018, *57* (10): p. 1830-37.
42. Jones, I. A., Togashi, R., Wilson, M. L., *et al.*, Intra-articular treatment options for knee osteoarthritis. *Nat Rev Rheumatol*. 2019, *15* (2): p. 77-90.
43. Maudens, P., Jordan, O. and Allemann, E., Recent advances in intra-articular drug delivery systems for osteoarthritis therapy. *Drug discovery today*. 2018, *23* (10): p. 1761-75.
44. Towheed, T. E., Maxwell, L., Judd, M. G., *et al.*, Acetaminophen for osteoarthritis. *Cochrane Database Syst Rev*. 2006, (1): p. 1-47.
45. Crofford, L. J., Use of NSAIDs in treating patients with arthritis. *Arthritis Res Ther*. 2013, *15*: p. 1-10.
46. Geenen, R., Overman, C. L., Christensen, R., *et al.*, EULAR recommendations for the health professional's approach to pain management in inflammatory arthritis and osteoarthritis. *Ann Rheum Dis*. 2018, *77* (6): p. 797-807.
47. Roth, S. H., A new role for opioids in the Treatment of arthritis. *Drugs*. 2002, *62* (13): p. 1852-9.
48. Benjamin, O. and Lappin, S. L., *Disease Modifying Anti-Rheumatic Drugs (DMARD)*, in *StatPearls*. 2019: Treasure Island (FL).
49. Rein, P. and Mueller, R. B., Treatment with Biologicals in Rheumatoid Arthritis: An Overview. *Rheumatol Ther*. 2017, *4* (2): p. 247-61.
50. Zhang, W., Ouyang, H., Dass, C. R., *et al.*, Current research on pharmacologic and regenerative therapies for osteoarthritis. *Bone Res*. 2016, *4*: p. 15040-57.
51. Aletaha, D. and Smolen, J. S., Diagnosis and Management of Rheumatoid Arthritis: A Review. *Jama*. 2018, *320* (13): p. 1360-72.
52. Zhang, W., Moskowitz, R. W., Nuki, G., *et al.*, OARSI recommendations for the management of hip and knee osteoarthritis, Part II: OARSI evidence-based, expert consensus guidelines. *Osteoarthr Cartilage*. 2008, *16* (2): p. 137-62.
53. Ofman, J. J., MacLean, C. H., Straus, W. L., *et al.*, A metaanalysis of severe upper gastrointestinal complications of nonsteroidal antiinflammatory drugs. *J Rheumatol*. 2002, *29* (4): p. 804-12.

54. Vandewalle, J., Luypaert, A., De Bosscher, K.*, et al.*, Therapeutic Mechanisms of Glucocorticoids. *Trends Endocrin Met*. 2018, *29* (1): p. 42-54.
55. Savvidou, O., Milonaki, M., Goumenos, S.*, et al.*, Glucocorticoid signaling and osteoarthritis. *Mol Cell Endocrinol*. 2019, *480*: p. 153-66.
56. Day, A. L. and Curtis, J. R., Opioid use in rheumatoid arthritis: trends, efficacy, safety, and best practices. *Curr Opin Rheumatol*. 2019, *31* (3): p. 264-70.
57. Yip, K. and Oettinger, J., Why are we still using opioids for osteoarthritis? *J Int J Clin Pract.* 2019. *11*. p 1-4.
58. Alam, J., Jantan, I. and Bukhari, S. N. A., Rheumatoid arthritis: Recent advances on its etiology, role of cytokines and pharmacotherapy. *Biomed Pharmacother*. 2017, *92*: p. 615-33.
59. Friedman, B. and Cronstein, B., Methotrexate mechanism in treatment of rheumatoid arthritis. *Joint Bone Spine*. 2019, *86* (3): p. 301-7.
60. Caspi, R. R., Immunotherapy of autoimmunity and cancer: the penalty for success. *Nat Rev Immunol*. 2008, *8* (12): p. 970-6.
61. Cui, Y., Cui, P., Chen, B.*, et al.*, Monoclonal antibodies: formulations of marketed products and recent advances in novel delivery system. *Drug Dev Ind Pharm*. 2017, *43* (4): p. 519-30.
62. Mitragotri, S., Burke, P. A. and Langer, R., Overcoming the challenges in administering biopharmaceuticals: formulation and delivery strategies. *Nat Rev Drug Discov*. 2014, *13* (9): p. 655-72.
63. Awwad, S. and Angkawinitwong, U., Overview of Antibody Drug Delivery. *Pharmaceutics*. 2018, *10* (3): p. 1-24.
64. Nam, J. L., Ramiro, S., Gaujoux-Viala, C.*, et al.*, Efficacy of biological disease-modifying antirheumatic drugs: a systematic literature review informing the 2013 update of the EULAR recommendations for the management of rheumatoid arthritis. *Ann Rheum Dis*. 2014, *73* (3): p. 516-28.
65. Lim, H. and Lee, S. H., Structural Biology of the TNFalpha Antagonists Used in the Treatment of Rheumatoid Arthritis. *Int J Mol Sci*. 2018, *19* (3): p. 1-14.
66. Grunke, M. and Schulze-Koops, H., Successful treatment of inflammatory knee osteoarthritis with tumour necrosis factor blockade. *Ann Rheum Dis*. 2006, *65* (4): p. 555-6.
67. Chevalier, X., Ravaud, P., Maheu, E.*, et al.*, A Randomized, Multicentre, Double Blind, Placebo-Controlled Trial of Anti Tnf Alpha (Adalimumab) in Refractory Hand Osteoarthritis. The Dora Study. *Osteoarthr Cartilage*. 2013, *21*: p. S146-7.
68. Chevalier, X., Eymard, F. and Richette, P., Biologic agents in osteoarthritis: hopes and disappointments. *Nat Rev Rheumatol*. 2013, *9* (7): p. 400-10.
69. Tanaka, Y. O., A.; Kishimoto, T., Targeting of Interleukin-6 for the Treatment of Rheumatoid Arthritis: A Review and Update. *Rheumatol Curr Res*. 2013, *S4* (2): p. 1-14.
70. Kang, S. J., Tanaka, T., Narazaki, M.*, et al.*, Targeting Interleukin-6 Signaling in Clinic. *Immunity*. 2019, *50* (4): p. 1007-23.
71. Mertens, M. and Singh, J. A., Anakinra for rheumatoid arthritis: a systematic review. *J Rheumatol*. 2009, *36* (6): p. 1118-25.
72. Thompson, C., Davies, R. and Choy, E., Anti cytokine therapy in chronic inflammatory arthritis. *Cytokine*. 2016, *86*: p. 92-9.
73. Smolen, J. S., Agarwal, S. K., Ilivanova, E.*, et al.*, A randomised phase II study evaluating the efficacy and safety of subcutaneously administered ustekinumab and guselkumab in patients with active rheumatoid arthritis despite treatment with methotrexate. *Ann Rheum Dis*. 2017, *76* (5): p. 831-9.

74. Ridgley, L. A., Anderson, A. E. and Pratt, A. G., What are the dominant cytokines in early rheumatoid arthritis? *Curr Opin Rheumatol*. 2018, *30* (2): p. 207-14.
75. Genovese, M. C., Greenwald, M., Cho, C. S., *et al.*, A Phase II Randomized Study of Subcutaneous Ixekizumab, an Anti-Interleukin-17 Monoclonal Antibody, in Rheumatoid Arthritis Patients Who Were Naive to Biologic Agents or Had an Inadequate Response to Tumor Necrosis Factor Inhibitors. *Arthritis Rheumatol*. 2014, *66* (7): p. 1693-1704.
76. Blanco, F. J., Moricke, R., Dokoupilova, E., *et al.*, Secukinumab in Active Rheumatoid Arthritis: A Phase III Randomized, Double-Blind, Active Comparator- and Placebo-Controlled Study. *Arthritis Rheumatol*. 2017, *69* (6): p. 1144-53.
77. Yin, H., Kanasty, R. L., Eltoukhy, A. A., *et al.*, Non-viral vectors for gene-based therapy. *Nat Rev Genet*. 2014, *15* (8): p. 541-55.
78. Evans, C. H. and Huard, J., Gene therapy approaches to regenerating the musculoskeletal system. *Nat Rev Rheumatol*. 2015, *11* (4): p. 234-42.
79. Grol, M. W. and Lee, B. H., Gene therapy for repair and regeneration of bone and cartilage. *Curr Opin Pharmacol*. 2018, *40*: p. 59-66.
80. Kim, M. K., Ha, C. W., In, Y., *et al.*, A Multicenter, Double-Blind, Phase III Clinical Trial to Evaluate the Efficacy and Safety of a Cell and Gene Therapy in Knee Osteoarthritis Patients. *Hum Gene Ther Clin Dev*. 2018, *29* (1): p. 48-59.
81. Cho, J. J., Kim, T. W., Park, Y. M., *et al.*, Tissuegene-C (Invossatm) in Patients with Osteoarthritis: A Phase Ii Trials. *Cytotherapy*. 2015, *17* (6): p. S84.
82. Rodriguez-Merchan, E. C. and Valentino, L. A., The Role of Gene Therapy in Cartilage Repair. *Arch Bone Jt Surg*. 2019, *7* (2): p. 79-90.
83. Strebhardt, K. and Ullrich, A., Paul Ehrlich's magic bullet concept: 100 years of progress. *Nat Rev Cancer*. 2008, *8* (6): p. 473-80.
84. Buzea, C., Pacheco, I. I. and Robbie, K., Nanomaterials and nanoparticles: Sources and toxicity. *Biointerphases*. 2007, *2* (4): p. MR17-71.
85. Whatmore, R. W., Nanotechnology - what is it? Should we be worried? *Occup Med-Oxford*. 2006, *56* (5): p. 295-9.
86. Filipponi, L. and Sutherland, D., EUR 24957 NANOTECHNOLOGIES: Principles, Applications, Implications and Hands-on Activities. A compendium for educators, ed. European Commission, D.-G.f.R.a.I.I.t.N.p. 2013: Luxembourg: Publications Office of the European Union.
87. Bawa, R., Bawa, S. R., Maebius, S. B., *et al.*, Protecting new ideas and inventions in nanomedicine with patents. *Nanomedicine: NBM*. 2005, *1* (2): p. 150-8.
88. Lövestam, G., Rauscher, H., Roebben, G., *et al.*, Considerations on a Definition of Nanomaterial for Regulatory Purposes. 2010: Luxembourg: Publications Office of the European Union.
89. Lima, A. C., Ferreira, H., Reis, R. L., *et al.*, Biodegradable polymers: an update on drug delivery in bone and cartilage diseases. *Expert Opin Drug Deliv*. 2019, *16* (8): p. 795-813.
90. Qureshi, Z. P., Seoane-Vazquez, E., Rodriguez-Monguio, R., *et al.*, Market withdrawal of new molecular entities approved in the United States from 1980 to 2009. *Pharmacoepidemiol Drug Saf*. 2011, *20*: p. 772-7.
91. Kaitin, K. I. and DiMasi, J. A., Pharmaceutical Innovation in the 21st Century: New Drug Approvals in the First Decade, 2000–2009. *Clin Pharmacol Ther*. 2011, *89* (2): p. 183-88.
92. Vieira, S., Vial, S., Reis, R. L., *et al.*, Nanoparticles for Bone Tissue Engineering. *Biotechnol Progr*. 2017, *33* (3): p. 590-611.
93. Silva, R., Ferreira, H. and Cavaco-Paulo, A., Sonoproduction of liposomes and protein particles as templates for delivery purposes. *Biomacromolecules*. 2011, *12*: p. 3353-68.

94. Liechty, W. B., Kryscio, D. R., Slaughter, B. V., *et al.*, Polymers for Drug Delivery Systems. *Annu Rev Chem Biomol Eng*. 2010, *1* (1): p. 149-73.
95. Kost, J. and Langer, R., Responsive polymeric delivery systems. *Adv Drug Deliver Rev*. 2012, *64*: p. 327-41.
96. Martins, A., Ferreira, H., Reis, R. L., *et al.*, *Delivery Systems Made of Natural-Origin Polymers for Tissue Engineering and Regenerative Medicine Applications*, in *Biomaterials from Nature for Advanced Devices and Therapies*. 2016.
97. Carvalho, A. M., Teixeira, R., Novoa-Carballal, R., *et al.*, Redox-Responsive Micellar Nanoparticles from Glycosaminoglycans for CD44 Targeted Drug Delivery. *Biomacromolecules*. 2018, *19* (7): p. 2991-9.
98. Torchilin, V. P., Drug targeting. *Eur J Pharm Sci*. 2000, *11*: p. S81-91.
99. Cartaxo, A. L., Costa-Pinto, A. R., Martins, A., *et al.*, Influence of PDLA nanoparticles size on drug release and interaction with cells. *J Biomed Mater Res A*. 2019, *107* (3): p. 482-93.
100. Evans, C. H., Kraus, V. B. and Setton, L. A., Progress in intra-articular therapy. *Nat Rev Rheumatol*. 2014, *10* (1): p. 11-22.
101. Giannoni, P. and Narcisi, R., Nano-approaches in cartilage repair. *J Appl Biomater Biom*. 2009, *7* (1): p. 1-12.
102. Ng, L., Grodzinsky, A. J., Patwari, P., *et al.*, Individual cartilage aggrecan macromolecules and their constituent glycosaminoglycans visualized via atomic force microscopy. *J Struct Biol*. 2003, *143* (3): p. 242-57.
103. Bajpayee, A. G., Wong, C. R., Bawendi, M. G., *et al.*, Avidin as a model for charge driven transport into cartilage and drug delivery for treating early stage post-traumatic osteoarthritis. *Biomaterials*. 2014, *35* (1): p. 538-49.
104. Elsaid, K. A., Ferreira, L., Truong, T., *et al.*, Pharmaceutical nanocarrier association with chondrocytes and cartilage explants: influence of surface modification and extracellular matrix depletion. *Osteoarthr Cartilage*. 2013, *21* (2): p. 377-84.
105. Rothenfluh, D. A., Bermudez, H., O'Neil, C. P., *et al.*, Biofunctional polymer nanoparticles for intra-articular targeting and retention in cartilage. *Nat Mater*. 2008, *7*: p. 248-55.
106. Torchilin, V. P., Tat peptide-mediated intracellular delivery of pharmaceutical nanocarriers. *Adv Drug Deliver Rev*. 2008, *60* (4-5): p. 548-58.
107. Cheung, C. S., Lui, J. C. and Baron, J., Identification of chondrocyte-binding peptides by phage display. *J Orthop Res*. 2013, *31* (7): p. 1053-8.
108. Loffredo, F. S., Pancoast, J. R., Cai, L., *et al.*, Targeted Delivery to Cartilage Is Critical for In Vivo Efficacy of Insulin-like Growth Factor 1 in a Rat Model of Osteoarthritis. *Arthritis Rheumatol*. 2014, *66* (5): p. 1247-55.
109. Chen, M., Daddy, J. C. K., Xiao, Y., *et al.*, Advanced nanomedicine for rheumatoid arthritis treatment: focus on active targeting. *Expert Opin Drug Deliv*. 2017, *14* (10): p. 1141-4.
110. Yuan, F. L., Li, X., Lu, W. G., *et al.*, Epidermal growth factor receptor (EGFR) as a therapeutic target in rheumatoid arthritis. *Clin Rheumatol*. 2013, *32* (3): p. 289-92.
111. Leblond, A., Allanore, Y. and Avouac, J., Targeting synovial neoangiogenesis in rheumatoid arthritis. *Autoimmun Rev*. 2017, *16* (6): p. 594-601.
112. Varghese, B., Vlashi, E., Xia, W., *et al.*, Folate receptor-beta in activated macrophages: ligand binding and receptor recycling kinetics. *Mol Pharm*. 2014, *11* (10): p. 3609-16.
113. Varki, A., Sialic acids as ligands in recognition phenomena. *Faseb J*. 1997, *11* (4): p. 248-255.
114. Krieger, M. and Herz, J., Structures and Functions of Multiligand Lipoprotein Receptors - Macrophage Scavenger Receptors and Ldl Receptor-Related Protein (Lrp). *Annu Rev Biochem*. 1994, *63*: p. 601-37.

115. Misra, S., Hascall, V. C., Markwald, R. R., *et al.*, Interactions between hyaluronan and its receptors (CD44, RHAMM) regulate the activities of inflammation and cancer. *Front Immunol*. 2015, *6*: p. 1-31.
116. Graversen, J. H., Svendsen, P., Dagnaes-Hansen, F., *et al.*, Targeting the Hemoglobin Scavenger receptor CD163 in Macrophages Highly Increases the Anti-inflammatory Potency of Dexamethasone. *Mol Ther*. 2012, *20* (8): p. 1550-8.
117. Kamperidis, P., Kamalati, T., Ferrari, M., *et al.*, Development of a novel recombinant biotherapeutic with applications in targeted therapy of human arthritis. *Arthritis Rheum*. 2011, *63* (12): p. 3758-67.
118. Sullivan, T., Benjamin, C. G., Kempf, P. W., *et al.*, Cetuximab in the treatment of rheumatoid arthritis. *J Clin Rheumatol*. 2010, *16* (1): p. 32-3.
119. Kok, R. J., Schraa, A. J., Bos, E. J., *et al.*, Preparation and functional evaluation of RGD-modified proteins as alpha(v)beta(3) integrin directed therapeutics. *Bioconjugate Chem*. 2002, *13* (1): p. 128-35.
120. Delgado, M., Abad, C., Martinez, C., *et al.*, Vasoactive intestinal peptide in the immune system: potential therapeutic role in inflammatory and autoimmune diseases. *J Mol Med (Berl)*. 2002, *80* (1): p. 16-24.
121. Barshavit, Z., Goldman, R., Stabinsky, Y., *et al.*, Tuftsin-Macrophage Interaction - Specific Binding and Augmentation of Phagocytosis. *J Cell Physiol*. 1979, *100* (1): p. 55-62.
122. Mi, Z., Lu, X., Mai, J. C., *et al.*, Identification of a synovial fibroblast-specific protein transduction domain for delivery of apoptotic agents to hyperplastic synovium. *Mol Ther*. 2003, *8* (2): p. 295-305.
123. Li, Z., Zhao, R., Wu, X., *et al.*, Identification and characterization of a novel peptide ligand of epidermal growth factor receptor for targeted delivery of therapeutics. *Faseb j*. 2005, *19* (14): p. 1978-85.
124. Yang, Y. H., Rajaiah, R., Ruoslahti, E., *et al.*, Peptides targeting inflamed synovial vasculature attenuate autoimmune arthritis. *Proc Natl Acad Sci U S A*. 2011, *108* (31): p. 12857-62.
125. Akbarzadeh, A., Rezaei-Sadabady, R., Davaran, S., *et al.*, Liposome: classification, preparation, and applications. *Nanoscale Res Lett*. 2013, *8* (1): p. 102-9.
126. Bangham, A. D. and Horne, R. W., Negative Staining of Phospholipids + Their Structural Modification by-Surface Active Agents as Observed in Electron Microscope. *J Mol Biol*. 1964, *8* (5): p. 660-4.
127. Monteiro, N., Martins, A., Pires, R. A., *et al.*, Dual release of a hydrophilic and a hydrophobic osteogenic factor from a single liposome. *Rsc Adv*. 2016, *6* (115): p. 114599-612.
128. Monteiro, N., Martins, A., Reis, R. L., *et al.*, Liposomes in tissue engineering and regenerative medicine. *J R Soc Interface*. 2014, *11* (101): p. 1-24.
129. Bulbake, U., Doppalapudi, S., Kommineni, N., *et al.*, Liposomal Formulations in Clinical Use: An Updated Review. *Pharmaceutics*. 2017, *9* (2): p. 1-33.
130. Jia, M. D., Deng, C. F., Luo, J. W., *et al.*, A novel dexamethasone-loaded liposome alleviates rheumatoid arthritis in rats. *Int J Pharmaceut*. 2018, *540* (1-2): p. 57-64.
131. Metselaar, J. M., Wauben, M. H. M., Wagenaar-Hilbers, J. P. A., *et al.*, Complete remission of experimental arthritis by joint targeting of glucocorticoids with long-circulating liposomes. *Arthritis Rheum-Us*. 2003, *48* (7): p. 2059-66.
132. Metselaar, J. M., van den Berg, W. B., Holthuysen, A. E. M., *et al.*, Liposomal targeting of glucocorticoids to synovial lining cells strongly increases therapeutic benefit in collagen type II arthritis. *Ann Rheum Dis*. 2004, *63* (4): p. 348-53.

133. Srinath, P., Vyas, S. P. and Diwan, P. V., Preparation and pharmacodynamic evaluation of liposomes of indomethacin. *Drug Dev Ind Pharm*. 2000, *26* (3): p. 313-21.
134. Williams, A., Goodfellow, R., Topley, N., *et al.*, The suppression of rat collagen-induced arthritis and inhibition of macrophage derived mediator release by liposomal methotrexate formulations. *Inflamm Res*. 2000, *49* (4): p. 155-61.
135. Williams, A. S., Topley, N., Dojcinov, S., *et al.*, Amelioration of rat antigen-induced arthritis by liposomally conjugated methotrexate is accompanied by down-regulation of cytokine mRNA expression. *Rheumatology*. 2001, *40* (4): p. 375-83.
136. Gottschalk, O., Metz, P., Trong, M. L. D., *et al.*, Therapeutic effect of methotrexate encapsulated in cationic liposomes (EndoMTX) in comparison to free methotrexate in an antigen-induced arthritis study in vivo. *Scand J Rheumatol*. 2015, *44* (6): p. 456-63.
137. Poh, S., Chelvam, V., Kelderhouse, L. E., *et al.*, Folate-conjugated liposomes target and deliver therapeutics to immune cells in a rat model of rheumatoid arthritis. *Nanomedicine*. 2017, *12* (20): p. 2441-51.
138. Koning, G. A., Schiffelers, R. M., Wauben, M. H. M., *et al.*, Targeting of angiogenic endothelial cells at sites of inflammation by dexamethasone phosphate-containing RGD peptide liposomes inhibits experimental arthritis. *Arthritis Rheum-Us*. 2006, *54* (4): p. 1198-1208.
139. Vanniasinghe, A. S., Manolios, N., Schibeci, S., *et al.*, Targeting fibroblast-like synovial cells at sites of inflammation with peptide targeted liposomes results in inhibition of experimental arthritis. *Clin Immunol*. 2014, *151* (1): p. 43-54.
140. Meka, R. R., Venkatesha, S. H. and Moudgil, K. D., Peptide-directed liposomal delivery improves the therapeutic index of an immunomodulatory cytokine in controlling autoimmune arthritis. *J Control Release*. 2018, *286*: p. 279-88.
141. Meka, R. R., Venkatesha, S. H., Acharya, B., *et al.*, Peptide-targeted liposomal delivery of dexamethasone for arthritis therapy. *Nanomedicine-Uk*. 2019, *14* (11): p. 1455-69.
142. Khoury, M., Escriou, V., Courties, G., *et al.*, Efficient suppression of murine arthritis by combined anticytokine small interfering RNA lipoplexes. *Arthritis Rheum-Us*. 2008, *58* (8): p. 2356-67.
143. Wang, S., Wei, X., Sun, X., *et al.*, A novel therapeutic strategy for cartilage diseases based on lipid nanoparticle-RNAi delivery system. *Int J Nanomedicine*. 2018, *13*: p. 617-31.
144. Banik, B. L., Fattahi, P. and Brown, J. L., Polymeric nanoparticles: the future of nanomedicine. *Wires Nanomed Nanobi*. 2016, *8* (2): p. 271-99.
145. Assali, M., Shawahna, R., Dayyeh, S., *et al.*, Dexamethasone-diclofenac loaded polylactide nanoparticles: Preparation, release and anti-inflammatory activity. *Eur J Pharm Sci*. 2018, *122*: p. 179-84.
146. Chiesa, E., Pisani, S., Colzani, B., *et al.*, Intra-Articular Formulation of GE11-PLGA Conjugate-Based NPs for Dexamethasone Selective Targeting-In Vitro Evaluation. *Int J Mol Sci*. 2018, *19* (8): p. 1-22.
147. Colzani, B., Speranza, G., Dorati, R., *et al.*, Design of smart GE11-PLGA/PEG-PLGA blend nanoparticulate platforms for parenteral administration of hydrophilic macromolecular drugs: synthesis, preparation and in vitro/ex vivo characterization. *Int J Pharm*. 2016, *511* (2): p. 1112-23.
148. Higaki, M., Ishihara, T., Izumo, N., *et al.*, Treatment of experimental arthritis with poly(D, L-lactic/glycolic acid) nanoparticles encapsulating betamethasone sodium phosphate. *Ann Rheum Dis*. 2005, *64* (8): p. 1132-36.
149. Ishihara, T., Kubota, T., Choi, T., *et al.*, Treatment of Experimental Arthritis with Stealth-Type Polymeric Nanoparticles Encapsulating Betamethasone Phosphate. *J Pharmacol Exp Ther*. 2009, *329* (2): p. 412-17.

150. Lee, S. J., Lee, A., Hwang, S. R., *et al.*, TNF-alpha Gene Silencing Using Polymerized siRNA/Thiolated Glycol Chitosan Nanoparticles for Rheumatoid Arthritis. *Mol Ther*. **2014**, *22* (2): p. 397-408.
151. Kim, M. J., Park, J. S., Lee, S. J., *et al.*, Notch1 targeting siRNA delivery nanoparticles for rheumatoid arthritis therapy. *J Control Release*. **2015**, *216*: p. 140-148.
152. Shi, Q., Rondon-Cavanzo, E. P., Dalla Picola, I. P., *et al.*, In vivo therapeutic efficacy of TNFalpha silencing by folate-PEG-chitosan-DEAE/siRNA nanoparticles in arthritic mice. *Int J Nanomedicine*. **2018**, *13*: p. 387-402.
153. Deng, R. H., Qiu, B. and Zhou, P. H., Chitosan/hyaluronic acid/plasmid-DNA nanoparticles encoding interleukin-1 receptor antagonist attenuate inflammation in synoviocytes induced by interleukin-1 beta. *J Mater Sci Mater Med*. **2018**, *29* (10): p. 155-68.
154. Kim, Y. J., Chae, S. Y., Jin, C. H., *et al.*, Ionic complex systems based on hyaluronic acid and PEGylated TNF-related apoptosis-inducing ligand for treatment of rheumatoid arthritis. *Biomaterials*. **2010**, *31* (34): p. 9057-64.
155. Jain, S., Tran, T. H. and Amiji, M., Macrophage repolarization with targeted alginate nanoparticles containing IL-10 plasmid DNA for the treatment of experimental arthritis. *Biomaterials*. **2015**, *61*: p. 162-77.
156. Zheng, Y., Xiao, L., Yu, C., *et al.*, Enhanced Antiarthritic Efficacy by Nanoparticles of (-)-Epigallocatechin Gallate-Glucosamine-Casein. *J Agric Food Chem*. **2019**, *67* (23): p. 6476-86.
157. Deshmukh, A. S., Chauhan, P. N., Noolvi, M. N., *et al.*, Polymeric micelles: Basic research to clinical practice. *Int J Pharmaceut*. **2017**, *532* (1): p. 249-68.
158. McBain, J. W., Mobility of highly charged micelles. *Trans. Faraday Soc*. **1913**, *9*: p. 99.
159. Wang, Q., Li, Y., Chen, X. Y., *et al.*, Optimized in vivo performance of acid-liable micelles for the treatment of rheumatoid arthritis by one single injection. *Nano Res*. **2019**, *12* (2): p. 421-28.
160. Zhang, N., Xu, C. Y., Li, N., *et al.*, Folate receptor-targeted mixed polysialic acid micelles for combating rheumatoid arthritis: in vitro and in vivo evaluation. *Drug Deliv*. **2018**, *25* (1): p. 1182-91.
161. Yang, M. D., Ding, J. X., Feng, X. R., *et al.*, Scavenger Receptor-Mediated Targeted Treatment of Collagen-Induced Arthritis by Dextran Sulfate-Methotrexate Prodrug. *Theranostics*. **2017**, *7* (1): p. 97-105.
162. Yang, M. D., Ding, J. X., Zhang, Y., *et al.*, Activated macrophage-targeted dextran-methotrexate/folate conjugate prevents deterioration of collagen-induced arthritis in mice. *J Mater Chem B*. **2016**, *4* (12): p. 2102-13.
163. Xu, X. L., Li, W. S., Wang, X. J., *et al.*, Endogenous sialic acid-engineered micelles: a multifunctional platform for on-demand methotrexate delivery and bone repair of rheumatoid arthritis. *Nanoscale*. **2018**, *10* (6): p. 2923-35.
164. Liang, H., Peng, B., Dong, C., *et al.*, Cationic nanoparticle as an inhibitor of cell-free DNA-induced inflammation. *Nat Commun*. **2018**, *9* (1): p. 4291-99.
165. Fan, Z., Li, J., Liu, J., *et al.*, Anti-Inflammation and Joint Lubrication Dual Effects of a Novel Hyaluronic Acid/Curcumin Nanomicelle Improve the Efficacy of Rheumatoid Arthritis Therapy. *ACS Appl Mater Interfaces*. **2018**, *10* (28): p. 23595-604.
166. Sherje, A. P., Jadhav, M., Dravyakar, B. R., *et al.*, Dendrimers: A versatile nanocarrier for drug delivery and targeting. *Int J Pharmaceut*. **2018**, *548* (1): p. 707-20.
167. Buhleier, E., Wehner, W. and Vogtle, F., Cascade-Chain-Like and Nonskid-Chain-Like Syntheses of Molecular Cavity Topologies. *Synthesis-Stuttgart*. **1978**, (2): p. 155-8.
168. Qi, R., Majoros, I., Misra, A. C., *et al.*, Folate Receptor-Targeted Dendrimer-Methotrexate Conjugate for Inflammatory Arthritis. *J Biomed Nanotechnol*. **2015**, *11* (8): p. 1431-41.

169. Geiger, B. C., Wang, S., Padera, R. F., Jr., *et al.*, Cartilage-penetrating nanocarriers improve delivery and efficacy of growth factor treatment of osteoarthritis. *Sci Transl Med*. 2018, *10* (469): p. 1-10.
170. Pandey, P. K., Maheshwari, R., Raval, N., *et al.*, Nanogold-core multifunctional dendrimer for pulsatile chemo-, photothermal- and photodynamic- therapy of rheumatoid arthritis. *J Colloid Interface Sci*. 2019, *544*: p. 61-77.
171. Peng, B., Liang, H., Li, Y., *et al.*, Tuned Cationic Dendronized Polymer: Molecular Scavenger for Rheumatoid Arthritis Treatment. *Angew Chem Int Ed Engl*. 2019, *58* (13): p. 4254-58.
172. Vial, S., Reis, R. L. and Oliveira, J. M., Recent advances using gold nanoparticles as a promising multimodal tool for tissue engineering and regenerative medicine. *Curr Opin Solid St M*. 2017, *21* (2): p. 92-112.
173. Ferreira, H., Martins, A., da Silva, M. L. A., *et al.*, The functionalization of natural polymer-coated gold nanoparticles to carry bFGF to promote tissue regeneration. *J Mater Chem B*. 2018, *6* (14): p. 2104-15.
174. Lee, H., Lee, M. Y., Bhang, S. H., *et al.*, Hyaluronate-Gold Nanoparticle/Tocilizumab Complex for the Treatment of Rheumatoid Arthritis. *Acs Nano*. 2014, *8* (5): p. 4790-8.
175. Kim, J. and Kim, H. Y., Synergistic Oxygen Generation and Reactive Oxygen Species Scavenging by Manganese Ferrite/Ceria Co-decorated Nanoparticles for Rheumatoid Arthritis Treatment. *ACS Nano*. 2019, *13* (3): p. 3206-17.
176. Dai, F. Y., Du, M. H., Liu, Y. G., *et al.*, Folic acid-conjugated glucose and dextran coated iron oxide nanoparticles as MRI contrast agents for diagnosis and treatment response of rheumatoid arthritis. *J Mater Chem B*. 2014, *2* (16): p. 2240-7.
177. Behzadi, S., Serpooshan, V., Tao, W., *et al.*, Cellular uptake of nanoparticles: journey inside the cell. *Chem Soc Rev*. 2017, *46* (14): p. 4218-44.
178. Foroozandeh, P. and Aziz, A. A., Insight into Cellular Uptake and Intracellular Trafficking of Nanoparticles. *Nanoscale Res Lett*. 2018, *13*: p. 1-12.
179. Albanese, A., Tang, P. S. and Chan, W. C. W., The Effect of Nanoparticle Size, Shape, and Surface Chemistry on Biological Systems. *Annu Rev Biomed Eng*. 2012, *14*: p. 1-16.
180. Yameen, B., Choi, W. I., Vilos, C., *et al.*, Insight into nanoparticle cellular uptake and intracellular targeting. *J Control Release*. 2014, *190*: p. 485-99.
181. Pryor, P. R., Analyzing Lysosomes in Live Cells. *Method Enzymol*. 2012, *505*: p. 145-57.
182. Murugan, K., Choonara, Y. E., Kumar, P., *et al.*, Parameters and characteristics governing cellular internalization and trans-barrier trafficking of nanostructures. *Int J Nanomedicine*. 2015, *10*: p. 2191-206.
183. Swanson, J. A., Shaping cups into phagosomes and macropinosomes. *Nat Rev Mol Cell Bio*. 2008, *9* (8): p. 639-49.
184. Pauwels, A. M., Trost, M., Beyaert, R., *et al.*, Patterns, Receptors, and Signals: Regulation of Phagosome Maturation. *Trends Immunol*. 2017, *38* (6): p. 407-22.
185. Kaksonen, M. and Roux, A., Mechanisms of clathrin-mediated endocytosis. *Nat Rev Mol Cell Bio*. 2018, *19* (5): p. 313-26.
186. Ferguson, J. P., Huber, S. D., Willy, N. M., *et al.*, Mechanoregulation of clathrin-mediated endocytosis. *J Cell Sci*. 2017, *130* (21): p. 3631-6.
187. Parton, R. G. and Simons, K., The multiple faces of caveolae. *Nat Rev Mol Cell Bio*. 2007, *8* (3): p. 185-94.
188. Sandvig, K., Pust, S., Skotland, T., *et al.*, Clathrin-independent endocytosis: mechanisms and function. *Curr Opin Cell Biol*. 2011, *23* (4): p. 413-20.

189. Grant, B. D. and Donaldson, J. G., Pathways and mechanisms of endocytic recycling. *Nat Rev Mol Cell Bio*. 2009, *10* (9): p. 597-608.
190. Lim, J. P. and Gleeson, P. A., Macropinocytosis: an endocytic pathway for internalising large gulps. *Immunol Cell Biol*. 2011, *89* (8): p. 836-43.
191. Li, Z. H., Zhang, Y. H., Zhu, D. H., *et al.*, Transporting carriers for intracellular targeting delivery via non-endocytic uptake pathways. *Drug Deliv*. 2017, *24* (2): p. 45-55.
192. Yang, J., Bahreman, A., Daudey, G., *et al.*, Drug Delivery via Cell Membrane Fusion Using Lipopeptide Modified Liposomes. *Acs Central Sci*. 2016, *2* (9): p. 621-30.
193. Zhu, M. T., Nie, G. J., Meng, H., *et al.*, Physicochemical Properties Determine Nanomaterial Cellular Uptake, Transport, and Fate. *Accounts Chem Res*. 2013, *46* (3): p. 622-31.
194. Chithrani, B. D. and Chan, W. C. W., Elucidating the mechanism of cellular uptake and removal of protein-coated gold nanoparticles of different sizes and shapes. *Nano Lett*. 2007, *7* (6): p. 1542-50.
195. Rejman, J., Oberle, V., Zuhorn, I. S., *et al.*, Size-dependent internalization of particles via the pathways of clathrin- and caveolae-mediated endocytosis. *The Biochemical journal*. 2004, *377* (1): p. 159-69.
196. Gratton, S. E., Ropp, P. A., Pohlhaus, P. D., *et al.*, The effect of particle design on cellular internalization pathways. *Proc Natl Acad Sci U S A*. 2008, *105* (33): p. 11613-8.
197. Walkey, C. D., Olsen, J. B., Guo, H., *et al.*, Nanoparticle size and surface chemistry determine serum protein adsorption and macrophage uptake. *J Am Chem Soc*. 2012, *134* (4): p. 2139-47.
198. Chithrani, B. D., Ghazani, A. A. and Chan, W. C. W., Determining the size and shape dependence of gold nanoparticle uptake into mammalian cells. *Nano Lett*. 2006, *6* (4): p. 662-8.
199. Banerjee, A., Qi, J. P., Gogoi, R., *et al.*, Role of nanoparticle size, shape and surface chemistry in oral drug delivery. *J Control Release*. 2016, *238*: p. 176-85.
200. Muthu, M. S. and Singh, S., Studies on biodegradable polymeric nanoparticles of risperidone: in vitro and in vivo evaluation. *Nanomedicine-Uk*. 2008, *3* (3): p. 305-19.
201. Marano, F., Hussain, S., Rodrigues-Lima, F., *et al.*, Nanoparticles: molecular targets and cell signalling. *Arch Toxicol*. 2011, *85* (7): p. 733-41.
202. Harush-Frenkel, O., Rozentur, E., Benita, S., *et al.*, Surface charge of nanoparticles determines their endocytic and transcytotic pathway in polarized MDCK cells. *Biomacromolecules*. 2008, *9* (2): p. 435-43.
203. Dausend, J., Musyanovych, A., Dass, M., *et al.*, Uptake Mechanism of Oppositely Charged Fluorescent Nanoparticles in HeLa Cells. *Macromol Biosci*. 2008, *8* (12): p. 1135-43.
204. Zhang, L. W. and Monteiro-Riviere, N. A., Mechanisms of Quantum Dot Nanoparticle Cellular Uptake. *Toxicol Sci*. 2009, *110* (1): p. 138-55.
205. Desai, D., Akerfelt, M., Prabhakar, N., *et al.*, Factors Affecting Intracellular Delivery and Release of Hydrophilic Versus Hydrophobic Cargo from Mesoporous Silica Nanoparticles on 2D and 3D Cell Cultures. *Pharmaceutics*. 2018, *10* (4): p. 1-18.
206. Chompoosor, A., Saha, K., Ghosh, P. S., *et al.*, The Role of Surface Functionality on Acute Cytotoxicity, ROS Generation and DNA Damage by Cationic Gold Nanoparticles. *Small*. 2010, *6* (20): p. 2246-9.
207. Jiang, X. E., Dausend, J., Hafner, M., *et al.*, Specific Effects of Surface Amines on Polystyrene Nanoparticles in their Interactions with Mesenchymal Stem Cells. *Biomacromolecules*. 2010, *11* (3): p. 748-53.
208. Patel, L. N., Zaro, J. L. and Shen, W. C., Cell penetrating peptides: Intracellular pathways and pharmaceutical perspectives. *Pharm Res*. 2007, *24* (11): p. 1977-92.

209. Burch, E. E., Patil, V. R. S., Camphausen, R. T.*, et al.*, The N-terminal peptide of PSGL-1 can mediate adhesion to trauma-activated endothelium via P-selectin in vivo*. Blood*. 2002, *100* (2): p. 531-8.
210. Fujimoto, T., Kogo, H., Nomura, R.*, et al.*, Isoforms of caveolin-1 and caveolar structure*. J Cell Sci*. 2000, *113* (19): p. 3509-17.
211. Murray, P. J. and Wynn, T. A., Protective and pathogenic functions of macrophage subsets*. Nat Rev Immunol*. 2011, *11* (11): p. 723-37.
212. MacParland, S. A., Tsoi, K. M., Ouyang, B.*, et al.*, Phenotype Determines Nanoparticle Uptake by Human Macrophages from Liver and Blood*. ACS nano*. 2017, *11* (3): p. 2428-43.
213. Qie, Y., Yuan, H., von Roemeling, C. A.*, et al.*, Surface modification of nanoparticles enables selective evasion of phagocytic clearance by distinct macrophage phenotypes*. Sci Rep*. 2016, *6*: p. 1-10.
214. Sahay, G., Kim, J. O., Kabanov, A. V.*, et al.*, The exploitation of differential endocytic pathways in normal and tumor cells in the selective targeting of nanoparticulate chemotherapeutic agents*. Biomaterials*. 2010, *31* (5): p. 923-33.
215. Carvalho, M. R., Maia, F. R., Silva-Correia, J.*, et al.*, A semiautomated microfluidic platform for real-time investigation of nanoparticles' cellular uptake and cancer cells' tracking*. Nanomedicine-Uk*. 2017, *12* (6): p. 581-96.

SECTION 2

EXPERIMENTAL SECTION

Chapter II

Materials and Methods

Chapter II

Materials and Methods

OVERVIEW

This chapter aims to provide a detailed overview on the experimental procedures behind the results presented in the following sections of this thesis. In addition, aspects concerning the selection of the materials, production and characterization of nanoparticles (NPs), the biological performance of the cells when exposed to them and the *in vivo* assays will be explained in detail and in a comprehensive manner.

II-1. MATERIALS

The various biomaterials used in this thesis are presented in the following sub-sections, detailing its main properties and methods of production used.

II-1.1. Chitosan

Chitosan (Ch) is obtained usually by the alkaline deacetylation of chitin [1]. Chitin is a naturally occurring mucopolysaccharide present in the exoskeleton of invertebrates such as crustaceans (crabs, shrimp, etc), insects and fungal and algae cell walls [2]. After cellulose, it is one of the most abundant polysaccharides on earth [3]. Ch is also known as poly-(β-1/4)-2-amino-2-deoxy-D-glucopyranose, it is a linear polysaccharide composed of randomly distributed D-glucosamine (deacetylated unit) and N-acetyl-D-glucosamine (acetylated unit), which are linked with β (1–4) bonds (**Figure II-1**). The chemical structure of this hydrophilic polycationic copolymer offer many interesting properties to be used in the biomedical field. Besides its non-toxicity and reported biocompatibility [4], several beneficial pharmacological properties include anti-ulcer and anti-acid [5], hemostatic [6], wound-healing [7], bacteriostatic [8], fungistatic [9] and anti-tumor [10, 11]. Recently, it has also been exploited in the pharmaceutical industry for drug delivery and tissue engineering applications [12, 13]. Several formulations are in development, such as nanoparticles (NPs) [14], microparticles/microcapsules [15], hydrogels [16], scaffolds [17], beads [18], films [19] and fibers [20]. Ch has been widely applied in nanotechnology, due to the following properties: *(i)* biocompatibility and biodegradability, *(ii)* non-toxicity, *(iii)* amine functional groups enables the functionalization and modification with other polymers, cross-linkers or biomolecules, *(iv)* potential for sustained and controlled release, *(v)* potential for targeted delivery to a specific organ or cells (e.g. mucoadhesive features), and *(vi)* Food and Drug Administration (FDA) approval for wound dressings and dietetic applications [21].

Ch degradation, degree of crystallinity, mechanical properties and cellular adhesion deeply depends on its molecular weight (MW) and its degree of deacetylation (DD) [1]. DD of chitosan refers to the ratio between the deacetylated and acetylated units. Consequently, those properties strongly affect the aqueous solubility, hydrophobicity, drug encapsulation efficiency as well as its interactions with cells. Moreover, while some studies reported the use of Ch as vaccine adjuvant [22], the capacity to promote cellular immunity is also related with the DD of the polymer [23]. Indeed, the DD and immunogenicity are inversely correlated in this biomaterial.

The Ch used in the experimental work of this thesis had a high DD of 95% to avoid immunogenicity, and a low MW of 150 kDa, to enable the production of the polymeric NPs presented in the **Chapters III, VI and VII**. It was purchased from Heppe Medical Chitosan GmbH (Germany), being a highly purified powder.

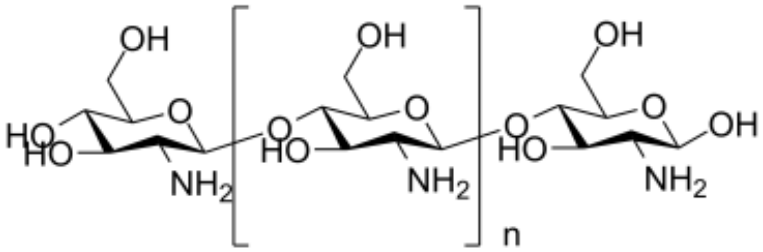

Figure II-1 – Chemical structure of chitosan (Ch).

II-1.2. Hyaluronic acid

Hyaluronic acid (also designated as hyaluronan, sodium hyaluronate or HA) is a glycosaminoglycan that is found in the extracellular matrix (ECM) of human and animal tissues, especially in the aqueous humor of the eye, synovial fluid, skin and umbilical cord [24]. It is a linear and anionic polymer composed of D-glucuronic acid and N-acetyl-D-glucosamine, linked via alternating β (1–4) and β (1–3) glycosidic bonds (**Figure II-2**) [25]. It is naturally synthesized by hyaluronan synthases and degraded by hyaluronidases. HA is responsible for many biological functions including maintenance of the elastoviscosity of liquid connective tissues, regulation of water transport and tissue hydration, supramolecular assembly of proteoglycans in the ECM, and several receptor-mediated roles in cell detachment, migration, mitosis, tumor development and metastasis, and inflammation. Yet, HA physicochemical and biological properties depend on its MW [26]. While high MW HA has been associated with anti-inflammatory, anti-angiogenic and immunosuppressive functions, low MW HA is a potent pro-inflammatory molecule, involved in different pathophysiogical processes, such as angiogenesis, wound healing and cancer.

Its unique viscoelastic nature, biocompatibility, bioactive properties and non-immunogenicity has led the use of HA in several clinical applications, including the supplementation of synovial fluid in arthritis (also known as viscosupplementation), surgical aid in eye surgery, wound healing and cosmetic

applications [27]. Recently, it has also been exploited for drug delivery and tissue engineering applications [28, 29]. As previously reported, HA with MW of 700–6000 kDa is the most adequate for cartilage repair, avoiding the inflammatory properties of low MW HA [30]. In this thesis, pharmaceutical grade HA with a MW of 750 kDa was used to enable the production of the polymeric NPs in the **Chapters III, VI and VII**, and it was acquired from Lifecore Biomedical (USA).

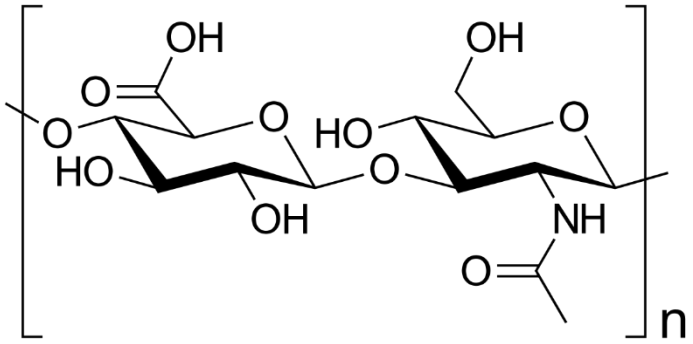

Figure II-2 – Chemical structure of Hyaluronic Acid (HA).

II-1.3. Lipids

Lipids are hydrophobic or amphipathic small molecules with a vital role in many biological functions as they are responsible for stabilizing the cell membranes, storing energy and participating in signaling pathways [31]. They are defined as a group of organic compounds that are insoluble in water but soluble in organic solvents [32]. As these chemical features include a wide range of molecules, such as fatty acids, phospholipids, sterols, sphingolipids, terpenes and many others, they are extremely heterogeneous. Regarding the scope of this thesis, fatty acids, phospholipids and steroids will be presented and discussed in more detail.

II-1.3.1. Fatty acids

Fatty acids are carboxylic acids with a hydrophobic tail playing an important role in the cell function and metabolism [33]. Based on the number of carbons, they are termed short, medium, long or very long-chained. They can also be designated as saturated (C–C without double bonds) or unsaturated (C=C double bond), which are further named monounsaturated when they have one bond and polyunsaturated when they possess two or more double bonds.

Palmitic acid (PA) is the most common saturated fatty acid (16:0) found in animals, plants and microorganisms (**Figure II-3**) [34]. Considering the ubiquitous nature of fatty acids in living organisms, PA and other fatty acids, including stearic acid (18:0) and myristic acid (14:0), are frequently combined with other polymers, such as Ch [35, 36], polyethylene glycol (PEG) [37, 38], polycaprolactone (PCL) [39], and many others to produce core-shell type NPs and polymeric micelles.

Analytical grade PA (≥98% PA basis-GC) was acquired from Sigma-Aldrich (USA) and used for the production of the polymeric micelles in the **Chapters V and VI**.

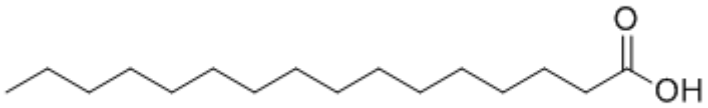

Figure II-3 – Chemical structure of palmitic acid (PA).

II-1.3.2. Phospholipids

Phospholipids are the most abundant type of lipid constituents in the cell membranes, having a key role in the structural integrity of the membrane bilayer [40]. They are composed of a glycerol ester in which two of the glyceride hydroxyl (OH) groups are linked to fatty acids whereas the other is attached to a phosphate group. The phosphate is then linked to a simple and polar organic molecule, such as ethanolamine or choline. The most common phospholipids are phosphatidylcholine, phosphatidylethanolamine, phosphatidylinositol and phosphatidylserine. Due to their excellent biocompatibility and remarkable amphiphilicity characteristics, phospholipids are being widely used in the formulation of drug delivery systems [41]. Indeed, several phospholipid-related formulations have already reached the clinic, including Doxil®, Myocet® and Cleviprex®, offering several advantages, for instance improvement of hydrophobic drugs bioavailability, uptake and release profiles, protecting the drug from degradation (e.g. in the gastrointestinal tract), and also reducing side effects [42, 43].

In this thesis, L-alfa-phosphatidylcholine from egg yolk (EPC) and 1,2-distearoyl-sn-glycero-3-phosphoethanolamineN-[maleimide(polyethyleneglycol)-2000] (ammonium salt) (DSPE-PEG-Mal) phospholipids were used to prepare the unilamellar liposomes (LUVs) in the **Chapters IV and VI**. Phosphatidylcholine, also known as lecithin, is the most abundant class of lipids in animal and plant cell

membranes [44]. It contains a positively charged choline group and negatively charged phosphate group, thus being as a zwitterionic molecule (**Figure II-4A**) [45]. DSPE-PEG-Mal is a conjugation of the lipid DSPE and the polymer PEG with an end functional group of maleimide (**Figure II-4B**). DSPE is a synthetic saturated negative charged lipid from the unsaturated phosphatidylethanolamine (PE). PEG (sub-section II-1.6) is a hydrophilic polymer that prevents protein adsorption and, consequently, increases the blood circulation half-life [46]. Maleimide functional group can react with ligands (e.g. antibodies, peptides) using thiol chemistry [47]. Recently, DSPE-PEG with several end functional groups are attracting much attention, due to its biomaterial characteristics, including safety, biocompatibility and low toxicity [48].

EPC from egg yolk, Type XVI-E, ≥99% (TLC), lyophilized powder was acquired from Sigma-Aldrich (USA) and DSPE-PEG-Mal lyophilized powder from Avanti Polar Lipids (USA).

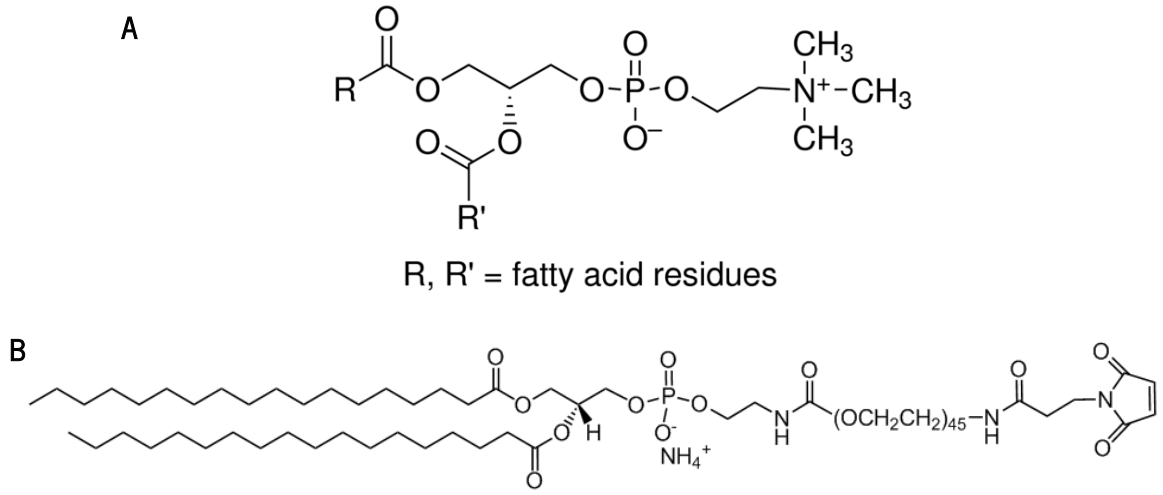

Figure II-4 – Chemical structure of (A) L-alfa-phosphatidylcholine (EPC) and (B) 1,2-distearoyl-sn-glycero-3-phospho ethanolamineN-[maleimide(polyethyleneglycol)-2000] (DSPE-PEG-Mal).

II-1.3.3. Steroids

Unlike other lipids, sterols are composed by a common steroid nucleus of a fused 4-ring structure with a hydrocarbon side chain linked to one end and an OH group linked to the other end. Depending on the side chain, many steroids including cholesterol, vitamin D and hormones (e.g. cortisol, testosterone), have different key biological functions in the organism.

Cholesterol, a sterol biosynthesized in all animal cells, is essential in the cell membranes structure as it affects their mechanical properties including mechanical strength, elasticity and packing density (**Figure II-5**) [33]. Thus, cholesterol has been widely applied in liposomes preparation in order to modulate

their structural and dynamic properties, including the stability (improve the resistance to vesicle aggregation), permeability (reduce bilayer permeability to solutes), thickness (increase the packing of the phospholipid molecules), fluidity (reduces the fluidity of the lipid bilayer of the vesicles) and rigidity (the change the fluidity make the vesicles more rigid) [49, 50]. Moreover, since it also influence drug incorporation efficiency (reduce in the case of hydrophobic drugs), the ratio between cholesterol and phospholipids in liposomal formulations needs to be optimized, in order to provide a high stability without reducing the efficacy of drug delivery.

Cholesterol (ovine wool, >98%) was acquired from Avanti Polar Lipids (USA) and NBD-Cholesterol (22-(N-(7-Nitrobenz-2-Oxa-1,3-Diazol-4-yl)Amino)-23,24-Bisnor-5-Cholen-3β-Ol) from Thermo Fisher Scientific (USA), which were used for the preparation of LUVs and fluorescent LUVs present in the **Chapters IV and VI**, respectively.

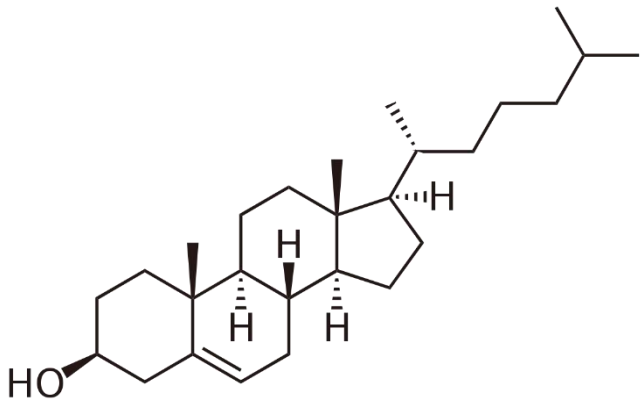

Figure II-5 – Chemical structure of cholesterol.

II-1.4. Gold nanoparticles

Gold nanoparticles (AuNPs) have been widely employed in the biomedical field, due to their unique properties, such as good biocompatibility, easy synthesis, chemical stability and inertness, facile surface modification and tunable optical properties [51, 52]. Currently there are several techniques to synthetize AuNPs, being the commonly used protocols categorized into: *(i)* top-down protocols, where physical-chemical processes are used to degrade a bulk material into smaller pieces, achieving the nanometric scale, or *(ii)* bottom-up protocols, where the syntheses of the NPs starts from smaller precursors, such as metallic salts or molecular seeds that through nucleation form nanostructures [53]. It is possible to synthesize AuNPs with controlled size, shape and surface functionality, for a wide variety of applications.

Computer Assisted Tomography scanning and X-Ray, for example, have been used to monitor the *in vivo* biodistribution of these contrast agents encapsulated or not into NPs. Moreover, they are promising new drugs for treatment of arthritic diseases attributed to their anti-inflammatory, anti-oxidant and antiangiogenic actions [54].

Stabilized suspension of AuNPs with 20 nm diameter in 0.1 mM phosphate buffered saline (PBS) was acquired from Sigma-Aldrich (USA), and used in the production of LUVs in **Chapter IV**.

II-1.5. Glutathione

Glutathione (GSH), also designed as γ-l-glutamyl-l-cysteinyl-glycine, is a tripeptide synthesized by the sequential addition of cysteine to glutamate followed by the addition of glycine (**Figure II-6**) [55]. It is the most important low MW antioxidant synthesized in cells, since besides removing peroxides, free radicals and many xenobiotic compounds, GSH is also involved in the regulation of the cell cycle. The sulfhydryl group (–SH) of the cysteine is involved in reduction and conjugation reactions where in the present of an antioxidant (or other xenobiotic compound) two GSH molecules become oxidized and join together via a disulfide bond to form glutathione disulfide (GSSG). Furthermore, GSSG can be reduced by glutathione reductase (GR) to regenerate GSH [56]. Thus, GSH is the key regulator of the intracellular redox state, being intracellularly in the range of 1-10 mM, whereas outside cells it is reportedly much lower within the range of 2-20 μM [57].

Recently, drug delivery systems that respond to biochemical differences between the extra and intracellular environments were explored to target and control the delivery of drugs inside cells. Thus, GSH can be used to coat the surface of NPs [58, 59] or to produce NPs, micelles and polymers that are sensible to the redox medium [38, 60-63].

In this thesis, L-glutathione reduced ≥98% was acquired from Sigma-Aldrich (USA), being used in the production of the micelles in **Chapters V and VI**.

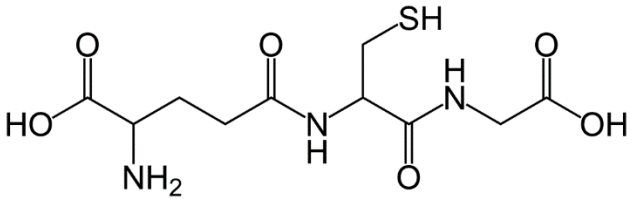

Figure II-6 – Chemical structure of glutathione (GSH).

II-1.6. Polyethylene glycol

PEG is a linear synthetic polyether that can have a wide range of sizes and terminal functional groups [46]. It is widely used in the pharmaceutical and nanotechnology field, due to its biocompatibility, non-immunogenicity and good physical properties. Indeed, it can be dissolved in both aqueous and organic solvents, which enhances its applications for end-group derivatization and chemical conjugation to a huge variety of biological molecules, such as polypeptides, polysaccharides, polynucleotides, drugs and other small molecules under mild physiological conditions [64]. Besides being widely applied in the pharmaceutical field as vehicle in oral, topical and intravenous formulations, it has been widely explored for drug delivery and tissue engineering applications [65].

Among the drug delivery field, PEGylation have an important role in avoiding the adsorption of opsonin proteins [66]. Due to the steric repulsive effect, PEG not only increases the blood circulation half-life of the formulation by several orders of magnitude, but also prevents their aggregation during storage [67]. Therefore, PEG reduces the immunogenicity of therapeutic formulations and increases their pharmacokinetic properties.

In this thesis, the PEG has a methoxy (OCH_3) group in one side and an amine (NH_2) group in the other side as terminal functional groups (**Figure II-7**). Methoxypolyethylene glycol amine 5,000 (extent of labeling: ≥0.17 mmol/g NH_2 loading) was acquired from Sigma-Aldrich (USA) and used in the production of the micelles in **Chapters V and VI**.

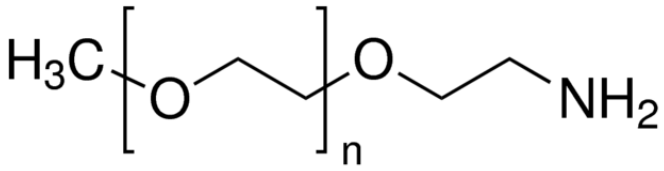

Figure II-7 – Chemical structure of methoxypolyethylene glycol amine (mPEG).

II-2. REAGENTS

Unless addressed otherwise, all the reagents used in this thesis were purchased from Sigma-Aldrich (USA).

II-3. NPS PREPARATION

Currently, NPs can be prepared by several techniques. In the following sub-sections the preparation methods and chemical coupling reactions performed in this thesis will be described in greater detail.

II-3.1. Preparation methods

The appropriate method for NPs preparation extremely depends on the characteristics of the polymer used or the biosynthesis molecules and the bioactive agent. Hence, in order to achieve the desirable properties of interest, such as particle size, surface charge, encapsulation efficiency and stability, the preparation method plays a vital role. Different techniques employed in this thesis for the preparation and synthesis of the NPs are discussed below.

II-3.1.1. Polyelectrolyte complexation

Polyelectrolyte complexes (PECs) are formed due to the electrostatic interactions established between oppositely charged polyions (e.g. polymer-polymer, polymer-drug and polymer-drug-polymer) [68]. PECs are usually obtained by simple, cost-effective and mild methods, presenting the benefit of using organic solvent-free and surfactant-free formulations. The main techniques employed are ionic gelation (cross-linking) or coacervation (phase separation) with the latter not requiring any extra excipient in addition to the polymers and the bioactive molecules. Different parameters are known to influence the

formation of PECs, namely charge density, polyelectrolytes concentration, pH, ionic strength and solvents [69]. In the last years, PECs gained much interest due to their potential applications in the drug delivery field. These systems offer many advantages over conventional delivery systems as they are able to encapsulate different compounds into the polymer matrix at the molecular level, which enhances the efficacy of the biological agents. Nevertheless, drug loading efficacy is normally low and they can also lose the cargo along the time [70].

Polyelectrolyte complexation was used in **Chapters III, VI and VII** to produce Ch-HA polymeric NPs.

II-3.1.2. Thin-film hydration method

The thin-film hydration method is one of the simplest ways to prepare LUVs in a research laboratory [71]. This method involves making a thin lipid film in a round-bottom flask by the removal of the organic solvent. Upon the addition and agitation of the dispersion medium, heterogeneous liposomes are formed. After extrusion through polycarbonate membranes, homogeneous liposomes are obtained. It can be used for all different kinds of lipid mixtures, being the drugs encapsulated into the liposomal formulation by introducing them to the aqueous phase in the case of hydrophilic drugs or to the organic phase for hydrophobic drugs.

The thin-film hydration method was used in **Chapters IV and VI** to produce LUVs.

II-3.1.3. Nanoprecipitation

Nanoprecipitation, also called solvent displacement method or interfacial deposition method, relies on the principle known as Marangoni effect [72]. This method requires the addition of two solvents that are miscible with each other and results in spontaneous formation of NPs by phase separation. The two solvents are selected such that the first solvent (usually organic) dissolves the polymer and the drug. The second system is a non-solvent (usually aqueous solution) in the presence or absence of a surfactant. Hence, this method results in the instantaneous formation of NPs, being an easy and one-step technique that can be easily scaled up [73]. This method is mostly used to encapsulate hydrophobic drugs, but it is also employed in some cases to incorporate hydrophilic drugs. The key parameters in the fabrication procedure are the organic phase injection rate, aqueous phase agitation rate and the organic phase/aqueous phase ratio, which have great influence on the NPs size distribution. Indeed, it can be

synthesized particles with sizes of very narrow distribution, because of the absence of shearing stress [74]. Hence, the nanoprecipitation technique has been widely used in the pharmaceutical and agricultural research as a clean alternative for other drug carrier formulations.

Nanoprecipitation method was used in **Chapters V and VI** to produce polymeric micelles.

II-3.2. Chemical coupling reactions

Coupling reaction in organic chemistry is a general term for a variety of reactions where two fragments are joined together, normally using coupling reagents. In comparison with the physical methods, chemical coupling reactions result in higher affinities between ligands in the nanocarrier. This increases the biological agent efficacy by improving its bioavailability and targeted delivery, improved safety, extending the molecule half-life in the target tissue and enhancing its stability against chemical and/or enzymatic degradation. The coupling reactions applied in this thesis will be presented in the following sub-sections.

II-3.2.1. EDC/NHS

Carboiimide reactions have been widely used to couple carboxyl groups to primary amines in a variety of conjugation techniques. 1-ethyl-3-(3-(dimethylaminopropyl) carbodiimide (EDC) reacts with the carboxyl group to form an active ester intermediate, which is stabilized though the presence of N-hydroxysuccinimide (NHS), reacting subsequently with a primary amine to form an amide bond (**Figure II-8**) [75, 76]. The addition of sulfo-NHS stabilizes the amine-reactive intermediate by converting it into an amine-reactive sulfo-NHS ester, thus increasing the efficiency of EDC-mediated coupling reactions. It is called a 'zero-length' cross-linker since the amide linkages are formed without leaving a spacer molecule. This reaction is nontoxic as the remained products and by-products (isourea) can be easily removed in the washing steps [77]. Indeed, several works have demonstrated the *in vitro* and *in vivo* cytocompatibility of EDC/NHS chemistry.

In **Chapter III, VI and VII**, EDC/NHS chemistry was used to stabilize the produced Ch-HA NPs and/or immobilize the antibodies at the NPs' surface. In **Chapter V**, EDC/NHS chemistry was used to synthesize the copolymers for the micelles preparation.

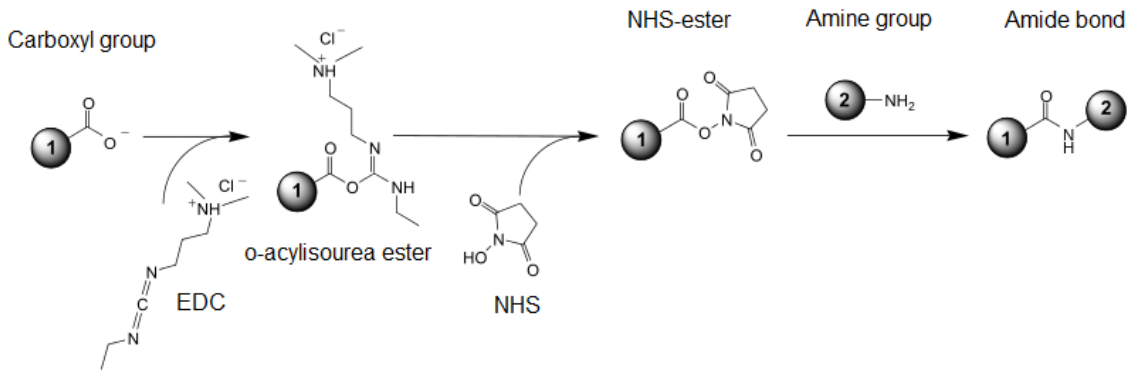

Figure II-8 – ECD/NHS chemistry (adapted from [76]).

II-3.2.2. TBTU

2-(1H-Benzotriazole-1-yl)-1,1,3,3-tetramethylaminium tetrafluoroborate (TBTU) is one of the most commonly used coupling reagents for amide bond formation in organic solvents, and it is also called a 'zero-length' cross-linker [78]. In the presence of a catalyzer (e.g. triethylamine - TEA), TBTU reacts with the carboxyl group forming an active ester that then reacts with the amine group to form an amide bond (**Figure II-9**).

In **Chapter V and VI**, TBTU chemistry was used to synthesize the copolymers for the micelles preparation.

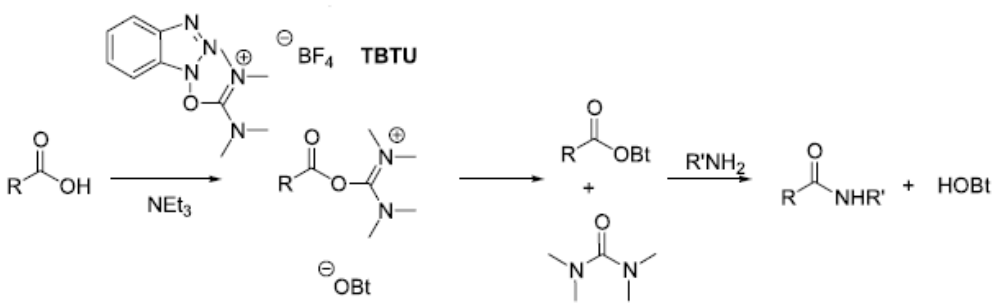

Figure II-9 – TBTU chemistry (adapted from [78]).

II-3.2.3. Thiols

Thiols, also called sulfhydryls, are considered analogs of alcohols where OH group is replaced with SH group [79]. They are an integral part of biological systems and have significant roles in protein

structure, detoxification, cell signaling and enzyme activities as well as being cofactors. Despite being used in many chemical reactions and applications [80], in the scope of this thesis thiol-disulfide and thiol-maleimide reactions will be explained in greater detail.

The interconversion between thiols and disulfide groups is a redox reaction: the thiol is the reduced state, and the disulfide is the oxidized state. Hence, disulfide bonds are usually formed from the oxidation of sulfhydryl groups (**Figure II-10A**). Despite being a covalent bond, disulfide bonds are susceptible to reduction while in biological systems. In **Chapter V**, the oxidation of the thiol group of GSH allows for the encapsulation of a hydrophobic drug into the polymeric micelles.

The maleimide group reacts specifically with sulfhydryl groups when the pH of the reaction mixture is between 6.5 and 7.5 (**Figure II-10B**). The result of this reaction forms a stable thioether linkage that is not reversible (i.e., the bond cannot be cleaved with reducing agents). In order to perform this reaction sometimes is necessary to introduce first the sulfhydryl groups, which can be achieved with 2-iminothiolane (2-IT, also known as Traut's reagent) [81]. The cyclic imidothioester reacts with primary amines in a ring-opening reaction regenerating a free sulfhydryl group. In order to prevent disulfide bond formation as a result of the oxidation of the sulfhydryl groups, a chelator (e.g. ethylenediamine tetraacetic acid - EDTA) should be added to the reaction. In **Chapter IV**, those reactions were performed in order to covalently immobilize the antibodies at the surface of the liposomes.

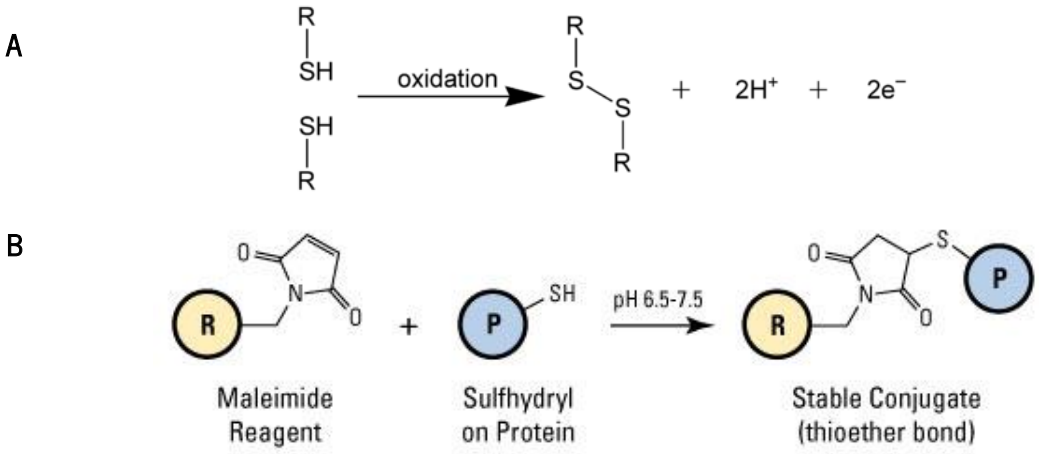

Figure II-10 – Thiol chemistry: (A) thiol-disulfide reaction, and (B) thiol-maleimide reaction.

II-3.3. Polymeric NPs preparation

In the **Chapters III, VI and VII**, Ch-HA NPs were prepared by polyelectrolyte complexation of both natural-based polyelectrolytes (**Figure II-11**).

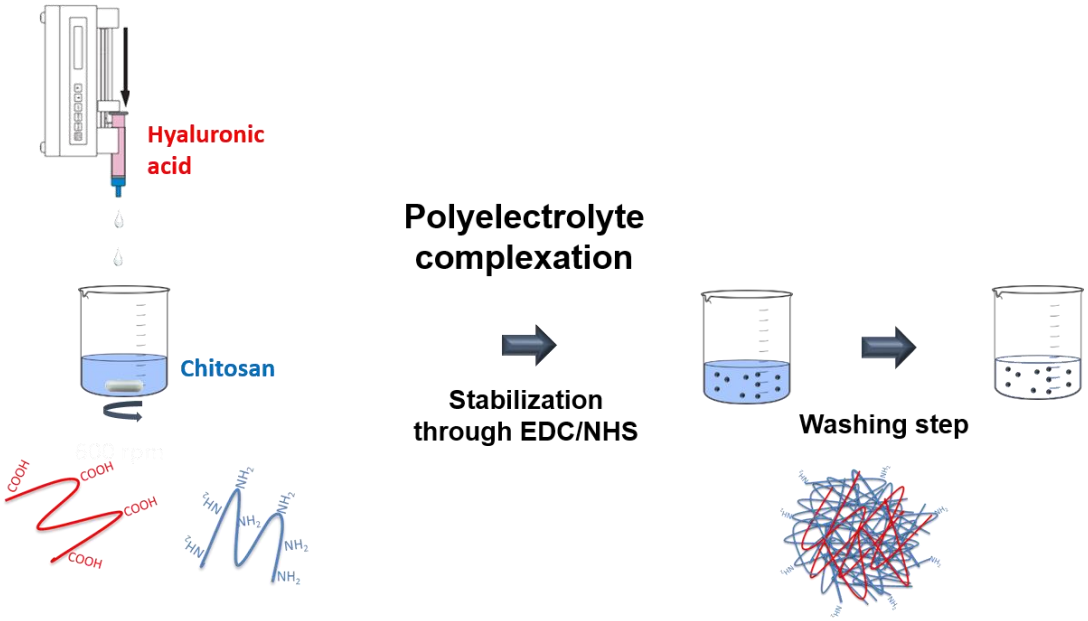

Figure II-11 – Ch-HA NPs production.

For the Ch-HA NPs formation, Ch was dissolved in 1% (v/v) acetic acid, while HA was dissolved in ultrapure water, overnight at room temperature (RT). Both solutions were filtered through a 0.22 μm pore membrane. The NPs formation occurred spontaneously when the HA solution was added dropwise at 1 mL/min rate to the Ch solution under strong magnetic stirring (600 rpm). Different initial polymer

concentrations (0.25, 0.5 and 1 mg/mL) and pH values (3, 4, 5, 6 and 7) were used to evaluate the influence of these parameters on the properties of the NPs. During the preparation, the NPs were stabilized through carbodiimide chemistry. EDC/NHS reagents were dissolved in 0.1 M MES buffer (pH 4.7) with 0.9% (w/w) NaCl. Five different EDC/NHS ratios were tested, namely 400/100, 100/400, 200/200, 50/200, and 200/50 mM.

To remove unreacted compounds, the NPs were washed twice with ultrapure water by centrifugation (30 min, 4000 rpm at 20 °C) using Vivaspin 300 kDa Filter Units (Fisher Scientific, USA). To avoid NPs aggregation, glucose at 2 mg/mL was added before centrifugation [82].

For the fluorescence biological assays, 200 µL of fluorescein isothiocyanate (FITC, 2 mg/mL in ethanol/water, 1:10) was added to the Ch solution before the NPs formation.

In order to assess the optimal production conditions in terms of size distribution and zeta potential, the different parameters evaluated are summarized in **Table II-1**. The optimal conditions for producing the NPs are highlighted in the table in bold.

Table II-1 – Parameters evaluated for CH-HA NPs production.

Parameter	[CH/HA] (mg/ml)	pH (solutions)	[EDC/NHS] (mM)
Tested conditions		3	400/100
	0.25	4	100/400
	0.5	**5**	200/200
	1	6	**50/200**
		7	200/50

II-3.4. LUVs preparation

In **Chapter IV and VI**, LUVs were prepared by the thin-film hydration method followed by extrusion (**Figure II-13**).

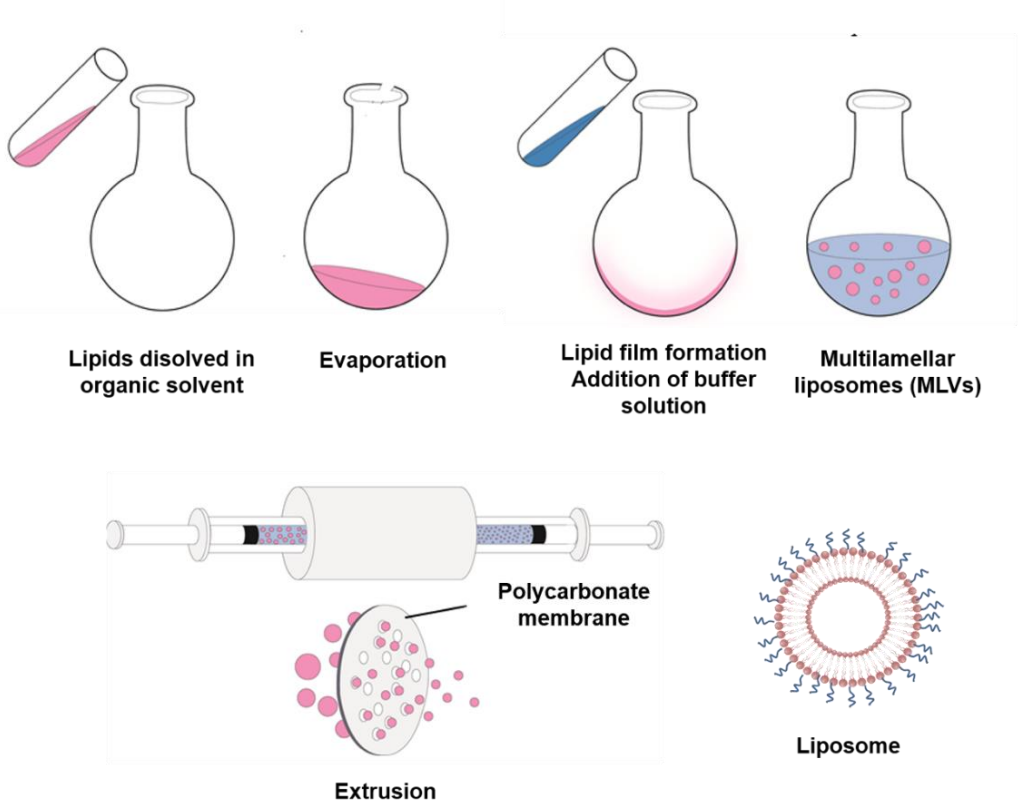

Figure II-12 – Liposomes production (adapted from [83]).

A lipid film of cholesterol/EPC/DSPE-PEG-Mal at 1:0.85:0.15 (n/n) and α-tocopherol at 1:200 (M/M) was obtained after complete ethanol evaporation in a rotary evaporator. The hydration of the dried lipid film was performed with *(i)* a suspension of 20 nm AuNPs in HEPES buffer (pH 7.4) in **Chapter IV** and *(ii)* a solution of HEPES buffer (pH 7.4) in **Chapter VI**, and the vigorous vortex of this mixture produced multilamellar liposomes (MLVs). MLVs were then extruded forty three times through polycarbonate filters of 0.1 μm pore diameter, using an Avanti Mini-Extruder. For fluorescence biological assays, NBD Cholesterol from Thermo Fisher Scientific (USA) was added to the lipid solution at 0.05 (n/n).

II-3.5. Micelles preparation

In **Chapters V and VI**, first mPEG-GSH-PA copolymers were synthesized, and then polymeric micelles were produced though the nanoprecipitation method (**Figure II-12**).

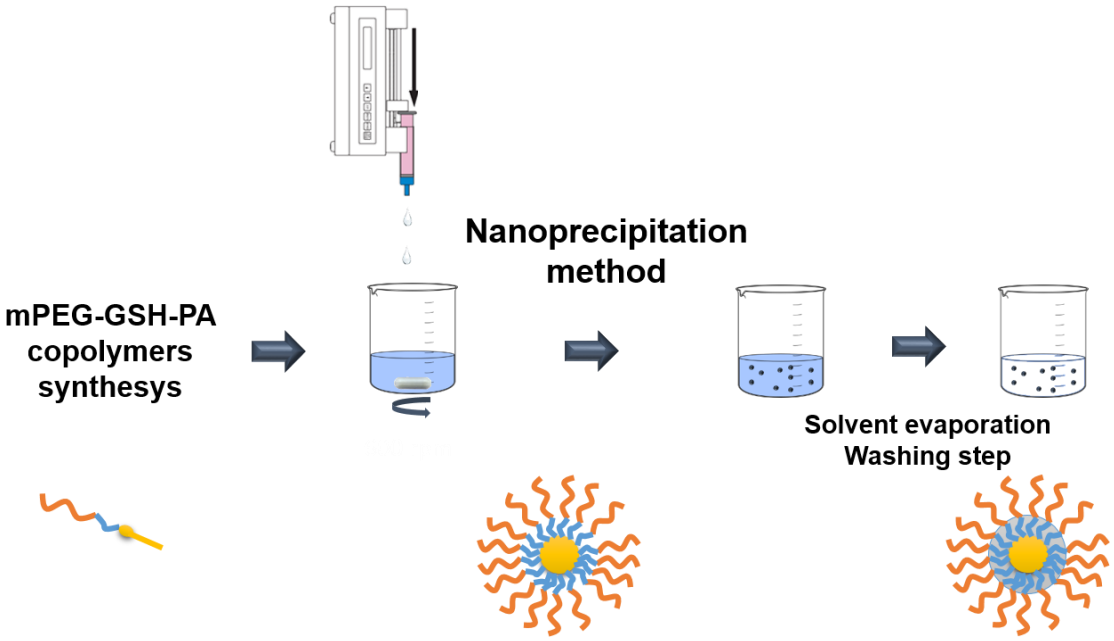

Figure II-13 – Micelles production.

In order to prepare mPEG-GSH-PA copolymers, firstly mPEG (0.01 mmol) and GSH (0.02 mmol) reacted in ultra-pure water for 24 h at RT, using as coupling agents EDC/NHS at 50/200 mM in MES hydrate at pH 4.7. The product of the reactions was placed in dialysis systems with 3.5-5 kDa cut-off (Micro Float-A-Lyzer®) to remove the unreacted compounds. After removing the water by freeze drying, mPEG-GSH reacted with PA (0.011 mmol) in tetrahydrofuran (THF) using TBTU (0.011 mmol) and TEA (0.02 mmol) for 24 h at RT.

The micelles were produced by the nanoprecipitation method. The polymeric solutions were added dropwise at a rate of 1 mL/min to ultra-pure water with strong magnetic stirring (600 rpm) during 48 h. To remove unreacted compounds, the micelles were washed twice with ultrapure water by centrifugation (45 min, 5000 rpm at 20 °C) using Vivaspin 300 kDa Filter Units.

For fluorescence biological assays, 0.5 mg of FITC was dissolved in the polymer solution before the micelles production.

II-4. NPs CHARACTERIZATION

As physicochemical properties of nanomaterials contribute to their biological behavior, an adequate characterization of the NPs is crucial to obtain reliable data with high translational output [84]. Hence, it is of paramount importance to analyze their physical and chemical properties.

II-4.1. Particle size, polydispersity index and zeta potential

NPs size distribution (size and polydispersity index - PDI) and charge are important parameters to be determined during development of nanocarriers. Size distribution were assessed by dynamic light scattering (DLS) and the zeta potential was determined by laser Doppler microelectrophoresis using a Zetasizer Nanoseries ZS equipment (Malvern Instruments, Portugal).

II-4.1.1. Size - Dynamic Light Scattering

DLS, also referred as Photon Correlation Spectroscopy or Quasi-Elastic Light Scattering, is a technique for measuring the size of particles, usually at the submicron range [85]. It relies on the fundament that the illumination by light of a suspension of particles in a solution provides different refraction indexes of the suspending solvent. Thus, DLS measures Brownian motion and relates this to the size of the particles. Brownian motion is defined as the random movement of particles and, consequently, larger particles have slower Brownian motions. As DLS depends on the temperature, which is related to the viscosity, this is a critical parameter that must be fixed. The size of a particle is calculated from the translational diffusion coefficient (D). Therefore, as it refers to the diffusion of a particle within a fluid, the particle diameter measured in DLS is a hydrodynamic diameter.

A typical DLS system comprises: a laser that provides a light source to illuminate the sample contained in a cell, a detector (173°) measures the scattered light and an attenuator reduces the intensity of the laser source and therefore reduce the intensity of scattering. DLS has emerged as a simple table-top technique with several advantages, including the capacity to measure in native environments, high sensitivity to small quantities of particles, minimal sample volume, little concentration and preparation requirements, and user friendly equipment [86]. However, this technique does not give other important information as the shape or number of particles. Moreover, sample preparation and proper training is required to achieve high quality data, as it can yield bias towards reporting larger diameters in the presence of aggregates or impurities.

DLS measurements also give an important information about the size distribution of the particles, the PDI [87]. While suspensions with a PDI lower than 0.2 is considered to be highly monodisperse, values of 0.2 - 0.4 or > 0.4 are considered to be moderately and highly polydisperse, respectively.

Through this thesis, measurements of Ch-HA NPs and micelles were performed at 25.0 °C and/or 37.0 °C, being the NPs diluted in ultra-pure water (1:20; v/v) and the micelles undiluted. LUVs were measure using a concentration of 500 μM in HEPES buffer at 37.0 °C.

II-4.1.2. Surface electric charge - Zeta potential

Zeta potential, also designated as electrokinetic potential, is the potential at the slipping/shear plane of a colloid particle moving under an electric field [88]. It is the key parameter that controls electrostatic interactions in particle dispersions. Indeed, the magnitude of the zeta potential gives an indication of the NPs suspension stability [89]. Higher absolute values of this parameter, give rise to stronger repellent electrostatic interactions between the particles dispersed in suspending solvent, which leads to a higher stability of the suspension. Guidelines classifying NP suspensions with zeta potential values of ±0 - 10 mV as highly unstable, ±10 - 20 mV as relatively stable, ±20 - 30 mV as moderately stable, and >±30 mV as highly stable [86].

Laser Doppler microelectrophoresis measures small frequency shifts in the scattered light that arise owing to the movement of particles in an applied electric field. Then, the instrument calculated the zeta potential from the electrophoretic mobility.

In this thesis, the zeta potential was determined with the same dilutions and buffers as previously described using a universal 'dip' cell.

II-4.2. Stability studies

Stability studies are very important to determine the colloidal stability of the particles over the time. During the development of new pharmaceutical drug products, including nanomedicines, it is required to establish a shelf-life and recommend the suitable storage conditions [90]. Hence, in this thesis all NPs formulations were kept at 4 °C under static conditions and during the experimental time (6 months) their storage stability was assessed by measuring their size, PDI and zeta potential, as previously described.

II-4.3. Morphology

Several techniques have been used to characterize the morphology of the NPs. In the following sub-sections, the techniques performed in this thesis will be described, highlighting their strengths and limitations.

II-4.3.1. Scanning electron microscopy

Scanning Electron Microscopy (SEM) is an imaging technique that enables obtaining high resolution images of a sample by scanning the surface with focused beam of electrons [91]. Those electrons interact with the atoms of the sample at various depths, and scattered electrons produce diverse type of signals that are detectable by the SEM equipment, and then transformed into a 2D image. Thus, SEM provides quantitative and qualitative information regarding surface morphology of the sample. Nevertheless, the quality of the results deeply depends on the sample preparation. For instance, polymeric materials should be coated with conductive materials (e.g. gold or palladium) by sputtering, as non-conducting materials saturate with the electrons leading to an incapacity in detecting the surface features by this technique.

The morphology of the produced NPs (Ch-HA NPs and micelles) was analyzed by SEM in **Chapters III and V**. Prior to analysis, samples were diluted in water (1:20; v/v) and disposed into the surface of a glass slide for air-dry. After being sputter-coated with palladium (EM ACE600, LEICA), the samples were analyzed using High-Resolution Field Emission Scanning Electron Microscope (Auriga Compact, ZEISS).

II-4.3.2. Transmission Electron Microscopy

Transmission Electron Microscopy (TEM) is a destructive imaging technique that gives high resolution images of a sample by passing through it an electron beam [92]. Those electrons interact with the atoms of the sample at various depths, and transmitted electrons produce diverse type of signals that are detectable by the TEM equipment and transformed into a 2D image. TEM magnification and resolution is higher than SEM. In addition, TEM also provides information relatively to the internal composition.

A JEOL JEM 1400 TEM (Tokyo, Japan) was used to analyze the morphology of AuNPs and LUVs incorporating AuNPs in **Chapter IV**. For negative staining TEM, 10 μL of samples were mounted on a Formvar/carbon film-coated mesh nickel grids (Electron Microscopy Sciences, USA) and left standing for

2 min. After removing the excess liquid with filter paper, 10 μL of 1% uranyl acetate was added to the grids and left standing for 10 s. The excess of liquid was once more removed with filter paper. Morphology assessment was carried out at 80 kV.

II-4.3.3. Atomic Force Microscopy

Atomic Force Microscopy (AFM) is a scanning probe technique that allows obtaining an image and measurement of the surface topography of samples with nanometer resolution [93]. The AFM principle relies on using a tip with a cantilever that scans the sample surface and, consequently, builds a topographical image with an exceptional resolution and accuracy. Typically, these micro-cantilever systems can operate in three open-loop modes: non-contact mode, contact mode and tapping mode, depending on the surface properties. AFM provides additional capabilities and advantages relative to other microscopic methods, as it can reach a magnification greater than 1000 x and gives 3D projections of the sample surface. Indeed, it is possible to acquire images showing the arrangement of individual atoms or the structure of individual molecules in a surface sample.

AFM measurements of the Ch-HA NPs were performed using the Tapping Mode™ with a MultiMode AFM connected to a NanoScope III controller from Veeco (USA) in **Chapters III and VII**. Prior to the analysis, the samples were diluted in water (1:20; v/v) and disposed into the surface of a glass slide for air-dry. Then, the surface of the samples were recorded by scanning the surface in tapping mode at a frequency of 1 Hz using vacuum, and afterwards being analyzed with the NanoScope software version 4.43r8.

II-4.4. Chemical characterization

Despite the chemical modifications of the NPs can be performed using several techniques, in this thesis it was used Fourier Transform Infrared Spectroscopy (FTIR).

II-4.4.1. Fourier Transform Infrared Spectroscopy

FTIR is a technique that is used to acquire an infrared spectrum of chemical compounds [94]. It has the advantages of high spectral resolution, good signal-to-noise ratios, and exceptional cost-effectiveness as it measures a broad region of the spectrum in a short period of time. Hence, this spectroscopic

technique relies on the absorption of energy from a photon that promotes the transition from a lower-energy state to a higher-energy (i.e. an excited state), which results in vibrations of molecular bonds (e.g. stretching, bending, twisting, rocking, wagging and out-of-plane deformation) in the infrared (IR) region of the spectrum. Fourier transformation algorithm allied to IR spectroscopy gives a spectrum of IR absorption per frequency/wavelength. Taking into consideration that each compound has a specific IR spectrum and that similar chemical groups absorb in the IR at similar frequencies, FTIR analysis enables to identify the chemical structure of a compound and subsequent chemical modifications.

An IR Prestige-21 FTIR spectrometer (Shimadzu, Japan) with the attenuated total reflectance (ATR) technique was used to identify the chemical structure of the produced micelles in **Chapter V**. A transmittance spectrum was obtained by performing 50 scans in each spectrum over a range of 500-4000 cm^{-1} at a 4 cm^{-1} resolution by the KBr disk method.

II-5. BIOACTIVE AGENTS

The bioactive agents used in this thesis as well as their loading/encapsulation efficacy are described in the following sub-sections.

II-5.1. Antibodies

An antibody (Ab), also known as immunoglobulin (Ig), is a large Y-shaped glycoprotein composed of two different regions, a variable region that is specific of each Ab and a non-variable region that is common for each type of Ab (**Figure II-14**). The antigens are specifically recognized via the fragment antigen-binding variable region [95]. They are mainly produced by B-cells and used by the immune system to identify and neutralize pathogens, such as bacteria and viruses [96].

In recent years, monoclonal Ab therapy have been approved for over 30 targets and diseases, which had dramatically advanced the therapy of chronic inflammatory diseases and cancer [97]. In this type of immunotherapy, the Ab bind specifically to certain cells or proteins in order to suppress/reduce the immune system activity or to eliminate and regulate immune cells that contribute to tissue damage. Despite their remarkable success, Abs-based therapies are associated with some limitations, including the short half-life of the Abs that decreases their therapeutic efficacy and severe systemic side effects, such as increased risk of infection, malignancy or administration reactions [98].

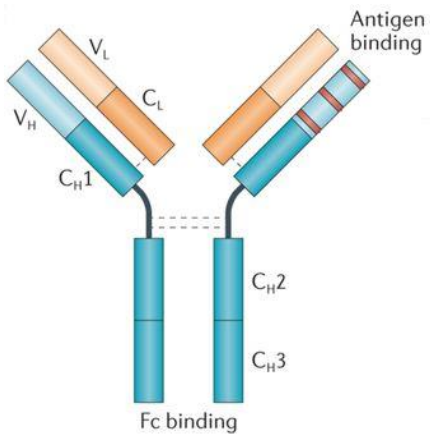

Figure II-14 – Antibody structure (adapted from [99]).

In this thesis, neutralizing Abs were used due to their ability to block the activity of the antigen after biding to the variable region. Three different Abs were used, namely anti-IL-6 Abs, anti-TNF-α Abs and anti-IL-23 Abs, being their properties summarized in **Table II-2**.

Table II-2 – Summary of antibodies properties.

Parameter	Anti-IL6 Abs		Anti-TNF-α Abs	Anti-IL-23 Abs
Clonality	Monoclonal	Monoclonal	Polyclonal	Monoclonal
Host specie	Mouse	Mouse	Rabbit	Mouse
Species reactivity	Human	Rat, Human	Rat, Human, Cynomolgus monkey, Rhesus monkey	Human
Application	Flow Cytometry, Blocking, Inhibition Assay	Immunochemistry, Neutralizing, Sandwich ELISA, Western Blot	Flow Cytometry, Inhibition Assay, Neutralizing, Western Blot	Neutralizing, Immunochemistry
Company	Abcam (UK)	Abcam (UK)	Abcam (UK)	Abcam (UK)
Chapters	**III**	**VII**	**VII**	**IV**

II-5.1.1. Polymeric NPs functionalization

Abs were immobilized at the surface of the optimized Ch-HA NPs, being anti-IL-6 Abs immobilized in **Chapter III**, and both anti-IL-6 Abs and anti-TNF-α Abs in **Chapter VII**. To determine the maximum immobilization capacity of the NPs, different concentrations of each Abs were used (from 0 to 20 μg/mL). First, the primary Abs were activated with a solution of 50/200 mM EDC/NHS in 0.1 M MES buffer for 15 min. Then, the NPs were incubated with the activated Abs, overnight at 4 °C. To remove the unbound Abs, the biofunctionalized NPs were washed twice by centrifugation, as previously described.

To determine the degree of Abs immobilization, the biofunctionalized NPs were incubated with the secondary Abs for 1 h at RT. NPs without immobilized Abs were used (0 μg/mL) as negative control. After centrifugation, the fluorescence of the unbound secondary Abs (in supernatant) were determined in a microplate reader (Synergie HT, Bio-Tek, USA). The concentration of Abs at the NPs surface corresponds to the difference between the initial and unbound secondary Abs.

II-5.1.2. Liposomes functionalization

Anti-IL-23 Abs were linked to the maleimide groups of PEG ends after their thiolation with 2IT [47]. For that, a 100-fold molar excess of 2IT was incubated with the Abs (20 μg per 1 mL of LUVs suspension at 30 mM) in the presence of 5 mM EDTA (to avoid the oxidation of the thiol groups) in PBS (pH 8.0) during 1 h at RT [100]. Before linking the thiolated Abs to liposomes, a dialysis (Micro Float-A-Lyzer®, MWCO: 3.5-5 kDa) was performed to remove the excess of 2IT. As thiol groups have a rapid rate of recyclization [101], the buffer replacement was performed each 15-20 min during a period of time lower than 4 h. After LUVs overnight incubation at 4 °C with the thiolated anti-IL-23 Abs, they were washed twice with HEPES buffer using Vivaspin 300 kDa Filter Units to remove unbound Abs.

To quantify the anti-IL-23 Abs immobilized at the LUVs surface, first they were immersed in a solution of 3% (w/v) bovine serum albumin (BSA) for 1 h at RT (to block nonspecific sites), and then the secondary Abs Alexa Fluor® 488 were added. After 1 h at RT, the fluorescence intensity of the supernatant (unbound secondary Abs) was measured using a microplate reader (Synergy HT, BioTek, USA).

II-5.2. Dexamethasone

Dexamethasone (Dex), also known as 9α-Fluoro-16α-methylprednisolone, is a potent synthetic member of the glucocorticoids (GCs) class of steroid drugs (**Figure II-15**), which acts as an anti-inflammatory and immunosuppressant [102]. Generally, GCs are among the most commonly prescribed drugs for various inflammatory, autoimmune and allergic disorders. Nevertheless, their use is severely hampered by the risk of developing serious side effects, such as osteoporosis, hyperglycemia, insulin resistance and hypertension. Moreover, the therapeutic efficiency is limited, due to inadequate pharmacokinetics, with low drug bioavailability and off-targeted biodistribution profile [66]. These therapeutic drawbacks can be overcomed by designing nanomedicines, namely drug delivery systems, which have been successfully introduced in the clinic for the treatment of cancer, pain and infectious diseases [103].

In this thesis, Dex ≥ 98% in HPLC was acquired from Sigma-Aldrich (USA), and was encapsulated in the polymeric micelles in the **Chapter V**.

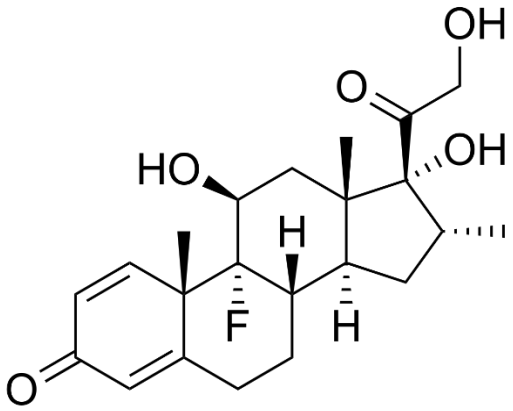

Figure II-15 – Chemical structure of Dexamethasone (Dex).

II-5.2.1. Encapsulation efficiency

The Dex loading content in the micelles was determined with micelle:Dex feed weight ratios varying from 1:0.2 to 1:0.8 at a micelle concentration of 1 mg/mL. Dex was added to THF solution and then the micelles were produced as previously described. The non-encapsulated Dex was measured in the supernatant of the centrifuged solution using an UV-Vis spectroscopy (Shimadzu, Japan). As Dex is a hydrophobic drug (soluble in organic solvents), samples were diluted in ethanol (0.5:0.5 v/v) in order to allow the Dex dissolution.

Entrapment efficiency (EE) was calculated by measuring the initial concentration and non-encapsulated Dex, according to the following formula:

$$\%EE = \frac{(\text{Initial concentration} - \text{ not encapsulated drug})}{\text{Initial concentration}} \text{ x } 100$$

II-5.2.2. Release studies

The *in vitro* Dex release profiles of micelles under different external conditions were obtained and measured through a dialysis method. Firstly, 5 mL of micelle suspensions were added to a dialysis system (Micro Float-A-Lyzer®, 3.5 - 5 MWCO) before putting it in a centrifugation tube containing 15 mL PBS (pH 7.4). The tube was shaken at 100 rpm at 37 °C. At the defined time points, an aliquot of solution (0.5 mL) was retrieved from the outside tube with equal volume replenishment. After dilution of the aliquot with 0.5 mL ethanol, Dex concentration was measured using an UV-Vis spectroscopy equipment (Shimadzu, Japan). The enzymatically- and GSH-responsive properties were evaluated using the same method but with different external media - PBS containing *(i)* 10 mM of GSH or *(ii)* 50 mU of GR (with 0.14 mM NADPH and 0.1 mM EDTA). All the characterization experiments were performed in triplicate.

II-5.2.3. UV-Vis spectrophotometry

UV-Vis spectrophotometry is a very simple, rapid and low cost technique that has been used extensively in analytical chemistry for characterization and quantitative analysis [104]. It uses light in the visible and adjacent regions near ultraviolet (UV) and near infrared (NIR) ranges to acquire the absorption or reflectance spectroscopy of photons of a compound. Hence, it is possible to determine concentrations of an absorbing chemical in solution by using Beer-Lambert law. This is based in the principle that the absorbance of a solution is directly proportional to the concentration of the absorbing species in the solution and the light path length. The concentration can be determined using a calibration curve.

In this thesis, UV-Vis spectrophotometry was used to determine the EE and release profile of the Dex loaded into the polymeric micelles in the **Chapter V**.

II-6. *IN VITRO* BIOLOGICAL TESTS

Several biological assays performed in this thesis are explained in greater detail in the following sub-sections. After discussing the selection of the cells sources used in this thesis, it is described the cell seeding, the methods used for the study and quantification of metabolic activity and viability and the production of pro-inflammatory cytokines as well as the NPs internalization.

II-6.1. Cell sources

Inflammatory arthritis compromises many cell types including endothelial cells, chondrocytes, synovial like fibroblasts and inflammatory cells, such as macrophages [105]. Hence, nanomedicines should take in consideration this dynamic environment in order to provide an increased therapeutic action, without affect cell function.

In vitro studies performed in this thesis were carried out using both primary cells and cell lines of human origin. Primary cells are isolated directly from a tissue through mechanical, chemical or enzymatic digestion methods [106]. Their use presents some challenges, due to their heterogeneity, sensitivity, lower proliferation rates and limited lifespan in culture. Moreover, they usually require additional nutrients in the culture medium. An important advantage is their accurately representation of the host tissues. In contrast to primary cells, cells lines are immortalized cells that present the ability to proliferate indefinitely either due to a random mutation or due to a programmed modification [107]. They offer several advantages including cost-effectiveness, easy to culture, unlimited supply of cells with high proliferative rates and bypass ethical concerns associated with the use of animal- and/or human-derived tissues. Moreover, as they provide a consistent sample, they present reliable and reproducible experimental results. However, they do not always accurately replicate the primary cells and, consequently, results needs to be carefully interpreted.

Taking into consideration the dynamic environment of arthritic diseases, two primary cells types, human articular chondrocytes (hACs) and human monocyte-derived macrophages, and two cell lines, human monocyte-like cell line - THP-1 and human umbilical vein endothelial cell line (EA.hy926), were used throughout this thesis. All cells were incubated at 37 °C in a humidified 5% CO_2 atmosphere.

II-6.1.1. Human Articular Chondrocytes

Chondrocytes, the only cell type of cartilage tissue, have a critical role in the synthesis and turnover of a large volume of ECM components in cartilage including collagen, glycoproteins, proteoglycans and HA [108]. Imbalance in their function leads to degenerative diseases like OA and RA. Thus, hACs from diseased knee arthroplasties, which have a phenotype associated with arthritis disease, are a relevant model to study the biological actions of the developed nanoformulations. In a monolayer culture, hACs acquire a fibrolastic-like morphology after several days in culture [109].

hACs were isolated from knee cartilage samples collected from arthroplasties surgeries biopsies. Samples were obtained through the cooperation agreement between Centro Hospitalar do Alto Ave, Guimarães, Portugal, and I3Bs – Research Institute on Biomaterials, Biodegradables and Biomimetics, in accordance to the established Protocol (67/CA), and after obtaining the donor informed consent. Cells were isolated by enzymatic digestion, according to a previously described protocol [110]. In detail, human cartilage samples were dissected in small full-depth pieces and washed twice with sterile PBS. Then, samples were digested using 0.25% (w/v) trypsin solution for 30 min at 37 °C under agitation, and after removing the solution, cartilage was washed and incubated with a 2 mg/mL collagenase type II solution overnight at 37 °C under agitation. In the next day, after washing the cells twice with sterile PBS, they were counted and plated at a density of 2×10^6 cells per 25 cm^2 culture flask. hACs cells were cultured in Dulbecco's modified Eagle's medium (DMEM), supplemented with 10% Fetal Bovine Serum (FBS, Thermo Fisher Scientific, USA), 10 mM HEPES buffer, 10 mM L-lanyl-L-glutamine, 10 mM MEM nonessential amino acids, 100 units/mL of penicillin, 100 μg/mL of streptomycin and 10 ng/mL of human basic Fibroblast Growth Factor (bFGF, Peprotech, USA). Culture medium was changed every 3 days, until reaching approximately 80 % confluence. Cells were routinely trypsinized with TripLE express (Life Technologies, USA) for 3-5 min at 37 °C, centrifuged (300 g, 5 min) and re-suspended in T150 cell culture flasks. Cells were used until passage 4.

In this thesis, hACs were used in all chapters of **Section 3, 4 and 5**.

II-6.1.2. Human monocyte-derived macrophages

Macrophages are an important population of immune cells that play a key role either in maintaining tissue homeostasis or in inflammatory states [111]. The study of human macrophages is frequently

hampered by access to tissue and inability of this cell type to survive *in vitro* following isolation. Hence, the culture of human monocyte-derived macrophages represent a tool to study macrophages, since monocytes can give rise to tissue macrophages when influenced by certain environmental cues. Despite the advantage of their natural origin, they are not able to replicate *in vitro*, which limits their applicability.

Human monocyte-derived macrophages were generated from peripheral blood mononuclear cells (PBMCs). Buffy coats from healthy donors were acquired after obtaining written informed consent at the Hospital de Braga, Braga, Portugal (SECVS 014/2015). Briefly, PBMCs were enriched from buffy coats by density gradient using Histopaque-1077. The cells in the enriched mononuclear fraction were washed twice in PBS and resuspended in Roswell Park Memorial Institute (RPMI)-1640 media (Thermo Fisher Scientific, USA) with 2 mM glutamine and 2 g/L $NaHCO_3$ supplemented with 10% human serum, 100 units/mL of penicillin, 100 μg/mL of streptomycin and 10 mM HEPES buffer. In the case of frozen PBMCs from RA patients, they were acquired from StemCell Tecnhology (Canada), and used as described in the manufactures' protocol.

In this thesis, healthy human macrophages were used in the **Chapter III and IV**, while diseased macrophages were used only in **Chapter IV**.

II-6.1.3. Human monocyte-like cell line THP-1

THP-1 designates a spontaneously immortalized monocyte-like cell line, derived from the peripheral blood of a childhood case of acute monocytic leukemia (M5 subtype) [112]. As the human monocyte-derived macrophages, THP-1 cell line can also give rise to tissue macrophages when stimulated with phorbol 12-myristate-13-acetate (PMA). Hence, taking into consideration the limited availability of PBMC-derived monocytes, THP-1 represent a valuable tool for investigating monocyte structure and function in both health and disease [113]. Several publications have compared responses between the THP-1 monocytes and human PBMC-monocytes. In most cases, both types showed relatively similar response patterns, with some variable regarding the degree of expression (e.g. gene expression, surface markers and cytokine secretion). In addition, it is important to emphasize that they are still a cell line and, consequently, present the same abovementioned limitations.

THP-1 cell line was kindly provided by Dr. Agostinho Carvalho (Life and Health Science Research Institute, University of Minho, ICVS/3B's – PT Government Associate Laboratory, Portugal). They were maintained in complete RPMI, containing RPMI-1640 media supplemented with 2 mM of L-glutamine,

100 units/mL of penicillin, 100 μg/mL of streptomycin, 10 mM HEPES buffer and 10% FBS. When started with a frozen cryotube, cells were added to a conical based centrifuge with 5 ml of culture medium. After the centrifugation at low speed (150 g, 5 min), the cell pellet was resuspended at a density of 3 - 5 x 100,000 cells/mL in fresh medium containing 20% FBS. The flask was kept in a vertical position until the cells reach the exponential phase of growth (usually this can take up to 7 days). Once the culture is established, the FBS concentration was reduced to 10%. Cells were maintained at a concentration of 3 - 8 x 100,000 cells/mL, in order to keep the cells in the exponential growth phase.

This cell line was used in all chapters of **Section 3, 4 and 5**.

II-6.1.4. Human umbilical vein endothelial cell line

EA.hy926 was established by fusing human umbilical vein endothelial cells with the permanent human cell line A549 [114]. Despite culturing them at high passages, EA cells still continue to express a wide range of differentiated endothelial cell properties [115]. As endothelial cells are the main cells of blood vessels, this cell line was used to assess any cytotoxic effects caused by micelles and LUVs as they would be used in systemic injection. Those cells were used in the **Chapters IV and V**, and in the internalization assays in **Chapter VI**.

Endothelial cells were cultured in DMEM low glucose (D5523) supplemented with 10% FBS, 100 units/mL of penicillin and 100 μg/mL of streptomycin. Culture medium was changed every 3 days, until reaching approximately 80% confluence. Cells were routinely trypsinized with TripLE express for 3-5 min at 37 °C, centrifuged (300 g, 5 min) and re-suspended in T150 cell culture flasks.

II-6.2. Cryopreservation

The cryopreservation of the cells used in this thesis was performed using a Statebourne Biosystem 24 cryogenic tank (Statebourne Cryogenics Ltd., UK). Briefly, cell suspensions of 1×10^6 cells/mL were prepared in a cryopreservation solution, consisting of 10 % (v/v) Dimethyl sulfoxide - DMSO (VWR, USA) in FBS, and transferred into 1.5 mL cryovials (VWR, USA). Then, cell suspensions were gently cooled down, first at -20 °C for at least 2 h and then moved to -80 °C freezer for a minimum period of 12 h. The cryovials were subsequently stored at -176 °C in the gas nitrogen phase of the cryogenic tank.

II-6.3. Cell seeding

II-6.3.1. Seeding on the bottom of well-plates

In **Chapter III, IV and V**, the cytocompatibility of the nanoformulations in contact with the different cell types was evaluated as described below.

Both hACs and EA were seeded at 5×10^4 cells per well into 24-well plates. To perform the SEM analyses, cells were added to tissue culture polystyrene (TCPS) coverslips in 24-well plates. After cell attachment during 5 h, culture medium was added to complete a final volume of 1 mL.

For the induction of THP-1 cell differentiation, cells were seeded at 5×10^5 cells per well in 24-well plates in cRPMI with 100 nM PMA for 24 h. After incubation, non-adherent cells were removed by aspiration, and the adherent cells were washed three times with cRPMI. To ensure reversion of cells to a resting macrophage phenotype before its stimulation, the cells were incubated for an additional 48 h in cRPMI without PMA. For the stimulation and the retrieval of conditioned media, cells were further incubated for 24 h with 100 ng/mL of lipopolysaccharide (LPS) (and 100 ng/mL of Interferon-gamma, IFN-γ, in **Chapter IV**) in fresh medium (the supernatants were collected and stored at -80 °C).

Regarding the human primary macrophages, isolated monocytes were resuspended in complete RPMI medium and seeded at 5×10^5 cells per well in 24-well plates for 7 days in the presence of 20 ng/mL of granulocyte-macrophage colony-stimulating factor (GM-CSF).

Cells cultured without nanoformulations (only with culture medium) were used as control. After the defined timepoints of culture with different concentrations of the nanoformulations, the different samples in triplicate were washed with sterile PBS and evaluated regarding cell viability, proliferation, total protein synthesis and SEM analyses.

In **Chapter III**, hACs were seeded as previously described to assess the ability of biofunctionalized NPs to capture IL-6. For that, the hACs were stimulated for 24 h with monocyte-derived macrophage conditioned medium containing 500 pg/mL of IL-6. Three different conditions were tested: *(i)* no treatment, *(ii)* treatment with biofunctionalized NPs, and *(ii)* treatment with soluble anti-IL-6 Abs. The Abs were added to the culture medium in a concentration of 1 μg/mL. hACs cultured without macrophage conditioned medium (only culture medium) were used as controls. After 1, 3, 7 and 14 days, samples were collected and evaluated regarding cell viability, proliferation, total protein synthesis and SEM

analyses. The amount of IL-6 in the supernatants was assessed by Enzyme-linked Immunosorbent Assay (ELISA). During the time of experiment 300 μL of fresh media was added each 3 days, but no media was removed to keep the NPs and the conditioned media in contact with the cells.

In **Chapter IV**, PBMCs obtained from healthy donors and from RA patients were used to assess the effect of biofunctionalized LUVs on IL-17A production. Cells were cultured at 1.5×10^6/mL in culture medium under neutral activation (anti-CD3/CD28 beads, Miltenyl Biotec) or Th17 condition (anti-CD3/anti-CD28 beads, 10 ng/mL of IL-1β and 10 ng of IL-23, R&D Systems, USA) [116]. After 24 h stimulation, LUVs and/or biofunctionalized LUVs (LUVs+Abs) were added to the culture. At the defined time points, the cell viability was assessed and the supernatants were collected in order to quantify the IL-17A production by ELISA.

The flow cytometry analyses (cellular uptake and internalization profiles) was performed with cells seeded at a density of 2.5×10^5 cells per well (hACs and EA cell line in 24-well plates and THP-1 cell line in 48-well plates) and incubated at 37 °C in a humidified 5% CO_2 atmosphere for 24 h (**Chapter VI**). For the induction of THP-1 cell differentiation, cells were seeded in cRPMI with 100 nM PMA. After 24h incubation, adherent cells were washed three times with cRPMI. Cells were then incubated for an additional 48 h in cRPMI without PMA. Then, the medium was replaced by medium containing 100 ng/mL LPS and 20 ng/mL IFN-γ for M1 differentiation, or 20 ng/mL IL-4 and IL-13 for M2 differentiation during 120 h, as previously reported [117]. For cellular uptake analyses, hACs and EA cell line were cultured in normal conditions and in inflammatory conditions (cells were stimulated with macrophage conditioned medium for 24 h).

In **Chapters III and VI**, for confocal analyses, all cell types were seeded as previously described on μ-slides (Ibidi, Germany).

II-6.3.2. Cell seeding in the co-culture system

To validate the biological effects of the nanoformulations, a co-culture system was established in **Chapters V and VII**. Indeed, *in vitro* models play a vital role not only to advance research on the etiological mechanisms, but also to help in the design and assessment of the safety and efficacy of new treatments. A plethora of *in vitro* models was developed to understand the pathogenesis of OA, however there is still no consensus on the most representative model [118]. Despite the advantages and disadvantages of each model, until now no single *in vitro* model was able to mimic the disease as a whole. Accordingly to

the aim of this thesis, we used an *in vitro* inflammation model involving a co-culture system of osteoarthritic chondrocytes and macrophages in a transwell system, closely resembling the permeable synovial joint (**Figure II-16**) [119].

hACs and THP-1 cell line were seeded as previously described, being the THP-1 seeded at 2.5×10^5 cells per well in 24-well cell culture inserts (pore size: 1 mm) for the co-culture systems. The inserts were transferred to the hACs culture, and the macrophages were activated to the M1 phenotype by adding 100 ng/mL of LPS. After 2 h of stimulation, the following conditions were tested in **Chapter V**: *(i)* no treatment, *(ii)* micelles encapsulating Dex, and *(iii)* free Dex, in order to compare their efficacy in an inflammatory scenario. Those conditions were also tested in the hACs and THP-1 cells seeded alone (monoculture) to compare their harmful effects in normal conditions. GR was added to the co-culture system at 50 mU to mimicking synovial inflammation (no GR was added to the monocultures). In **Chapter VII**, the following conditions were tested: *(i)* no treatment, *(ii)* treatment with anti-TNF-α Abs, *(iii)* treatment with anti-IL-6 Abs, *(iv)* treatment with anti-TNF-α and anti-IL-6 Abs, *(v)* treatment with biofunctionalized NPs with anti-TNF-α Abs, *(vi)* treatment with biofunctionalized NPs with anti-IL-6 Abs, and *(vii)* treatment with biofunctionalized NPs with anti-TNF-α and anti-IL-6 Abs. The Abs were administered at 1 μg/mL.

After 1, 3, 7 and 14 days, the samples were collected and evaluated regarding cell viability, proliferation and morphology. The quantity of TNF-α and IL-6 in the media were both evaluated by ELISA. During the time of the experiment 300 μL of fresh media was added each 3 days, but no media was removed to maintain constant the quantity of nanoformulations in the culture medium.

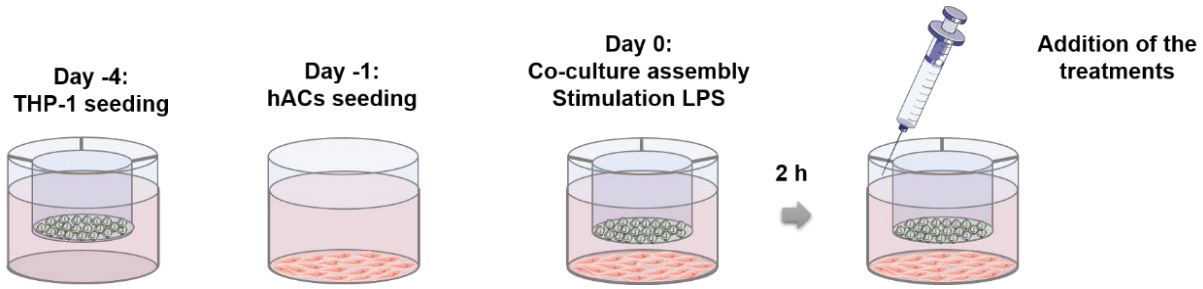

Figure II-16 – Schematic representation of the establishment of the co-culture system.

II-6.4. Metabolic activity and cell viability examination

Several assays were performed to evaluate the cells metabolic activity and viability, which are described in the following sub-sections.

II-6.4.1. Alamar Blue assay

The alamar blue (AB) assay is used to quantitatively measure the metabolic activity of cells by using the reducing power of living cells. Indeed, metabolically active cells have a reducing environment within the cytosol [120]. Hence, the active molecule of AlamarBlue® reagent, resazurin, is blue in color, non-cytotoxic and cell permeable. Inside the cells, the reagent is reduced to resorufin, turning from blue to pink and highly fluorescent. Viable cells continuously convert resazurin to resorufin, increasing the overall fluorescence and color of the media surrounding the cells, that can be measured [121]. It is a simple and rapid assay with high sensitivity, specially using its fluorescent properties. Moreover, since AB is nontoxic to cells, the same cells can be reused for further investigations.

In **Chapters IV, V and VII**, AB assay was performed according to the instructions of the manufacturer. At the defined timepoints, cells were washed twice with sterile PBS solution, and 350 µL of working solution containing 10% (v/v) AlamarBlue® (Bio-Rad, USA) solution and 90% culture medium was added to each well. The culture plates were kept in the dark, at 37°C in the CO_2 incubator for 4 h. The fluorescence was read in a microplate reader (Synergy HT, BioTek, USA) using 100 µL supernatant per well, at an excitation wavelength of 530/25 nm and at an emission wavelength of 590/35 nm. The metabolic activity values were calculated by normalization with the mean fluorescence value obtained for the controls with and without cells.

II-6.4.2. MTS assay

MTS is a colorimetric assay that also quantifies cell metabolic activity by using the reducing power of living cells [122]. The principle of this assay is based on the reduction of a tetrazolium compound, 3-(4,5-dimethylthiazol-2-yl)-5-(3-carboxymethoxyphenyl)-2-(4-sulfofenyl)-2H-tetrazolium (MTS), into a brown formazan by cells in culture, presumably accomplished by NADPH or NADH produced by dehydrogenase enzymes in metabolically active cells. The color intensity reflects the number of viable cells, as dying cells lose the capacity to reduce MTS.

In **Chapter V**, the CellTiter 96 AQueous One Solution cell proliferation assay (Promega, USA) was performed according to the instructions of the manufacturer. At the defined timepoints, cells were washed twice with sterile PBS solution, and 360 µL of a mixture of culture medium (without FBS and phenol red) and MTS reagent (5:1 ratio) was added to each well. The culture plates were kept in the dark, at 37°C in

the CO_2 incubator for 3 h. The absorbance of the MTS reaction was read in a microplate reader (Synergy HT, BioTek, USA) using 100 μL supernatant per well, at 490 nm.

II-6.4.3. 7-AAD/CFSE assay

Cell-Mediated Cytotoxicity Assay Kit contains carboxyfluorosuccinimide ester (CFSE), a green fluorescent probe that labels live target cells and 7-aminoactinomycin D (7-AAD), a red fluorescent probe that labels late apoptotic and necrotic target cells killed in the cytotoxicity assay. CFSE passively diffuses into the cells and its acetate groups are cleaved by intracellular esterases to produce highly fluorescent carboxyfluorescein succinimidyl ester. 7-AAD is a membrane-impermeable dye that is generally excluded from living cells but penetrate dead or damaged cells to label DNA. This assay does not require cell lysis and provides a direct measurement of cytotoxicity instead of indirect indicators. Despite providing roboust data, it has the disadvantage of being time consuming.

In **Chaper IV**, THP-1 cell line viability was assessed by the 7-AAD/CFSE assay as described in the instructions from the manufacturer. After 24 h of incubation with different concentrations of LUVs, untreated and treated cells were collected in tubes by centrifugation at 300 g for 5 min. Then, the cells were incubated for 30 min at 37 °C in a CO_2 incubator with 1 μL of CFSE Staining Solution and 1 μL of 7-AAD Staining Solution. The analyses were performed by flow cytometry.

II-6.4.4. DNA quantification

Cell proliferation can be quantified by measuring the total amount of double stranded DNA (dsDNA) of the samples [123]. DNA content can be determined by several fluorescence methods. For instance, the Pico-Green® dsDNA quantification assay allows the accurately measure of DNA from many sources, detecting selectively as little as 25 pg/ml of dsDNA in the presence of single-stranded DNA, RNA and free nucleotides. Hence, conversely to others methods, contaminants do not interfere with the results. In this assay, the addition of the PicoGreen® fluorescent marker to the samples enables the emission of fluorescence through its specifically binding to the dsDNA. DNA content is further determined through a DNA standard curve, prepared using standard dsDNA solutions with concentrations ranging from 0 to 2 μg/mL.

In the **Chapters III, IV, V and VII**, the Quant-iT™, PicoGreen® dsDNA Assay Kit (Invitrogen, Molecular Probes, USA) was used according to the manufacturer instructions. At the defined time points, samples were collected into sterile Eppendorf tubes containing 1 mL of ultrapure water and kept frozen at -80 °C. Prior to dsDNA quantification, the various specimens were thawed and sonicated for 15 min. Then, 28.7 μL of sample or standard were added to a 96-well opaque plate, mixed with 100 μL of 1X Tris-EDTA (TE) buffer and 71.3 μL of 1X Quant-iT™ PicoGreen® reagent, in a total volume of 200 μL. The plate was incubated at RT for 10 min and read using excitation 485/20 nm and emission 528/20 nm wavelengths in a microplate reader (Synergy HT, BioTek, USA). DNA concentration of the samples was inferred from the standard curve.

II-6.4.5. Total protein synthesis quantification

The quantification of total protein synthesis into the cell culture provides important information on the overall cell physiology, being the colorimetric methods, namely the Lowry method, the bicinchoninic acid assay (BCA) and the biuret method, the most used [124]. BCA assay remains widely recognized for its robustness and sensitiveness for the colorimetric detection and quantitation of total protein [125]. In this assay, BCA is the detection reagent for Cu^{+}, which is formed when Cu^{+2} is reduced by protein in an alkaline environment. A purple-colored reaction product is formed by the chelation of two molecules of BCA with one cuprous ion (Cu^{+}). This water-soluble complex has a linear absorbance at 562 nm with increasing protein concentration.

In **Chapters III, IV and V**, Micro BCA™ Protein Assay kit (Thermo Scientific, Pierce, USA) was used according to the manufacturer's instructions. Using the same cell lysates as for dsDNA quantification, 150 μL of samples or standards in triplicate and 150 μL of working reagent were added to each 96-well plate. The plate was sealed and incubated for 2 h at 37 °C. Then, the absorbance was measured at 562 nm using a microplate reader (Synergy HT, BioTek, USA). Protein concentration was inferred from the standard curve ranging from 0 to 40 μg/mL.

II-6.4.6. Cell morphology

In the **Chapters III, IV, V and VII**, cell morphology was assessed by SEM. In order to maintain cells structure, after washing twice with sterile PBS, cells were fixed with 2.5% glutaraldehyde and kept at 4

°C. Dehydration was performed using increasing concentrations of ethanol (10%, 20%, 40%, 60%, 80%, 90%, 95% and 100%) and air-dried overnight. Then, the samples were sputter-coated (EM ACE600, LEICA) with a thin layer (8–12 nm) of palladium and analyzed by High-Resolution Field Emission Scanning Electron Microscope (Auriga Compact, ZEISS). Microphotographs were recorded at 5 kV at x200, x1000, and x10000 magnifications.

II-6.5. Enzyme-linked Immunosorbent Assay

ELISA is a method for detection and quantification of specific antigens (e.g. peptides, proteins, Abs and hormones) [126]. The principle of this technique relies on antigen-Ab binding, as the antigen is quantified using a solid-phase enzyme immunoassay. A primary Ab of interest is attached to the surface of a multi well-plate and then the sample (antigen) is added and binds to the Ab. Following, a secondary Ab is added to the well, an enzyme is added to bind the Ab and, finally, a substrate for the enzyme is added. The color change is measured using a spectrometer and the antigen concentration is determined using a standard curve.

In the **Chapters III, IV, V and VII**, ELISA was performed to quantify the amount of the pro-inflammatory cytokines (IL-6, TNF-α, IL-23 or IL-17A) in the medium. In the **Chapter III**, it was also used to evaluate the amount of IL-6 capture by the biofunctionalized NPs. In all the cases, samples were collected and frozen at -80°C until further analysis.

For the quantification of the pro-inflammatory cytokines, human IL-6 and TNF-α Standard ABTS ELISA development kits were acquired from Peprotech (USA), human IL-23 TMB ELISA Development Kit was purchased from R&D Systems (USA) and human ELISA MAX™ Deluxe Set IL-17A with TMB subtract was purchased from BioLegend (USA). The quantification was performed according to manufactures' protocol, and the main steps can be observed in **Table I-3**. Briefly, the primary Abs were incubated overnight in a 96-well plate (Nunc-Immuno MicroWell 96-well solid plates). Then, a blocking step was performed to assure that the antigen will be specifically binding to the immobilized Abs. Both the standards and the samples were incubated for 2 h at RT. For the ABTS ELISA kits, in the last step, 100 μL of an 2,2'-azino-bis(3-ethylbenzthiazoline-6-sulphonic acid (ABTS) liquid substrate was added to each well, and a color development was monitored in a microplate (Synergy HT, BioTek, USA) at 405 nm, with a wavelength correction set at 650 nm. For the TMB ELISA kits, the last steps compromise the addition of 100 μL of 3,3′,5,5′-Tetramethylbenzidine (TMB) liquid substrate. The reaction was stopped by the

addition of a stop solution and the absorbance read in a microplate (Synergy HT, BioTek, USA) at 450 nm, with a wavelength correction set at 540 nm.

Table II-3 – ELISA procedure summary.

	IL-6	TNF-α	IL-23	IL-17A
Capture antibody	100 μL, overnight at RT			
Blocking	300 μL, 1% BSA in PBS, 1h at RT			
Sample/Standard	100 μL, 2h at RT			
Biotinylated detection antibody	Rabbit Anti-Human IL-6 100 μL, 2 h at RT	Rabbit Anti-Human TNF-α 100 μL, 2 h at RT	Goat Anti-Human IL-23 100 μL, 2 h at RT	Goat Anti-human IL-17A 100 μL, 2 h at RT
HRP	Avidin-HRP Conjugate 100 μL, 1:2000, 30 min at RT		Streptavidin-HRP 100 μL, 20 min at RT	Avidin-HRP 100 μL, 30 min at RT
Substrate	100 μL of ABTS		100 μL of 1:1 mixture of H_2O_2 and TMB, 20 min at RT	100 μL of TMB solution, 30 min at RT
Stop Solution	-	-	50 μL stop solution	100 μL stop solution
Absorbance	405/560 nm		450/540 nm	
Sensitivity	2000 pg/mL	3000 pg/mL	8000 pg/mL	250 pg/mL

II-6.6. Internalization studies

The cellular uptake of the NPs by the cells was performed using flow cytometry and confocal analyses, as described in the following sub-sections.

II-6.6.1. Flow cytometry analyses

Flow cytometry is a sophisticated instrument with the ability to measure the optical and fluorescence characteristics of a single cell or any other particle in a fluid stream when they pass through a light source [127]. Other parameters can be used to analyze and differentiate the cells including size, granularity and fluorescent features of the cells, resulting from either Abs or dyes. The principle of flow cytometry is related to light scattering and fluorescence emission that occurs as light from the excitation source (commonly a laser beam) strikes the moving cells, giving valuable information about biochemical,

biophysical and molecular aspects of them. Structural and morphological properties of the cells are directly related to the light scattering while the amount of fluorescent probe bound to the cell is proportional to the fluorescence emission derived from a fluorescence probe. Hence, flow cytometry is a powerful tool for detailed analysis of complex populations in a short period of time.

In **Chapter VI**, flow cytometry was performed to quantify and compare the internalization levels along time. Cells were seeded and stimulated as previously described, and afterwards they were incubated with the different fluorescent labelled formulations of NPs for 2, 6 and 24 h at 37 °C in a humidified 5% CO_2 atmosphere. Ch-HA NPs and micelles were added at 50 μg/mL and LUVs at 500 μM. After each incubation time, cells were washed twice with PBS in order to remove any cellular debris or non-internalized NPs, and harvested with TripLE express. Afterwards, cells were centrifuged and cell pellets were re-suspended and fixed with 4% formalin in DPBS and kept in the dark at 4 °C (for less than 1 week) [128]. The analyses of the samples were performed in a BD FACSCalibur™ flow cytometer (Biosciences, Belgium), after and before the addition of 0.11% trypan blue during 1 min, in order to quench the fluorescent signal coming from NPs adsorbed to the cell surface (and also giving an indication of the amount of NPs that were at the cells' surface) [129]. Data were analyzed using Flowing Software 2.5.1. The results were reported as the mean of the percentage of cellular uptake obtained by measuring 20000 cells and normalized relatively to the cells incubated without NPs.

In the same **Chapter VI**, flow cytometry was also used to study the internalization pathways involved in the cellular uptake of the different NP formulations. After seeding the cells as previously described, they were pre-incubated for 30 min at 37 °C in a humidified 5% CO_2 atmosphere with three pharmacological pathway inhibitor solutions: *(i)* 10 μg/mL of chlorpromazine, *(ii)* 1 μg/mL of filipin, or *(iii)* 5 μg/mL of cytochalasin D [20]. Moreover, to study whether the cellular uptake was energy dependent, cells were incubated at 4 °C for 30 min and then incubated with each NP formulation at 4 °C. The time of culture was dependent on previous results of the maximum internalization for each cell type and NP formulation. Cells were collected and analyzed by flow cytometric analyses as previously described.

II-6.6.2. Confocal microscopy analyses

Confocal microscope is broadly used to resolve the detailed structure of specific objects within the cell [130]. Instead of illuminating the whole sample at once, the laser light is focused onto a defined spot

at a specific depth within the sample. Hence, confocal microscopy enables the creation of sharp images of the exact plane of focus, without any disturbing fluorescent light from the background or other regions of the specimen. This tool allows to conveniently visualize structures within thicker objects, and 3D structures can also be analyzed by stacking several images from different optical planes. As such, confocal microscopy has a number of significant advantages over conventional fluorescence microscopy, including increased effective resolution, improved signal-to-noise ratio, depth perception in z-sectioned image, reduced blurring of the image from light scattering and electronic magnification adjustment. Nevertheless, the sample penetration depth is limited.

In **Chapters III and VI**, to assess the NPs internalization and cell morphology microscopy confocal analyses were performed. Cells were seeded as previously described, and at the defined time point (12 h and 6 h for Chapters III and VI, respectively), cells were fixed with 10% formalin in PBS and stored at 4 °C. Then, samples were stained (between each step samples were washed three times with PBS): *(i)* cell membranes were permeated with 0.2% (v/v) Triton X-100 for 5 min, *(ii)* nonspecific proteins were blocked with 3% (w/v) BSA for 30 min, *(iii)* the cytoskeleton was staining with phalloidin (0.25 μg/mL) and cell nuclei labeled with DAPI (1 μg/mL) during 15 min. Images of fluorescent-labeled cells and NPs were obtained by using excitation wavelengths of 405 nm (DAPI), 488 nm (FITC labeled NPs) and 561 nm (phalloidin). Images were acquired using a laser scanning confocal microscopy imaging system (TCS SP8, Leica).

II-7. *IN VIVO* STUDIES

The experimental protocol was approved by the Institutional Ethical Commission (SECVS 109/2016) and followed the European Community Council Directive 86/609/EEC and 2010/63/EU concerning the use of animals for scientific purposes. Animal manipulation was performed only by qualified personnel and following the Principle of the 3Rs.

Animals were housed in pairs in a limited-access rodent facility, with food and water available *ad libitum*. The temperature was maintained at 22.0 ± 0.5 °C with a 12/12 h light/dark cycle (starting at 8:00 a.m.). General health parameters were surveyed twice per week by the resident veterinary in order to check for pain and distress, and the weight of each animal was recorded every week throughout the experimental period. On the day of the experiments, animals were left in the experimental room for 1 h

in order to get acquainted with the surroundings. Efforts were always made to minimize the number of animals used per experiment or test and their potential suffering.

In vivo studies were performed in an experimental carrageenan-induced arthritis rat model to assess the safety and efficacy of the biofunctionalized Ch-HA NPs in the **Chapter VII**.

II-7.1. Arthritis rat model

Several animal models using different species were proposed to study the pathological features of arthritic diseases including pain, synovial inflammation, cartilage degeneration and bone remodeling [118, 131]. They can be categorized into induced or spontaneous models, whereas they are chemically or surgically induced or they occur spontaneously either naturally or due to genetically modification, respectively. Regarding the animal species used in the models of research, they always present advantages and disadvantages. Smaller animal models, such as mice, rats, rabbits and guinea pigs are much easier, cheaper and more readily available than larger animal models, such as horses, pigs and dogs. Nevertheless, the smaller size of those animals makes their anatomical and physiological structure considerably different when compared to humans, which do not happen in larger animal models. Additionally, there are also greater ethical concerns around the use of larger animal models. Based on this, researchers need to make a careful reflection when selecting the animal models. In this thesis, the *in vivo* assays were performed in a rat model as they have a larger joint in comparison with mouse models, allowing an easier intra-articular (IA) injection of the biofunctionalized NPs.

Specifically, arthritis was induced though the IA injection of carrageenan [132]. Structurally, carrageenans are a complex group of polysaccharides composed of repeating galactose-related monomers and are of three main types: lambda, kappa, and iota. The lambda form does not gel strongly at RT and after injection it induces an inflammatory response. Inflammation induced by carrageenan is acute, nonimmune, well-documented and highly reproducible [133, 134]. Fundamental signs of inflammation, including edema, hyperalgesia and erythema, develop immediately by the action of pro-inflammatory agents. Such agents can be generated *in situ* at the site of insult or by infiltrating cells as neutrophils that rapidly migrate to sites of inflammation produce pro-inflammatory cytokines, reactive oxygen and other noxious chemicals such as glutamate, prostaglandins, histamine and serotonin [135]. The inflammatory response is usually quantified by increase in paw size (edema), mechanical allodynia

and hyperalgesia, and also by the histological changes in the synovial membrane (development of synovitis) [135]. Therefore, this model has a vital role in testing novel drugs and nanoformulations.

II-7.2. Behavioral assessments & clinical parameters

Behavioral and clinical parameters were assessed to analyze the edema and nociception of the animals by measuring the knee perimeter, performing the flexion/extension test and the pressure application measurement (PAM), and evaluating the footprint area.

II-7.2.1. Evaluation of knee perimeter

Measuring the joint volume allows the quantification of the severity and the extension of the edema in the developed animal model [136]. The knee circumference is a widely used technique that measures the articular volume using a measuring tape, from an anatomical point previously established. It is a quick, low cost, accessible and easy to handle technique in comparison with other more recent evaluation methods, such as the Leg-O-Meter (equipment to measure the circumference of the lower limb), the water displacement method, optical electronic methods, computerized tomography, among others, all characterized as expensive devices and more time consuming. Nevertheless, the results may be highly influenced by the researcher training.

In this thesis, joint perimeter was assessed as an indirect indicator of the development of an inflammatory state with edema. Knee perimeters of both hind paws were measured using a paper strip with a ruler.

II-7.2.2. Flexion/extension test

Mechanical allodynia is defined as a painful sensation in response to a non-nociceptive stimulus (e.g. innocuous stimuli like light touch) [137]. Unlike inflammatory hyperalgesia that has a protective role, allodynia has no obvious biological utility. It has been reported a higher mechanical allodynia in arthritic diseases.

In this thesis, mechanical allodynia was evaluated by the flexion/extension test, in which animals were submitted to five consecutive flexion/extension movements in both knees. While normal animals do

not vocalize with this stimulus, arthritic rats had an increased number of vocalizations representing high mechanical allodynia. The number of vocalizations during each flexion/extension movement was registered.

II-7.2.3. Pressure application measurement

Mechanical hyperalgesia is defined as an increased pain sensitivity (i.e. increased pain response produced by a stimulus that normally causes pain) [138]. A classical approach to measure mechanical hyperalgesia is the application of noxious pressure to the primary site of injury [139]. The PAM applies a force range of 0–1500 g and allows an accurate behavioral quantification of the mechanical hypersensitivity in rodents with chronic inflammatory joint pain [140].

In this thesis, the PAM method was used as previously described [141]. Briefly, with the animal securely held, an increasing force was gradually applied across the joint until a behavioral response was observed (paw-withdrawal, freezing of whisker movement, wriggling or vocalization) with a cut-off of 5 s. Limb withdrawal threshold (LWT) was recorded as the peak force (in grams force - gf) applied immediately prior to the behavioral response. LWT was measured twice in both paws at 1 min intervals. The mean LWTs were calculated per animal.

II-7.2.4. Footprint area

Gait disturbance has also been detected using the knee joint incapacitation test in rats with knee joint arthritis induced by IA injections of carrageenan [142]. Indeed, analyses of the gait gives important information regarding the sensitivity of the animals to the pain.

In this thesis, the animals performed the catwalk gait analyses and the footprint area of both feet was measured using the Image J software.

II-7.3. Experimental design

In vivo studies were divided in two main experiments: *(i)* assessment of NPs biocompatibility after IA delivery and their therapeutic potential, and *(ii)* evaluation of the NPs therapeutic efficacy and its

comparison with the injection of both free Abs. Both experiments used a carrageenan-induced inflammatory arthritis model of OA.

In the first experiment (**Figure II-17A**), three days after the arthritis induction through an IA injection of carrageenan into the right knee joint of adult male and female Wistar rats, the development of arthritis was verified as previously described (time point 0) and the animals were treated with NPs or NPs+Abs. The control (SHAM) animals were injected with saline during the induction and then treated with the NPs. At the end of the behavioral session, after 4 days of treatment, animals were sacrificed with a lethal dose of pentobarbital and the knee joints were removed for further histological analyses.

In the second *in vivo* experiment (**Figure II-17B**), arthritis induction (after 3 days of the carrageenan injection) in male Wistar rats was assessed as previously described (time point 0), and four groups were tested: *(i)* saline, *(ii)* NPs, *(iii)* Abs and *(iv)* NPs+Abs. At time points 4 and 10, the disease progression was assessed, and in the last time point the animals were sacrificed as described and the joints removed for subsequent histological analyses.

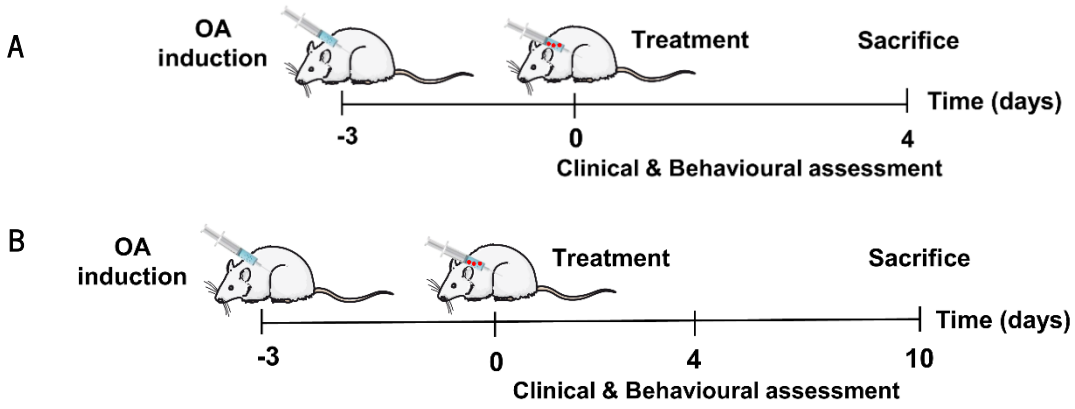

Figure II-17 – Experimental design of (A) Experiment 1 - NPs biocompatibility, and (B) Experiment 2 - therapeutic effects of the biofunctionalized NPs.

II-7.4. Histological analyses

Histological analyses is the gold standard for tissue examination for both qualitative and quantitative measurements in research and medical diagnosis [143]. It is used to assess the inflammation or healing stage and to monitor the presence and distribution of degradation products that dissolved into the surrounding tissue. The process of histological staining takes five key stages: fixation, processing,

embedding, sectioning and staining [144]. Different staining is used to identify specific structures, cells and tissues.

Joints were fixed with 10% (v/v) of formalin, decalcified in Biodec R (BioOptica, Italy) until all the mineral part of the bone was removed. Then, samples were transferred to histological cassettes, processed and embedded in paraffin. Sagittal sections (5 μm) were cut through the knee joint using a manual rotary microtome (Micron Technology, USA). Afterwards, histological sections were analyzed though hematoxylin and eosin (H&E) staining and immunohistochemistry (IHC).

II-7.4.1. Hematoxylin & Eosin Staining

H&E staining is widely used in histology either in research and in medical diagnosis as it allows the visualization of different cell components [145]. Hematoxylin is a natural basic dye that preferentially stains the acidic components (basophilic cell components), such as nucleic acids in the nucleus. Eosin is a synthetic acidic dye that stains basic components of cells with a pink color, including the cytoplasm or connective tissue.

In this thesis, H&E staining was performed following a routine protocol [146]. Briefly, sections were deparaffinized with xylene, rehydrated in ethanol and stained with Gill hematoxylin and alcoholic eosin. Afterwards, the sections were dehydrated and mounted with resinous mounting medium. The histological sections were analyzed under Leica DM750 microscope.

II-7.4.2. Immunohistochemistry

IHC is a technique to specifically label a cellular antigen (e.g. a protein) in tissue sections using Abs [147]. Hence, these localization methods fundamentally rely on the high specificity, affinity and sensitivity of Ab-antigen interactions. Abs are visualized either directly or indirectly (usually via a secondary Ab), with a stain that is easily detectable under a light or electron microscope.

In this thesis, IHC analyses were performed as herein described. After deparaffinization in xylene and rehydration, the tissue sections were subjected to heat-induced antigen-retrieval with sodium citrate buffer (10 mM sodium citrate, 0.05 % (v/v) tween 20 acquired from Bio-Rad (USA), pH 6) for 20 min at 98 °C. To block nonspecific antigen binding, sections were incubated for 30 min with 3 % (w/v) BSA. Sections were incubated with the mouse anti-IL-6 Abs and rabbit anti-TNF-α Abs at 4 °C overnight. Then,

sections were incubated with the secondary Abs Alexa Fluor 488 or 594 for 2 h at RT. After removing unbound secondary Abs, the sections were mounted using aqueous mounting medium. For negative controls, the incubation step for primary Abs was replaced with Abs diluent solution alone. The samples were examined using a confocal laser scanning microscope (TCS SP8, Leica).

II-8. STATISTICAL ANALYSES

All quantitative data are presented as mean ± standard deviation (SD). Statistical analyses were performed using a GraphPad Prism 5.0 software (GraphPad Software, USA). A Shapiro-Wilk normality test was performed to assess data normality. As data do not followed a normal distribution, the Mann–Whitney U test was used when two groups were compared and the Kruskal-Wallis test followed by Dunn's multiple comparison test when more than two groups were compared.

II-9. REFERENCES

1. Islam, S., Bhuiyan, M. A. R. and Islam, M. N., Chitin and Chitosan: Structure, Properties and Applications in Biomedical Engineering. *J Polym Environ*. 2017, *25* (3): p. 854-66.
2. Yang, T. L., Chitin-based materials in tissue engineering: applications in soft tissue and epithelial organ. *Int J Mol Sci*. 2011, *12* (3): p. 1936-63.
3. Jayakumar, R., Chennazhi, K. P., Srinivasan, S., *et al.*, Chitin scaffolds in tissue engineering. *Int J Mol Sci*. 2011, *12* (3): p. 1876-87.
4. VandeVord, P. J., Matthew, H. W., DeSilva, S. P., *et al.*, Evaluation of the biocompatibility of a chitosan scaffold in mice. *J Biomed Mater Res*. 2002, *59* (3): p. 585-90.
5. Hillyard, I. W., Doczi, J. and Kiernan, P. B., Antacid and Antiulcer Properties of the Polysaccharide Chitosan in the Rat. *Proc Soc Exp Biol Med*. 1964, *115*: p. 1108-12.
6. Millner, R. W., Lockhart, A. S., Bird, H., *et al.*, A new hemostatic agent: initial life-saving experience with Celox (chitosan) in cardiothoracic surgery. *Ann Thorac Surg*. 2009, *87* (2): p. e13-4.
7. Dai, T. H., Tanaka, M., Huang, Y. Y., *et al.*, Chitosan preparations for wounds and burns: antimicrobial and wound-healing effects. *Expert Rev Anti-Infe*. 2013, *11* (8): p. 866-76.
8. Zheng, L. Y. and Zhu, J. A. F., Study on antimicrobial activity of chitosan with different molecular weights. *Carbohyd Polym*. 2003, *54* (4): p. 527-30.
9. Chatterjee, S. and Guha, A. K., A study on biochemical changes during cultivation of Rhizopus oryzae in deproteinized whey medium in relation to chitosan production. *Lett Appl Microbiol*. 2014, *59* (2): p. 155-60.
10. Ignatova, M., Kalinov, K., Manolova, N., *et al.*, Quaternized chitosan-coated nanofibrous implants loaded with gossypol prepared by electrospinning and their efficacy against Graffi myeloid tumor. *J Biomat Sci-Polym E*. 2014, *25* (3): p. 287-306.

11. Xu, X. F., Li, Y. G., Shen, Y. Y., *et al.*, Synthesis and in vitro cellular evaluation of novel anti-tumor norcantharidin-conjugated chitosan derivatives. *Int J Biol Macromol*. 2013, *62*: p. 418-25.
12. Ali, A. and Ahmed, S., A review on chitosan and its nanocomposites in drug delivery. *Int J Biol Macromol*. 2018, *109*: p. 273-86.
13. Lima, A. C., Ferreira, H., Reis, R. L., *et al.*, Biodegradable polymers: an update on drug delivery in bone and cartilage diseases. *Expert Opin Drug Deliv*. 2019, *16* (8): p. 795-813.
14. Santo, V. E., Gomes, M. E., Mano, J. F., *et al.*, Chitosan-chondroitin sulphate nanoparticles for controlled delivery of platelet lysates in bone regenerative medicine. *J Tissue Eng Regen M*. 2012, *6*: p. s47-59.
15. Cui, X. J., Guan, X. Y., Zhong, S. L., *et al.*, Multi-stimuli responsive smart chitosan-based microcapsules for targeted drug delivery and triggered drug release. *Ultrason Sonochem*. 2017, *38*: p. 145-53.
16. Hamedi, H., Moradi, S., Hudson, S. M., *et al.*, Chitosan based hydrogels and their applications for drug delivery in wound dressings: A review. *Carbohyd Polym*. 2018, *199*: p. 445-60.
17. da Silva, M. L. A., Crawford, A., Mundy, J. M., *et al.*, Chitosan/polyester-based scaffolds for cartilage tissue engineering: Assessment of extracellular matrix formation. *Acta Biomater*. 2010, *6* (3): p. 1149-57.
18. Neto, J. D. M., Bellato, C. R., Milagres, J. L., *et al.*, Preparation and Evaluation of Chitosan Beads Immobilized with Iron(III) for the Removal of As(III) and As(V) from Water. *J Brazil Chem Soc*. 2013, *24* (1): p. 121-32.
19. Cui, L. Q., Gao, S. S., Song, X. M., *et al.*, Preparation and characterization of chitosan membranes. *Rsc Adv*. 2018, *8* (50): p. 28433-9.
20. Albanna, M. Z., Bou-Akl, T. H., Blowytsky, O., *et al.*, Chitosan fibers with improved biological and mechanical properties for tissue engineering applications. *J Mech Behav Biomed*. 2013, *20*: p. 217-26.
21. Naskar, S., Sharma, S. and Kuotsu, K., Chitosan-based nanoparticles: An overview of biomedical applications and its preparation. *J Drug Deliv Sci Tec*. 2019, *49*: p. 66-81.
22. Carroll, E. C., Jin, L., Mori, A., *et al.*, The Vaccine Adjuvant Chitosan Promotes Cellular Immunity via DNA Sensor cGAS-STING-Dependent Induction of Type I Interferons. *Immunity*. 2016, *44* (3): p. 597-608.
23. Patel, S. and Goyal, A., Chitin and chitinase: Role in pathogenicity, allergenicity and health. *Int J Biol Macromol*. 2017, *97*: p. 331-8.
24. Necas, J., Bartosikova, L., Brauner, P., *et al.*, Hyaluronic acid (hyaluronan): a review. *Vet Med-Czech*. 2008, *53* (8): p. 397-411.
25. Vigetti, D., Karousou, E., Viola, M., *et al.*, Hyaluronan: Biosynthesis and signaling. *Bba-Gen Subjects*. 2014, *1840* (8): p. 2452-9.
26. Litwiniuk, M., Krejner, A., Speyrer, M. S., *et al.*, Hyaluronic Acid in Inflammation and Tissue Regeneration. *Wounds*. 2016, *28* (3): p. 78-88.
27. Fakhari, A. and Berkland, C., Applications and emerging trends of hyaluronic acid in tissue engineering, as a dermal filler and in osteoarthritis treatment. *Acta Biomater*. 2013, *9* (7): p. 7081-92.
28. Huang, G. L. and Huang, H. L., Application of hyaluronic acid as carriers in drug delivery. *Drug Deliv*. 2018, *25* (1): p. 766-72.
29. Collins, M. N. and Birkinshaw, C., Hyaluronic acid based scaffolds for tissue engineering-A review. *Carbohyd Polym*. 2013, *92* (2): p. 1262-79.

30. Muzzarelli, R. A., Greco, F., Busilacchi, A., *et al.*, Chitosan, hyaluronan and chondroitin sulfate in tissue engineering for cartilage regeneration: a review. *Carbohydr Polym*. 2012, *89* (3): p. 723-39.
31. Fahy, E., Cotter, D., Sud, M., *et al.*, Lipid classification, structures and tools. *Bba-Mol Cell Biol L*. 2011, *1811* (11): p. 637-47.
32. Fahy, E., Subramaniam, S., Murphy, R. C., *et al.*, Update of the LIPID MAPS comprehensive classification system for lipids. *J Lipid Res*. 2009, *50*: p. S9-14.
33. Ratnayake, W. M. and Galli, C., Fat and fatty acid terminology, methods of analysis and fat digestion and metabolism: a background review paper. *Ann Nutr Metab*. 2009, *55* (1-3): p. 8-43.
34. Carta, G., Murru, E., Banni, S., *et al.*, Palmitic Acid: Physiological Role, Metabolism and Nutritional Implications. *Front Physiol*. 2017, *8*: p. 1-14.
35. Thotakura, N., Dadarwal, M., Kumar, R., *et al.*, Chitosan-palmitic acid based polymeric micelles as promising carrier for circumventing pharmacokinetic and drug delivery concerns of tamoxifen. *Int J Biol Macromol*. 2017, *102*: p. 1220-25.
36. Hu, F. Q., Zhao, M. D., Yuan, H., *et al.*, A novel chitosan oligosaccharide-stearic acid micelles for gene delivery: Properties and in vitro transfection studies. *Int J Pharmaceut*. 2006, *315* (1-2): p. 158-66.
37. Lee, J. H., Jung, S. W., Kim, I. S., *et al.*, Polymeric nanoparticle composed of fatty acids and poly(ethylene glycol) as a drug carrier. *Int J Pharm*. 2003, *251* (1-2): p. 23-32.
38. Kim, H. C., Kim, E., Ha, T. L., *et al.*, Highly stable and reduction responsive micelles from a novel polymeric surfactant with a repeating disulfide-based gemini structure for efficient drug delivery. *Polymer*. 2017, *133*: p. 102-9.
39. Silva, C. O., Rijo, P., Molpeceres, J., *et al.*, Polymeric nanoparticles modified with fatty acids encapsulating betamethasone for anti-inflammatory treatment. *Int J Pharm*. 2015, *493* (1-2): p. 271-84.
40. Wang, B. and Tontonoz, P., Phospholipid Remodeling in Physiology and Disease. *Annu Rev Physiol*. 2019, *81*: p. 165-88.
41. Singh, R. P., Gangadharappa, H. V. and Mruthunjaya, K., Phospholipids: Unique carriers for drug delivery systems. *J Drug Deliv Sci Tec*. 2017, *39*: p. 166-79.
42. Balazsovits, J. A. E., Mayer, L. D., Bally, M. B., *et al.*, Analysis of the Effect of Liposome Encapsulation on the Vesicant Properties, Acute and Cardiac Toxicities, and Antitumor Efficacy of Doxorubicin. *Cancer Chemoth Pharm*. 1989, *23* (2): p. 81-6.
43. Leonard, R. C. F., Williams, S., Tulpule, A., *et al.*, Improving the therapeutic index of anthracycline chemotherapy: Focus on liposomal doxorubicin (Myocet (TM)). *Breast*. 2009, *18* (4): p. 218-24.
44. van der Veen, J. N., Kennelly, J. P., Wan, S., *et al.*, The critical role of phosphatidylcholine and phosphatidylethanolamine metabolism in health and disease. *Bba-Biomembranes*. 2017, *1859* (9): p. 1558-72.
45. Pasenkiewicz-Gierula, M., Takaoka, Y., Miyagawa, H., *et al.*, Charge pairing of headgroups in phosphatidylcholine membranes: A molecular dynamics simulation study. *Biophys J*. 1999, *76* (3): p. 1228-40.
46. Suk, J. S., Xu, Q. G., Kim, N., *et al.*, PEGylation as a strategy for improving nanoparticle-based drug and gene delivery. *Adv Drug Deliver Rev*. 2016, *99*: p. 28-51.
47. Manjappa, A. S., Chaudhari, K. R., Venkataraju, M. P., *et al.*, Antibody derivatization and conjugation strategies: application in preparation of stealth immunoliposome to target chemotherapeutics to tumor. *J Control Release*. 2011, *150* (1): p. 2-22.
48. Che, J., Okeke, C. I., Hu, Z. B., *et al.*, DSPE-PEG: A Distinctive Component in Drug Delivery System. *Curr Pharm Design*. 2015, *21* (12): p. 1598-605.

49. Hosta-Rigau, L., Zhang, Y., Teo, B. M., *et al.*, Cholesterol - a biological compound as a building block in bionanotechnology. *Nanoscale*. 2013, *5* (1): p. 89-109.
50. Briuglia, M. L., Rotella, C., McFarlane, A., *et al.*, Influence of cholesterol on liposome stability and on in vitro drug release. *Drug Deliv Transl Re*. 2015, *5* (3): p. 231-42.
51. Yeh, Y. C., Creran, B. and Rotello, V. M., Gold nanoparticles: preparation, properties, and applications in bionanotechnology. *Nanoscale*. 2012, *4* (6): p. 1871-80.
52. Ferreira, H., Martins, A., da Silva, M. L. A., *et al.*, The functionalization of natural polymer-coated gold nanoparticles to carry bFGF to promote tissue regeneration. *J Mater Chem B*. 2018, *6* (14): p. 2104-15.
53. de Freitas, L. F., Varca, G. H. C., Batista, J. G. D., *et al.*, An Overview of the Synthesis of Gold Nanoparticles Using Radiation Technologies. *Nanomaterials (Basel)*. 2018, *8* (11): p. 1-23.
54. Carneiro, M. F. H. and Barbosa, F., Gold nanoparticles: A critical review of therapeutic applications and toxicological aspects. *J Toxicol Env Heal B*. 2016, *19* (3-4): p. 129-48.
55. Forman, H. J., Zhang, H. Q. and Rinna, A., Glutathione: Overview of its protective roles, measurement, and biosynthesis. *Mol Aspects Med*. 2009, *30* (1-2): p. 1-12.
56. Lu, S. C., Regulation of glutathione synthesis. *Mol Aspects Med*. 2009, *30* (1-2): p. 42-59.
57. Chiang, Y. T., Yen, Y. W. and Lo, C. L., Reactive oxygen species and glutathione dual redox-responsive micelles for selective cytotoxicity of cancer. *Biomaterials*. 2015, *61*: p. 150-61.
58. Vinluan, R. D., Liu, J. B., Zhou, C., *et al.*, Glutathione-Coated Luminescent Gold Nanoparticles: A Surface Ligand for Minimizing Serum Protein Adsorption. *Acs Appl Mater Inter*. 2014, *6* (15): p. 11829-33.
59. Ma, Y. F., Wang, L. J., Zhou, Y. L., *et al.*, A facilely synthesized glutathione-functionalized silver nanoparticle-grafted covalent organic framework for rapid and highly efficient enrichment of N-linked glycopeptides. *Nanoscale*. 2019, *11* (12): p. 5526-34.
60. Quinn, J. F., Whittaker, M. R. and Davis, T. P., Glutathione responsive polymers and their application in drug delivery systems. *Polym Chem-Uk*. 2017, *8* (1): p. 97-126.
61. Zhang, H. Y., Sun, C. Y., Adu-Frimpong, M., *et al.*, Glutathione-sensitive PEGylated curcumin prodrug nanomicelles: Preparation, characterization, cellular uptake and bioavailability evaluation. *Int J Pharmaceut*. 2019, *555*: p. 270-9.
62. Li, Y., Xiao, K., Luo, J., *et al.*, Well-defined, reversible disulfide cross-linked micelles for on-demand paclitaxel delivery. *Biomaterials*. 2011, *32* (27): p. 6633-45.
63. Ling, X., Tu, J., Wang, J., *et al.*, Glutathione-Responsive Prodrug Nanoparticles for Effective Drug Delivery and Cancer Therapy. *ACS nano*. 2019, *13* (1): p. 357-70.
64. Roberts, M. J., Bentley, M. D. and Harris, J. M., Chemistry for peptide and protein PEGylation. *Adv Drug Deliv Rev*. 2002, *54* (4): p. 459-76.
65. D'Souza A, A. and Shegokar, R., Polyethylene glycol (PEG): a versatile polymer for pharmaceutical applications. *Expert Opin Drug Deliv*. 2016, *13* (9): p. 1257-75.
66. Cabral, H., Miyata, K., Osada, K., *et al.*, Block Copolymer Micelles in Nanomedicine Applications. *Chem Rev*. 2018, *118* (14): p. 6844-92.
67. Owens, D. E. and Peppas, N. A., Opsonization, biodistribution, and pharmacokinetics of polymeric nanoparticles. *Int J Pharm*. 2006, *307* (1): p. 93-102.
68. Lankalapalli, S. and Kolapalli, V. R. M., Polyelectrolyte Complexes: A Review of their Applicability in Drug Delivery Technology. *Indian J Pharm Sci*. 2009, *71* (5): p. 481-87.
69. Carneiro-da-Cunha, M. G., Cerqueira, M. A., Souza, B. W. S., *et al.*, Influence of concentration, ionic strength and pH on zeta potential and mean hydrodynamic diameter of edible polysaccharide solutions envisaged for multinanolayered films production. *Carbohyd Polym*. 2011, *85* (3): p. 522-28.

70. Lima, A. C., Sher, P. and Mano, J. F., Production methodologies of polymeric and hydrogel particles for drug delivery applications. *Expert Opin Drug Del*. 2012, *9* (2): p. 231-48.
71. Zhang, H., Thin-Film Hydration Followed by Extrusion Method for Liposome Preparation. *Methods Mol Biol*. 2017, *1522*: p. 17-22.
72. Mora-Huertas, C. E., Fessi, H. and Elaissari, A., Polymer-based nanocapsules for drug delivery. *Int J Pharmaceut*. 2010, *385* (1-2): p. 113-42.
73. Rivas, C. J. M., Tarhini, M., Badri, W., *et al.*, Nanoprecipitation process: From encapsulation to drug delivery. *Int J Pharmaceut*. 2017, *532* (1): p. 66-81.
74. Wang, Y. C., Li, P. W., Tran, T. T. D., *et al.*, Manufacturing Techniques and Surface Engineering of Polymer Based Nanoparticles for Targeted Drug Delivery to Cancer. *Nanomaterials (Basel)*. 2016, *6* (2): p. 1-18.
75. Pieper, J. S., Hafmans, T., Veerkamp, J. H., *et al.*, Development of tailor-made collagen-glycosaminoglycan matrices: EDC/NHS crosslinking, and ultrastructural aspects. *Biomaterials*. 2000, *21* (6): p. 581-93.
76. Bart, J., Tiggelaar, R., Yang, M., *et al.*, Room-temperature intermediate layer bonding for microfluidic devices. *Lab Chip*. 2009, *9* (24): p. 3481-8.
77. Ahmad, Z., Shepherd, J. H., Shepherd, D. V., *et al.*, Effect of 1-ethyl-3-(3-dimethylaminopropyl) carbodiimide and N-hydroxysuccinimide concentrations on the mechanical and biological characteristics of cross-linked collagen fibres for tendon repair. *Regen Biomater*. 2015, *2* (2): p. 77-85.
78. Montalbetti, C. A. G. N. and Falque, V., Amide bond formation and peptide coupling. *Tetrahedron*. 2005, *61* (46): p. 10827-52.
79. Poole, L. B., The basics of thiols and cysteines in redox biology and chemistry. *Free Radical Bio Med*. 2015, *80*: p. 148-57.
80. Nair, D. P., Podgorski, M., Chatani, S., *et al.*, The Thiol-Michael Addition Click Reaction: A Powerful and Widely Used Tool in Materials Chemistry. *Chem Mater*. 2014, *26* (1): p. 724-44.
81. Traut, R. R., Bollen, A., Sun, T. T., *et al.*, Methyl 4-Mercaptobutyrimidate as a Cleavable Crosslinking Reagent and Its Application to Escherichia-Coli 30s Ribosome. *Biochemistry*. 1973, *12* (17): p. 3266-73.
82. Paiva, A. M., Pinto, R. A., Teixeira, M., *et al.*, Development of noncytotoxic PLGA nanoparticles to improve the effect of a new inhibitor of p53-MDM2 interaction. *Int J Pharmaceut*. 2013, *454* (1): p. 394-402.
83. An, S. Y., Bui, M. P. N., Nam, Y. J., *et al.*, Preparation of monodisperse and size-controlled poly(ethylene glycol) hydrogel nanoparticles using liposome templates. *J Colloid Interf Sci*. 2009, *331* (1): p. 98-103.
84. Treuel, L., Eslahian, K. A., Docter, D., *et al.*, Physicochemical characterization of nanoparticles and their behavior in the biological environment. *Phys Chem Chem Phys*. 2014, *16* (29): p. 15053-67.
85. Dzakpasu, R. and Axelrod, D., Dynamic light scattering microscopy. A novel optical technique to image submicroscopic motions. I: theory. *Biophys J*. 2004, *87* (2): p. 1279-87.
86. Bhattacharjee, S., DLS and zeta potential - What they are and what they are not? *J Control Release*. 2016, *235*: p. 337-51.
87. Panchal, J., Kotarek, J., Marszal, E., *et al.*, Analyzing subvisible particles in protein drug products: a comparison of dynamic light scattering (DLS) and resonant mass measurement (RMM). *The AAPS journal*. 2014, *16* (3): p. 440-51.
88. Kaszuba, M., Corbett, J., Watson, F. M., *et al.*, High-concentration zeta potential measurements using light-scattering techniques. *Philos T R Soc A*. 2010, *368* (1927): p. 4439-51.

89. Silva, R., Ferreira, H., Azoia, N. G., *et al.*, Insights on the mechanism of formation of protein microspheres in a biphasic system. *Mol Pharm*. 2012, *9* (11): p. 3079-88.
90. Muthu, M. S. and Feng, S. S., Pharmaceutical stability aspects of nanomedicines. *Nanomedicine*. 2009, *4* (8): p. 857-60.
91. Hayes, T. L. and Pease, R. F., The scanning electron microscope: principles and applications in biology and medicine. *Adv Biol Med Phys*. 1968, *12*: p. 85-137.
92. De Graef, M., Introduction to conventional transmission electron microscopy. 2003, Cambridge, U.K.: Cambridge University Press. xxi, 718 p.
93. Marrese, M., Guarino, V. and Ambrosio, L., Atomic Force Microscopy: A Powerful Tool to Address Scaffold Design in Tissue Engineering. 2017, *8* (1): p. 7.
94. Lopes, C. D. A., Limirio, P. H. J. O., Novais, V. R., *et al.*, Fourier transform infrared spectroscopy (FTIR) application chemical characterization of enamel, dentin and bone. *Appl Spectrosc Rev*. 2018, *53* (9): p. 747-69.
95. Litman, G. W., Rast, J. P., Shamblott, M. J., *et al.*, Phylogenetic Diversification of Immunoglobulin Genes and the Antibody Repertoire. *Mol Biol Evol*. 1993, *10* (1): p. 60-72.
96. Murphy, K. and Weaver, C., Janeway's Immunobiology, 9th Edition. 2017: p. 1-904.
97. Shepard, H. M., Phillips, G. L., Thanos, C. D., *et al.*, Developments in therapy with monoclonal antibodies and related proteins. *Clin Med*. 2017, *17* (3): p. 220-32.
98. Woodrick, R. S. and Ruderman, E. M., Safety of biologic therapy in rheumatoid arthritis. *Nat Rev Rheumatol*. 2011, *7* (11): p. 639-52.
99. Lerner, R. A., Combinatorial antibody libraries: new advances, new immunological insights. *Nat Rev Immunol*. 2016, *16* (8): p. 498-508.
100. Kouchakzadeh, H., Shojaosadati, S. A., Tahmasebi, F., *et al.*, Optimization of an anti-HER2 monoclonal antibody targeted delivery system using PEGylated human serum albumin nanoparticles. *Int J Pharmaceut*. 2013, *447* (1-2): p. 62-9.
101. Deng, L., Zhang, Y. Y., Ma, L. L., *et al.*, Comparison of anti-EGFR-Fab' conjugated immunoliposomes modified with two different conjugation linkers for siRNA delivery in SMMC-7721 cells. *Int J Nanomed*. 2013, *8*: p. 3271-83.
102. Vandewalle, J., Luypaert, A., De Bosscher, K., *et al.*, Therapeutic Mechanisms of Glucocorticoids. *Trends Endocrin Met*. 2018, *29* (1): p. 42-54.
103. Petros, R. A. and DeSimone, J. M., Strategies in the design of nanoparticles for therapeutic applications. *Nat Rev Drug Discov*. 2010, *9* (8): p. 615-27.
104. Ingle, J. D. a. C., Stanley R, Spectrochemical analysis, ed. Hall, P. 1988.
105. Pap, T. and Korb-Pap, A., Cartilage damage in osteoarthritis and rheumatoid arthritis-two unequal siblings. *Nat Rev Rheumatol*. 2015, *11* (10): p. 606-15.
106. Uysal, O., Sevimli, T., Sevimli, M., *et al.*, *Cell and Tissue Culture: The Base of Biotechnology*, in *Omics Technologies and Bio-Engineering: Towards Improving Quality of Life, Vol 1: Emerging Fields, Animal and Medical Biotechnologies*. 2018. p. 391-429.
107. Kaur, G. and Dufour, J. M., Cell lines: Valuable tools or useless artifacts. *Spermatogenesis*. 2012, *2* (1): p. 1-5.
108. Akkiraju, H. and Nohe, A., Role of Chondrocytes in Cartilage Formation, Progression of Osteoarthritis and Cartilage Regeneration. *J Dev Biol*. 2015, *3* (4): p. 177-92.
109. Ahmed, N., Gan, L., Nagy, A., *et al.*, Cartilage Tissue Formation Using Redifferentiated Passaged Chondrocytes In Vitro. *Tissue Eng Pt A*. 2009, *15* (3): p. 665-73.
110. da Silva, M. L. A., Costa-Pinto, A. R., Martins, A., *et al.*, Conditioned medium as a strategy for human stem cells chondrogenic differentiation. *J Tissue Eng Regen M*. 2015, *9* (6): p. 714-23.

111. Kelly, A., Grabiec, A. M. and Travis, M. A., Culture of Human Monocyte-Derived Macrophages. *Methods Mol Biol*. 2018, *1784*: p. 1-11.
112. Tsuchiya, S., Yamabe, M., Yamaguchi, Y., *et al.*, Establishment and characterization of a human acute monocytic leukemia cell line (THP-1). *Int J Cancer*. 1980, *26* (2): p. 171-6.
113. Bosshart, H. and Heinzelmann, M., THP-1 cells as a model for human monocytes. *Ann Transl Med*. 2016, *4* (21): p. 1-10.
114. Edgell, C. J., McDonald, C. C. and Graham, J. B., Permanent cell line expressing human factor VIII-related antigen established by hybridization. *Proc Natl Acad Sci U S A*. 1983, *80* (12): p. 3734-7.
115. Bauer, J., Margolis, M., Schreiner, C., *et al.*, In vitro model of angiogenesis using a human endothelium-derived permanent cell line: contributions of induced gene expression, G-proteins, and integrins. *J Cell Physiol*. 1992, *153* (3): p. 437-49.
116. Xue, X., Soroosh, P., De Leon-Tabaldo, A., *et al.*, Pharmacologic modulation of RORgammat translates to efficacy in preclinical and translational models of psoriasis and inflammatory arthritis. *Sci Rep*. 2016, *6*: p. 1-17.
117. Binnemars-Postma, K. A., ten Hoopen, H. W. M., Storm, G., *et al.*, Differential uptake of nanoparticles by human M1 and M2 polarized macrophages: protein corona as a critical determinant. *Nanomedicine*. 2016, *11* (22): p. 2889-902.
118. Cope, P. J., Ourradi, K., Li, Y., *et al.*, Models of osteoarthritis: the good, the bad and the promising. *Osteoarthritis Cartilage*. 2019, *27* (2): p. 230-9.
119. Bauer, C., Niculescu-Morzsa, E., Jeyakumar, V., *et al.*, Chondroprotective effect of high-molecular-weight hyaluronic acid on osteoarthritic chondrocytes in a co-cultivation inflammation model with M1 macrophages. *J Inflamm (Lond)*. 2016, *13* (31): p. 1-9.
120. Rampersad, S. N., Multiple Applications of Alamar Blue as an Indicator of Metabolic Function and Cellular Health in Cell Viability Bioassays. *Sensors*. 2012, *12* (9): p. 12347-60.
121. O'Brien, J., Wilson, I., Orton, T., *et al.*, Investigation of the Alamar Blue (resazurin) fluorescent dye for the assessment of mammalian cell cytotoxicity. *Eur J Biochem*. 2000, *267* (17): p. 5421-6.
122. Mosmann, T., Rapid colorimetric assay for cellular growth and survival: application to proliferation and cytotoxicity assays. *J Immunol Methods*. 1983, *65* (1-2): p. 55-63.
123. Freshney, R. I., *Cytotoxicity*, in *Culture of Animal Cells: A Manual of Basic Technique and Specialized Applications, 7th Edition*, FRESHNEY, R.I., Editor. 2016, Wiley-Blackwell.
124. Krohn, R. I., The colorimetric detection and quantitation of total protein. *Curr Protoc Cell Biol*. 2011, *3*: p. 1-28.
125. Reichelt, W. N., Waldschitz, D., Herwig, C., *et al.*, Bioprocess monitoring: minimizing sample matrix effects for total protein quantification with bicinchoninic acid assay. *J Ind Microbiol Biot*. 2016, *43* (9): p. 1271-80.
126. Rudge, T. L., Jr., Sankovich, K. A., Niemuth, N. A., *et al.*, Development, qualification, and validation of the Filovirus Animal Nonclinical Group anti-Ebola virus glycoprotein immunoglobulin G enzyme-linked immunosorbent assay for human serum samples. *PLoS One*. 2019, *14* (4): p. e0215457-8.
127. Adan, A., Alizada, G., Kiraz, Y., *et al.*, Flow cytometry: basic principles and applications. *Crit Rev Biotechnol*. 2017, *37* (2): p. 163-76.
128. dos Santos, T., Varela, J., Lynch, I., *et al.*, Effects of Transport Inhibitors on the Cellular Uptake of Carboxylated Polystyrene Nanoparticles in Different Cell Lines. *Plos One*. 2011, *6* (9): p. 1-10.

129. Gouveia, V. M., Lopes-de-Araujo, J., Costa Lima, S. A., *et al.*, Hyaluronic acid-conjugated pH-sensitive liposomes for targeted delivery of prednisolone on rheumatoid arthritis therapy. *Nanomedicine*. 2018, *13* (9): p. 1037-49.
130. Robinson, J. P., Principles of confocal microscopy. *Method Cell Biol*. 2001, *63*: p. 89-106.
131. Choudhary, N., Bhatt, L. K. and Prabhavalkar, K. S., Experimental animal models for rheumatoid arthritis. *Immunopharmacol Immunotoxicol*. 2018, *40* (3): p. 193-200.
132. Amorim, D., David-Pereira, A., Pertovaara, A., *et al.*, Amitriptyline reverses hyperalgesia and improves associated mood-like disorders in a model of experimental monoarthritis. *Behav Brain Res*. 2014, *265*: p. 12-21.
133. Morris, C. J., Carrageenan-induced paw edema in the rat and mouse. *Methods Mol Biol*. 2003, *225*: p. 115-21.
134. Winter, C. A., Risley, E. A. and Nuss, G. W., Carrageenin-induced edema in hind paw of the rat as an assay for antiiflammatory drugs. *Proc Soc Exp Biol Med*. 1962, *111*: p. 544-7.
135. Radhakrishnan, R., Moore, S. A. and Sluka, K. A., Unilateral carrageenan injection into muscle or joint induces chronic bilateral hyperalgesia in rats. *Pain*. 2003, *104* (3): p. 567-77.
136. Yu, Y. C., Koo, S. T., Kim, C. H., *et al.*, Two variables that can be used as pain indices in experimental animal models of arthritis. *J Neurosci Meth*. 2002, *115* (1): p. 107-13.
137. Lolignier, S., Eijkelkamp, N. and Wood, J. N., Mechanical allodynia. *Pflug Arch Eur J Phy*. 2015, *467* (1): p. 133-39.
138. Sandkuhler, J., Models and Mechanisms of Hyperalgesia and Allodynia. *Physiol Rev*. 2009, *89* (2): p. 707-58.
139. Randall, L. O. and Selitto, J. J., A method for measurement of analgesic activity on inflamed tissue. *Arch Int Pharmacodyn Ther*. 1957, *111* (4): p. 409-19.
140. Leite-Almeida, H., Almeida-Torres, L., Mesquita, A. R., *et al.*, The impact of age on emotional and cognitive behaviours triggered by experimental neuropathy in rats. *Pain*. 2009, *144* (1-2): p. 57-65.
141. Amorim, D., David-Pereira, A., Pertovaara, A., *et al.*, Amitriptyline reverses hyperalgesia and improves associated mood-like disorders in a model of experimental monoarthritis. *Behavioural brain research*. 2014, *265*: p. 12-21.
142. Tonussi, C. R. and Ferreira, S. H., Rat knee-joint carrageenin incapacitation test: an objective screen for central and peripheral analgesics. *Pain*. 1992, *48* (3): p. 421-7.
143. Narayan, R., Monitoring and evaluation of biomaterials and their performance in vivo. Woodhead Publishing series in biomaterials. 2013.
144. Titford, M., Progress in the Development of Microscopical Techniques for Diagnostic Pathology. *J Histotechnol*. 2009, *32* (1): p. 9-19.
145. Gurcan, M. N., Boucheron, L. E., Can, A., *et al.*, Histopathological image analysis: a review. *IEEE Rev Biomed Eng*. 2009, *2*: p. 147-71.
146. Fischer, A. H., Jacobson, K. A., Rose, J., *et al.*, Hematoxylin and eosin staining of tissue and cell sections. *CSH Protoc*. 2008, *3* (4): p. 1-3.
147. van der Loos, C. M., Immunohistochemistry is not the same as immunocytochemistry. *Biotech Histochem*. 2010, *85* (5): p. 325-6.

SECTION 3

NANOPARTICLES DEVELOPMENT AND *IN VITRO* EVALUATION

Chapter III

Interleukin-6 neutralization by antibodies immobilized at the surface of polymeric nanoparticles as a therapeutic strategy for arthritic diseases

Chapter III

Interleukin-6 neutralization by antibodies immobilized at the surface of polymeric nanoparticles as a therapeutic strategy for arthritic diseases[1]

ABSTRACT

Arthritic diseases are disabling conditions affecting millions of patients worldwide. Pro-inflammatory cytokines, particularly interleukin-6 (IL-6), plays a crucial role in inflammation and cartilage destruction. Although the beneficial effects of antibody therapy, its efficacy is limited. Therefore, this work proposes the immobilization of antibodies at the surface of biodegradable polymeric nanoparticles (NPs) to capture and neutralize IL-6. Our system is intended to protect, extend and enhance the therapeutic efficacy after delivery. Chitosan-hyaluronic acid NPs are synthetized as a stable monodisperse population. After determining the maximum immobilization capacity (10 μg/mL), the capture ability was confirmed. Biological assays demonstrate the NPs cytocompatibility with human articular chondrocytes (hACs) and human macrophages. hACs stimulated with macrophage conditioned medium shows the beneficial role of IL-6 capture and neutralization. Biofunctionalized NPs exhibit a prolonged action and stronger efficacy than the free antibodies. In conclusion, this system can be an effective and long lasting treatment for arthritic diseases.

[1]This chapter is based on the following publication:

Lima A. C., Cunha C., Carvalho A., Ferreira H., Neves N. M. Interleukin-6 Neutralization by Antibodies Immobilized at the Surface of Polymeric Nanoparticles as a Therapeutic Strategy for Arthritic Diseases. *Acs Appl Mater Inter*. 2018, *10* (16): p. 13839-50.

III-1. INTRODUCTION

Arthritic diseases are inflammatory joint disorders, associated with synovitis and articular cartilage destruction. The most common forms of arthritis are osteoarthritis (OA) and rheumatoid arthritis (RA) [1]. OA, a local degenerative joint disease, is the leading cause of morbidity and disability in the elderly, affecting around 10% of men and 18% of women over 60 years of age [2]. In contrast to OA, RA is a systemic autoimmune disease that usually involves multiple joints, affecting 0.3-1.0% of the general population [2].

Even though joint damage in OA and RA proceeds via different pathways, in both the normal balance of extracellular matrix (ECM) is disrupted and shifts towards degradation [3]. Cartilage disruption is associated with an increase of the levels of pro-inflammatory cytokines such as tumor necrosis factor-α (TNF-α) and interleukins (IL, particularly IL-1β and IL-6), mainly produced by mononuclear cells, chondrocytes or synoviocytes [1]. These cytokines increases the production of catabolic factors and down-regulates the anabolic mediators [4, 5]. Hence, pro-inflammatory cytokines up-regulates injurious enzymes, especially matrix metalloproteinases. Simultaneously, they inhibit the production of their physiological regulators, stimulate the production of nitric oxide, and hinder the synthesis of ECM components such as collagen type II and aggrecan.

IL-6 is a key mediator in the pathophysiology of OA and RA, as it regulates a wide range of fundamental biological activities, including acute-phase responses, inflammation, and immune responses [6]. Indeed, OA and RA patients present high concentrations of this pleiotropic cytokine [7], and many efforts are being made to create biosensors to monitor IL-6 secretion *in vivo* [8]. In addition, higher levels of IL-6 in OA was found to be a significant predictor of superior risk of cartilage loss and reduced response to treatment [9]. Thus, strategies targeting IL-6 or its receptors are promising treatments for arthritic diseases [10]. The first humanized anti-IL-6 receptor antibody (Ab), tocilizumab, has demonstrated its outstanding clinical efficacy and tolerable safety profile in phase III clinical trials for RA patients, resulting in its worldwide approval to treat moderate-to-severe active RA. This successful approach led to the development of other IL-6 inhibitors, including fully human anti-IL-6 receptor mAb (sarilumab, sirukumab and olokizumab) [11]. This cytokine is being also considered the most interesting new target for OA treatment with clinical trials currently in progress [ClinicalTrials.gov Identifier: NCT02477059].

Although these treatments seem very attractive, systemic injection of biological agents are associated with serious side effects, such as risk of infection, administration reactions, congestive heart failure, demyelinating diseases, hyperlipidemia, among other conditions that affect patient health [12]. In this

sense, intra-articular (IA) injections offers several benefits by achieving high local bioavailability, reducing systemic exposure and requiring lower doses [13, 14]. However, due to the rapid clearance of Abs by the synovium, the therapy has limited efficacy. Hence, there is an unmet need for the development of new effective approaches, with prolonged efficacy and reduced side effects.

Nanoparticles (NPs) are promising approaches to solve limitations of conventional therapies [14]. The unique properties of NPs make them highly attractive for the design of novel modalities for arthritis treatment. Nanoscale features can be used to protect the therapeutic agent from degradation and to have targeted and controlled delivery, which improves drug efficacy, reduces the dosage and significantly reduces the side effects. Actually, polymeric NPs are one of the most studied strategies for nanomedicine [15]. Polymers are widely used as building blocks, due to the flexible design based on functionalization, macromolecular synthesis methods, and polymer diversity. Regarding degradation properties, biodegradable polymeric NPs are highly preferred for medical applications, providing outstanding bioavailability, stability, compatibility and controlled release [16]. In this work, natural-derived polymers were used, namely chitosan (Ch) and hyaluronic acid (HA). They possess a high level of functional groups, such as amino (NH_2) and carboxylic acid (COOH) groups that can be further modified and functionalized with other polymers, crosslinkers and/or biomolecules [17, 18]. Ch, the second most abundant polysaccharide in nature, is particularly attractive due to its advantages, such as non-cytotoxicity, low immunogenicity, high stability and reasonable cost [19, 20]. Although there are some studies reporting Ch as vaccine adjuvant [21], the capacity to promote cellular immunity is related with the deacetylation degree (DD) of the polymer [22]. Indeed the DD and immunogenicity are inversely correlated in this biomaterial. Therefore, in this work, Ch with a high degree of deacetylation was used to avoid any immunogenicity. HA is a natural component of the ECM of articular cartilage and synovial fluid. Due to the interaction with CD44 receptors of the cells, especially chondrocytes, HA plays an important role on cartilage function [23]. Nonetheless, HA physicochemical and biological properties depend on its molecular weight (MW) [24]. High MW HA displays anti-inflammatory and immune-suppressive properties, whereas low MW HA is a potent pro-inflammatory molecule. It has been reported that HA with MW of 700–6000 kDa are the best suited for cartilage repair [19].

The aim of this study was to develop a carrier intended for IA administration and allowing the capture and neutralization of IL-6, a crucial pro-inflammatory mediator in arthritic joints (**Figure III-1**). Ch and HA were used to produce biofunctionalized NPs with anti-IL-6 Abs immobilized at NPs' surface. The maximum immobilization of Abs and the capture capability was assessed. NPs cytocompatibility was validated by their culturing with human articular chondrocytes (hACs) and human macrophages. Our system was also

validated by stimulating hACs with macrophage conditioned medium, and then treating with biofunctionalized NPs or the free Abs. Considering the drawbacks of the current treatments, we hypothesized that this strategy offers a maximum therapeutic effect of the immobilized Abs, avoiding unnecessary exposure to healthy tissues and systemic side-effects.

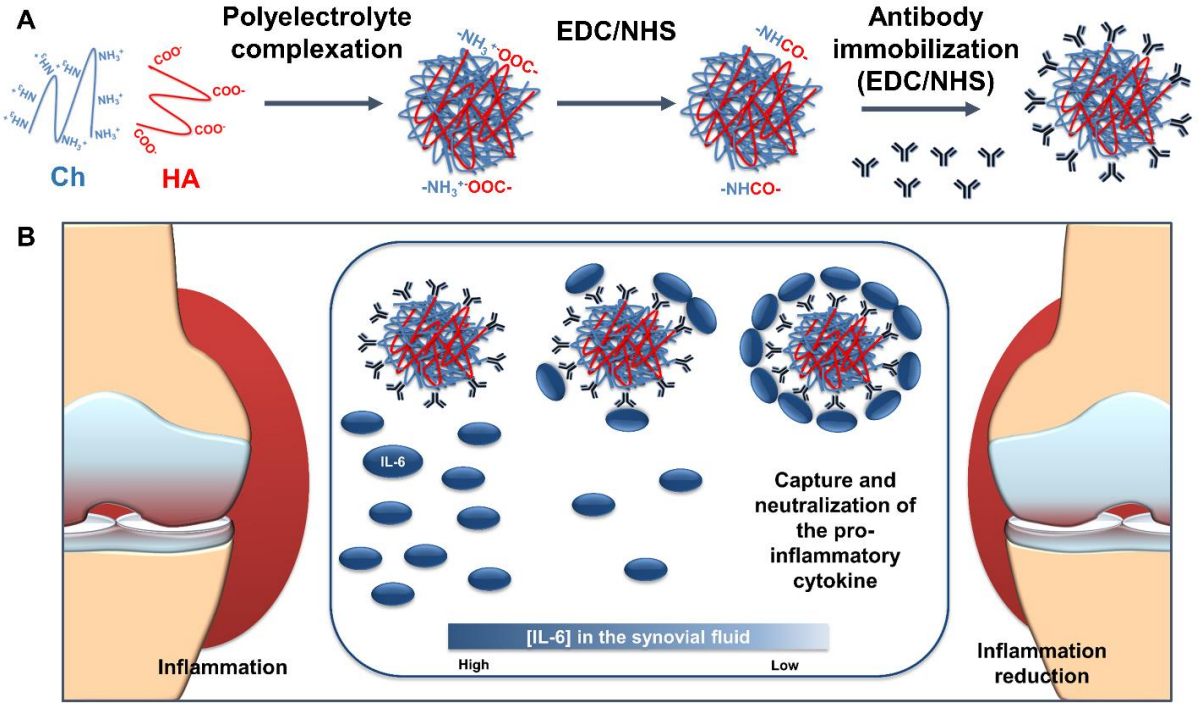

Figure III-1 – Schematic illustration of the biofunctionalized NPs role in arthritis treatment. (A) Production of the biofunctionalized polymeric NPs. (B) Inflammation reduction in the synovial fluid after the neutralization of IL-6 by the NPs. Abbreviations: Ch, chitosan; HA, hyaluronic acid; EDC, ethyl-3-(3-(dimethylaminopropyl)carbodiimide; NHS, N-hydroxysuccinimide.

III-2. MATERIALS AND METHODS

This section provides details on the NPs preparation and characterization, the maximum Abs immobilization and their performance in capture as well as their cytocompatibility and biologic activity.

III-2.1. Materials

Ch with a MW of 150 kDa and 95% of DD was purchased from Heppe Medical Chitosan GmbH (Germany). HA with a MW of 750 kDa was bought from Lifecore Biomedical (USA). Mouse monoclonal anti-IL-6 Abs and human IL-6 full length protein was purchased from Abcam (UK). Alexa Fluor® 594 donkey

anti-mouse IgG, Roswell Park Memorial Institute (RPMI)-1640 media and Fetal Bovine Serum (FBS) were purchased from Thermo Fisher Scientific (USA). Human IL-6 Standard ABTS ELISA Development Kits and human basic Fibroblast Growth Factor (bFGF) was acquired from Peprotech (USA). CD14 MicroBeads and recombinant human granulocyte macrophage colony-stimulating factor (GM-CSF) was obtained from Miltenyi Biotec (USA). All other reagents were purchased from Sigma-Aldrich (USA).

III-2.2. NPs preparation

Ch-HA NPs were prepared by polyelectrolyte complexation of both natural-based polyelectrolytes. Briefly, Ch was dissolved in 1% (v/v) acetic acid, while HA was dissolved in ultrapure water, overnight at room temperature (RT). Both solutions were filtered through a 0.22 μm pore membrane. The NPs formation occurred spontaneously when the HA solution was added dropwise at 1 mL/min rate to the Ch solution under strong magnetic stirring (600 rpm). Different initial polymers concentration (0.25, 0.5 and 1 mg/mL) and pH values (3, 4, 5, 6 and 7) were used to evaluate the influence of these parameters on the properties of the NPs.

During preparation, NPs were stabilized through carbodiimide chemistry. 1-ethyl-3-(3-(dimethylaminopropyl)carbodiimide (EDC)/N-hydroxysuccinimide (NHS) reagents were dissolved in 0.1 M MES buffer (pH 4.7) with 0.9% (w/w) NaCl. Five different EDC/NHS ratios were tested, namely 400/100, 100/400, 200/200, 50/200 and 200/50 mM.

For fluorescence biological assays, 200 μL of fluorescein isothiocyanate (FITC, 2 mg/mL in ethanol:water, 1:10) was added to the Ch solution before the NPs formation.

To remove unreacted compounds, the NPs were washed twice with ultrapure water by centrifugation (30 min, 4000 rpm at 20 °C) using Vivaspin 300 kD Filter Units (Fisher Scientific, USA). To avoid NPs aggregation, glucose at 2 mg/mL was added before centrifugation [25].

III-2.3. NPs characterization

The developed NPs were characterized regarding their size distribution, surface charge, stability and morphology, as described in the following sub-sections.

III-2.3.1. Size distribution and zeta potential measurements

The size and polydispersity index (PDI) of the produced NPs were assessed by dynamic light scattering (DLS) and the zeta potential was determined by laser Doppler micro-electrophoresis using a Zetasizer Nanoseries ZS equipment (Malvern Instruments, Portugal). The measurements were performed at 25 °C using samples diluted in ultra-pure water (1:20; v/v).

III-2.3.2. Stability studies

For pH stability assessment the pH was increased until 7.4 using NaOH 1M. For storage stability, the NPs suspensions were kept at 4 °C under static conditions. During the experimental time (6 months), it was determined the size, PDI and zeta potential, as just described.

III-2.3.3. NPs morphology

Morphological analyses of the developed Ch-HA NPs were performed by scanning electron microscopy (SEM) and atomic force microscopy (AFM). Prior to analysis, Ch-HA NPs were diluted in water (1:20; v/v) and disposed into the surface of a glass slide for air-dry. For SEM analyses, the NPs were sputter-coated with palladium (EM ACE600, LEICA) and analyzed using High-Resolution Field Emission Scanning Electron Microscope (Auriga Compact, ZEISS). AFM measurements were performed using a MultiMode STM microscope controlled by a NanoScope III from Digital Instruments system, operating in tapping mode at a frequency of 1 Hz.

III-2.4. Abs immobilization determination

The anti-IL-6 Abs were immobilized at the surface of the optimized Ch-HA NPs. In order to determine the NPs' maximum immobilization capacity, a range of primary Abs concentrations were tested (from 5 to 20 μg/mL). First, the anti-IL-6 Abs were activated with a solution of 50/200 mM EDC/NHS in 0.1 M MES buffer for 15 min. Then, the NPs were incubated with the activated anti-IL-6 Abs, overnight at 4 °C. To remove the unbound Abs, the biofuncionalized NPs were washed twice by centrifugation, as previously described.

To determine the degree of anti-IL-6 Abs immobilization, the biofunctionalized NPs were incubated with the secondary Abs Alexa Fluor® 594 solution for 1 h at RT. As negative control, NPs without immobilized Abs were used (0 μg/mL). After centrifugation, the fluorescence of the unbound secondary Abs (in supernatant) were determined using an excitation-emission wavelengths of 590/20 - 645/40 nm, respectively, in a microplate reader (Synergy HT, BioTek, USA). The concentration of the anti-IL-6 Abs at the NPs surface corresponds to the difference between the initial and unbound secondary Abs.

III-2.5. IL-6 capturing

Ch-HA NPs biofunctionalized with anti-IL-6 Abs (5-20 μg/mL) were incubated with 1.25 μg/mL of human IL-6 full length protein, overnight at RT. After centrifugation, the supernatants were collected and the unbound IL-6 was assessed using the ELISA Development Kit. The amount of IL-6 captured by the biofunctionalized NPs corresponds to the difference between the initial and unbound amount of the added cytokine.

III-2.6. Biological Assays

In order to assess the cytocompatibility and biological effects of the developed NPs, the cell isolation and culture, viability, proliferation, protein content and morphology were performed as described in the following sub-sections.

III-2.6.1. Isolation and cell culture

hACs were isolated from knee cartilage samples collected from arthroplasties surgeries biopsies. Samples were obtained through the cooperation agreement between Centro Hospitalar do Alto Ave, Guimarães, Portugal, and 3B's Research Group, and after informed donor consent. Cells were isolated by enzymatic digestion, according to a previously described protocol [26]. hACs cells were cultured in Dulbecco's modified Eagle's medium (DMEM), supplemented with 10% FBS, 10 mM HEPES buffer, L-lanyl-L-glutamine, MEM Non Essential Aminoacids, 100 units/mL of penicillin, 100 μg/mL of streptomycin and 10 ng/mL human bFGF, and incubated at 37 °C in a humidified 5% CO_2 atmosphere.

The human monocytic cell line THP-1 was maintained in complete RPMI, containing RPMI-1640 media supplemented with 2 mM L-glutamine, 100 units/mL of penicillin, 100 μg/mL of streptomycin, 10 mM HEPES buffer and 10% FBS.

Human monocyte-derived macrophages were generated from peripheral blood mononuclear cell (PBMCs). Buffy coats from healthy donors were obtained after written informed consent at the Hospital de Braga, Braga, Portugal. Briefly, PBMCs were enriched from buffy coats by density gradient using Histopaque®-1077. Cells present in the enriched mononuclear fraction were washed twice in PBS and re-suspended in RPMI-1640 culture medium with 2 mM glutamine and 2 g/L $NaHCO_3$ supplemented with 10% human serum, 100 units/mL of penicillin, 100 μg/mL of streptomycin and 10 mM HEPES buffer. Monocytes were then separated by positive selection using magnetically labelled CD14 MicroBeads on a MiniMACS separator. Isolated monocytes were re-suspended in complete RPMI medium and seeded at 5×10^5 cells per well in 24-well plates for 7 days in the presence of 20 ng/mL of GM-CSF. Acquisition of macrophage morphology was confirmed by visualization in a BX61 microscope (Olympus, Japan).

III-2.6.2. Cell seeding

For hACs seeding, cells at 5×10^4 cells per well were added to tissue culture polystyrene (TPCS) coverslips in 24-well plates. After cell attachment during 5h, culture medium was added to a final volume of 1 mL. Different concentrations of sterilized Ch-HA NPs were added to hACs subsequently to 24 h of incubation.

For the induction of THP-1 cell differentiation, cells were seeded at 5×10^5 cells per well in 24-well plates in cRPMI with 100 nM phorbol 12-myristate-13-acetate (PMA) for 24 h. After incubation, non-attached cells were removed by aspiration, and the adherent cells were washed three times with cRPMI. To ensure reversion of cells to a resting macrophage phenotype before stimulation, cells were incubated for an additional 48 h in cRPMI without PMA. For stimulation and retrieval of conditioned media, cells were further incubated for 24 h with 100 ng/mL of lipopolysaccharide (LPS) in fresh media and the supernatants were collected and stored at -80 °C. IL-6 production by cells was assessed in the supernatants by commercial ELISA. Then, Ch-HA NPs were added at different concentrations.

Regarding the human primary macrophages, after 7 days in the presence of GM-CSF, culture medium was replaced and different concentrations of Ch-HA NPs were added.

Cells cultured without NPs (only with culture medium) were used as control. After 1, 2, 3 and 7 days of culture with NPs, the different samples in triplicate were washed with sterile PBS and analyzed

regarding cell viability (MTS assay), cell proliferation (DNA quantification), total protein synthesis and SEM analyses.

III-2.6.2.1 *Cell viability*

The metabolic activity of cells treated or not with different concentrations of Ch-HA NPs was determined by MTS assay (CellTiter 96 AQueous One Solution, Promega, USA), according to the instructions of the manufacturer. Briefly, a mixture of culture medium, without FBS and phenol red, and MTS reagent (5:1 volume ratio) were added to each well. Samples were incubated for 3 h at 37 °C in a humidified 5% CO_2 atmosphere. The absorbance was read in triplicate at 490 nm, using a microplate reader (Synergy HT, BioTek, USA).

III-2.6.2.2 *Cell proliferation*

Cell proliferation was assessed using a fluorimetric dsDNA quantification kit (Quant-iT™, PicoGreen®, Molecular Probes, Invitrogen, USA). First, cell samples were transferred to Eppendorf tubes containing 1 mL of ultrapure water and frozen at -80 °C until further analysis. Prior to DNA quantification, samples were defrosted and sonicated for 15 min. DNA standards were prepared at concentrations ranging from 0 to 2 μg/mL in ultrapure water. To each well of an opaque 96-well plate (Falcon) were added 28.7 μL of sample or standard (n=3), 71.3 μL of PicoGreen solution, and 100 μL of Tris-EDTA (TE) buffer. The plate was incubated for 10 min in the dark, and the fluorescence of each sample was measured in a microplate reader (Synergy HT, BioTek, USA), using an excitation wavelength of 485 nm and an emission wavelength of 528 nm. DNA concentration of the samples was inferred from the standard curve.

III-2.6.2.3 *Total protein*

Total protein content was quantified using a Micro BCA protein assay kit (Thermo Scientific, Pierce, USA), according to the manufacturer's instructions. Briefly, samples were collected in triplicate as described above. Standards were prepared in ultrapure water in concentrations ranging from 0 to 40 μg/mL. Then, 150 μL of samples or standards in triplicate and 150 μL of working reagent were added to each 96-well plate. The plate was sealed and incubated for 2 h at 37 °C. Then, the absorbance was

measured at 562 nm using a microplate reader (Synergy HT, BioTek, USA). Protein concentration was inferred from the standard curve.

III-2.6.2.4 *SEM analyses*

SEM was used to analyze the morphology of cells in the presence of Ch-HA NPs. Briefly, cells were fixed with 2.5% glutaraldehyde and kept at 4 °C. Dehydration was performed using increasing concentrations of ethanol (10, 20, 40, 60, 80, 90, 95 and 100%). Then, the samples were sputter-coated (EM ACE600, LEICA) with a thin layer (8-12 nm) of palladium and analyzed by High-Resolution Field Emission Scanning Electron Microscope (Auriga Compact, ZEISS). Microphotographs were recorded at 5 kV with magnifications of 200, 1000 and 10000 x.

III-2.6.3. NPs internalization

For internalization assays, hACs were seeded at a concentration of $2x10^4$ cells per well on μ-slides (Ibidi, Germany) for confocal microscopy analysis. Ch-HA NPs functionalized or not with the anti-IL-6 Abs were added at a concentration of 50 μg/mL to the cultured cells. After 12 h, cells were fixed with 10% formalin in PBS and stored at 4 °C. Then, samples were stained (between each step samples were washed three times with PBS): *(i)* cell membranes were permeated with 0.2% (v/v) Triton X-100 for 5 min, *(ii)* nonspecific proteins were blocked with 3% (w/v) BSA for 30 min, *(iii)* the cytoskeleton was staining with phalloidin (0.25 μg/mL) and cell nuclei labeled with DAPI (1 μg/mL) during 15 min. Images of fluorescent-labelled cells and NPs were obtained by using excitation wavelengths of 405 nm (DAPI), 488 nm (FITC labelled NPs) and 561 nm (phalloidin). Images were acquired using a laser scanning confocal microscopy imaging system (TCS SP8, Leica).

III-2.6.4. Biofunctionalized NPs capturing ability of IL-6

hACs were seeded as previously described. After cell attachment, hACs were stimulated for 24 h with monocyte-derived macrophage conditioned medium containing 500 pg/mL of IL-6. hACs cultured without macrophage conditioned medium (only culture medium) were used as controls. Three different conditions were tested: *(i)* no treatment, *(ii)* treatment with biofunctionalized NPs presenting a concentration of anti-IL-6 Abs equal to 1 μg/mL; and *(iii)* treatment with soluble anti-IL-6 Abs at a

concentration of 1 μg/mL. After 1, 3, 7 and 14 days, samples were collected and evaluated regarding cell viability, proliferation, total protein synthesis and SEM analyses as previously described. The amount of IL-6 in the supernatants was assessed by ELISA. During the time of experiment 300 μL of fresh media was added each 3 days, but no media was removed in order to keep the NPs and the conditioned media in contact with the cells.

III-2.7. IL-6 quantification

For the quantification of the IL-6, human sandwich IL-6 ELISA Kit was performed according to the manufacturer procedure. ABTS liquid substrate was added to each well and color development was assessed by measuring the absorbance at 405 and 650 nm, in a microplate reader (Synergy HT, BioTek, USA). The IL-6 concentration was inferred from the standard curve.

III-2.8. Statistical analyses

Data are presented as the mean ± standard deviation (SD) of at least three independent assays. Statistical analyses were performed using GraphPad Prism Software. First, a Shapiro-Wilk test was used to establish the assumption of data normality. Since data not followed a normal distribution, a nonparametric test was used (Kruskal-Wallis test) followed by Dunn's test where $p < 0.01$ was considered statistically significant.

III-3. RESULTS

Ch-HA NPs characterization, biofunctionalization, capability to capture the pro-inflammatory cytokine as well as biological effects are herein described.

III-3.1. Characterization of Ch-HA NPs

Ch-HA NPs were successfully prepared by polyelectrolyte complexation. The influence of the initial polymer concentration and pH values on size, PDI and zeta potential of Ch-HA NPs are shown in **Figure III-2A** and **Table III-1**, respectively. Both particle size and PDI increased with the increase of the concentration of Ch and HA polymers, within a linear range relationship. Concerning the aim of this study,

it was selected the condition that originates smaller NPs (0.25 mg/mL) to obtain a higher surface area for enlarged biofunctionalization. Regarding the influence of pH (**Table III-1**), it can be inferred that the initial pH of Ch solution has a huge influence on particle size and PDI, in contrast with the initial pH of HA solution. The same behavior was observed for zeta potential measurements. The initial pH of the Ch solution has a significant impact on the zeta potential, presenting a higher value at pH 5. The pH of the HA solution has no impact over the zeta potential, but higher values were also found for a pH value of 5. Since we aimed to produce monodisperse NPs with higher stability, we selected pH 5 for both Ch and HA solutions. Additionally, it was observed that adding glucose to the NPs suspension before centrifugation avoids their aggregation (121.8 ± 2.4 nm, 0.11 ± 0.01 of PDI and 178.8 ± 51.1 nm, 0.24 ± 0.08 of PDI in the presence or in the absence of glucose, respectively, after centrifugation). Although the Ch-HA NPs were stable in water, the particle size and PDI increased at pH 7.4. In order to increase the NPs stability at physiological pH, carbodiimide chemistry (EDC/NHS) was tested. As shown in **Figure III-2B**, the optimal concentrations of EDC/NHS for stabilization were 50 mM/200 mM, since it is required lower concentrations of reagents to have the same effect over NPs size distribution.

Storage stability was also assessed, and as shown in **Figure III-2C** the produced NPs were stable during time without a significant increase of size and PDI for at least 6 months.

From SEM and AFM analyses (**Figure III-2D** and **E**, respectively), it was possible to observe that Ch-HA NPs presented a spherical shape with dimensions around 130 nm, which is in agreement with the DLS measurements.

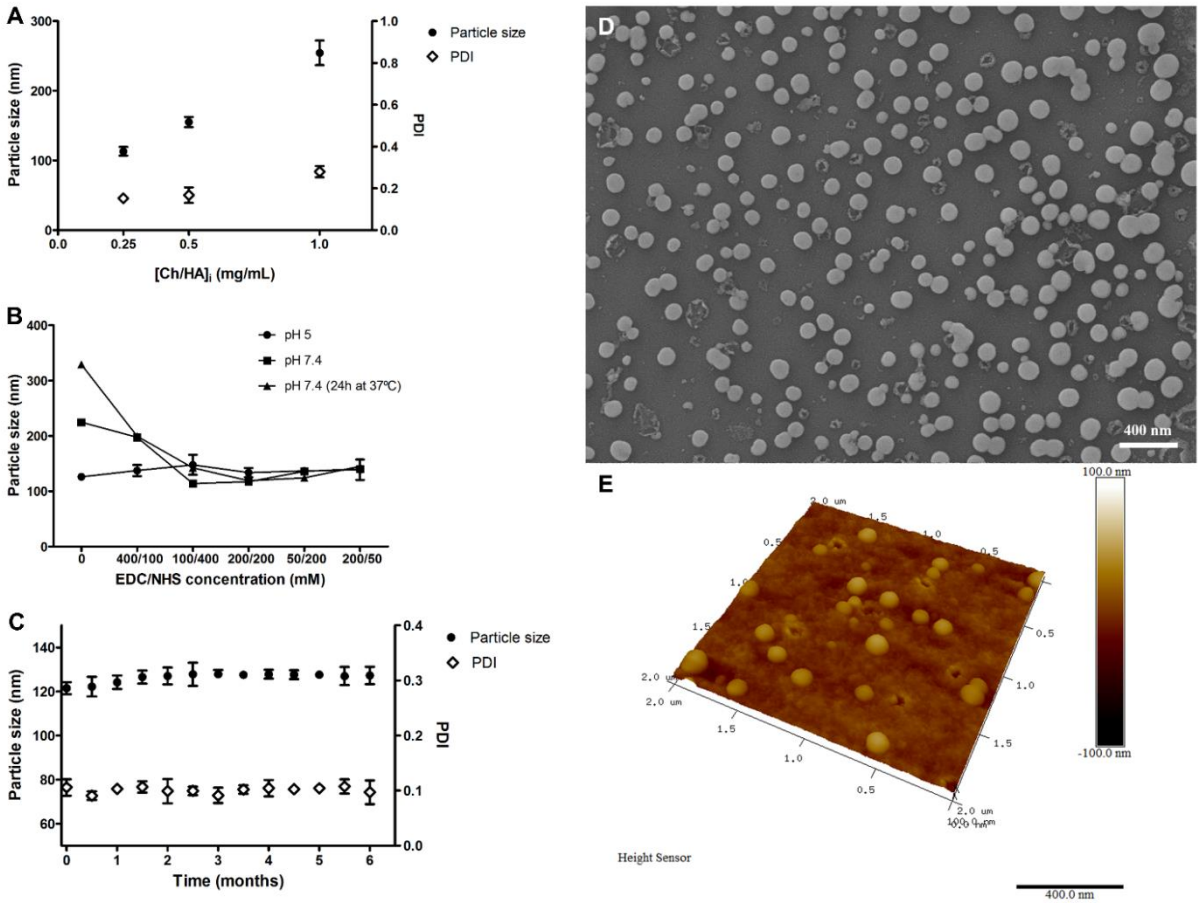

Figure III-2 – (A) Particle size and polydispersity index (PDI) of Ch-HA NPs obtained for different initial concentrations of Ch and HA, at pH 5. (B) Influence of EDC/NHS concentration on the particle size at pH 5 and 7.4. (C) Stability evaluation of NPs kept in water at 4°C for 6 months. (D) SEM and (E) AFM micrographs of the produced Ch-HA NPs.

Table III-1 – Influence of pH values on the diameter, PDI and zeta potential of Ch-HA NPs. The pH of the solutions used to produce the selected NPs are highlighted in the table.

Solution pH		Size (nm)	PDI	Zeta Potential (mV)
Ch	HA			
3		859.1 ± 427.6	0.66 ± 0.26	5.77 ± 0.58
4		1134.0 ± 139.1	0.16 ± 0.19	7.10 ± 2.24
5	**5**	**121.8 ± 2.4**	**0.11 ± 0.01**	**25.12 ± 1.86**
6		430.5 ± 82.6	0.31 ± 0.18	5.87 ± 4.43
7		3337.0 ± 640.4	0.78 ± 0.31	-19.68 ± 3.31
	4	128.2 ± 13.5	0.20 ± 0.04	16.33 ± 2.40
5	6	121.3 ± 6.7	0.19 ± 0.04	16.96 ± 5.38
	7	117.8 ± 4.29	0.17 ± 0.08	18.00 ± 0.99

III-3.2. Optimization of Abs immobilization at the NPs surface

Anti-IL-6 Abs were covalently immobilized at the NPs surface using the same chemistry previously described. In order to quantify the amount of primary Abs immobilized at the NPs surface, an indirect method was used, based on the measurement of the fluorescence of the unbound secondary Abs (**Figure III-3**). Higher fluorescence values of secondary Abs correspond to lower concentrations of immobilized anti-IL-6 Abs. As can be observed in **Figure III-3**, concentrations above 10 μg/mL displayed significantly lower values of fluorescence intensity than control (0 μg/mL). Moreover, these concentrations did not display significantly differences between them. Therefore, the maximum immobilization capacity of anti-IL-6 Abs is 10 μg/mL. After this point, the NPs surface becomes saturated and the fluorescence intensity reaches a plateau.

Afterwards Abs immobilization, the biofunctionalized NPs presented 132.05 ± 2.58 nm of diameter, 0.12 ± 0.01 of PDI and +20.07 ± 2.10 mV of zeta potential. Additionally, the NPs remained stable.

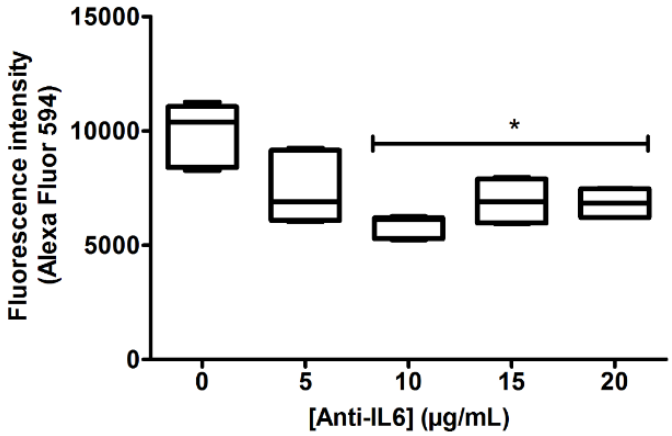

Figure III-3 – Box plot of anti-IL-6 Abs immobilization at 0 to 20 μg/mL concentrations. Asterisk (*) denotes significant differences (p<0.01) compared to control (0 μg/mL).

III-3.3. Capture of IL-6

To confirm the ability of the primary anti-IL-6 Abs immobilized at the NPs' surface to capture and neutralize IL-6, a human full length recombinant IL-6 protein was added at 1.250 μg/mL to the biofunctionalized NPs. The amount of unbound IL-6 determined in NPs without functionalization (**Table III-2**) revealed their ineffectiveness of capturing IL-6. For biofunctionalized NPs, the maximum capture (1.222 ± 0.020 μg/mL) was achieved with an initial Abs concentration of 10 μg/mL, which comprises

around 98% of capture. No significant differences were found for higher initial concentrations of anti-IL-6 Abs.

Table III-2 – Amount of the human recombinant IL-6 captured by biofunctionalized NPs.

Initial [anti-IL6 Abs] (μg/mL)	[IL-6] unbound (supernatant) (μg/mL)	[IL-6] capture by NPs (μg/mL)	% capture
0	1.245 ± 0.025	-	-
5	0.068 ± 0.007	1.182 ± 0.007	94.56 ± 0.56
10	0.028 ± 0.020	1.222 ± 0.020	97.79 ± 1.6
15	0.067 ± 0.017	1.183 ± 0.017	94.64 ± 1.36
20	0.057 ± 0.018	1.193 ± 0.018	95.44 ± 1.44

III-3.4. Biological assays

Biological assays were performed to assess the NPs cytocompatibility and evaluate the biologic effects of IL-6 capture by the biofunctionalized NPs.

III-3.4.1. NPs cytocompatibility

To use Ch-HA NPs as a platform of Abs carrying to treat arthritic diseases, it was performed an assessment of their potential toxicity for: *(i)* hACs, *(ii)* human monocyte-like cell line, THP-1, and *(iii)* human primary macrophages. hACs isolated from diseased knee arthroplasties have a phenotype associated with arthritic diseases, being a relevant model to assess any toxic interaction. Macrophages were also used since they represent a suitable model to assess the cytocompatibility of NPs with the immune system.

Different biological assays were conducted to assess cell viability (MTS assay), proliferation (DNA quantification), total protein synthesis and morphology (SEM) after 1, 2, 3 and 7 days of culture.

For hACs a wide range of NPs concentration (10-500 μg/mL) was tested. Even though cell viability (**Figure III-4A**) was not affected, considering the cell proliferation at NPs concentrations above 50 μg/mL, there was a significantly decrease compared to the control. Nonetheless, SEM analyses confirm that the cell morphology was not affected by NPs (**Figure III-5A**). From these results, we can infer that the

maximum NPs concentration that does not have a harmful effect to the cells is 50 μg/mL. For NPs internalization assessment, hACs were exposed during 12 h to NPs, subjected or not to biofunctionalization, at a concentration of 50 μg/mL (**Figure III-5C**). Comparing the results of the samples with NPs to the control, it seems that the hACs do not internalize NPs.

Taking into account the previous results, for THP-1 cell line (**Figure III-4B** and **5B**) and human primary macrophages (**Figure III-4C**) three different NPs concentrations (25, 50 and 100 μg/mL) were tested. Since there were no significant differences between the NPs and the control, it can be concluded that the NPs are not cytotoxic at these concentrations for those cells.

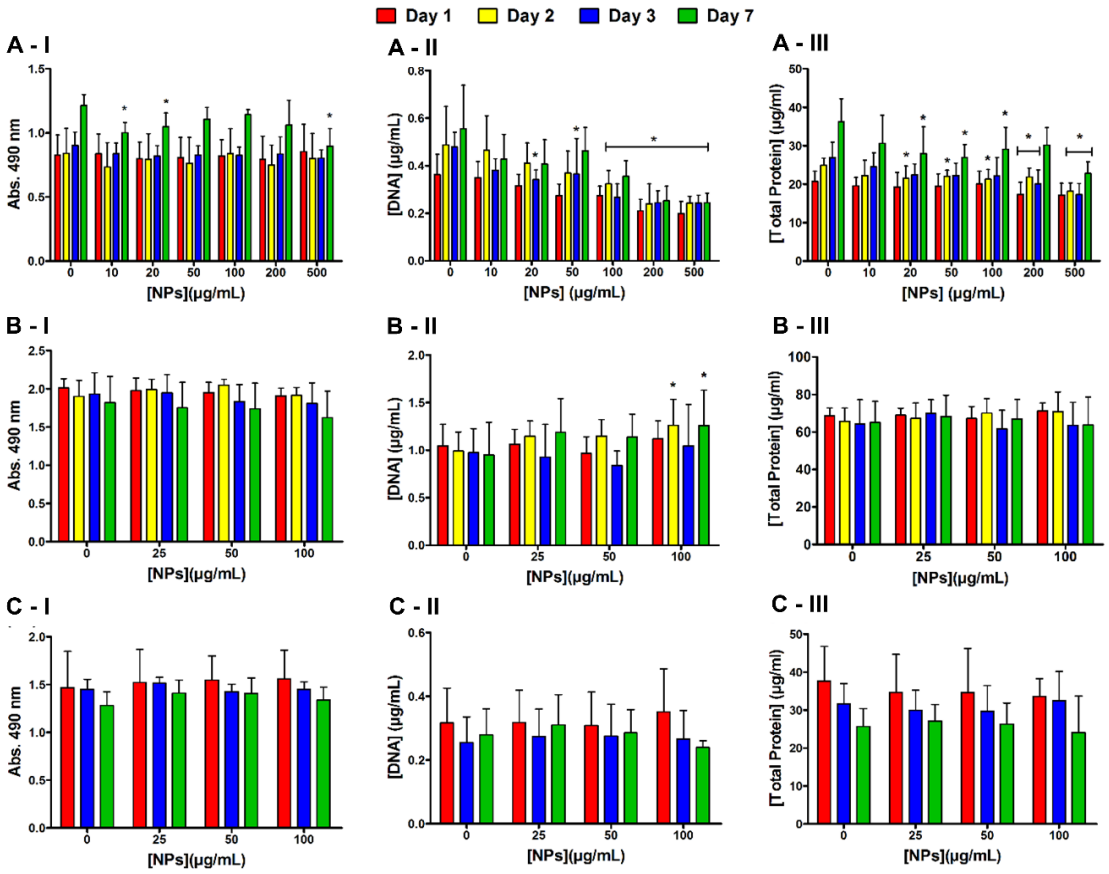

Figure III-4 – Biological performance of the (A) hACs, (B) THP-1 cell line and (C) primary human macrophages cultured with different concentrations of Ch-HA NPs: (I) cell viability, (II) cell proliferation and (III) total protein synthesis after 1, 2, 3 and 7 days of culture. Asterisk (*) denotes significant differences (p<0.01) compared to the control (0 μg/mL).

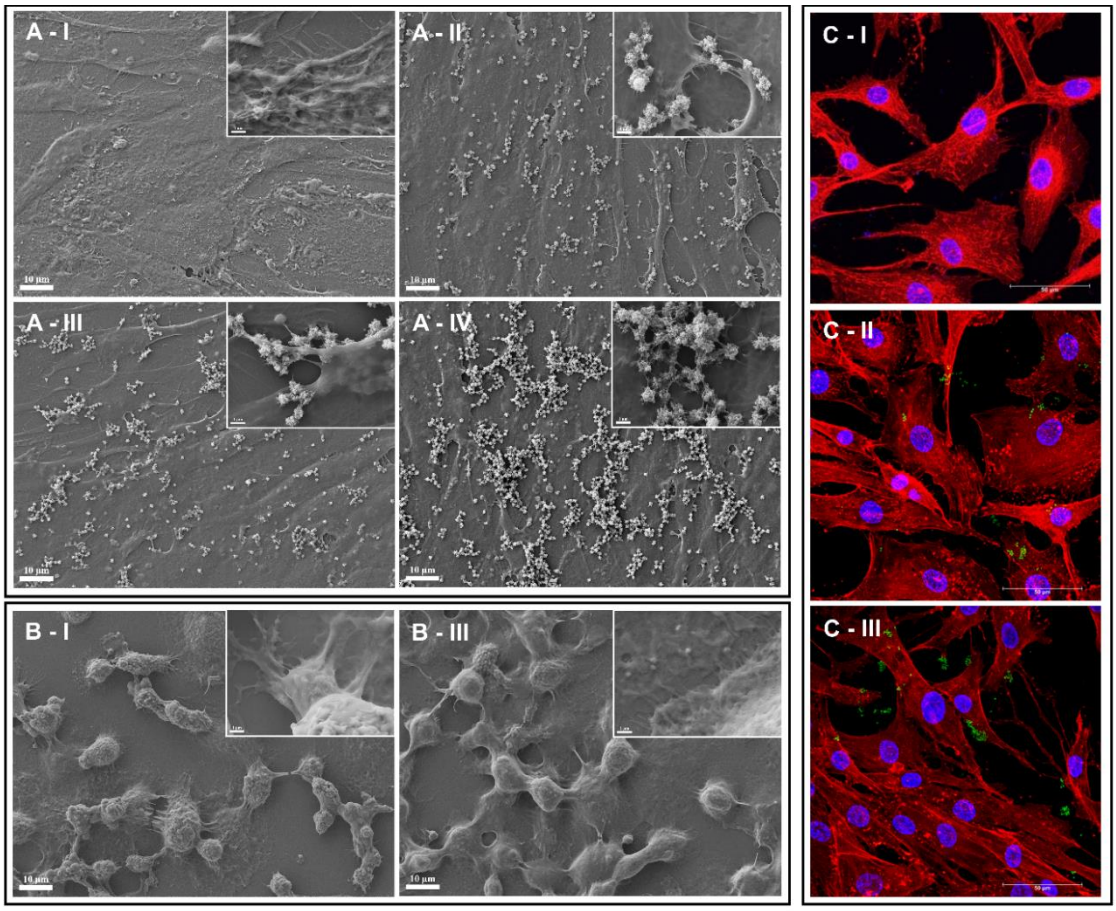

Figure III-5 – SEM micrographs of Ch-HA NPs cultured with (A) hACs or (B) THP-1 cells in the absence (control, I) and in the presence of NPs at different concentrations: (II) 20 μg/mL, (III) 50 μg/mL, and (IV) 100 μg/mL. Confocal microscopy images of hACs (C): (I) control, (II) NPs, and (III) biofunctionalized NPs, being the NPs green (FITC), nuclei blue (DAPI) and the cytoskeleton red (phalloidin).

III-3.4.2. Evaluation of IL-6 capture by biofunctionalized NPs and its biologic effects

To confirm the capacity of the primary anti-IL-6 Abs immobilized at the NPs' surface to capture and neutralize IL-6, hACs were stimulated with macrophage conditioned medium containing 500 pg/mL of IL-6, for 24 h. Then, three different conditions were tested: *(i)* hACs without treatment (no treat), *(ii)* treatment with biofunctionalized NPs (NPs+Ab); and *(iii)* treatment with soluble anti-IL-6 Abs (Ab). hACs cultured without macrophage conditioned medium were used as controls (Ctr).

Regarding the amount of unbound IL-6 in the medium (**Figure III-6A**), the results showed that macrophage conditioned medium had a huge impact on IL-6 production by cells, which corroborates the susceptibility to inflammation of hACs isolated from osteoarthritic patients. These cells produce around 8

ng/mL of IL-6 without any stimulus. Given the macrophage conditioned medium, they increased in 85 to 190 times the amount of this cytokine (0.68 to 1.51 μg/mL at 1 and 14 days, respectively). Moreover, there was a higher reduction of free IL-6 in the medium with biofunctionalized NPs comparing to the soluble Abs. Therefore, the results confirmed the initial hypothesis that the primary Abs immobilized at the NPs' surface had a longer effect than the soluble Abs.

After hACs stimulation with macrophage conditioned medium there was a significant decrease in cell viability and DNA concentration comparatively to the control (**Figure III-6B** and **C**). Alternatively, the condition with biofunctionalized NPs had an improvement in cell viability and proliferation, since there was no significant difference when compared with the control. Furthermore, this improvement was significantly higher in comparison with the soluble Abs, especially at 7 and 14 days. Despite these results, total protein concentration was almost the same for all conditions under evaluation (**Figure III-6D**).

The analyses of cell morphology (**Figure III-7**) revealed that the stimulated cells showed altered morphology with cell shrinkage, especially after 14 days. As shown in **Figure III-7**, hACs remained widely normal with the addition of functionalized NPs, while the addition of soluble Abs didn't prevent cell shrinkage.

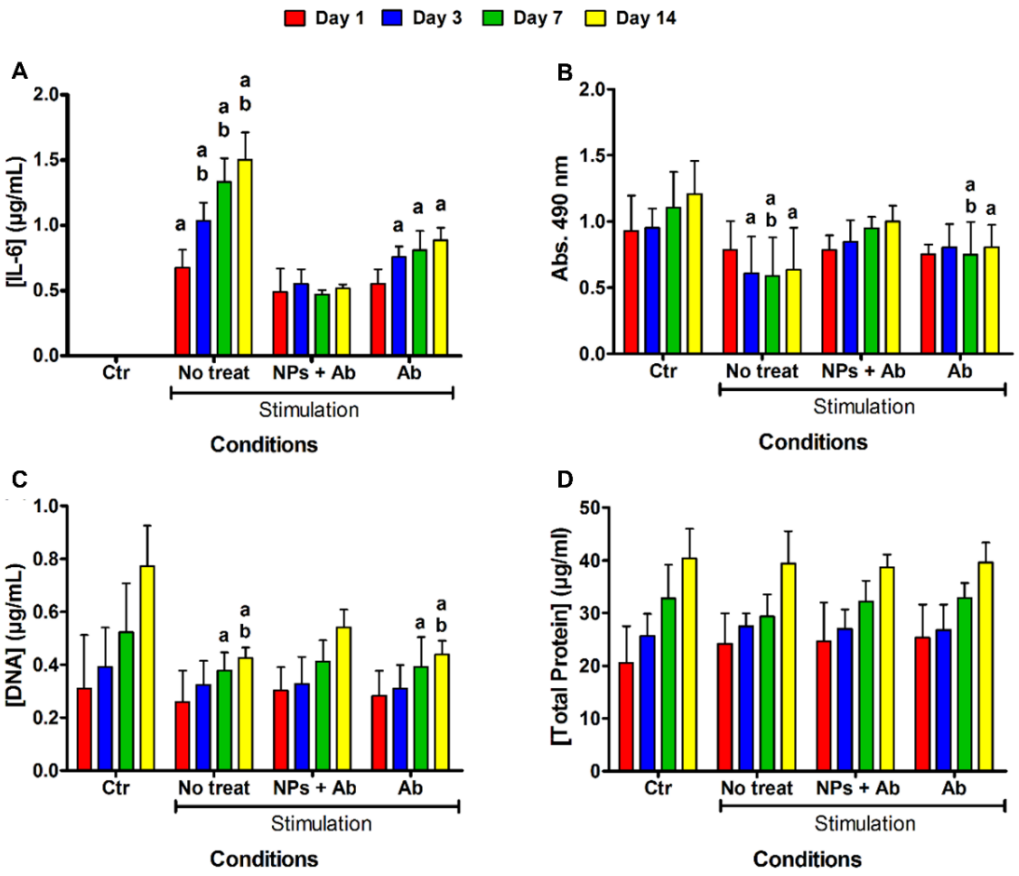

Figure III-6 – Biochemical performance of the stimulated hACs: *(i)* without stimulation (Ctr), *(ii)* hACs without treatment (no treat), *(iii)* treatment with biofunctionalized NPs (NPs+Ab), and *(iv)* treatment with soluble antibody (Ab), and analyzed regarding (A) unbound IL-6 concentration, (B) cell viability, (C) cell proliferation and (D) total protein synthesis. Letter "a" denotes significant difference (p<0.01) compared to the Ctr, and "b" denotes significant difference (p<0.01) compared to NPs+Ab.

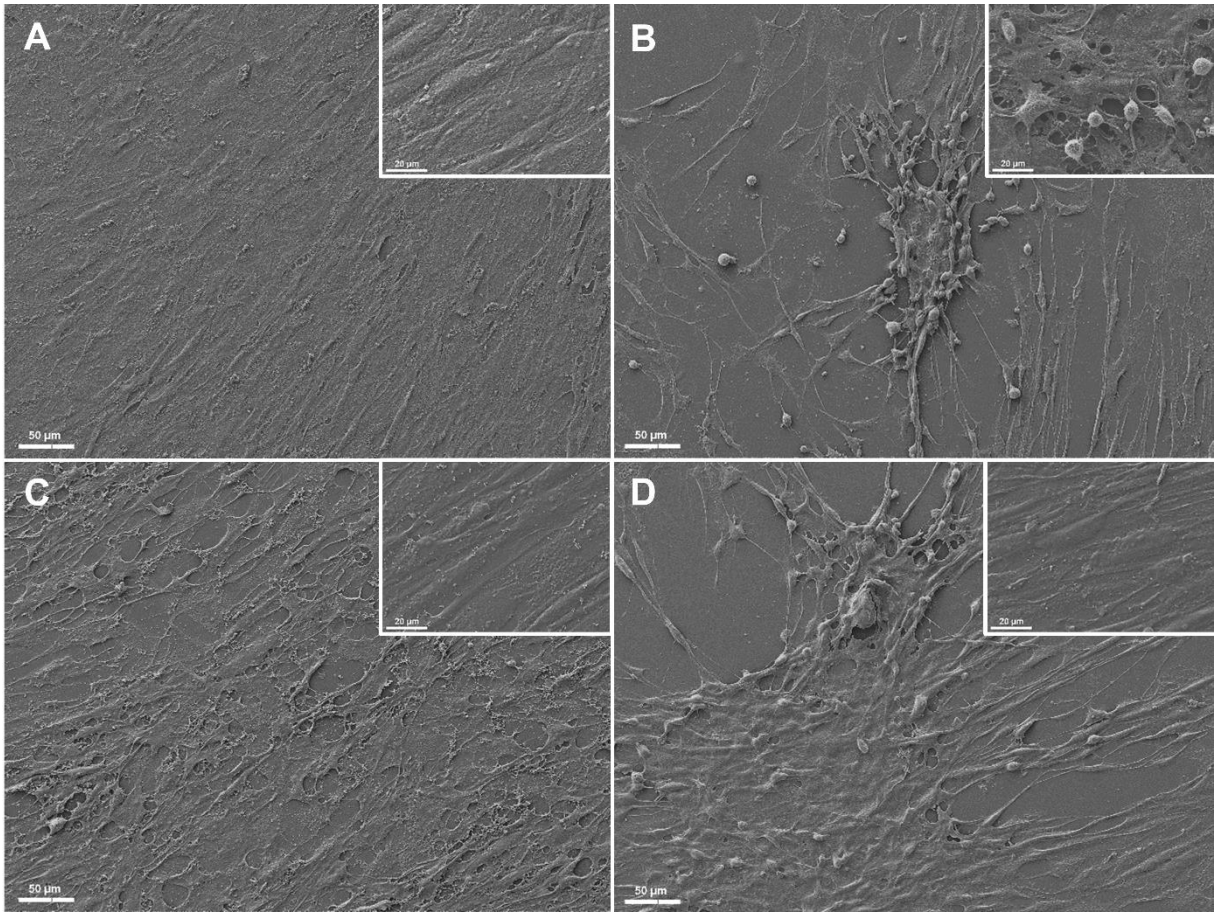

Figure III-7 – SEM micrographs of stimulated hACs: (A) control without stimulation, (B) stimulation without treatment, (C) biofunctionalized NPs and (D) soluble Ab after 14 days of culture. Micrographs obtained after 7 days of culture are shown to evaluate the effect during time (small images).

III-4. DISCUSSION

The aim of this study was to develop a carrier intended for local administration and allowing the capture and inactivation of a central pro-inflammatory mediator, IL-6, in arthritic joints. Ch and HA polysaccharides were used as the NPs building blocks. The backbone of Ch consists of glucosamine units, which has a high density of NH_2 (pKa ≈ 6.5), giving to Ch its cationic nature. This property allows Ch to electrostatically bind with negatively charged molecules. HA is an anionic biopolymer containing glucuronic acid with COOH as functional groups (pKa 3–4), at a proportion of 1:2 comparing to NH_2 of Ch. These two functional groups were used to produce NPs by polyelectrolyte complexation. As in the literature [27, 28], the initial polymer concentrations were optimized according to the experimental conditions and the aim of the work. Therefore, we selected 0.25, 0.5 and 1 mg/mL. The concentration of Ch and HA was observed to affect the size and PDI of the resulting NPs. Additionally, different initial

pH of the polymers solutions was tested to evaluate the impact of the protonation/deprotonation of NH_2 and COOH groups on the properties of the NPs. Indeed, the pH of the Ch solution has a strong impact in the particle size. NH_2 groups of Ch are protonated at pH 5, NH_3^+, which is necessary to interact with COOH groups of the HA that are deprotonated at pH 5 (COO^-). Therefore, at pH 5 electrostatic interactions between the opposite charges can be established, resulting in NPs formation [29]. However, those interactions are a reversible physical crosslinking. Consequently, due to the electrostatic interactions weakness of the NPs taking place at pH 7.4 (physiological pH) there is an increase of the NPs size.

Hence, crosslinkers are essential to increase pH stability and mechanical strength [30]. In this work, EDC/NHS were used to catalyze the reaction between the NH_2 of Ch and the COOH of HA to form amide bonds [31]. The resulting NPs were stable at physiological pH, even after 24 h at 37 °C. This chemical reaction does not represent a problem in terms of cytotoxicity, since EDC/NHS chemistry is a zero-length cross-linker [32]. Additionally, the only by-product of the reaction, urea, is non-toxic, and as all products are water soluble they are easily removed in the washing steps. Therefore, an absence of cytotoxicity is expected. Indeed, several works have being demonstrated the *in vitro* and *in vivo* cytocompatibility of EDC/NHS chemistry [33].

Stable NPs with 121.8 ± 2.4 nm of diameter, 0.11 ± 0.01 of PDI and +25.12 ± 1.86 mV of zeta potential were produced with 0.25 mg/mL of concentration of the initial polymers solutions, at pH 5, and with 50/200 mM of EDC/NHS concentration, after their centrifugation with glucose. NPs size and PDI significantly increased without the addition of this sugar to the NPs suspension. As reported for lyophilization [34], the centrifugation with glucose leads to the development of a layer around the NPs in the pellet, avoiding their aggregation when re-suspended. From these results, it can be inferred that the NPs suspension are homogeneous in terms of size, since typically monodisperse suspensions have PDI values less than 0.2 [35]. As expected from the ratio of NH_2:COOH (2:1), the zeta potential of the produced NPs was positive. Recent reports have been described that cationic proteins and particles increase the retention of therapeutic agents in articular joints [36, 37]. Hence, it will be expectable higher retention in the target tissue of the developed NPs. Moreover, the value of zeta potential gives an indication of the NPs suspension stability [38]. Higher absolute values of this parameter, give rise to stronger repellent electrostatic interactions between the NPs dispersed in water, which leads to a higher stability of the suspension. Guidelines classifying NP suspensions with zeta potential values of ±0-10 mV as highly unstable, ±10-20 mV as relatively stable, ±20-30 mV as moderately stable and >±30 mV as highly stable [39]. Regarding the value obtained around +25 mV, it is possible to conclude that the NPs are moderately

stable. Stability assays also corroborated the suspension stability, since they showed that NPs conserved their size distribution for at least 6 months, under the tested conditions.

After optimization of the process for NPs preparation, anti-IL-6 Abs was immobilized at their surface using the same chemistry previously referred. In this case, the COOH groups of the Abs reacted specifically with the NH_2 groups present at the NPs' surface. The maximum concentration of Abs immobilized by NPs was obtained when it was used an initial anti-IL-6 Abs concentration of 10 μg/mL. After this point, the values of the Abs immobilization reached a plateau, and despite the increment of Abs concentration, no significant differences were observed in its quantity on the NPs' surface. Moreover, it can be concluded that the immobilization of the Abs at the NPs' surface did not affect significantly the NPs properties.

Since the goal of the present study was to produce NPs for IL-6 neutralization, after the primary Abs immobilization, the cytokine capture capacity was assessed. The maximum binding ability was obtained for an initial concentration of Abs of 10 μg/mL, which corresponds to the capture of 1.22 ± 0.02 μg/mL of the protein added (1.25 μg/mL). Despite the increment of the anti-IL-6 Abs concentration added to the NPs suspension, the biofunctionalized NPs neutralized equivalent amounts of the cytokine, which corroborates the maximum immobilization capacity of the anti-IL-6 Abs at NPs' surface, obtained for an initial Abs concentration of 10 μg/mL.

To use Ch-HA NPs as a platform to treat arthritic diseases, an assessment of their potential toxicity for both chondrocytes and immune cells was performed. Ch-HA NPs in a concentration until 50 μg/mL did not present toxicity for hACs, THP-1 cells and human primary macrophages. For the hACs, higher amounts of NPs (10-500 μg/mL) were assessed and besides none of the concentrations had a huge impact in cell viability, for concentrations higher than 50 μg/mL, the cell proliferation was negatively affected. These results can be explained by analyzing SEM micrographs, where it can be seen that at higher concentrations, the NPs form agglomerates around hACs that can inhibit cell spreading. Concerning the immune cells, the Ch-HA NPs were not cytotoxic under the tested conditions (25, 50 and 100 μg/mL). In summary, it is possible to conclude that Ch-HA NPs are cytocompatible for concentrations up to 50 μg/mL.

Since inflammation had an important role in the pathological process of these diseases, it was investigated if the biofunctionalized NPs could avoid the negative impact of inflammation into human chondrocytes. hACs were stimulated with macrophage conditioned medium and three different conditions were tested: *(i)* hACs without treatment, *(ii)* treatment with biofunctionalized NPs and *(iii)* treatment with

soluble Abs. hACs cultured without macrophage conditioned medium (only culture medium) were used as controls (Ctr).

The IL-6 of the conditioned media was quantified in order to insure the presence of 500 pg/mL of IL-6 which is within the range of the IL-6 levels found in the synovial fluid of OA and RA patients (119.4 ± 193.2 and 354.7 ± 1851.6 pg/mL, respectively) [40]. This experiment showed that the macrophage conditioned medium has a huge impact in the hACs production of IL-6, since they increase in 85 to 190 times the amount of IL-6, when compared to the control. Additionally, it corroborates the susceptibility to inflammation of hACs isolated from osteoarthritic patients. The reduction of the interleukin amount obtained in the conditions with biofunctionalized NPs or with soluble Abs confirms the neutralization of IL-6 by the primary Abs and, consequently, the reduction of its negative effects. Moreover, there was a higher reduction of IL-6 in the medium with biofunctionalized NPs comparing to the soluble Abs, which confirmed the initial hypothesis that the primary Abs immobilized at the NPs' surface had a longer effect than the soluble Abs.

A previous study demonstrated that the synovial fluid obtained from OA and RA patients led to altered cell morphology, to a highly significant decrease of vital chondrocytes and also activates the synthesis of pro-inflammatory cytokines in primary human chondrocytes [41]. In the present work, we used macrophage conditioned medium to stimulate hACs, and observed similar effects, since there was a significant decrease in cell viability and DNA concentration, and cell morphology shift in the stimulation condition. Since the addition of the biofunctionalized NPs was able to reduce these effects (more than the free Abs), it was demonstrated that the Abs immobilized at the NPs' surface has a prolonged action and stronger efficacy than the free Abs. The Abs immobilization can increase its stability and reduce its degradation, explaining the prolonged effect observed. Therefore, the conjugation of Abs to NPs combines the advantages of NPs support, with lower degradability, and longer half-life time and efficacy of the Abs. Moreover, they retain the specific and selective recognition of the antigens to capture and neutralize them [42].

In a recent study, anti-IL-6 Abs were encapsulated into poly(lactic-co-glycolic acid) NPs to antagonize the effect of IL-6 locally in the heart, as a therapeutic procedure to prevent/ameliorate organ ischemia–reperfusion injury [43]. The localized delivery of anti-IL-6 significantly reduced immune rejection of transplants with a lower amount administered, comparing with the systemic delivery. In this context, the covalent immobilization of anti-IL-6 into Ch-HA NPs' surface can be a viable and effective strategy to increase the Abs efficacy when injected locally in joint cavities, which can reduce the dosage and significantly avoid associated systemic side effects.

Although the controversy about the size necessary to retain longer the particles in the joint cavity, preclinical studies clearly demonstrate that NPs can be effective for IA delivery [44]. The prescribed dose of anti-IL-6 in RA patients (for OA patients is not yet an available therapy) is around 8 mg/kg intravenously, which can be dramatically reduced using this system injected IA. Indeed, with 1 μg/mL of Abs immobilized in NPs the inflammatory scenario was significantly reduced. Furthermore, as the NPs are composed of well-known biodegradable polymers, they can be further degraded by biological processes, without any toxic effects for the cells, enabling subsequent treatments.

III-5. CONCLUSION

In the present work, we developed natural biodegradable polymeric NPs biofunctionalized with anti-IL-6 Abs able to selectively capture and inactivate the pro-inflammatory cytokine IL-6. Due to the key role of IL-6 in arthritis, its effective neutralization by the NPs will reduce inflammation, leading to a possible decrease of swelling and pain in such diseases.

Current treatments present serious side effects and limited efficacy mainly because of the rapid clearance of Abs by the body. Presently, in order to have an improvement in arthritis, higher doses and extended periods of treatments are needed. Therefore, it is foreseeable that the developed NPs will overcome the limitations of the above-mentioned treatments, since they will increase the Abs therapeutic efficacy as a result of their subcellular size, cytocompatibility, high functionalization and stability, avoiding associated side effects. Indeed, these systems have enhanced efficacy and prolonged action in the capture and neutralization of IL-6 when compared with the free Abs.

In conclusion, the biofunctionalized NPs are a valid approach for the local and sustained treatment of inflammatory arthritic diseases. Hence, the outcomes of this work have important implications for increasing the efficacy of currently available treatments, by prolonging the therapeutic action of the Abs and avoiding most of their side effects. Those benefits will be further tested in relevant arthritis animal models.

III-6. ACKNOWLEDGMENT

Authors acknowledge the financial support from FCT/MCTES (Portuguese Foundation for Science and Technology / Ministry of Science, Technology and Higher Education) and the FSE/POCH (European

Social Fund through the Operational Program of Human Capital), for the PhD scholarship PD/BD/11384/2015 of A. C. Lima (PD/59/2013), the FCT for the grant of A. Carvalho (IF/00735/2014) and C. Carvalho (SFRH/BPD/96176/2013). Authors would also like to acknowledge FCT for the project PTDC/CTM-BIO/4388/2014 – SPARTAN, and the Northern Portugal Regional Operational Programme (NORTE 2020), under the Portugal 2020 Partnership Agreement, through the European Regional Development Fund (FEDER) (NORTE-01-0145-FEDER-000023 - FROnTHERA and NORTE-01-0145-FEDER-000013 - PersonalizedNOS).

III-7. REFERENCES

1. Roy, K., Kanwar, R. K. and Kanwar, J. R., Molecular targets in arthritis and recent trends in nanotherapy. *Int J Nanomed*. 2015, *10*: p. 5407-20.
2. Woolf, A. D. and Pfleger, B., Burden of major musculoskeletal conditions. *Bull World Health Organ*. 2003, *81* (9): p. 646-56.
3. Pap, T. and Korb-Pap, A., Cartilage damage in osteoarthritis and rheumatoid arthritis-two unequal siblings. *Nat Rev Rheumatol*. 2015, *11* (10): p. 606-15.
4. Martel-Pelletier, J., Wildi, L. M. and Pelletier, J. P., Future therapeutics for osteoarthritis. *Bone*. 2012, *51* (2): p. 297-311.
5. Alcaraz, M. J., Megias, J., Garcia-Arnandis, I., *et al.*, New molecular targets for the treatment of osteoarthritis. *Biochem Pharmacol*. 2010, *80* (1): p. 13-21.
6. Kimura, A. and Kishimoto, T., IL-6: regulator of Treg/Th17 balance. *Eur J Immunol*. 2010, *40* (7): p. 1830-5.
7. Savio, A. S., Diaz, A. C. M., Capote, A. C., *et al.*, Differential expression of pro-inflammatory cytokines IL-15Ralpha, IL-15, IL-6 and TNFalpha in synovial fluid from Rheumatoid arthritis patients. *Bmc Musculoskel Dis*. 2015, *16* (51): p. 1-8.
8. Qi, M., Huang, J. W., Wei, H., *et al.*, Graphene Oxide Thin Film with Dual Function Integrated into a Nanosandwich Device for in Vivo Monitoring of Interleukin-6. *Acs Appl Mater Inter*. 2017, *9* (48): p. 41659-68.
9. Livshits, G., Zhai, G., Hart, D. J., *et al.*, Interleukin-6 Is a Significant Predictor of Radiographic Knee Osteoarthritis The Chingford Study. *Arthritis Rheum*. 2009, *60* (7): p. 2037-45.
10. Adachi, Y., Yoshio-Hoshino, N. and Nishimoto, N., The blockade of IL-6 signaling in rational drug design. *Curr Pharm Design*. 2008, *14* (12): p. 1217-24.
11. Tanaka, Y. O., A.; Kishimoto, T., Targeting of Interleukin-6 for the Treatment of Rheumatoid Arthritis: A Review and Update. *Rheumatol Curr Res*. 2013, *S4* (2): p. 1-14.
12. Woodrick, R. S. and Ruderman, E. M., Safety of biologic therapy in rheumatoid arthritis. *Nat Rev Rheumatol*. 2011, *7* (11): p. 639-52.
13. Iannitti, T., Lodi, D. and Palmieri, B., Intra-articular injections for the treatment of osteoarthritis: focus on the clinical use of hyaluronic acid. *Drugs R D*. 2011, *11* (1): p. 13-27.
14. O'Mary, H., Del Rincomicronn, I. and Cui, Z., Nanomedicine for Intra-Articular Drug Delivery in Rheumatoid Arthritis. *Curr Med Chem*. 2016, *23* (23): p. 2490-506.
15. Banik, B. L., Fattahi, P. and Brown, J. L., Polymeric nanoparticles: the future of nanomedicine. *Wires Nanomed Nanobi*. 2016, *8* (2): p. 271-99.

16. Kumari, A., Yadav, S. K. and Yadav, S. C., Biodegradable polymeric nanoparticles based drug delivery systems. *Colloids Surf B Biointerfaces*. 2010, *75* (1): p. 1-18.
17. Wen, Y. F. and Oh, J. K., Recent Strategies to Develop Polysaccharide-Based Nanomaterials for Biomedical Applications. *Macromol Rapid Comm*. 2014, *35* (21): p. 1819-32.
18. Oliveira, C., Costa-Pinto, A. R., Reis, R. L., *et al.*, Biofunctional nanofibrous substrate comprising immobilized antibodies and selective binding of autologous growth factors. *Biomacromolecules*. 2014, *15* (6): p. 2196-205.
19. Muzzarelli, R. A., Greco, F., Busilacchi, A., *et al.*, Chitosan, hyaluronan and chondroitin sulfate in tissue engineering for cartilage regeneration: a review. *Carbohydr Polym*. 2012, *89* (3): p. 723-39.
20. Grenha, A., Gomes, M. E., Rodrigues, M., *et al.*, Development of new chitosan/carrageenan nanoparticles for drug delivery applications. *J Biomed Mater Res A*. 2010, *92* (4): p. 1265-72.
21. Carroll, E. C., Jin, L., Mori, A., *et al.*, The Vaccine Adjuvant Chitosan Promotes Cellular Immunity via DNA Sensor cGAS-STING-Dependent Induction of Type I Interferons. *Immunity*. 2016, *44* (3): p. 597-608.
22. Patel, S. and Goyal, A., Chitin and chitinase: Role in pathogenicity, allergenicity and health. *Int J Biol Macromol*. 2017, *97*: p. 331-8.
23. Umerska, A., Corrigan, O. I. and Tajber, L., Intermolecular interactions between salmon calcitonin, hyaluronate, and chitosan and their impact on the process of formation and properties of peptide-loaded nanoparticles. *Int J Pharmaceut*. 2014, *477* (1-2): p. 102-12.
24. Litwiniuk, M., Krejner, A., Speyrer, M. S., *et al.*, Hyaluronic Acid in Inflammation and Tissue Regeneration. *Wounds*. 2016, *28* (3): p. 78-88.
25. Paiva, A. M., Pinto, R. A., Teixeira, M., *et al.*, Development of noncytotoxic PLGA nanoparticles to improve the effect of a new inhibitor of p53-MDM2 interaction. *Int J Pharmaceut*. 2013, *454* (1): p. 394-402.
26. da Silva, M. L. A., Costa-Pinto, A. R., Martins, A., *et al.*, Conditioned medium as a strategy for human stem cells chondrogenic differentiation. *J Tissue Eng Regen M*. 2015, *9* (6): p. 714-23.
27. de la Fuente, M., Seijo, B. and Alonso, M. J., Novel hyaluronic acid-chitosan nanoparticles for ocular gene therapy. *Invest Ophth Vis Sci*. 2008, *49* (5): p. 2016-24.
28. Lu, H. D., Zhao, H. Q., Wang, K., *et al.*, Novel hyaluronic acid-chitosan nanoparticles as non-viral gene delivery vectors targeting osteoarthritis. *Int J Pharmaceut*. 2011, *420* (2): p. 358-65.
29. Denuziere, A., Ferrier, D., Damour, O., *et al.*, Chitosan-chondroitin sulfate and chitosan-hyaluronate polyelectrolyte complexes: biological properties. *Biomaterials*. 1998, *19* (14): p. 1275-85.
30. Mavila, S., Eivgi, O., Berkovich, I., *et al.*, Intramolecular Cross-Linking Methodologies for the Synthesis of Polymer Nanoparticles. *Chem Rev*. 2016, *116* (3): p. 878-961.
31. Kang, M. L., Ko, J. Y., Kim, J. E., *et al.*, Intra-articular delivery of kartogenin-conjugated chitosan nano/microparticles for cartilage regeneration. *Biomaterials*. 2014, *35* (37): p. 9984-94.
32. Yang, X. X., Wang, X. Y., Yu, F., *et al.*, Hyaluronic acid/EDC/NHS-crosslinked green electrospun silk fibroin nanofibrous scaffolds for tissue engineering. *Rsc Adv*. 2016, *6* (102): p. 99720-8.
33. Ahmad, Z., Shepherd, J. H., Shepherd, D. V., *et al.*, Effect of 1-ethyl-3-(3-dimethylaminopropyl) carbodiimide and N-hydroxysuccinimide concentrations on the mechanical and biological characteristics of cross-linked collagen fibres for tendon repair. *Regen Biomater*. 2015, *2* (2): p. 77-85.
34. Wang, Y. C., Zheng, Y., Zhang, L., *et al.*, Stability of nanosuspensions in drug delivery. *J Control Release*. 2013, *172* (3): p. 1126-41.

35. Panchal, J., Kotarek, J., Marszal, E.*, et al.*, Analyzing subvisible particles in protein drug products: a comparison of dynamic light scattering (DLS) and resonant mass measurement (RMM). *The AAPS journal*. 2014, *16* (3): p. 440-51.
36. Bajpayee, A. G., De la Vega, R. E., Scheu, M.*, et al.*, Sustained intra-cartilage delivery of low dose dexamethasone using a cationic carrier for treatment of post traumatic osteoarthritis. *Eur Cell Mater*. 2017, *34*: p. 341-64.
37. Morgen, M., Tung, D., Boras, B.*, et al.*, Nanoparticles for Improved Local Retention after Intra-Articular Injection into the Knee Joint. *Pharm Res-Dordr*. 2013, *30* (1): p. 257-68.
38. Silva, R., Ferreira, H., Azoia, N. G.*, et al.*, Insights on the mechanism of formation of protein microspheres in a biphasic system. *Mol Pharm*. 2012, *9* (11): p. 3079-88.
39. Bhattacharjee, S., DLS and zeta potential - What they are and what they are not? *J Control Release*. 2016, *235*: p. 337-51.
40. Kokebie, R., Aggarwal, R., Lidder, S.*, et al.*, The role of synovial fluid markers of catabolism and anabolism in osteoarthritis, rheumatoid arthritis and asymptomatic organ donors. *Arthritis Res Ther*. 2011, *13* (2): p. 1-10.
41. Hoff, P., Buttgereit, F., Burmester, G. R.*, et al.*, Osteoarthritis synovial fluid activates pro-inflammatory cytokines in primary human chondrocytes. *Int Orthop*. 2013, *37* (1): p. 145-51.
42. Arruebo, M., Valladares, M. and Gonzalez-Fernandez, A., Antibody-Conjugated Nanoparticles for Biomedical Applications. *J Nanomater*. 2009: p. 3103-27.
43. Solhjou, Z., Uehara, M., Bahmani, B.*, et al.*, Novel Application of Localized Nanodelivery of Anti-Interleukin-6 Protects Organ Transplant From Ischemia-Reperfusion Injuries. *Am J Transplant*. 2017, *17* (9): p. 2326-37.
44. Holyoak, D. T., Tian, Y. F., van der Meulen, M. C.*, et al.*, Osteoarthritis: Pathology, Mouse Models, and Nanoparticle Injectable Systems for Targeted Treatment. *Ann Biomed Eng*. 2016, *44* (6): p. 2062-75.

Chapter IV

Interleukin-23 neutralization by biofunctionalized liposomes encapsulating gold nanoparticles for the treatment of rheumatoid arthritis

Chapter IV

Interleukin-23 neutralization by biofunctionalized liposomes encapsulating gold nanoparticles for the treatment of rheumatoid arthritis[1]

ABSTRACT

Biologic drugs revolutionized the management of rheumatoid arthritis (RA), however this debilitating disease remains a major clinical problem. The outstanding outcomes of the systemic administration of antibodies (Abs) are narrowed by the risk of serious side effects and limited efficacy due to their short half-life in circulation. The present work proposes the immobilization of anti-interleukin-23 (IL-23) Abs at the surface of large unilamellar liposomes (LUVs) in order to increase their therapeutic efficacy. IL-23 is a crucial pro-inflammatory cytokine in the regulation of the cellular mechanisms involved in inflammation. For instance, IL-23 potently enhances the generation of pathogenic T helper type 17 (Th17) cells, which are central drivers of inflammation in autoimmune diseases (ADs), such as RA. Gold nanoparticles (AuNPs) were incorporated in the biofunctionalized LUVs to increase the anti-inflammatory activity of this novel strategy and to confer it theranostic properties. LUVs encapsulating AuNPs were produced as a stable monodisperse suspension (129.4 ± 4.0 nm of diameter, 0.114 ± 0.012 of polydispersity index and - 21.9 ± 1.8 of zeta potential). The anti-IL-23 Abs were efficiently immobilized at the LUVs surface and their capture capacity was confirmed using cultures of activated macrophages. Biological assays demonstrated their cytocompatibility in the presence of human articular chondrocytes (hACs), human macrophages (THP-1 cell line) and endothelial cells (Ea.hy936 cell line). Moreover, the neutralization of IL-23 by the biofunctionalized liposomes efficiently decreased the production of IL-17A by peripheral blood mononuclear cells (PBMCs) of healthy donors and RA patients, activated to Th17 differentiation. Therefore, the overall results reveal that the developed formulation is a promising strategy to treat RA and likely, other ADs.

[1]This chapter is based on the following publication:

Lima A. C., Campos C. F., Cunha C., Carvalho A., Reis R. L., Ferreira H., Neves N. M. Interleukin-23 neutralization by biofunctionalized liposomes encapsulating gold nanoparticles for the treatment of rheumatoid arthritis. *(Submitted)*. 2019.

IV-1. INTRODUCTION

Rheumatoid arthritis (RA) is an autoimmune disease that primarily affects joints of up to 1% of the worldwide population [1]. It is characterized by inflammation and hyperplasia of the synovial membrane, pannus formation, as well as cartilage and bone destruction [2]. Consequently, its clinical features can severely impair the physical function and quality of life of the patients. In addition to the progressive disability, RA patients present a higher risk of developing serious infections, respiratory and cardiovascular disorders, cancer, and have higher mortality than the general population.

Although the exact etiology of RA remains unclear, environmental, immunological and genetic factors contribute to increase its susceptibility and severity. Its pathogenesis is related to an uncontrolled and specific immune response against self-antigens [3]. It is generally accepted that joint damage in RA begins with the proliferation of synovial fibroblasts and accumulation and infiltration of activated inflammatory cells in the synovium [4]. In healthy joints, synovial fibroblasts produce extracellular matrix (ECM) components that are crucial for joint lubrication and cartilage integrity [5]. In RA, the alteration of the synovial fibroblast phenotype enhances the expression of pro-inflammatory and matrix-degrading mediators and, consequently, promote cartilage degradation.

Inflammatory cells in the synovial membrane include innate (e.g., monocytes, dendritic cells, mast cells and innate lymphoid cells) and adaptive immune cells (e.g., T helper (Th) type-1 and Th17 cells, B cells and T cells). These cells release several pro-inflammatory cytokines, such as tumor necrosis factor-α (TNF-α) and interleukins (ILs, particularly IL-6, IL-1β and IL-17A), producing an inflammatory milieu in the synovium that has a crucial role in the development and progression of RA [6]. Moreover, the combinatory effects of the activation of fibroblasts and immune cells enhances chondrocyte catabolism and synovial osteoclastogenesis, which further promotes the destruction of the articular cartilage [3].

In the past decade, the development of new biological agents to inhibit cytokine activity revolutionized the treatment of RA [4]. After the outstanding outcomes of infliximab, a chimeric antibody (Ab) specific for TNF-α neutralization, further anti-TNF-α agents and other cytokine inhibitors have been developed and reached the clinic. Indeed, these agents have not only improved the treatment of RA but also yielded crucial insights into the pathophysiology of this disorder. One of those important findings was the crucial role of IL-23/Th17 pathway in autoimmunity [7]. IL-23 plays a central role in T cell-mediated responses and is considered a key promoter of immune-mediated conditions, such as colitis, gastritis, psoriasis and arthritis [8]. It is a heterodimeric cytokine and a member of the IL-12 cytokine family, sharing the subunit

IL-12p40 with the IL-12 and having a specific p19 subunit. However, despite a strong structural relationship, IL-12 and IL-23 maintain different biological roles, such as the driving of Th1 or Th17 cell responses, respectively [9]. While Th1 cells promote cellular immunity (protection against pathogens), Th17 cells are typically associated to autoimmune tissue inflammation [10]. IL-23 induces the differentiation of naive $CD4^+$ T cells into Th17 cells in the presence of other factors (such as IL-6 and transforming growth factor -TGF-β), which stimulates the production of other pro-inflammatory cytokines (e.g. IL-17, IL-22, TNF-α and granulocyte-macrophage colony-stimulating factor -GM-CSF). IL-17 produced by these differentiated cells also stimulates the upregulation of pro-inflammatory cytokines (IL-6, IL-8, TNF-α), chemokines and metalloproteinases, being also crucial for the T cell-mediated activation of osteoclastogenesis. Moreover, IL-17A and TNF-α act synergistically to promote increased expression of endothelial cell adhesion molecules, further increasing granulocyte recruitment to the sites of inflammation. Considering the high expression of IL-23 in the serum and synovial fluid of RA patients, it may be also a useful biomarker for the diagnosis of the different stages of RA [11, 12].

Since IL-23 is an early and important factor of the immune cascade, monoclonal Abs were investigated to inhibit its function and treat various ADs, including RA [8]. For instance, ustekinumab, a human monoclonal Ab that inhibits both IL-12 and IL-23 was approved by the Food and Drug Administration (FDA) for Psoriatic Arthritis (PsA) treatment. Guselkumab is a human monoclonal Ab that binds specifically to the p19 subunit of IL-23 to inhibit its downstream signaling. It is currently approved for the treatment of moderate to severe plaque psoriasis, and it is in clinical trials for pustular psoriasis (phase III, NCT02343744), PsA (phase III, NCT0315828, NCT03162796), and RA (phase II, NCT01645280). Many other anti-IL-23 Abs are under clinical evaluation for several immune-mediated conditions. In a phase II clinical trial, the signs and symptoms of RA were not significantly reduced by guselkumab and ustekinumab after subcutaneous administration [13]. However, rather than being interpreted as evidence that IL-23 is irrelevant in RA, these results should instigate further studies considering other therapeutic conditions (e.g. route of administration, doses, time of treatment and concomitant administration of other drugs) [14]. Moreover, due to the short half-life of Abs, they have limited therapeutic efficacy [15]. Indeed, considering their rapidly clearance from circulation, repeated drug administration and prolonged times of treatment are required. In addition, biological agents are associated with serious side effects such as increased risk of infection and malignancy [15]. Hence, novel drug delivery systems are required to improve the efficacy and safety of the biological agents.

Nanomedicine is a branch of the nanotechnology field that addresses the limitations of conventional therapies [16]. Among all types of nanoparticles, unilamellar liposomes (LUVs) have been widely used due to their advantages such as biocompatibility, versatility and *in vivo* long-term circulation [17]. Indeed, FDA and European Medicines Agency (EMA) already approved several liposome formulations [18]. After the first liposomal formulation was introduced in the market (Doxil® in 1995), many others followed the same trend. These phospholipid bilayer-based carriers can be designed with specific characteristics adjusted to the requirements of the therapeutic agent chemical properties and mode of action as well as to the specificity of the disease [19]. Moreover, the incorporation of imaging agents allows monitoring the LUVs biodistribution and efficacy [20]. Actually, despite the huge diversity of metal NPs, gold (Au) NPs are one of the most used in biomedical applications due to their unique properties, such as good biocompatibility, easy synthesis, chemical stability and inertness, facile surface modification and tunable optical properties [21, 22]. Computer Assisted Tomography scanning and X-Ray, for example, have been used to monitor the *in vivo* biodistribution of these contrast agents encapsulated or not into NPs. Moreover, the binding ability of AuNPs to vascular endothelial growth factor (VEGF) confers them an antiangiogenic effect [23]. The antioxidant effects of these imaging agents were also well-demonstrated, for instance, after intra-articular injection in arthritic rats [24]. Indeed, by quenching reactive oxygen species (ROS), AuNPs inhibit the receptor activator of nuclear factor κB ligand (RANKL)-induced osteoclast formation that promote bone and cartilage erosion. Therefore, AuNPs can have beneficial effects in the treatment of autoimmune arthritis (especially RA), as VEGF, osteoclasts and ROS are the main contributors to their pathogenesis [25]. Consequently, synergistic effects can be obtained with the therapeutic agents.

This work presents a therapy for RA based on a nanotherapeutic approach relying on the: *(i)* enhanced vascular permeability of inflamed synovial tissues for LUVs accumulation; *(ii)* antioxidant and antiangiogenic effects as well as disease monitoring capacity conferred by AuNPs; *(iii)* IL-23 neutralization by Abs immobilized at the surface of the LUVs to inhibit Th17 cell differentiation and, consequently, to reduce the production of IL-17A (**Figure IV-1**). Therefore, this innovative strategy presents a great potential to increase anti-IL-23 Abs bioavailability and hence boosted efficacy.

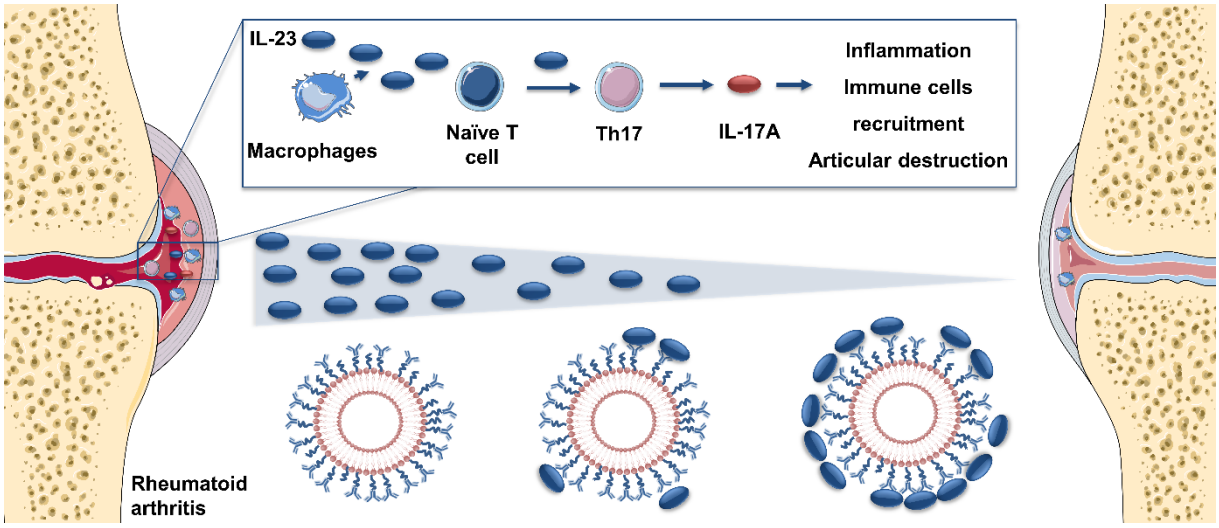

Figure IV-1 – Schematic illustration of the biofunctionalized liposomes role in RA treatment. The neutralization of IL-23 cytokine will inhibit the Th17 differentiation and, consequently, reduce inflammation, immune cells recruitment and articular destruction.

IV-2. MATERIALS AND METHODS

This section describes in detail the methods used in LUVs preparation, biofunctionalization and characterization. The biological assays performed to assess their cytocompatibility as well as the biologic effects of the pro-inflammatory cytokine capture and neutralization are presented also in detail.

IV-2.1. Materials

1,2-distearoyl-sn-glycero-3-phosphoethanolamineN-[maleimide(polyethyleneglycol)-2000] (ammonium salt) (DSPE-PEG-Mal) was purchased from Avanti Polar Lipids (USA). LabAssay™ Phospholipid was obtained from Wako (Japan). The secondary Abs Alexa Fluor® 488 Donkey Anti-Mouse, Roswell Park Memorial Institute (RPMI)-1640 media and Fetal Bovine Serum (FBS) were purchased from Thermo Fisher Scientific (USA). Human Fibroblast Growth Factor (bFGF) and Interferon-γ (IFN-γ) was acquired from Peprotech (USA). Human IL-23 TMB ELISA Development Kit was purchased from R&D Systems (USA). Human ELISA MAX™ Deluxe Set IL-17A and the recombinant human IL-23 was purchased from BioLegend (USA). Anti-IL-23 Abs was purchased from Abcam (Uk). All other reagents were purchased from Sigma-Aldrich (USA). The reagents were used as received. The glass material was washed with aqua regia to remove wholly Au.

IV-2.2. LUVs preparation and biofunctionalization

LUVs were prepared by the thin-film hydration method followed by extrusion as described [26, 27], with some modifications. Briefly, a lipid film of cholesterol/L-alfa-phosphatidylcholine (EPC)/DSPE-PEG-Mal at 1:0.85:0.15 (n/n) and α-tocopherol at 1:200 (M/M) was obtained after complete ethanol evaporation in a rotary evaporator. The hydration of the dried lipid film was performed with a suspension of 20 nm AuNPs in HEPES buffer (pH 7.4) and the vigorous vortex of this mixture produced multilamellar liposomes (MLVs). MLVs were then extruded forty three times through polycarbonate filters of 0.1 μm pore diameter, using an Avanti Mini-Extruder.

Anti-IL-23 Abs were linked to the maleimide groups of PEG ends after their thiolation with 2-iminothiolane (2IT) [28]. For that, a 100-fold molar excess of 2IT was incubated with the Abs (20 μg per 1 mL of LUVs suspension at 30 mM) in the presence of 5 mM ethylenediamine tetraacetic (EDTA, to avoid the oxidation of the thiol groups) in phosphate buffered saline (PBS, pH 8.0) during 1 h at room temperature (RT) [29]. Before linking the thiolated antibodies to LUVs, a dialysis (Micro Float-A-Lyzer®, MWCO: 3.5-5 kDa) was used to remove the excess of 2IT. As thiol groups have a rapid rate of recyclization [30], the buffer replacement was performed each 15-20 min during a period of time lower than 4 h [29]. After LUVs overnight incubation at 4 °C with the thiolated anti-IL-23 Abs, they were washed twice with HEPES buffer using Vivaspin 300 kDa Filter Units (Fisher Scientific, USA) to remove any unbound Abs. To quantify the anti-IL-23 Abs immobilized at the LUVs surface, first they were immersed in a solution of 3% (w/v) bovine serum albumin (BSA) for 1 h at RT (to block nonspecific sites), and then the secondary Abs Alexa Fluor® 488 was added. After 1 h at RT, the fluorescence intensity of the supernatant (unbound secondary Abs) was measured using a microplate reader (Synergy HT, BioTek, USA), setting the excitation wavelength at 485 nm and the emission wavelength at 530 nm.

The quantitative determination of phosphatidylcholine was performed using an enzymatic method, namely LabAssay™ Phospholipid, according to manufacturer's instructions. The absorbance at 600 nm was acquired using the microplate reader previously referred.

IV-2.3. LUVs characterization

LUVs were characterized regarding their size distribution, surface charge, stability and morphology, as described in the following sub-sections.

IV-2.3.1. Size distribution and zeta-potential measurements

Size, polydispersity index (PDI) and zeta-potential determinations of LUVs (500 μM; pH 7.4) were assessed using dynamic light scattering (DLS) in disposable polystyrene cuvettes and laser Doppler micro-electrophoresis using a dip cell, respectively, at 37.0 ± 0.1 °C, in a Malvern Zetasizer NS (Malvern Instruments) equipment.

IV-2.3.2. Stability Studies

For storage stability assessment, LUVs were kept at 4 °C under static conditions. During the experimental time (6 months), the size, PDI and zeta potential were determined as described previously.

IV-2.3.3. NPs Morphology

The morphology of AuNPs and LUVs incorporating AuNPs was assessed using transmission electron microscopy (TEM; Jeol JEM-1400). For negative staining TEM, 10 μL of samples were mounted on a Formvar/carbon film-coated mesh nickel grids (Electron Microscopy Sciences, USA) and left standing for 2 min. After removing the excess liquid with filter paper, 10 μL of 1% uranyl acetate was added to the grids and left standing for 10 s. The excess of liquid was once more removed with filter paper. The morphology assessment was carried out at 80 kV.

IV-2.4. Biological studies

Cell viability, proliferation, protein content and morphology were performed to assess LUVs cytocompatibility and their biological effects after biofunctionalization with anti-IL-23 Abs.

IV-2.4.1. Isolation and Cell Culture

Human articular chondrocytes (hACs) were isolated from knee cartilage samples collected after arthroplasties surgeries biopsies. Samples were obtained through the cooperation agreement established between the Centro Hospitalar do Alto Ave, Guimarães, Portugal, and the 3B's Research Group, and after informed donor consent. Isolation was performed by enzymatic digestion, as previously described [31].

hACs cells were cultured in Dulbecco's modified Eagle's medium (DMEM) high glucose (D5671), supplemented with 10% FBS, 10 mM L-lanyl-L-glutamine, MEM Non Essential Aminoacids, HEPES buffer, 100 units/mL of penicillin, 100 μg/mL of streptomycin and 10 ng/mL of human bFGF.

The human umbilical vein endothelial cell line (EA.hy926) was cultured in DMEM low glucose (D5523) supplemented with 10% FBS, 100 units/mL of penicillin and 100 μg/mL of streptomycin.

The human monocytic cell line THP-1 was maintained in complete RPMI, containing RPMI-1640 media supplemented with 2 mM of L-glutamine, 100 units/mL of penicillin, 100 μg/mL of streptomycin, 10 mM HEPES buffer and 10% FBS.

Human monocyte-derived macrophages were generated from peripheral blood mononuclear cells (PBMCs). Buffy coats from healthy donors were acquired after obtaining written informed consent at the Hospital de Braga, Braga, Portugal (SECVS 014/2015) Briefly, PBMCs were enriched from buffy coats by density gradient using Histopaque-1077. The cells in the enriched mononuclear fraction were washed twice in PBS and resuspended in RPMI-1640 culture medium with 2 mM glutamine and 2 g/L $NaHCO_3$ supplemented with 10% human serum, 100 units/mL of penicillin, 100 μg/mL of streptomycin and 10 mM HEPES buffer.

All cells were incubated at 37 °C in a humidified 5% CO_2 atmosphere.

IV-2.4.2. LUVs cytocompatibility

LUVs cytocompatibility was assessed in the presence of hACs as well as of EA and THP-1 cell lines. hACs and EA were cultured at 5×10^4 cells per well in 24-well plates. For THP-1 cell differentiation, 5×10^5 cells per well were seeded with 100 nM phorbol 12-myristate-13-acetate (PMA) for 24 h. Cells were washed three times with RPMI, and to ensure cells reversion to a resting macrophage phenotype, cells were incubated for 48 h in RPMI without PMA. Then, cells were stimulated for 24 h with 100 ng/mL of lipopolysaccharide (LPS). LUVs sterilized through 0.22 μm filters were used for all cell culture experiments. Cells cultured without being exposed to LUVs (only with culture medium) were used as control. After 1, 3 and 7 days of culture with the LUVs, the different triplicate cell culture were rinsed with sterile PBS. Cell cultures were characterized regarding cell viability, cell proliferation, total protein synthesis and morphology.

IV-2.4.2.1 *Cell viability*

Two different assays were used to assess cell viability, alamar blue (AB) and Cell-Mediated Cytotoxicity Fluorometric Assay Kit (7-AAD/CFSE). The metabolic activity of the hACs and EA cell line was determined by AB reagent (Bio-Rad, USA), according to the instructions of the manufacturer. Briefly, medium containing 10% AB were added to each well. Samples were incubated for 4 h at 37 °C in a humidified 5% CO_2 atmosphere. The fluorescence was measured using excitation wavelength of 530/25 nm and at an emission wavelength of 590/35 nm, in a microplate reader (Synergy HT, BioTek, USA). For THP-1 cell line, 7-AAD/CFSE assay was used as described in the manufacturer' instruction. Live cells were labelled with a green fluorescent probe, carboxyfluorosuccinimide ester (CFSE), and apoptotic and necrotic cells were labelled with a red fluorescent probe, 7-aminoactinomycin D (7-AAD). After 24 h of incubation with different concentrations of LUVs, untreated and treated cells were collected in tubes by centrifugation at 300 g for 5 min. Then, cells were incubated for 30 min at 37 °C in a CO_2 incubator with 1 µl of CFSE Staining Solution and 1 µl of 7-AAD Staining Solution. The analyses were performed by flow cytometry.

IV-2.4.2.2 *Cell proliferation*

A fluorimetric dsDNA quantification kit Quant-iT™, PicoGreen® dsDNA Assay Kit (Invitrogen, Molecular Probes, USA) was used to assess cell proliferation. Prior to DNA quantification, samples were defrosted from de -80 °C and sonicated for 15 min. DNA standards were prepared at concentrations ranging from 0 to 2 µg/mL in ultrapure water. To each well of an opaque 96-well plate (Falcon) were added 28.7 µL of sample or standard (n=3), 71.3 µL of PicoGreen solution and 100 µL of Tris-EDTA (TE) buffer. The plate was incubated for 10 min in the dark, and the fluorescence of each sample was quantified using excitation/emission wavelengths of 485/528 nm, respectively, in a microplate reader (Synergy HT, BioTek, USA). The standard curve was used to calculate the DNA concentration of the samples.

IV-2.4.2.3 *Total protein*

A Micro BCA protein assay kit (Thermo Scientific, Pierce, USA) was used to quantify the total amount of protein, according to the manufacturer's instructions. Briefly, samples were collected in triplicate as described above. Standards were prepared in ultrapure water in concentrations ranging from 0 to 40

μg/mL. Then, 150 μL of samples or standards and 150 μL of working reagent were added to each 96-well plate. After 2 h incubation at 37 °C, the absorbance was measured at 562 nm using a microplate reader (Synergy HT, BioTek, USA). The standard curve was used to calculate the protein concentration of the samples.

IV-2.4.2.4 *Cell morphology analyses*

SEM was used to analyze the morphology of cells in the presence of different concentrations of the LUVs. Briefly, cells were fixed with 2.5% glutaraldehyde (in PBS) at 4 °C. Dehydration was performed by exposing the cells to increasing concentrations of ethanol (10, 20, 40, 60, 80, 90, 95 and 100%). Then, the samples were sputter-coated (EM ACE600, LEICA) with a thin layer (8-12 nm) of palladium and analyzed by High-Resolution Field Emission Scanning Electron Microscope (Auriga Compact, ZEISS). Microphotographs were recorded at 5 kV with magnifications of 200, 1000 and 10000 x.

IV-2.4.3. IL-23 capture by biofunctionalized LUVs

After stimulation of THP-1 cells with 100 ng/mL of LPS and 100 ng/mL of IFNγ, 2000 μM of biofunctionalized LUVs were added to the cell cultures and incubated during 24 h. The amount of IL-23 in the supernatants was assessed by ELISA. The stimulated cells not being exposed to the LUVs were used as controls.

IV-2.4.4. Effect of biofunctionalized LUVs on IL-17A production from PBMCs of healthy and RA patients

PBMCs of healthy patients were isolated as described above. Frozen PBMCs from RA patients were obtained from StemCell Tecnhology (Canada). Cells were cultured at 1.5×10^{6}/mL in culture medium under neutral activation (anti-CD3/CD28 beads, Miltenyl Biotec) or Th17 condition (anti-CD3/anti-CD28 beads, 10 ng/mL of IL-1β and 10 ng of IL-23 from R&D) [32]. After 24 h stimulation, LUVs and/or biofunctionalized LUVs (LUVs+Abs) were added to the culture. At the time point 3 and/or 7 days, the cell viability was assessed by AB and the supernatants were collected. IL-17A production was quantified by ELISA.

IV-2.5. IL-23 and IL-17A quantification

Human IL-23 and IL-17A ELISA kits were used according to the manufacturer instructions. The reaction of the chromogen 3,3', 5,5;-tetramethylbenzidine (TMB) substrate was stopped by the addition of a stop solution and the absorbance read in a microplate (Synergy HT, BioTek, USA) at 450 nm, with a wavelength correction set at 540 nm. The cytokines concentrations were inferred from the standard curve.

IV-2.6. Statistical Analyses

Three independent experiments were performed and data are presented as the mean ± standard deviation (SD). GraphPad Prism Software was used to perform the statistical analyses. As results do not follow a normal distribution (by Shapiro-Wilk test), the variances were assessed by nonparametric tests. Mann–Whitney U test was used when two groups were compared and the Kruskal-Wallis test followed by Dunn's multiple comparison test when more than two groups were compared.

IV-3. RESULTS

LUVs characterization, biofunctionalization, capability to capture the pro-inflammatory cytokine as well as their biological effects are herein described.

IV-3.1. LUVs characterization and biofunctionalization

LUVs composed of cholesterol/EPC/DSPE-PEG-Mal incorporating or not AuNPs were characterized in terms of size, PDI and zeta potential (**Table IV-1** and **Figure IV-2A**). The size was ≈124 nm for empty LUVs and ≈129 nm for LUVs encapsulating AuNPs. Both formulations revealed PDI values < 0.2, which indicates the homogeneity of the LUVs populations. Additionally, zeta potential measurements revealed that their surface charge is around -20 to -22 mV. Storage stability was also assessed (**Figure IV-2B**) and demonstrated that liposomes are stable for 6 months (size increased ≈10%).

From TEM analyses, AuNPs have a spherical shape and a diameter around 20 nm (**Figure IV-2C**), which is in agreement with the manufacturer specifications. The size of the LUVs+AuNPs of 130 nm is in line to the DLS measurements (**Figure IV-2D**).

To quantify the amount of the anti-IL-23 Abs covalently immobilized at the LUVs surface, an indirect method was used, namely the measurement of the fluorescence of the unbound secondary Abs. The difference of the fluorescence obtained in the presence of the total amount and unbound of the secondary Abs demonstrated that 82.1 ± 8.4% of anti-IL-23 Abs were efficiently immobilized at the LUVs surface. The size distribution and zeta potential of the biofunctionalized LUVs remained approximately the same (**Table IV-1**).

Table IV-1 – Size distribution and zeta potential of LUVs incorporating or not AuNPs at pH 7.4 and 37 °C.

Formulation	Size (nm)	PDI	Zeta potential
LUVs	123.8 ± 4.6	0.127 ± 0.056	-20.2 ± 1.1
LUVs + AuNPs	129.4 ± 4.0	0.114 ± 0.012	- 21.9 ± 1.8
LUVs+AuNPs+Anti-IL-23	130.1 ± 2.8	0.099 ± 0.015	-23.5 ± 1.4

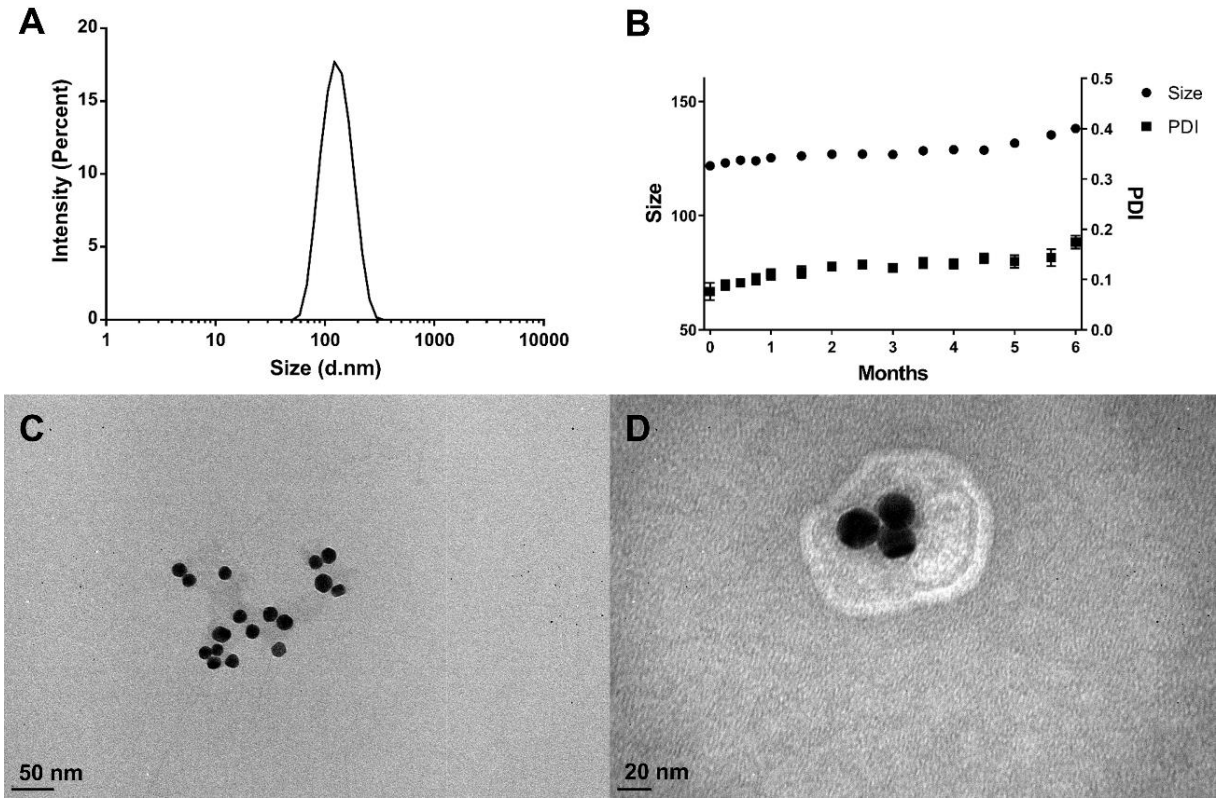

Figure IV-2 – (A) Size distribution of the LUVs+AuNPs. (B) Stability evaluation of LUVs+AuNPs kept in HEPES buffer at 4 °C for 6 months. TEM micrographs of the (C) AuNPs and (D) LUVs+AuNPs.

IV-3.2. LUVs cytocompatibility

To consider the use the proposed formulation in the RA treatment, it is critical to analyze the potential toxicity of the LUVs. For that it was used: *(i)* an endothelial cell line (EA.hy926), *(ii)* primary hACs and *(iii)* a human monocyte-like cell line (THP-1).

Different biological assays were conducted to assess cell viability (AB or 7-AAD/CFSE assay), proliferation (DNA quantification), total protein synthesis (MicroBCA) and morphology (SEM) after 1, 3 and 7 days of culture.

The *in vitro* studies with EA and hACs revealed that LUVs+AuNPs are biocompatible, since the cells viability and proliferation were not significantly affected (**Figure IV-3**). The culture of LUVs+AuNPs with EA cell line showed no differences in the metabolic activity for all the tested concentrations. Despite lower values of DNA and higher quantification of protein were obtained for the maximum concentration of liposomes, in general it can be assumed the non-toxicity of the produced LUVs incorporating AuNPs. For the hACs, although there is statically difference after 1 day of culture for the concentration of 2000 μM

LUVs in comparison to the control, after 3 and 7 days all tested conditions were not cytotoxic. Moreover, no significant differences were observed in the DNA and total protein quantification. These *in vitro* results were corroborated by SEM analyses (**Figure IV-4**), which shown no changes in both cells morphology.

Regarding the THP-1 cell line, **Figure IV-5A** shows that LUVs+AuNPs are cytocompatible for all the concentrations under evaluation. Indeed, no significant differences were observed in the cell activity percentages.

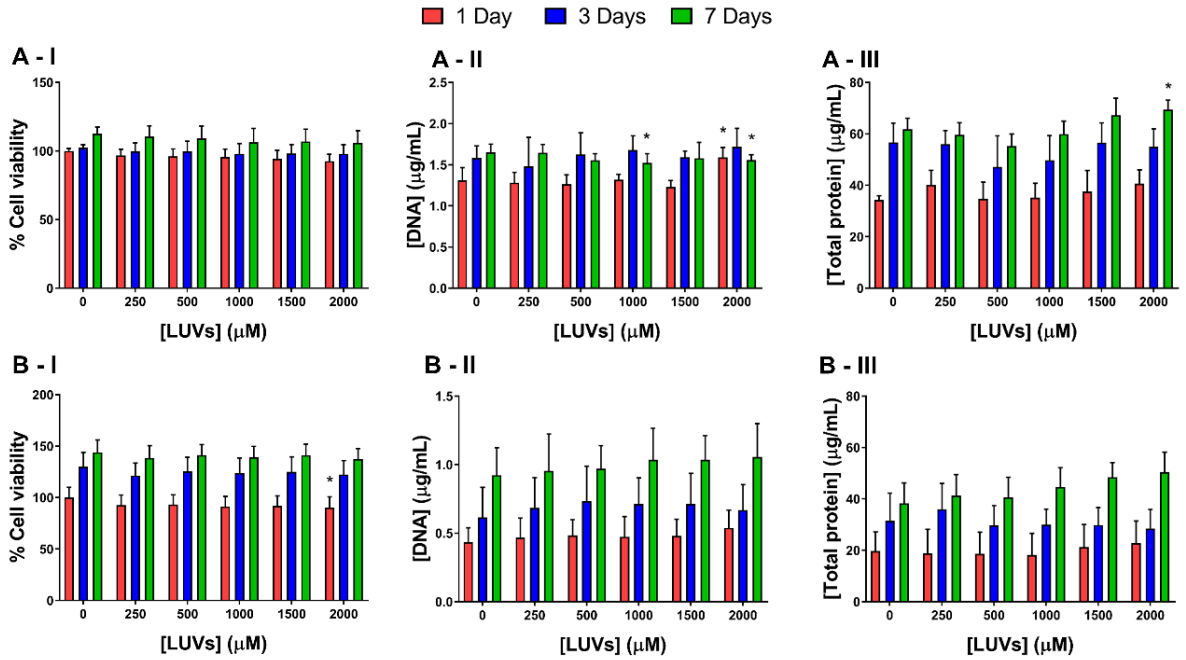

Figure IV-3 – Biological performance of the (A) EA cell line and (B) human articular chondrocytes (hACs) cultured with different concentrations of LUVs containing AuNPs: cell viability (I), cell proliferation (II) and total protein synthesis (III) after 1, 3 and 7 days of culture. Asterisk (*) denotes significant differences ($p < 0.01$) compared to the control (0 µM).

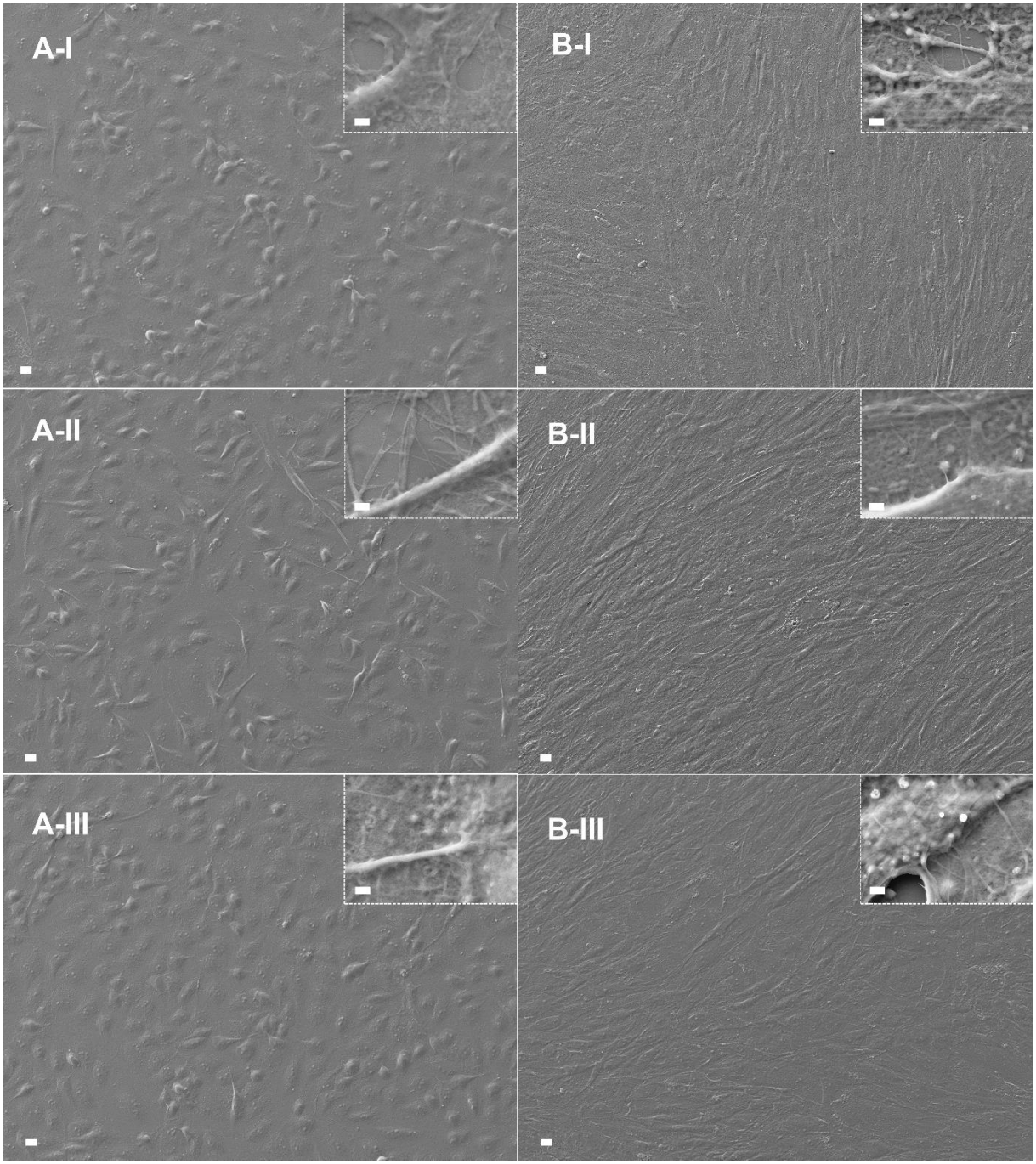

Figure IV-4 – SEM micrographs of (A) EA cell line and (B) hACs in the absence (control, I) and in the presence of different concentrations (II: 1000 μM and III: 2000 μM) of LUVs incorporating AuNPs after 7 days of culture. Scale bars: 10 μm (large images) and 1 μm (small images).

IV-3.3. IL-23 capture by biofunctionalized LUVs

To evaluate the capacity of the immobilized anti-IL-23 Abs to capture the IL-23 cytokine, a conditioned cultured medium of activated macrophages was used. After 24 h of incubation with 2000 μM of the biofunctionalized LUVs, they were able to capture 53.5 ± 9.6% of the produced cytokine (**Figure IV-5B**).

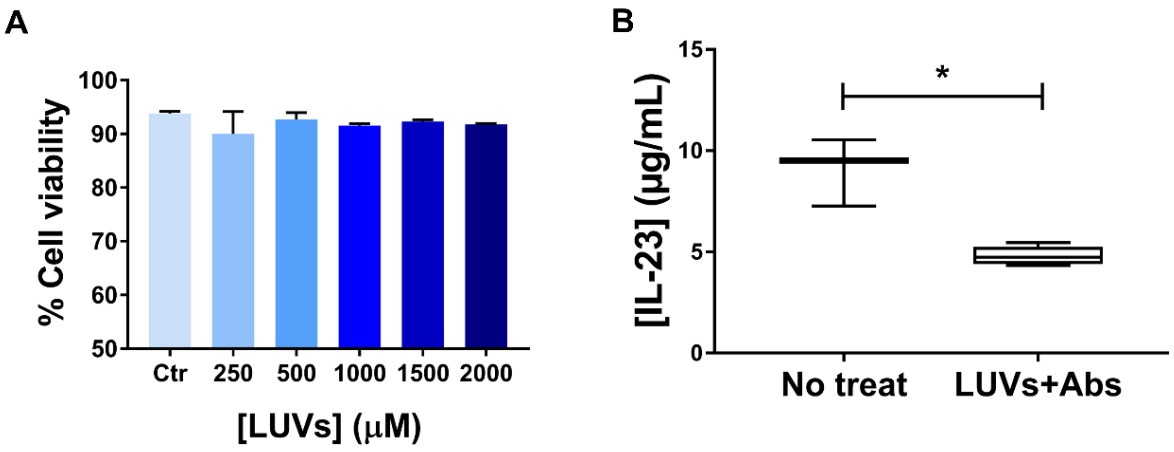

Figure IV-5 – (A) Percentage of THP-1 cell viability after cultured 24 h with different concentrations of LUVs incorporating AuNPs. (B) IL-23 quantification on the conditioned cultured medium of activated (LPS+IFNγ) THP-1 cell line in the absence and the presence of biofunctionalized LUVs incorporating AuNPs (LUVs+Abs). Asterisk (*) denotes significant differences ($p < 0.05$).

IV-3.4. Biological effects from IL-23 capture and neutralization by biofunctionalized LUVs

To confirm the inhibition of the IL-17A production by the anti-IL-23 Abs immobilized at the LUVs' surface, PBMCs from healthy and RA donors were activated for the Th17 phenotype (stimulation with anti-CD3/anti-CD28 beads, 10 ng/ml of IL-1β and 10 ng of IL-23) for 24 h. Then, three different conditions were tested: *(i)* no treatment (no treat), *(ii)* treatment with LUVs (LUVs) and *(iii)* treatment with biofunctionalized LUVs (LUVs+Abs). Non activated PBMCs were used as controls (Ctr).

Regarding the cell viability, the PBMCs differentiation reduced the metabolic activity in healthy donors (**Figure IV-6A-I**), since there is a significant decrease in the stimulation without treatment ($p < 0.05$) in comparison to the control. This reduction was prevented by LUVs addition. In the RA donors (**Figure IV-6B-II**), the capture and inactivation of the IL-23 conferred by the biofunctionalized LUVs significantly increased the metabolic activity.

From **Figure IV-6A-II**, there is a significant increase ($p < 0.0001$) in the amount of IL-17A production in the No treat group in comparison to the Ctr. Moreover, as observed in **Figure IV-6B-II**, PBMCs from RA patients produced more IL-17A than PBMCs from healthy donors when activated to the Th17 phenotype. This shown the high susceptibility to immune cell activation of the diseased patients. While LUVs had a little impact on the IL-17A production, the treatment with the biofunctionalized LUVs significantly reduced the IL-17A amount. Moreover, the reduction of IL-17A production followed a similar trend in both healthy and RA donors. Therefore, these results clearly indicate the positive impact of the IL-23 neutralization by the biofunctionalized LUVs.

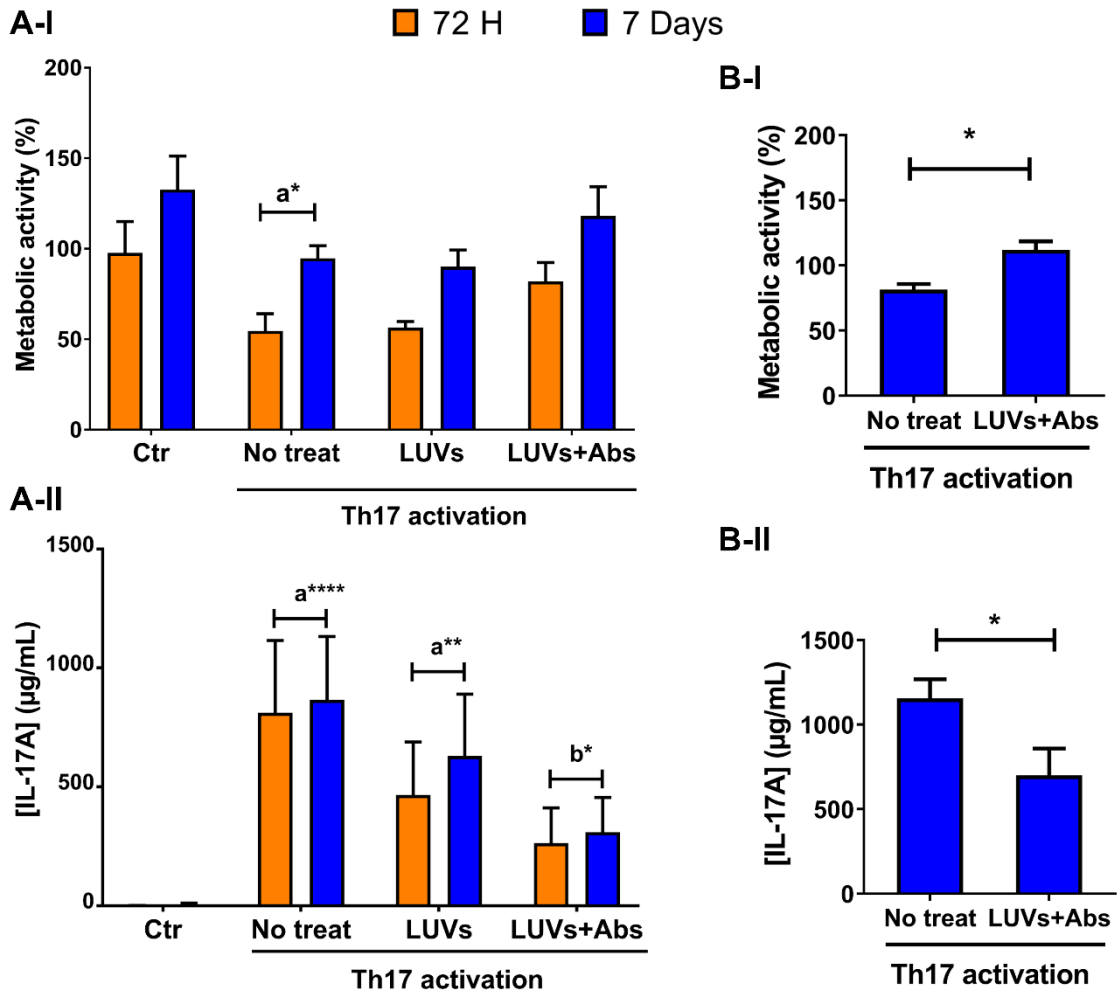

Figure IV-6 – Biological effects of the PBMCs of (A) healthy donors and (B) RA patients without (Ctr) and with Th17 activation in the absence (No treat) or in the presence of LUVs functionalized or not (LUVs) with anti-IL-23 Abs (LUVs+Abs) and analyzed regarding (I) metabolic activity and (II) IL-17A production. Letter "a" denotes significant difference compared to the Ctr, and "b" compared to No treat group, being * p<0.05, ** p<0.01, and **** p<0.0001.

IV-4. DISCUSSION

The aim of present study was to develop a carrier to capture and inactivate a central auto-immune mediator, IL-23, after systemic administration in RA patients. The short half-life of the Abs limits their therapeutic efficacy and considering the critical role of IL-23 in the pathogenesis of RA, the immobilization of the anti-IL-23 Abs at the LUVs surface will increase their beneficial effects. Indeed, as demonstrated in a previous study, immobilizing the Abs into a NPs surface can protect them from degradation, prolonging their half-life and increasing their efficacy [33]. Hence, biofunctionalized LUVs can be a viable carrier and provide an effective strategy to increase the Abs therapeutic efficacy after their systemic administration.

AuNPs were successfully incorporated into LUVs composed of cholesterol/EPC/DSPE-PEG-Mal/α-tocopherol. For the liposomal formulation composition, biomaterials with excellent biocompatibility and biological performance were selected to provide an efficient vehicle for RA treatment [34]. In this study, a 1:1 ratio of lipids and cholesterol was selected aiming to provide higher stability to the produced LUVs [35, 36]. EPC are the major class of phospholipids in biological membranes [37]. Since EPC obtained from egg yolk is biocompatible and biodegradable, formulations of this phospholipid are already in the clinical practice (e.g. Myocet® for the delivery of doxorubicin in metastatic breast cancer) [38, 39]. DSPE-PEG-Mal was introduced into the liposomal formulation to increase the blood circulation half-life. To avoid lipids oxidation that negatively affect the bilayer permeability and their storage life [40], α-tocopherol, a vitamin with antioxidant properties, was used. Additionally, it can also contribute to reduce reactive species that are upregulated in inflammation [41]. AuNPs were also incorporated into the liposomes due to their antioxidant and antiangiogenic effects, as well as, to allow monitoring the fate of the liposomes *in vivo*.

LUVs incorporating AuNPs presented around 130 nm of diameter, which is suitable for intravenous administration and for long-circulating times in the blood circulation. Moreover, due to the enhanced vascular permeability (EPR) effect of the inflamed tissues, LUVs will have enhanced ability to permeate into the synovial region [42]. The PDI value obtained (0.114 ± 0.012) was less than 0.2, indicating the presence of a monodisperse population in terms of size [43]. Due to the negative charge of DSPE-PEG-Mal, LUVs have a negative surface charge (-21.9 ± 1.8 mV). Indeed, neutral and negative surface charges reduce the adsorption of serum proteins, resulting in prolonged circulating half-lives [42]. In addition, the absolute value of zeta potential gives an indication of the particles suspension stability. Therefore, accordingly to the guidelines, a zeta-potential value around -22 mV indicates a moderately stable

suspension [44]. Storage stability studies also demonstrated their stability for at least 6 months, having only a marginal increase in size.

Thiol chemistry was used to immobilize the anti-IL-23 Abs to LUVs surface. Among a wide variety of methods reported for coupling Abs or proteins, thiolation has been widely used due to the fast aqueous reaction kinetics and mild reaction conditions [28]. In this work, thiol groups of the anti-IL-23 Abs were covalently linked to the terminal maleimide groups of DSPE-PEG-Mal on the LUVs surface. For that, first sulfhydryl groups were introduced in the Abs using 2-IT (Traut's reagent) [45]. The cyclic imidothioester react with primary amines in a ring-opening reaction regenerating a free sulfhydryl group. EDTA was added to the reaction to prevent disulfide bond formation as a result of sulfhydryl groups' oxidation. Then, the maleimide groups present on the LUVs surface reacts with the thiol groups of the Abs resulting in the formation of stable thioether bonds. In the present work, the amount of anti-IL-23 Abs added to the LUVs suspension was 1:20 of the DSPE-PEG-Mal molar ratio. The percentage of Abs immobilized at LUVs surface was of 82.1 ± 8.4%. Furthermore, the antibodies immobilization did not disturb significantly the LUVs properties.

*In vitr*o cellular studies were carried out to assess the cytotoxicity of the produced LUVs+AuNPs for endothelial cells, chondrocytes and immune cells. Endothelial cells and hACs are suitable models to assess any toxic interaction between the developed formulation with the blood vessels and the cells from the cartilage tissue, respectively. Indeed, hACs isolated from diseased knee arthroplasties have a phenotype associated with arthritic diseases. Additionally, since the immune system has an important role in these diseases, the cytocompatibility with macrophages was also assessed. Overall, the results obtained from the metabolic activity, DNA and total protein quantification clearly showed their cytocompatibility until the maximum concentration tested (2000 μM). In addition, SEM micrographs confirmed that LUVs+AuNPs did not affect cell morphology. Indeed, these results were predictable, since a reduced or even lack of cytotoxicity was reported in many studies with liposomes [17]. *In vitro* assays were also performed to assess the ability of the formulation to capture and inactivate the IL-23 cytokine. Macrophages can be differentiated from monocytes in two main phenotypes: pro-inflammatory phenotype (M1; producing high levels of TNF-α, IL-1, IL-6, IL-12, IL-23 and reactive oxygen species) and anti-inflammatory phenotype (M2; producing high levels of IL-10, IL-1Ra, TGF-β, and low levels of IL-12) [46]. Therefore, M1 phenotype has a major role in prolonging the inflammatory process in RA, while M2 is crucial for the anti-inflammatory response and tissue remodeling. Considering the aim of the present work, macrophages were stimulated to the inflammatory M1 phenotype in order to produce the IL-23

cytokine. After 24 h of incubation with M1 macrophages, the biofunctionalized LUVs efficiently captured the IL-23 cytokine (53.5 ± 9.6%). Thus, these results confirm the ability of this innovative system to capture the native form of the pro-inflammatory cytokine IL-23. Since IL-23 has a major role in the Th17 differentiation, we investigated whereas the biofunctionalized LUVs could avoid the activation of the PBMCs to the Th17 phenotype, reducing consequently the production of the pro-inflammatory cytokine IL-17A. PBMCs were activated for 24 h and then three conditions were tested: *(i)* no treatment, *(ii)* treatment with LUVs and *(iii)* treatment with biofunctionalized LUVs. PBMCs not submitted to the activation conditions were used as controls (Ctr). The increased amount of IL-17A in the stimulated conditions demonstrated the induction of the PBMCs to the Th17 phenotype. As previously reported [32], after stimulation, PBMCs from RA patients produce more IL-17A than PBMCs from healthy donors. The addition of biofunctionalized LUVs significantly reduced the amount of IL-17A cytokine produced from stimulated PBMCs obtained from both healthy and RA patients. Moreover, LUVs alone could reduce at some level the IL-17A production. Since AuNPs have the ability to reduce the oxidative stress, they could inhibit cytokine production. Indeed, previous studies reported that AuNPs can specifically inhibit TNFα and IL-17A cytokines production after macrophages stimulation with LPS [47]. Regarding the metabolic activity, the reduction observed in the stimulation conditions was suppressed by the biofunctionalized LUVs. Thus, by targeting IL-23, biofunctionalized LUVs can inhibit the key inflammatory cascade that leads to IL-17A production. The blocking of IL-17A production will reduce joint swelling and inflammation as well as cartilage erosion [8]. Therefore, the developed IL-23 axis targeted LUVs are a promising therapeutic approach for RA and other ADs.

IV-5. Conclusion

The anti-IL-23 Abs immobilized at the surface of LUVs encapsulating AuNPs were able to selectively capture and inactivate the pro-inflammatory cytokine IL-23. Due to the key role of IL-23 in the Th17 cells activation, the biofunctionalized LUVs efficiently reduced this process and, consequently, the production of the IL-17A cytokine by those cells. Since LUVs provide a platform to improve Abs biodistribution, they will be able to overcome the current limitations of the systemic administration of biological agents. Indeed, the limited therapeutic efficacy of the Abs is associated with their rapid clearance from the body, which demands higher doses and extended times of treatment in order to have a clinical positive effect. Moreover, the synergist effects of the reduction in IL-23 and IL-17A levels and anti-oxidant activity (vitamin E and AuNPs) will potentiate the therapeutic effect.

This innovative carrier can increase the efficacy of Abs for longer times and, consequently, the developed biofunctionalized LUVs are a better approach not only for RA treatment, but also for other inflammatory ADs.

IV-6. ACKNOWLEDGMENTS

Authors acknowledge the financial support from FCT/MCTES (Portuguese Foundation for Science and Technology/Ministry of Science, Technology and Higher Education) and the FSE/POCH (European Social Fund through the Operational Program of Human Capital), for the PhD scholarship PD/BD/11384/2015 of A. C. Lima (PD/59/2013), and the FCT for the contracts of A. Carvalho (CEECIND/03628/2017) and C. Cunha (CEECIND/04601/2017). Authors would also like to acknowledge FCT for the project PTDC/CTM-BIO/4388/2014 – SPARTAN, and the Northern Portugal Regional Operational Programme (NORTE 2020), under the Portugal 2020 Partnership Agreement, through the European Regional Development Fund (FEDER) (NORTE-01-0145-FEDER-000023-FROnTHERA and NORTE-01-0145-FEDER-000013-PersonalizedNOS). The authors also acknowledge NORTE 2020 Structured Project within the R&D&I Structured Project, co funded by Norte2020 - Programa Operacional Regional do Norte.

IV-7. REFERENCES

1. Smolen, J. S., Aletaha, D. and McInnes, I. B., Rheumatoid arthritis. *Lancet*. 2016, *388* (10055): p. 2023-38.
2. Sparks, J. A., Rheumatoid Arthritis. *Ann Intern Med*. 2019, *170* (1): p. 1-6.
3. Guo, Q., Wang, Y., Xu, D., *et al.*, Rheumatoid arthritis: pathological mechanisms and modern pharmacologic therapies. *Bone Res*. 2018, *6*: p. 1-15.
4. Siebert, S., Tsoukas, A., Robertson, J., *et al.*, Cytokines as Therapeutic Targets in Rheumatoid Arthritis and Other Inflammatory Diseases. *Pharmacol Rev*. 2015, *67* (2): p. 280-309.
5. Lefevre, S., Meier, F. M., Neumann, E., *et al.*, Role of synovial fibroblasts in rheumatoid arthritis. *Curr Pharm Des*. 2015, *21* (2): p. 130-41.
6. McInnes, I. B. and Schett, G., Cytokines in the pathogenesis of rheumatoid arthritis. *Nat Rev Immunol*. 2007, *7* (6): p. 429-42.
7. McKenzie, B. S., Kastelein, R. A. and Cua, D. J., Understanding the IL-23-IL-17 immune pathway. *Trends Immunol*. 2006, *27* (1): p. 17-23.
8. Tang, C. L., Chen, S., Qian, H., *et al.*, Interleukin-23: as a drug target for autoimmune inflammatory diseases. *Immunology*. 2012, *135* (2): p. 112-24.

9. Frieder, J., Kivelevitch, D., Haugh, I., *et al.*, Anti-IL-23 and Anti-IL-17 Biologic Agents for the Treatment of Immune-Mediated Inflammatory Conditions. *Clin Pharmacol Ther*. 2018, *103* (1): p. 88-101.
10. Paradowska-Gorycka, A., Grzybowska-Kowalczyk, A., Wojtecka-Lukasik, E., *et al.*, IL-23 in the pathogenesis of rheumatoid arthritis. *Scand J Immunol*. 2010, *71* (3): p. 134-45.
11. Yago, T., Nanke, Y., Kawamoto, M., *et al.*, IL-23 and Th17 Disease in Inflammatory Arthritis. *J Clin Med*. 2017, *6* (9): p. 1-9.
12. Zaky, D. S. E. and El-Nahrery, E. M. A., Role of interleukin-23 as a biomarker in rheumatoid arthritis patients and its correlation with disease activity. *Int Immunopharmacol*. 2016, *31*: p. 105-8.
13. Smolen, J. S., Agarwal, S. K., Ilivanova, E., *et al.*, A randomised phase II study evaluating the efficacy and safety of subcutaneously administered ustekinumab and guselkumab in patients with active rheumatoid arthritis despite treatment with methotrexate. *Ann Rheum Dis*. 2017, *76* (5): p. 831-9.
14. Ridgley, L. A., Anderson, A. E. and Pratt, A. G., What are the dominant cytokines in early rheumatoid arthritis? *Curr Opin Rheumatol*. 2018, *30* (2): p. 207-14.
15. Woodrick, R. S. and Ruderman, E. M., Safety of biologic therapy in rheumatoid arthritis. *Nat Rev Rheumatol*. 2011, *7* (11): p. 639-52.
16. Prasad, L. K., O'Mary, H. and Cui, Z., Nanomedicine delivers promising treatments for rheumatoid arthritis. *Nanomedicine (Lond)*. 2015, *10* (13): p. 2063-74.
17. Bulbake, U., Doppalapudi, S., Kommineni, N., *et al.*, Liposomal Formulations in Clinical Use: An Updated Review. *Pharmaceutics*. 2017, *9* (2): p. 1-33.
18. Anselmo, A. C. and Mitragotri, S., Nanoparticles in the clinic. *Bioeng Transl Med*. 2016, *1* (1): p. 10-29.
19. Monteiro, N., Martins, A., Reis, R. L., *et al.*, Liposomes in tissue engineering and regenerative medicine. *J R Soc Interface*. 2014, *11* (101): p. 1-24.
20. Kojima, C., Hirano, Y., Yuba, E., *et al.*, Preparation and characterization of complexes of liposomes with gold nanoparticles. *Colloid Surface B*. 2008, *66* (2): p. 246-52.
21. Yeh, Y. C., Creran, B. and Rotello, V. M., Gold nanoparticles: preparation, properties, and applications in bionanotechnology. *Nanoscale*. 2012, *4* (6): p. 1871-80.
22. Ferreira, H., Martins, A., da Silva, M. L. A., *et al.*, The functionalization of natural polymer-coated gold nanoparticles to carry bFGF to promote tissue regeneration. *J Mater Chem B*. 2018, *6* (14): p. 2104-15.
23. Bhattacharya, R., Mukherjee, P., Xiong, Z., *et al.*, Gold nanoparticles inhibit VEGF165-induced proliferation of HUVEC cells. *Nano Lett*. 2004, *4* (12): p. 2479-81.
24. Kirdaite, G., Leonaviciene, L., Bradunaite, R., *et al.*, Antioxidant effects of gold nanoparticles on early stage of collagen-induced arthritis in rats. *Res Vet Sci*. 2019, *124*: p. 32-7.
25. Dolati, S., Sadreddini, S., Rostamzadeh, D., *et al.*, Utilization of nanoparticle technology in rheumatoid arthritis treatment. *Biomed Pharmacother*. 2016, *80*: p. 30-41.
26. Bangham, A. D. and Horne, R. W., Negative Staining of Phospholipids and their Structural Modification by Surface-Active Agents as Observed in the Electron Microscope. *J Mol Biol*. 1964, *8*: p. 660-8.
27. Ferreira, H., Gonçalves, V. M. F., Silva, R., *et al.*, Development of Liposomes-in-Hydrogel Formulations Containing Betamethasone for Topical Therapy. *J Pharmaceut Drug Deliv Safety*. 2017, *1* (3): p. 1-8.

28. Manjappa, A. S., Chaudhari, K. R., Venkataraju, M. P., *et al.*, Antibody derivatization and conjugation strategies: application in preparation of stealth immunoliposome to target chemotherapeutics to tumor. *J Control Release*. 2011, *150* (1): p. 2-22.
29. Kouchakzadeh, H., Shojaosadati, S. A., Tahmasebi, F., *et al.*, Optimization of an anti-HER2 monoclonal antibody targeted delivery system using PEGylated human serum albumin nanoparticles. *Int J Pharmaceut*. 2013, *447* (1-2): p. 62-9.
30. Deng, L., Zhang, Y. Y., Ma, L. L., *et al.*, Comparison of anti-EGFR-Fab' conjugated immunoliposomes modified with two different conjugation linkers for siRNA delivery in SMMC-7721 cells. *Int J Nanomed*. 2013, *8*: p. 3271-83.
31. da Silva, M. L. A., Costa-Pinto, A. R., Martins, A., *et al.*, Conditioned medium as a strategy for human stem cells chondrogenic differentiation. *J Tissue Eng Regen M*. 2015, *9* (6): p. 714-23.
32. Xue, X., Soroosh, P., De Leon-Tabaldo, A., *et al.*, Pharmacologic modulation of RORgammat translates to efficacy in preclinical and translational models of psoriasis and inflammatory arthritis. *Sci Rep*. 2016, *6*: p. 1-17.
33. Lima, A. C., Cunha, C., Carvalho, A., *et al.*, Interleukin-6 Neutralization by Antibodies Immobilized at the Surface of Polymeric Nanoparticles as a Therapeutic Strategy for Arthritic Diseases. *Acs Appl Mater Inter*. 2018, *10* (16): p. 13839-50.
34. Ferreira, H., Fangueiro, J. F. and Neves, N. M., The Role of Natural-Based Biomaterials in Advanced Therapies for Autoimmune Diseases. *Adv Exp Med Biol*. 2018, *1077*: p. 127-46.
35. Hosta-Rigau, L., Zhang, Y., Teo, B. M., *et al.*, Cholesterol - a biological compound as a building block in bionanotechnology. *Nanoscale*. 2013, *5* (1): p. 89-109.
36. Briuglia, M. L., Rotella, C., McFarlane, A., *et al.*, Influence of cholesterol on liposome stability and on in vitro drug release. *Drug Deliv Transl Re*. 2015, *5* (3): p. 231-42.
37. van der Veen, J. N., Kennelly, J. P., Wan, S., *et al.*, The critical role of phosphatidylcholine and phosphatidylethanolamine metabolism in health and disease. *Bba-Biomembranes*. 2017, *1859* (9): p. 1558-72.
38. Balazsovits, J. A. E., Mayer, L. D., Bally, M. B., *et al.*, Analysis of the Effect of Liposome Encapsulation on the Vesicant Properties, Acute and Cardiac Toxicities, and Antitumor Efficacy of Doxorubicin. *Cancer Chemoth Pharm*. 1989, *23* (2): p. 81-6.
39. Leonard, R. C. F., Williams, S., Tulpule, A., *et al.*, Improving the therapeutic index of anthracycline chemotherapy: Focus on liposomal doxorubicin (Myocet (TM)). *Breast*. 2009, *18* (4): p. 218-24.
40. Hernandezcaselles, T., Villalain, J. and Gomezfernandez, J. C., Stability of Liposomes on Long-Term Storage. *J Pharm Pharmacol*. 1990, *42* (6): p. 397-400.
41. Quinn, P. J., The effect of tocopherol on the structure and permeability of phosphatidylcholine liposomes. *J Control Release*. 2012, *160* (2): p. 158-63.
42. Blanco, E., Shen, H. and Ferrari, M., Principles of nanoparticle design for overcoming biological barriers to drug delivery. *Nat Biotechnol*. 2015, *33* (9): p. 941-51.
43. Panchal, J., Kotarek, J., Marszal, E., *et al.*, Analyzing subvisible particles in protein drug products: a comparison of dynamic light scattering (DLS) and resonant mass measurement (RMM). *The AAPS journal*. 2014, *16* (3): p. 440-51.
44. Bhattacharjee, S., DLS and zeta potential - What they are and what they are not? *J Control Release*. 2016, *235*: p. 337-51.
45. Traut, R. R., Bollen, A., Sun, T. T., *et al.*, Methyl 4-Mercaptobutyrimidate as a Cleavable Crosslinking Reagent and Its Application to Escherichia-Coli 30s Ribosome. *Biochemistry*. 1973, *12* (17): p. 3266-73.

46. Rana, A. K., Li, Y., Dang, Q.*, et al.*, Monocytes in rheumatoid arthritis: Circulating precursors of macrophages and osteoclasts and, their heterogeneity and plasticity role in RA pathogenesis*. Int Immunopharmacol*. 2018, *65*: p. 348-59.
47. Kingston, M., Pfau, J. C., Gilmer, J.*, et al.*, Selective inhibitory effects of 50-nm gold nanoparticles on mouse macrophage and spleen cells*. J Immunotoxicol*. 2016, *13* (2): p. 198-208.

Chapter V

Enzymatic- and redox-responsive polymeric micelles for targeted and controlled drug delivery on arthritic diseases

Chapter V

Enzymatic- and redox-responsive polymeric micelles for targeted and controlled drug delivery on arthritic diseases[1]

ABSTRACT

Inflammation plays a vital role in arthritis development and progression. Despite the advances in the pharmaceutical field, currently available treatments still present low efficacy and severe side effects. To establish a distinctive drug delivery system sensitive to the articular inflammation microenvironment, this work proposes a newly enzymatic- and redox-responsive polymeric micelle for efficient dexamethasone (Dex) delivery. Thus, a linear copolymer composed of methoxypolyethylene glycol-glutathione-palmitic acid (mPEG-GSH-PA) was synthetized and the thiol groups of the GSH were oxidized intermolecularly to retain the drug into the micelles. The produced spherical micelles presented a uniform size of 100 nm, and a loading capacity of Dex up to 65%. In physiological conditions, Dex release from the micelles presented slow and sustained kinetics. However, in the presence of GSH at a concentration similar to the intracellular level and glutathione reductase (GR) enzyme activity found in the arthritic articular cavities, the drug release is significantly facilitated (burst release). Biological assays demonstrated their cytocompatibility in contact with human endothelial cells, human articular chondrocytes and human macrophages. Importantly, the assays with chondrocytes and macrophages in both monoculture and co-culture systems showed the beneficial role of encapsulating the drug into the micelles. Indeed, the micelles in the presence of GR and redox media promoted a targeted and sustained release of the drug. Moreover, the developed drug delivery system exhibited a higher efficacy than the free Dex while reducing the negative effects of the drug in normal cells. In conclusion, this formulation is a promising approach to treat arthritic diseases and other inflammatory conditions.

[1]This chapter is based on the following publication:

Lima A. C., Ferreira H., Neves N. M. Enzymatic- and redox-responsive polymeric micelles for targeted and controlled drug delivery on arthritic diseases. *(Submitted)*. 2019.

V-1. INTRODUCTION

The two most common forms of arthritis, osteoarthritis (OA) and rheumatoid arthritis (RA), are joint disorders associated with chronic synovial inflammation, pain and tissue damage [1]. The high worldwide prevalence, the long-term disability and the severe functional limitations in the patient quality of life, explain the significant economic burden associated to those diseases [2]. Although the etiology of both diseases is still unknown, recent studies recognized that matrix-degrading enzymes and inflammatory mediators, produced by numerous exogenous and endogenous factors, are important mechanisms to trigger the degradation of cartilage [3].

Since arthritis has currently no cure, the main objectives of the treatments focus in reducing the pain, to slow down the inflammatory progression and to delay the beginning of irreversible joint damage, as an attempt to improve physical function as well as quality of life of the patients [4]. The available treatment options include non-steroidal anti-inflammatory drugs (NSAIDs) and glucocorticoids (GCs) for OA and RA, and disease modifying anti-rheumatic drugs (DMARDs) and biologicals therapies for RA (still in clinical trials for OA). The European League Against Rheumatism (EULAR) emphasize the importance of an early intervention [5]. Consequently, immediately after the diagnosis, those guidelines recommend the administration of low-dose GCs, such as dexamethasone (Dex) and prednisolone, followed by longer term modulation of inflammation using DMARDs in the case of RA. Owing to their potent anti-inflammatory and immune-suppressive actions, GCs are among the most commonly prescribed drugs for various inflammatory, autoimmune and allergic disorders [6]. Nevertheless, their use is severely hampered by the risk of developing serious side effects, such as osteoporosis, hyperglycemia, insulin resistance and hypertension. Moreover, the therapeutic efficiency is limited, due to inadequate pharmacokinetics, with low drug bioavailability and off-targeted biodistribution profile [7]. These therapeutic drawbacks can be overcomed by designing nanomedicines, namely drug delivery systems, which have been successfully introduced in the clinic for the treatment of cancer, pain and infectious diseases [8].

Polymeric micelles are demonstrating promising potential as nanoparticles (NPs) to effectively encapsulate a wide variety of biological agents and to control their distribution and function in the body [7, 9]. Indeed, among the clinical nanomedicines with translation potential, polymeric micelles exhibit several features that favor their use for drug delivery applications, including biocompatibility, longevity, high *in vitro* and *in vivo* stability, as well as the ability to increase the drug bioavailability and accumulation in target tissues [9, 10]. The typical spherical core-shell structure in aqueous media is formed through

the self-assembling of amphiphilic copolymers, where the hydrophobic units of the copolymer aggregate in the inner core surrounded by the hydrophilic units [11].

Engineered NPs that respond to pathophysiological parameters, such as redox potential and pH were developed to control the spatiotemporal distribution of the drugs, to reduce the dosage and to avoid systemic side effects [12, 13]. Such signals can be endogenously present in the body, or intensified or distinctly overexpressed in diseased tissues. In this study, redox and glutathione reductase (GR) dual responsive micelles were explored as targeted drug delivery systems to inflamed articular tissues. Glutathione (GSH) is the key regulator of the intracellular redox state and is required for the detoxification of, for example, reactive oxygen species (ROS), peroxides and electrophilic xenobiotic compounds as well as for the regeneration of other endogenous and exogenous antioxidants [14]. In those reactions, two GSH molecules become oxidized and join together via a disulfide bond between the cysteine residues to form glutathione disulfide (GSSG). In its turn, GSSG can be reduced by glutathione reductase (GR) to regenerate GSH. Therefore, since GSH concentrations outside cells is reportedly as low as 2 - 20 μM whereas intracellularly it ranges from 2 to 10 mM, redox-responsive nanomedicines can be used for specific intracellular drug delivery [15]. Intracellular GSH exchanges with the thiol disulfide bond of GSSG in the polymeric micelles will promote their disruption and a rapid drug release. Furthermore, it was found higher activity of GR in the synovial fluid of RA and OA patients, in comparison with normal controls [16, 17]. Therefore, this enzyme can also selectively stimulate the drug release in arthritic tissues.

Polymeric micelles were made of methoxypolyethylene glycol amine-glutathione-palmitic acid (mPEG-GSH-PA) copolymers. PEG is widely used in the pharmaceutical and nanotechnology field, due to its essential role in avoiding the adsorption of opsonin proteins [7]. Indeed, PEG reduces the immunogenicity of therapeutic formulations, increases their pharmacokinetic profile and reduces the unspecific biodistribution [19, 20]. GSH is a tripeptide synthesized by the sequential addition of cysteine to glutamate followed by the addition of glycine (γ-l-glutamyl-l-cysteinyl-glycine) [23]. In recent years, many drug delivery system are taking advantages of this antioxidant to coat the surface of the NPs [24, 25] or to produce NPs, micelles and polymers that are responsive to a redox medium [26-29]. PA is the most common saturated fatty acid (16:0) found in animals, plants and microorganisms [30]. Fatty acids are carboxylic acids with a hydrophobic tail that play an important role in the cell function and metabolism. Considering the ubiquity of fatty acids in the organisms, PA and other fatty acids, including stearic acid (18:0) and myristic acid (14:0), are being combined with other polymers, such as chitosan [31, 32], PEG [26, 33] and polycaprolactone (PCL) [34] to produce core–shell type nanoparticles and polymeric micelles.

Therefore, the aim of this study is to develop a drug carrier intended for targeted delivery of an anti-inflammatory drug in inflamed articular joints. After systemic administration, the micelles will be passively accumulated in the articular inflammation through the enhanced permeability and retention (EPR) effect. Once in the joints, the extracellular GR and intracellular GSH will destabilize the micellar structure into monomeric ones through a thiol-disulfide exchange, triggering the drug release from the micelles. Micelles preparation and their dual mechanism of drug release is illustrated in **Figure V-1**. The produced micelles presented the ability to successfully entrap a lipophilic drug in its hydrophobic compartment. Dex was used as the model drug for this study and its maximum entrapment and *in vitro* release profile with different stimulus were assessed. The cytocompatibility of the polymeric micelles was validated by adding them to the medium of cultures of endothelial and monocytic cell lines, as well as human articular chondrocytes (hACs). To validate our system further, a co-culture model of articular inflammation was also established using hACs and stimulated macrophages. The differences in the cell viability and morphology, as well as the concentration of pro-inflammatory cytokines were all evaluated after the treatment with micelles encapsulating Dex or the free Dex. Considering the current limitations of GC treatments, we hypothesized that this strategy will increase the drug therapeutic efficacy, reducing the severe side effects by limiting the exposure of healthy tissues.

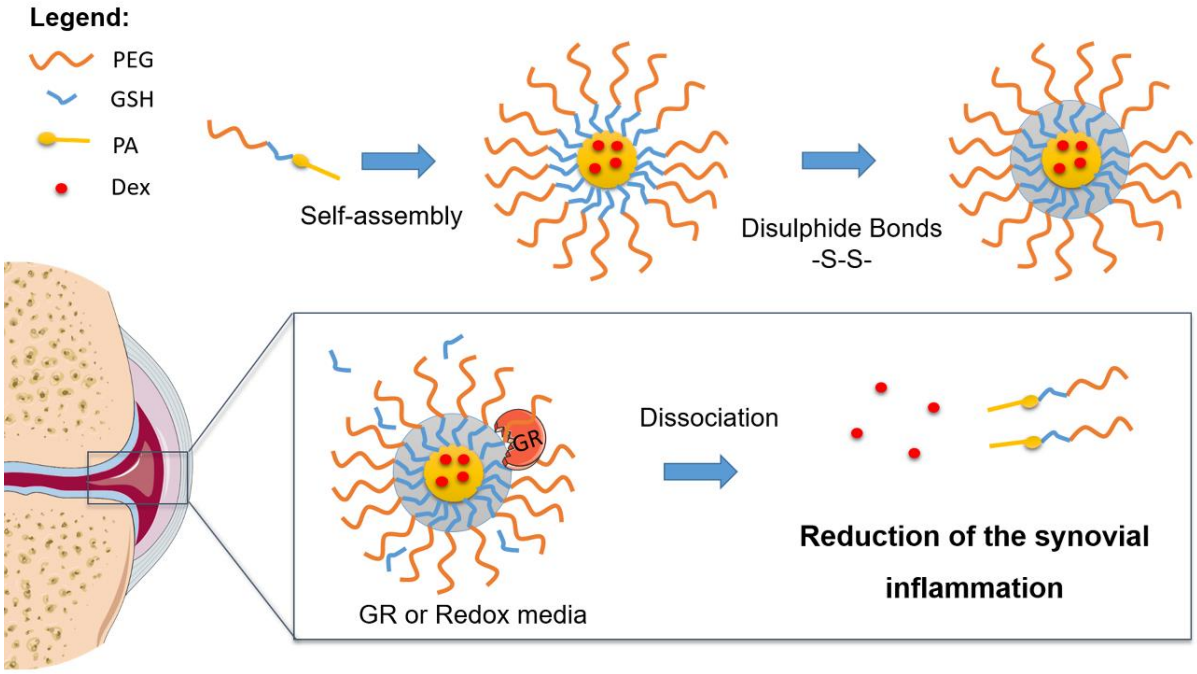

Figure V-1 – Schematic illustration of the enzymatically (Glutathione reductase –GR) and glutathione (GSH) responsive polymeric micelles rationale for arthritis treatment. Abbreviations: PEG, Polyethylene glycol; PA, Palmitic acid; Dex, Dexamethasone.

V-2. MATERIALS AND METHODS

The methods used for the synthesis of the copolymers, the micelles preparation and its characterization considering their chemical and physical properties and drug encapsulation efficacy are herein described. In addition, it is also reported the methods used to characterize the *in vitro* drug release kinetics from the micelles and their cytocompatibility and biologic effects.

V-2.1. Materials

Unless otherwise noted, all chemicals were purchased from Sigma-Aldrich (USA), stored and further used as supplied.

Roswell Park Memorial Institute (RPMI)-1640 Medium and Fetal Bovine Serum (FBS) were purchased from Thermo Fisher Scientific (USA). Human IL-6 and TNF-α Standard ABTS ELISA Development Kits and human Fibroblast Growth Factor (bFGF) was acquired from Peprotech (USA).

V-2.2. Synthesis of mPEG-GSH-PA copolymers

In order to prepare methoxypolyethylene glycol amine-glutathione-palmitic acid (mPEG-GSH-PA) copolymers, the first step was to covalently link mPEG OF 5000 kDa with GSH. For that mPEG (0.01 mmol) and GSH (0.02 mmol) reacted in ultra-pure water for 24 h at room temperature (RT), using as coupling agents 1-(3-Dimethylaminopropyl)-3-ethylcarbodiimide (EDC)/N-Hydroxysuccinimide (NHS) at 50/200 mM in MES hydrate at pH 4.7. The product of the reactions was placed in dialysis systems with 3.5-5 kDa cut-off to remove the unreacted compounds. Then, the water was removed by freeze drying. In the second step, mPEG-GSH reacted with PA (0.011 mmol) in tetrahydrofuran (THF) using 2-(1H-Benzotriazole-1-yl)-1,1,3,3-tetramethylaminium tetrafluoroborate (TBTU, 0.011 mmol) and triethylamine (TEA, 0.02 mmol) for 24 h at RT.

V-2.3. Micelles preparation

For the micelles production the polymer solutions were added dropwise at a rate of 1 mL/min to ultra-pure water with strong magnetic stirring (600 rpm) during 48 h.

To remove unreacted compounds, the micelles were washed twice with ultrapure water by centrifugation (45 min, 5000 rpm at 20 °C) using Vivaspin 300 kD Filter Units (Fisher Scientific, USA).

V-2.4. Micelles characterization

Several testing methods were conducted to demonstrate the main physical and chemical properties of the micelles.

V-2.4.1. Chemical characterization

Fourier-transform infrared spectroscopy (FTIR) was used to identify the chemical structures of all the products. The co-polymers were analyzed using an IRPrestige 21 spectrometer (Shimadzu, Japan) in the range of 500 - 4000 cm^{-1} by the KBr-disk method.

V-2.4.2. Particle size, polydispersity index (PDI) and zeta potential

The evaluation of size distribution and zeta-potential of the micelles was performed in a Zetasizer Nanoseries ZS equipment (Malvern Instruments, Portugal), using dynamic light scattering (DLS) and laser Doppler micro-electrophoresis, respectively. The measurements were performed at 25 °C.

V-2.4.3. Stability studies

Storage stability was assessed by measuring the micelles size, PDI and zeta potential during the experimental time (6 months). The micelles were kept at 4 °C under static conditions.

V-2.4.4. NPs morphology

Morphological analysis of the developed micelles was performed by scanning electron microscopy (SEM). Prior to SEM analysis, the micelles were disposed into the surface of a glass slide to air-dry, and then sputter-coated with palladium (EM ACE600, LEICA) and analyzed using High-Resolution Field Emission Scanning Electron Microscope (Auriga Compact, ZEISS).

V-2.5. Drug entrapment efficiency

The Dex loading content in the micelles was determined with micelle:Dex feed weight ratios varying from 1:0.2 to 1:0.8 at a micelle concentration of 1 mg/mL. Dex was added to THF solution and then the micelles were produced as previously described. The non-encapsulated Dex was measured in the supernatant of the centrifuged solution using an UV spectroscopy (Shimadzu, Japan) with the samples diluted in ethanol (0.5:0.5 v/v).

Entrapment efficiency (EE) was calculated by measuring the initial concentration and non-encapsulated Dex, according to the following formula:

$$\%EE = \frac{(\text{Initial concentration} - \text{ not encapsulated drug})}{\text{Initial concentration}} \text{ x } 100$$

V-2.6. *In vitro* drug release profile

The *in vitro* Dex release profiles of micelles under different external conditions were obtained and measured through a dialysis method. Firstly, 5 mL of micelle suspension were added to a dialysis system (3.5 - 5 MWCO) before putting it in a centrifugation tube containing 15 mL PBS (pH 7.4). The tube was shaken at 100 rpm at 37 °C. At the defined time points, an aliquot of solution (0.5 mL) was retrieved from the outside tube with equal volume replenishment. After dilution of the aliquot with 0.5 mL ethanol, Dex concentration was measured using an UV spectroscopy equipment (Shimadzu, Japan). The redox- and enzymatically-responsive properties were evaluated using the same method but with a different external media - PBS containing *(i)* 10 mM of GSH or *(ii)* 50 mU of GR (with 0.14 mM NADPH and 0.1 mM EDTA).

V-2.7. Biological Assays

In order to assess the cytocompatibility of the developed micelles and their biological effects after encapsulation of Dex, the cell isolation and culture, viability, proliferation, protein content and morphology were performed as described in the following sub-sections.

V-2.7.1. Cell Culture

Knee cartilage samples collected from arthroplasties surgeries were used for hACs isolation. Samples were obtained through the cooperation agreement established between the Centro Hospitalar do Alto Ave, Guimarães, Portugal, and the 3B's Research Group, after obtaining the donor informed consent. Cells were isolated by enzymatic digestion, according to a previously described protocol [18]. hACs cells were cultured in Dulbecco's modified Eagle's medium (DMEM) high glucose (D5671), supplemented with 10% FBS, 10 mM L-lanyl-L-glutamine, MEM with non-essential aminoacids, HEPES buffer, 100 units/mL of penicillin, 100 μg/mL of streptomycin and 10 ng/mL of human bFGF, and incubated at 37 °C in a humidified 5% CO_2 atmosphere.

Human umbilical vein endothelial (EA.hy926) cell line was cultured in DMEM low glucose (D5523) supplemented with 10% FBS, 100 units/mL of penicillin and 100 μg/mL of streptomycin.

The human monocytic cell line THP-1 was maintained in complete RPMI, containing RPMI-1640 media supplemented with 2 mM of L-glutamine, 100 units/mL of penicillin, 100 μg/mL of streptomycin, 10 mM HEPES buffer and 10% FBS.

V-2.7.2. Cytotoxicity of mPEG-GSH-PA micelles

The cytotoxicity of the micelles were evaluated over primary hACs, EA and THP-1 cell lines. hACs and EA were cultured at 5×10^4 cells per well in 24-well plates. The THP-1 cell line was seeded at 5×10^5 cells per well with 100 nM phorbol 12-myristate-13-acetate (PMA) for 24 h, to promote its differentiation. Cells were washed three times with RPMI, and to ensure cells reversion to a resting macrophage phenotype, cells were incubated for 48 h in RPMI without PMA. Then, cells were stimulated for 24 h with 100 ng/mL of lipopolysaccharide (LPS), in order to obtain M1-polarized macrophages. For all the cell types, an increasing concentration of micelles sterilized through 0.22 μm filters were used. The cells cultured without being exposed to micelles (only with culture medium) were used as controls. After 1, 3 and 7 days of culture with the micelles, the different samples in triplicate were rinsed with sterile PBS and analyzed regarding cell viability (Alamar blue assay), cell proliferation (DNA quantification), total protein synthesis and SEM analysis of the cell morphology.

V-2.7.2.1 *Cell viability*

The metabolic activity of cells treated or not with different concentrations of micelles was determined by Alamar blue (AB) reagent (Bio-Rad, USA), according to the instructions of the manufacturer. Briefly, medium containing 10% AB was added to each well. Samples were incubated for 4 h at 37 °C in a humidified 5% CO_2 atmosphere. The fluorescence was measured using excitation wavelength of 530/25 nm and at an emission wavelength of 590/35 nm, in a microplate reader (Synergy HT, BioTek, USA).

V-2.7.2.2 *Cell proliferation*

A fluorimetric dsDNA quantification kit (Quant-iT™, PicoGreen®, Invitrogen, Molecular Probes, USA) was used to assess cell proliferation. Prior to DNA quantification, samples were thawed from -80 °C and sonicated for 15 min. DNA standards were prepared at concentrations ranging from 0 to 2 μg/mL in ultrapure water. To each well of a 96-well plate (Falcon) was added 28.7 μL of sample or standard (n=3),

71.3 μL of PicoGreen solution and 100 μL of Tris-EDTA (TE) buffer. The plate was incubated for 10 min in the dark, and the fluorescence of each sample was measured using an excitation/emission wavelengths of 485/528 nm, respectively, in a microplate reader (Synergy HT, BioTek, USA). The standard curve was used to infer the DNA concentration of the samples.

V-2.7.2.3 *Total protein*

A Micro BCA protein assay kit (Thermo Scientific, Pierce, USA) was used to quantify the total amount of protein, according to the manufacturer's instructions. Briefly, samples were collected in triplicate as described above. Standards were prepared in ultrapure water in concentrations ranging from 0 to 40 μg/mL. Then, 150 μL of samples or standards and 150 μL of working reagent were added to each 96-well plate. After 2 h incubation at 37 °C, the absorbance was measured at 562 nm using a microplate reader (Synergy HT, BioTek, USA). The standard curve was used to infer the protein concentration of the samples.

V-2.7.2.4 *Cell morphology analyses*

SEM was used to analyze the morphology of the cells in the presence of different concentrations of the micelles. Briefly, cells were fixed with 2.5% glutaraldehyde at 4 °C. Dehydration was performed using increasing concentrations of ethanol (10, 20, 40, 60, 80, 90, 95 and 100%). Then, the samples were sputter-coated (EM ACE600, LEICA) with a thin layer (8-12 nm) of palladium and analyzed by High-Resolution Field Emission Scanning Electron Microscope (Auriga Compact, ZEISS). Microphotographs were recorded at 5 kV with magnifications of 200, 1000 and 10,000.

V-2.7.3. Biological effects of Dex encapsulated into micelles

The biological effects of the micelles encapsulating the drug were assessed in a co-culture system. hACs and THP-1 cell line were seeded as previously described, being the THP-1 seeded at 2.5×10^5 cells per well in 24-well cell culture inserts (pore size: 1 μm) for the co-culture systems. The inserts were transferred to the hACs culture, and the macrophages were activated to the M1 phenotype by adding 100 ng/mL of LPS. After 2 h of stimulation, 3 different conditions were tested: *(i)* no treatment, *(ii)* micelles encapsulating Dex, and *(iii)* free Dex. Those conditions were also tested in the hACs and THP-1 cells

seeded alone (monoculture). GR was added to the co-culture system at 50 mU (no GR was added to the monocultures). After 1, 3, 7 and 14 days, the samples were collected and evaluated regarding cell viability, proliferation and SEM analyses, as described. The amount of IL-6 and TNF-α in the media was assessed by ELISA. During the time of the experiment 300 μL of fresh media was added each 3 days, but no media was removed to maintain constant the quantity of micelles in the culture medium.

V-2.7.4. Cytokines quantification

For the quantification of the IL-6 and TNF-α, human sandwich ELISAs Kit were performed according to the manufacturer procedure. ABTS liquid substrate was added to each well and the color development was monitored in a microplate (Synergy HT, BioTek, USA) at 405 nm, with a wavelength correction set at 650 nm. Cytokines concentration was inferred from the standard curve.

V-2.8. Statistical Analyses

Data are presented as the mean ± standard deviation (SD) of at least three independent assays. GraphPad Prism Software was used to perform the statistical analyses. To access the normality of the data, a Shapiro–Wilk test was used, and since data not followed a normal distribution, it was performed the Kruskal–Wallis test (a nonparametric test) followed by Dunn's test. Statistically significance was considered with $p < 0.01$.

V-3. RESULTS

Micelles characterization, drug encapsulation efficacy, *in vitro* release kinetics as well as biological effects are herein described.

V-3.1. Micelles characterization

The triblock amphiphilic copolymer was synthesized via a two-step polymerization reaction. The first step involved the reaction of mPEG with the carboxylic groups of GSH. In the second step the free amine groups of GSH reacted with the carboxylic groups of PA. FTIR analysis of the micelles (**Figure V-2A**) showed a shift of the amine group from the mPEG and GSH (two N-H stretch absorptions at 3300-3000 cm^{-1}) to

amide in the micelles (one N-H stretch absorption at 3300 cm^{-1} and a C=O peak at 1680-1630 cm^{-1}). Moreover, while the GSH present a weak thiol (S-H) peak at 2550-2620 cm^{-1}, the micelles presented a weak disulfide (S-S) peak at 700-550 cm^{-1}. The size of the micelles (**Figure V-2B**) was 101.3 ± 3.4 nm with a zeta potential of -20.2 ± 3.42 mV and a PDI value of 0.092 ± 0.011. Since the PDI value was lower than 0.2, we can conclude that the population of obtained micelles is homogeneous in size. The assessment of the storage stability (**Figure V-2C**) demonstrated that the size of the micelles is stable for at least 6 months (without a significant variation of size and PDI). From the SEM micrographs (**Figure V-2D**), it is visible the spherical shape of the micelles and the diameter of around 100 nm, being this result in agreement with the DLS data.

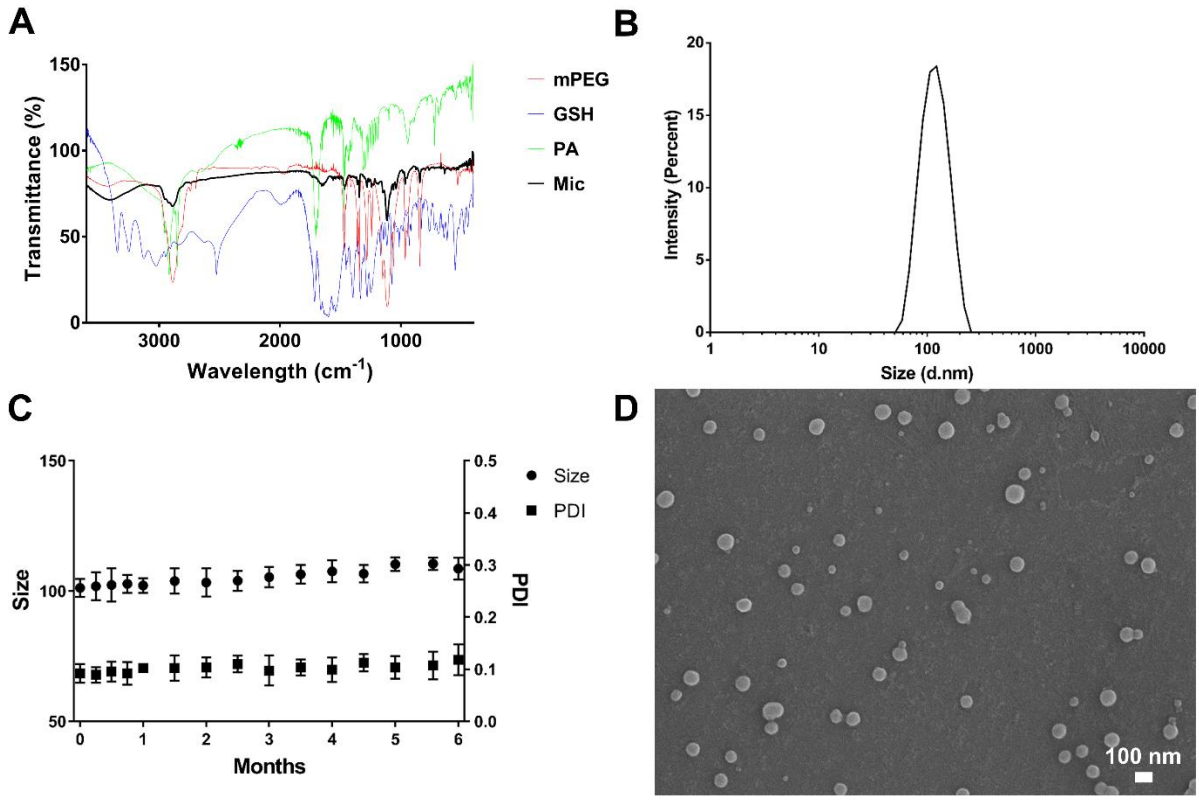

Figure V-1 – (A) FTIR analysis of the methoxypolyethylene glycol (mPEG), glutathione (GSH), palmitic acid (PA) and the micelles (Mic). (B) Size distribution of the micelles. (C) Evaluation of the size stability of the micelles kept in water at 4 °C during 6 months. (D) SEM micrographs of the micelles.

V-3.2. Efficacy of drug encapsulation and *in vitro* release kinetics

Dex was used as a model hydrophobic drug in this study. To obtain the drug loaded micelles, Dex was dissolved in the organic phase of the micelles using feed weight ratios varying from 1:0.2 to 1:0.8 at a polymer concentration of the micelles of 1 mg/mL. The **Table V-1** shows that the Dex loading content

and entrapment efficiency increased directly with the micelle:Dex feed weight ratio, reaching a maximum of 64% in the 1:0.8 condition. After the entrapment of the drug, the micelles presented a size of 118.8 ± 0.2 nm, with 0.105 ± 0.009 of PDI and a zeta potential of -17.4 ± 2.7 mV.

After quantifying the amount of encapsulated Dex, the 1:0.8 ratio was selected to evaluate its *in vitro* release profile (**Figure V-3**). Using the dialysis method, different artificial media were used. Micelles presented almost no release in the first 24 h in the presence of PBS at 37 °C and shown a maximum release of 20% after 5 days of incubation. In contrast, the addition of GSH at an intracellular level (10 mM) increased the kinetics of Dex release, reaching the maximum of ≈ 50% after 5 days. The addition of GR at 50 mU induced a burst release with ≈ 80% of the drug released in the first 24 h. These results show the slow release profile of Dex from the developed micelles and their sensitivity in the presence of GSH and GR enzyme.

Table V-1 – Dex loading content and entrapment efficiency into the micelles at a concentration of 1 mg/mL

Micelles:Dex feed weight ratio	Dex loading content (mg)	Entrapment efficiency (%)
1:0.2	0.57 ± 0.03	35.3 ± 1.9
1:0.4	1.38 ± 0.08	39.8 ± 1.3
1:0.6	2.50 ± 0.10	51.9 ± 2.1
1:0.8	4.65 ± 0.11	64.6 ± 1.6

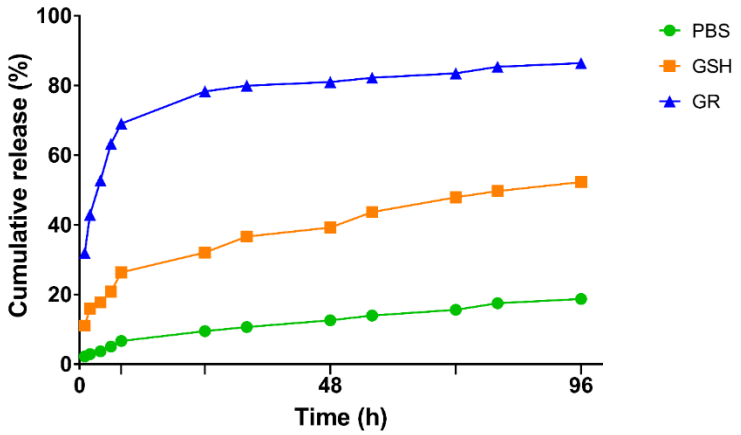

Figure V-2 – Release profile of Dex from the micelles when exposed to different environments: PBS, 10 mM of GSH and 50 mU of GR at 37°C.

V-3.3. Biological Assays

The cells metabolic activity, proliferation and morphology were assessed to demonstrate the cytocompatibility and biologic effects of the developed micelles.

V-3.3.1. Micelles cytocompatibility

In vitro cell studies were carried out to assess the viability of relevant cells that can be affected by our delivery device when systemically administered. Being the synovial cavity the main site of therapeutic action aimed, we used primary hACs from diseased knee arthroplasties (phenotype associated with arthritis disease), endothelial cells (main cells of the blood vessels) and macrophages (immune system). After 1, 3, and 7 days of culture, different biological assays were performed to assess the cell viability (AB assay), proliferation (DNA quantification), total protein synthesis and morphology (SEM). All cells tested shown excellent cytocompatibility of the micelles until a concentration of 50 μg/mL (**Figure V-4**). Considering the hACs and the EA cell line, the cell viability, DNA quantification and protein expression was not negatively affected for concentrations below 50 μg/mL. Above this concentration there is a significant reduction of the cytocompatibility in comparison with the control. For the THP-1 cell line, none of the concentrations reduce the cell viability, but there is a reduction in the DNA and protein quantification above 100 μg/mL of micelles. It can also be observed a decay over time regarding the DNA and the total protein concentration, both in the control and in the cells exposed to the micelles. This is a normal feature of those cells, since they do not replicate. Moreover, the SEM analyses of the cell cultures confirmed that

the cell morphology was not affected by the presence of the micelles even for concentrations of 100 μg/mL (**Figure V-5**). Thus, we can infer that the maximum concentration of micelles that does not have a harmful effect to the cells is 50 μg/mL.

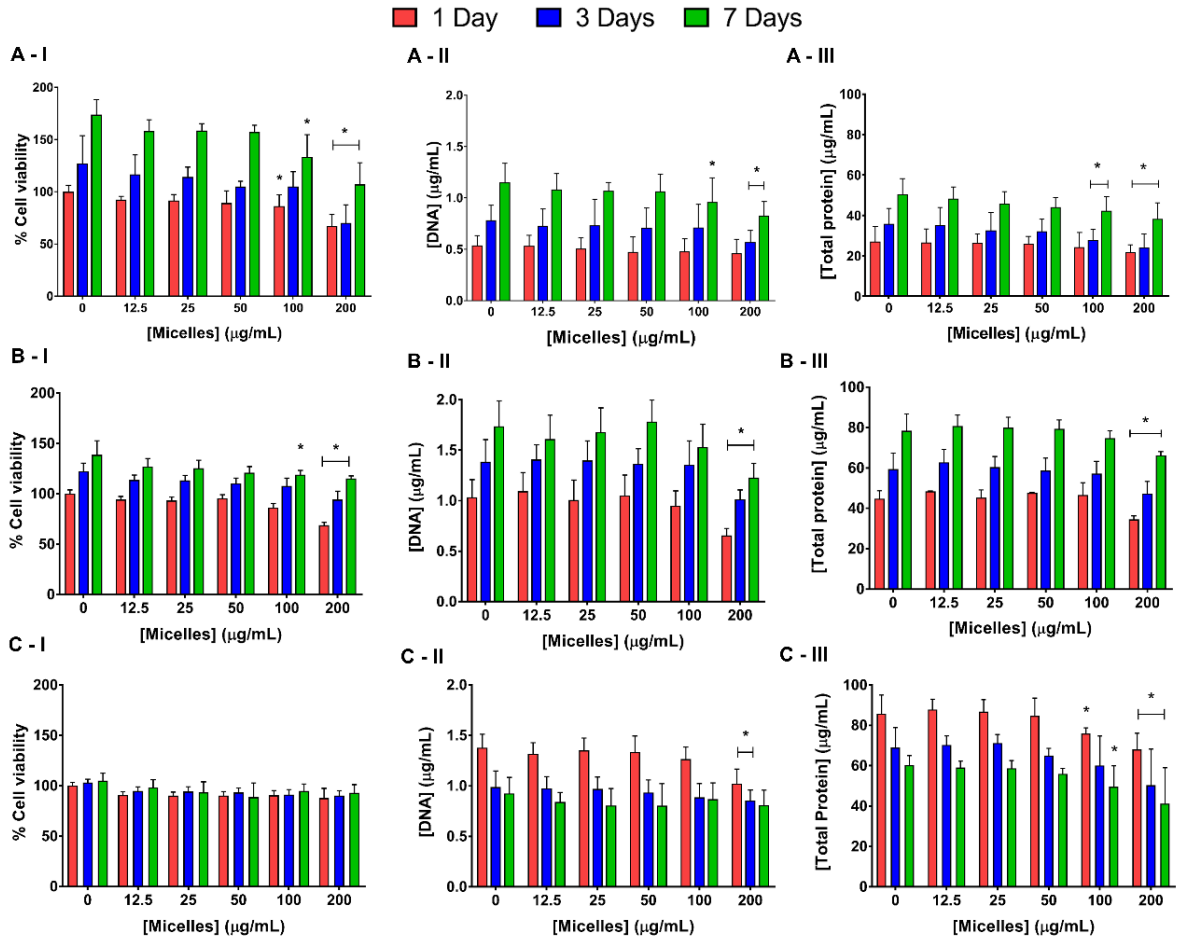

Figure V-3 – Biological performance of the (A) hACs, (B) EA cell line, and (C) THP-1 cell line cultured with different concentrations of micelles: (I) cell viability, (II) cell proliferation and (III) total protein synthesis after 1, 3, and 7 days of culture. Asterisk (*) denotes significant differences ($p < 0.01$) compared to the control (0 µg/mL).

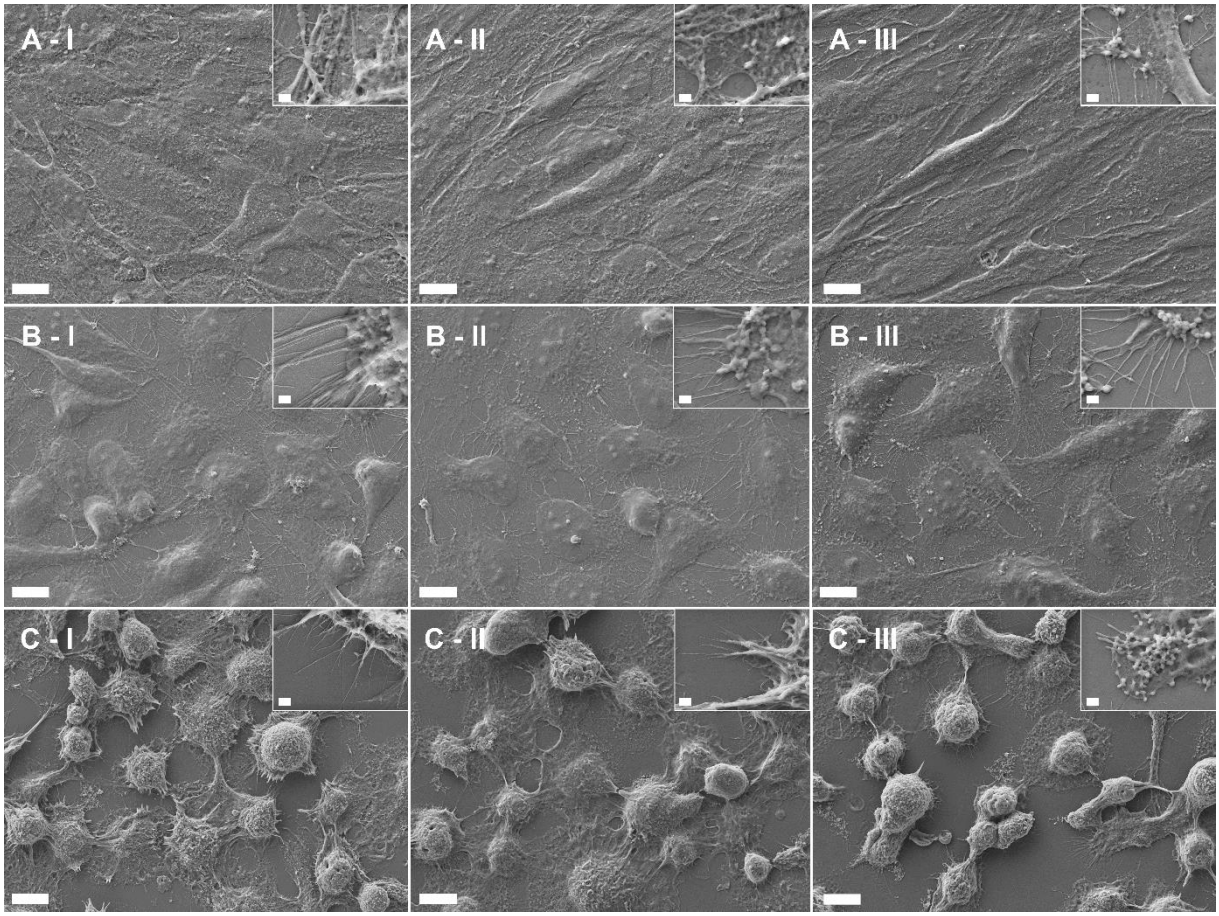

Figure V-4 – SEM micrographs of the micelles cultured with (A) hACs, (B) EA cell line and (C) THP-1 cell line in the absence (control, I) and in the presence of the micelles at different concentrations: (II) 50 and (III) 100 μg/mL. Scale bar 10 μm.

V-3.3.2. Biological effects of Dex in monocultures and co-culture of hACs and THP-1

To compare the biological effects of the micelles encapsulating Dex with the free Dex, both monoculture and co-culture of hACs and stimulated M1 macrophages were used. Three different conditions were tested: *(i)* no treatment (Ctr), *(ii)* treatment with micelles encapsulating Dex (Mic+Dex), and *(iii)* treatment with free Dex (Dex). The concentration of Dex was 100 μM, and in the co-culture system 50 mU of GR was added to the culture medium to accelerate the release kinetics, mimicking synovial inflammation.

In monoculture, the hACs viability and proliferation were significantly reduced with the free Dex treatment (**Figure V-6A**). Interestingly, the encapsulation of the Dex into the micelles was able to block the Dex negative effects over hACs, as there are no differences between the Ctr and Mic+Dex groups. In addition, the morphological analyses of the hACs (**Figure V-7A**) show that the encapsulation of the drug

did not affect the cell density nor the morphology of the cells observed in the Dex group. This effect was also observed in the THP-1 cell line (**Figure V-6B**), where in the presence of micelles a higher cell viability and proliferation were observed when compared with the treatment with free Dex. The co-culture of hACs with activated M1 macrophages significantly decreased the cell viability and proliferation comparatively to the hACs control (**Figure V-6A**). While the treatment with Mic+Dex was able to reduce this harmful effect over the chondrocytes, the treatment with free Dex was not. Indeed, the Mic+Dex treatment significantly increase the cell viability in comparison with the co-culture without treatment. These results were corroborated with the morphological analyses of the hACs (**Figure V-7B**). After 14 days of co-culture, the hACs presented altered morphology with cell shrinkage and a reduction of cell density. The treatment with the micelles encapsulating Dex was able to prevent these features more effectively than the free Dex. Additionally, the co-culture system do not present negative effects over THP-1 cells, but the addition of the Mic+Dex and Dex significantly reduced the amount of DNA, especially after 1 day of treatment.

The co-culture of hACs and activated macrophages had a huge impact on the amount of the pro-inflammatory cytokines produced by those cells. TNF-α and IL-6 cytokines (**Figures V-6C** and **D**, respectively) were quantified in the medium. While the hACs almost do not produce TNF-α, activated M1 macrophages produce around 1.3 ng/mL after 1 day, which was reduced to 0.1 ng/mL after 14 days. In this case, all conditions (Ctr, Mic+Dex and Dex in THP-1) presented a similar reduction of this cytokine in the medium. However, the micelles encapsulating Dex were able to reduce more TNF-α amount in the co-culture system than the free Dex, especially after 3 days. This result can be explained through the GR controlled release of the Dex from the micelles over the time. Regarding the IL-6, the establishment of the co-culture system increased the expression of this cytokine to a maximum ≈ 1.2 μg/mL. In this case, both encapsulating and free Dex were capable to effectively reduce the amount of this cytokine in the medium to ≈ 0.1 μg/mL.

One of the biggest problems of the treatments with GCs are the negative effects over normal cells. Herein, we show that the micelles were able to protect the chondrocytes from those effects. Importantly, the encapsulation of the Dex into the micelles did not compromise the biological activity of the drug and protects the chondrocytes in an inflammatory scenario by reducing the expression of pro-inflammatory cytokines. Therefore, the overall results confirmed the initial hypothesis that micelles can prolong and extend the half-life of the drug, increase its therapeutic efficacy and reducing the side effects.

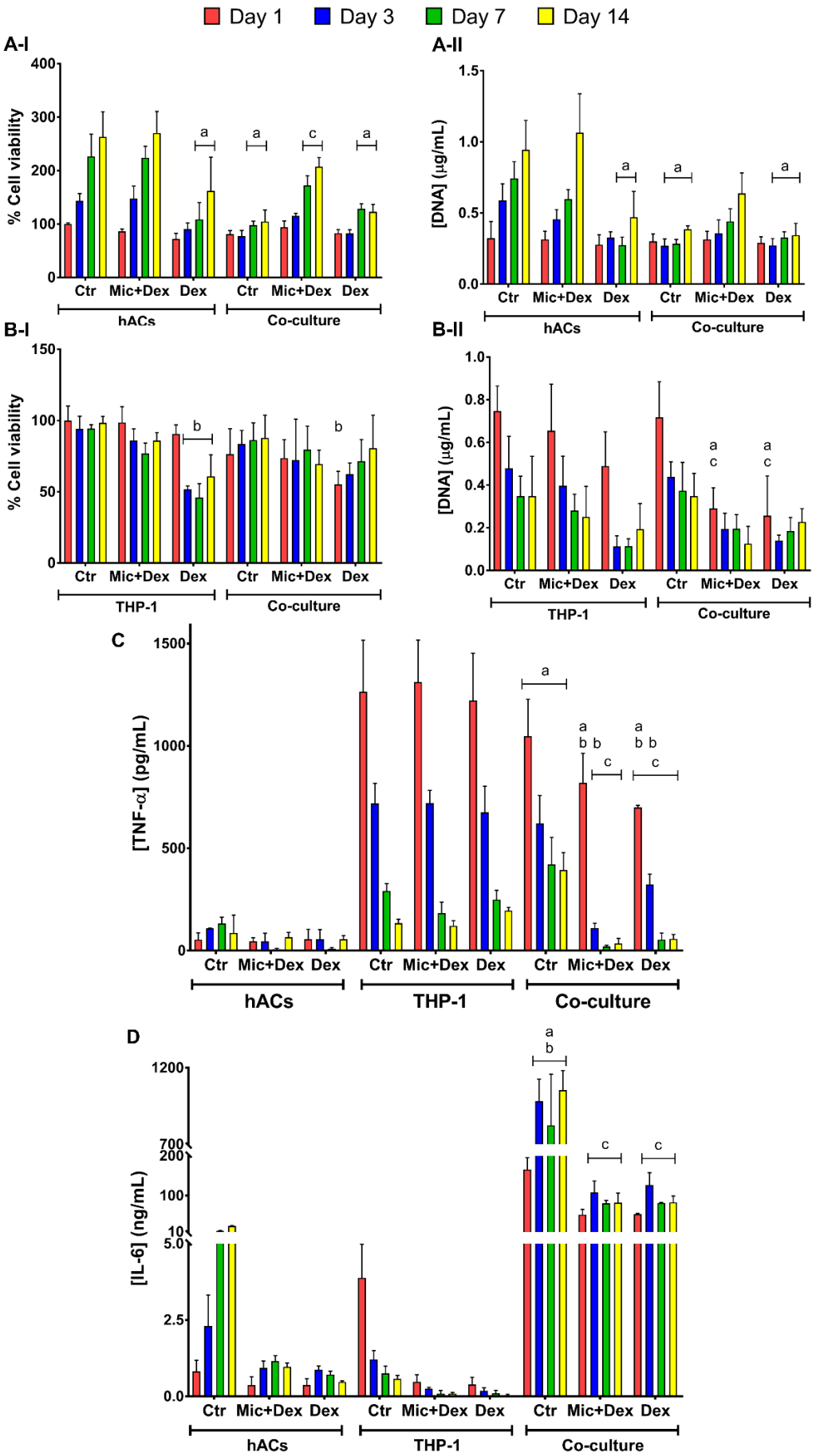
Day 1
Day 3
Day 7
Day 14
A-I
% Cell viability
A-II
[DNA] (µg/mL)
B-I
% Cell viability
B-II
[DNA] (µg/mL)
Ctr
Mic+Dex
Dex
hACs
Co-culture
THP-1
C
[TNF-α] (pg/mL)
D
[IL-6] (ng/mL)

Figure V-5 – Biochemical performance of (A) hACs and (B) THP-1 cultured in monolayers and hACs co-cultured with activated M1 macrophages after treatment with different conditions: control (Ctr, no treatment), micelles encapsulating Dex (Mic+Dex) and Dex. The samples were analyzed regarding (I) cell viability, (II) cell proliferation, (C) TNF-α concentration, and (D) IL-6 concentration. The alphabet "a" denotes significant difference as compared to hACs Ctr, "b" denotes significant difference as compared to THP-1 Ctr, and "c" denotes significant difference as compared to co-culture Ctr, where $p < 0.01$.

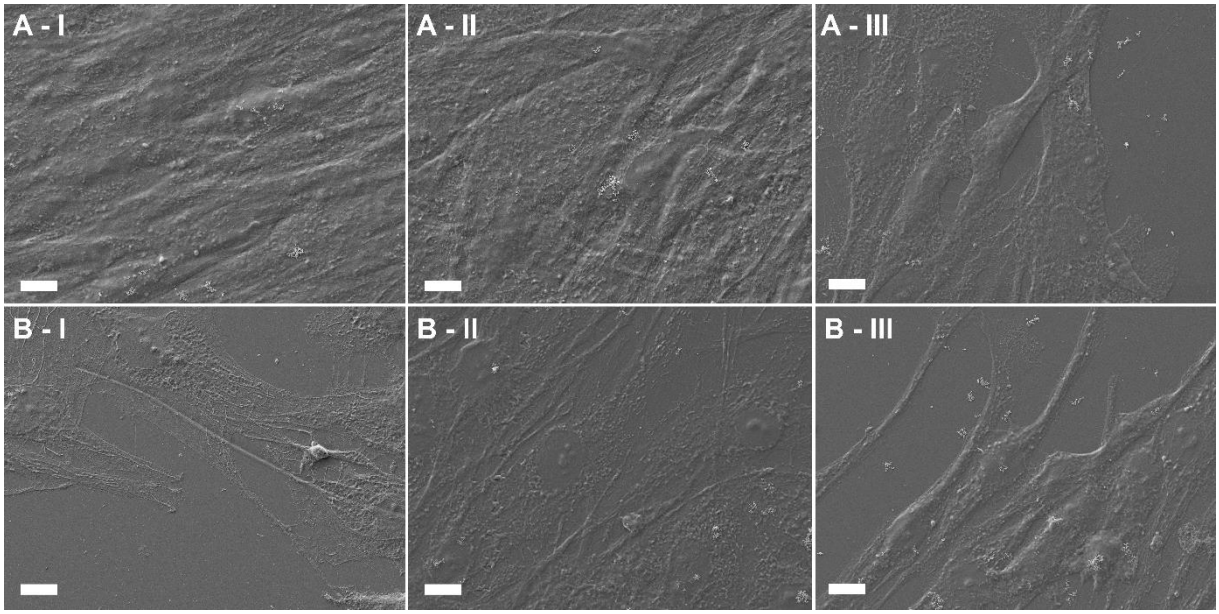

Figure V-6 – SEM micrographs of hACs cultured in (A) monolayer and (B) co-cultured with activated M1 macrophages after 14 days of treatment with different conditions: (I) no treatment, (II) micelles encapsulating Dex and (iii) Dex. Scale bars: 10 μm.

V-4. DISCUSSION

An efficient drug delivery device should facilitate a stable circulation in plasma and release the drug in therapeutic concentrations at the diseased site. The aim of this work was to developed novel polymeric micelles for the targeting of inflammatory conditions and controlled drug release. The oxidation of the adjacent GSH in the micelles avoid the leakage of the drug into the plasma, as the disulfide cross-linking provides a barrier against blood dilution. After accumulation in the inflammatory site via the EPR effect, the drug will undergo quick release triggered by both redox and GR activity. Thus, this innovative technology was designed to: *(i)* increase the therapeutic index of the drug through its encapsulation into the micelles; *(ii)* reduce the systemic side effects due to the controlled release profiles of the drug and consequently reducing the unnecessary exposure of healthy tissues to the drug; and *(iii)* maximize the performance of the currently used therapies. Our results demonstrate that mPEG-GSH-PA micelles are an efficient targeted drug delivery system for the treatment inflammatory arthritis.

FTIR results confirmed the synthesis of the triblock amphiphilic copolymers, due to the shift of the amine group from the mPEG and GSH and the carboxyl of the PA and GSH to amide in the micelles. This copolymer was produced via a two-step polymerization reaction. In the first, mPEG–GSH grafted copolymer was synthesized via the reaction of the amine group of mPEG with the carboxyl group of GSH using EDC/NHS chemistry. It is called a 'zero-length' cross-linker since the amide linkages are formed without leaving a spacer molecule [19]. This reaction is nontoxic as the remaining products and by-products (isourea) can be easily removed though dialysis with water [20], which was performed after the first reaction was completed. In the second step, TBTU in the presence of the catalytic TEA reacts with the carboxyl group of PA forming an active ester that then reacts with the amine group of the mPEG-GSH copolymer to form an amide bond [21]. TBTU is one of the most commonly used coupling reagents for amide bond formation in organic solvents, and it is also called a 'zero-length' cross-linker. After the synthesis of the copolymer mPEG-GSH-PA, micelles were successfully prepared through the nanoprecipitation method [22]. Since it is an easy, quick and one-step technique that results in instantaneous formation of NPs and consequently can be easily scaled up, the nanoprecipitation method is widely used to prepare a variety of NP systems, including polymeric micelles [23].

Stable micelles with 101.3 ± 3.4 nm of diameter, 0.092 ± 0.011 of PDI, and -20.2 ± 3.42 mV of zeta potential were produced. The size range around 100 nm enables the micelles to take full advantage of the EPR effect and accumulate at inflammatory sites [24]. Indeed, the expression of histamine, bradykinin, leukotrienes and serotonin in the inflamed tissues promotes the contraction of the inflammatory cells lining within capillaries, resulting in increased intra-endothelial gaps. This effect was widely explored not only for inflammatory conditions, but also for cancer therapies [25]. The micelles are monodisperse in size as confirmed with the PDI value lower than 0.2 [26], and present a negative surface charge, which may contribute for a prolonged circulation time in the bloodstream [27]. Moreover, since the absolute value of the zeta potential provides an indication of the stability of the particles in suspension, the obtained value of -20 mV ensure a moderately stable suspension [28]. The size stability of the micelles was also confirmed during 6 months.

Polymeric micelles exhibited good Dex loading capacity that increased with the increment of the micelle:Dex feed weight ratio. Indeed, the maximum entrapment efficiency (64%) occurred for the micelles:Dex feed weight ratio of 1:0.8, and comprises 4.65 ± 0.11 mg of Dex. Therefore, the amount drug present in the micelles is adequate to neutralize the inflammatory process [29]. It should also be mentioned that the micelles retained a similar particle size distribution after the encapsulation of the drug.

The kinetics of Dex release from the micelles is slow and it is lower in PBS at 37°C. While encapsulating the drug, the free thiol groups of GSH present into the copolymer were oxidized by oxygen to form disulfide linkages, which prevent the premature release of the drug. In the presence of redox and GR enzyme, there will be a dissociation of the disulfide linkages and, consequently, a fast release of the drug. These results indicate that the polymeric micelles are able to entrap a suitable amount of the drug, and release it in a targeted and controlled manner under specific local conditions.

The *in vitro* cytotoxicity of the produced micelles was studied on endothelial cells, chondrocytes and immune cells. Endothelial cells were used as a model of the cells lining the interior of the blood vessels, hACs isolated from diseased knee arthroplasties as a model of cartilage tissue, and THP-1 as a model of the immune system. Considering the rationale of the responsive micelles, all of these cell types represent a suitable model to assess any cytotoxic interaction after systemic injection. mPEG-GSH-PA micelles in a concentration until 50 μg/mL were cytocompatible in contact with hACs, EA and THP-1 cells. Since higher concentrations of the micelles negatively affected those cells, this was the maximum concentration of micelles used. Those results were comparable to other studies using amphiphilic copolymers of PEG and e.g. cholic acid [30]. SEM micrographs analyses of cell cultures also confirmed that the micelles did not affect cell morphology.

To confirm the ability of the micelles in counteracting inflammation and Dex side effects, it was investigated their effect on chondrocytes and macrophages in both monoculture and co-culture systems (as a model of an inflamed joint). In the present work, the chondrocytes viability and proliferation were compromised with the addition of the free Dex. Indeed, previous studies also reported a reduction in the ATDC5 chondrocyte cell line viability after administration of Dex at 100 μM, due to the induction of autophagy [31]. Importantly, the micelles encapsulating the drug prevented those negative effects in the hACs. Regarding the THP-1 cell line, while free Dex impairs the cell viability and proliferation, its incorporation into the micelles also reduced those negative effects. hACs were co-cultured with activated M1 macrophages using a transwell system, as a model of an inflamed joint [32], and GR was added to further mimic the synovial inflammation in arthritic diseases. This system enabled assessing if the drug loaded micelles could avoid the negative impact of inflammation on human chondrocytes. In order to obtain an inflammatory scenario, with high concentrations of the pro-inflammatory cytokines TNF-α, IL-1, IL-6, IL-12, IL-23 and reactive oxygen species, the THP-1 macrophages were activated to the M1 phenotype. Indeed, the higher amount of TNF-α and IL-6 in activated macrophages and in the co-culture systems confirmed their induction to the pro-inflammatory phenotype. Moreover, the amount of IL-6 was

much higher than TNF-α, which is also in agreement with the values found in the plasma and synovial fluid of arthritic patients [33]. In the co-culture system only the micelles encapsulating Dex were able to prevent the negative effects of the inflammation into the chondrocytes, especially after 14 days. Moreover, the Dex-loaded micelles were able to more effectively reduce the production of the pro-inflammatory cytokine IL-6 by macrophages. Overall these results confirm the initial hypothesis that the micelles in the presence of GR and redox medium ensure a targeted and fast release of the drug. Thus, this strategy is able to increase the drug therapeutic index, which can reduce the dosage and consequently circumvent the GCs associated systemic side effects.

V-5. CONCLUSION

In the present work, we developed enzymatic- and redox-responsive polymeric micelles for targeted and controlled release of an anti-inflammatory drug. The developed devices allow overcoming some drawbacks of current treatments, such as the limited solubility of some drugs, their inadequate pharmacokinetics and their limited efficacy and severe side effects. Our results clearly show that the release of the drug from the micelles is controlled by the presence of redox medium and GR enzyme. Therefore, an increase of the drug targeting and, consequently, its therapeutic efficacy in specific tissues is ensured, and a reduction of off-target effects can be expected by using our delivery device. Therefore, the polymeric micelles are a valid approach not only for arthritic diseases, but also for other systemic inflammatory conditions.

V-6. ACKNOWLEDGMENTS

Authors acknowledge the financial support from FCT/MCTES (Portuguese Foundation for Science and Technology/Ministry of Science, Technology and Higher Education) and the FSE/POCH (European Social Fund through the Operational Program of Human Capital), for the PhD scholarship PD/BD/11384/2015 of A. C. Lima (PD/59/2013. Authors would also like to acknowledge FCT for the project PTDC/CTM-BIO/4388/2014 – SPARTAN, and the Northern Portugal Regional Operational Programme (NORTE 2020), under the Portugal 2020 Partnership Agreement, through the European Regional Development Fund (FEDER) (NORTE-01-0145-FEDER-000023-FROnTHERA and NORTE-01-

0145-FEDER-000013-PersonalizedNOS). The authors also acknowledge NORTE 2020 Structured Project within the R&D&I Structured Project, co funded by Norte2020 - Programa Operacional Regional do Norte.

V-7. REFERENCES

1. Roy, K., Kanwar, R. K. and Kanwar, J. R., Molecular targets in arthritis and recent trends in nanotherapy. *Int J Nanomed*. 2015, *10*: p. 5407-20.
2. Reginster, J. Y., The prevalence and burden of arthritis. *Rheumatology*. 2002, *41 Supp 1*: p. 3-6.
3. Pap, T. and Korb-Pap, A., Cartilage damage in osteoarthritis and rheumatoid arthritis-two unequal siblings. *Nat Rev Rheumatol*. 2015, *11* (10): p. 606-15.
4. Ledingham, J., Snowden, N. and Ide, Z., Diagnosis and early management of inflammatory arthritis. *Bmj*. 2017, *358*: p. 1-8.
5. Geenen, R., Overman, C. L., Christensen, R., *et al.*, EULAR recommendations for the health professional's approach to pain management in inflammatory arthritis and osteoarthritis. *Ann Rheum Dis*. 2018, *77* (6): p. 797-807.
6. Vandewalle, J., Luypaert, A., De Bosscher, K., *et al.*, Therapeutic Mechanisms of Glucocorticoids. *Trends Endocrin Met*. 2018, *29* (1): p. 42-54.
7. Cabral, H., Miyata, K., Osada, K., *et al.*, Block Copolymer Micelles in Nanomedicine Applications. *Chem Rev*. 2018, *118* (14): p. 6844-92.
8. Petros, R. A. and DeSimone, J. M., Strategies in the design of nanoparticles for therapeutic applications. *Nat Rev Drug Discov*. 2010, *9* (8): p. 615-27.
9. Jhaveri, A. M. and Torchilin, V. P., Multifunctional polymeric micelles for delivery of drugs and siRNA. *Front Pharmacol*. 2014, *5*: p. 1-26.
10. Nicolas, J., Mura, S., Brambilla, D., *et al.*, Design, functionalization strategies and biomedical applications of targeted biodegradable/biocompatible polymer-based nanocarriers for drug delivery. *Chem Soc Rev*. 2013, *42* (3): p. 1147-235.
11. Kataoka, K., Harada, A. and Nagasaki, Y., Block copolymer micelles for drug delivery: design, characterization and biological significance. *Adv Drug Deliver Rev*. 2001, *47* (1): p. 113-31.
12. Kamaly, N., Yameen, B., Wu, J., *et al.*, Degradable Controlled-Release Polymers and Polymeric Nanoparticles: Mechanisms of Controlling Drug Release. *Chem Rev*. 2016, *116* (4): p. 2602-63.
13. Pu, H. L., Chiang, W. L., Maiti, B., *et al.*, Nanoparticles with Dual Responses to Oxidative Stress and Reduced pH for Drug Release and Anti-inflammatory Applications. *Acs Nano*. 2014, *8* (2): p. 1213-21.
14. Lu, S. C., Regulation of glutathione synthesis. *Mol Aspects Med*. 2009, *30* (1-2): p. 42-59.
15. Chiang, Y. T., Yen, Y. W. and Lo, C. L., Reactive oxygen species and glutathione dual redox-responsive micelles for selective cytotoxicity of cancer. *Biomaterials*. 2015, *61*: p. 150-61.
16. Ostalowska, A., Birkner, E., Wiecha, M., *et al.*, Lipid peroxidation and antioxidant enzymes in synovial fluid of patients with primary and secondary osteoarthritis of the knee joint. *Osteoarthr Cartilage*. 2006, *14* (2): p. 139-45.
17. Sredzinska, K., Galicka, A., Porowska, H., *et al.*, Glutathione reductase activity correlates with concentration of extracellular matrix degradation products in synovial fluid from patients with joint diseases. *Acta Biochim Pol*. 2009, *56* (4): p. 635-40.
18. da Silva, M. L. A., Costa-Pinto, A. R., Martins, A., *et al.*, Conditioned medium as a strategy for human stem cells chondrogenic differentiation. *J Tissue Eng Regen M*. 2015, *9* (6): p. 714-23.

19. Pieper, J. S., Hafmans, T., Veerkamp, J. H., *et al.*, Development of tailor-made collagen-glycosaminoglycan matrices: EDC/NHS crosslinking, and ultrastructural aspects. *Biomaterials*. 2000, *21* (6): p. 581-93.
20. Ahmad, Z., Shepherd, J. H., Shepherd, D. V., *et al.*, Effect of 1-ethyl-3-(3-dimethylaminopropyl) carbodiimide and N-hydroxysuccinimide concentrations on the mechanical and biological characteristics of cross-linked collagen fibres for tendon repair. *Regen Biomater*. 2015, *2* (2): p. 77-85.
21. Montalbetti, C. A. G. N. and Falque, V., Amide bond formation and peptide coupling. *Tetrahedron*. 2005, *61* (46): p. 10827-52.
22. Fessi, H., Puisieux, F., Devissaguet, J. P., *et al.*, Nanocapsule Formation by Interfacial Polymer Deposition Following Solvent Displacement. *Int J Pharm*. 1989, *55* (1): p. R1-4.
23. Rivas, C. J. M., Tarhini, M., Badri, W., *et al.*, Nanoprecipitation process: From encapsulation to drug delivery. *Int J Pharmaceut*. 2017, *532* (1): p. 66-81.
24. Nehoff, H., Parayath, N. N., Domanovitch, L., *et al.*, Nanomedicine for drug targeting: strategies beyond the enhanced permeability and retention effect. *Int J Nanomed*. 2014, *9*: p. 2539-55.
25. Golombek, S. K., May, J. N., Theek, B., *et al.*, Tumor targeting via EPR: Strategies to enhance patient responses. *Adv Drug Deliver Rev*. 2018, *130*: p. 17-38.
26. Panchal, J., Kotarek, J., Marszal, E., *et al.*, Analyzing subvisible particles in protein drug products: a comparison of dynamic light scattering (DLS) and resonant mass measurement (RMM). *The AAPS journal*. 2014, *16* (3): p. 440-51.
27. Blanco, E., Shen, H. and Ferrari, M., Principles of nanoparticle design for overcoming biological barriers to drug delivery. *Nat Biotechnol*. 2015, *33* (9): p. 941-51.
28. Bhattacharjee, S., DLS and zeta potential - What they are and what they are not? *J Control Release*. 2016, *235*: p. 337-51.
29. Hochhaus, G., Barth, J., Al-Fayoumi, S., *et al.*, Pharmacokinetics and pharmacodynamics of dexamethasone sodium-m-sulfobenzoate (DS) after intravenous and intramuscular administration: A comparison with dexamethasone phosphate (DP). *J Clin Pharmacol*. 2001, *41* (4): p. 425-34.
30. Li, Y., Xiao, K., Luo, J., *et al.*, Well-defined, reversible disulfide cross-linked micelles for on-demand paclitaxel delivery. *Biomaterials*. 2011, *32* (27): p. 6633-45.
31. Zhao, Y., Zuo, Y., Huo, H., *et al.*, Dexamethasone reduces ATDC5 chondrocyte cell viability by inducing autophagy. *Mol Med Rep*. 2014, *9* (3): p. 923-7.
32. Bauer, C., Niculescu-Morzsa, E., Jeyakumar, V., *et al.*, Chondroprotective effect of high-molecular-weight hyaluronic acid on osteoarthritic chondrocytes in a co-cultivation inflammation model with M1 macrophages. *J Inflamm (Lond)*. 2016, *13* (31): p. 1-9.
33. Mabey, T., Honsawek, S., Tanavalee, A., *et al.*, Plasma and synovial fluid inflammatory cytokine profiles in primary knee osteoarthritis. *Biomarkers*. 2016, *21* (7): p. 639-44.

SECTION 4

INTERNALIZATION STUDIES

Chapter VI

Cellular uptake of nanoparticles in an inflammatory arthritis scenario

Chapter VI

Cellular uptake of nanoparticles in an inflammatory arthritis scenario[1]

ABSTRACT

Nanoparticles (NPs) have huge potential applications in the biomedical field. To promote a targeted and controlled delivery of the encapsulated drugs, it is fundamentally important to understand the NPs uptake by different cells. Indeed, many factors affect the mechanism of NPs cellular internalization, including physicochemical properties of the NPs, protein-NPs and cell-NPs interactions as well as the cell type and cell state. Thus, the goal of the present study is to assess the internalization and pathways used for different NPs (polymeric NPs, micelles and unilamelar liposomes -LUVs) in a normal and inflammatory scenario by different cells, namely endothelial cells, chondrocytes and macrophages. The results show the important role of surface chemistry in the NPs internalization by the cells. Moreover, each NP had a similar uptake level regardless the cell type, but the same NP may exploit different cellular pathways depending on the cell type. Hence, since therapeutic efficacy of the loaded cargo depends on the NPs fate after cellular internalization, these outcomes highlight the importance of considering the targeted cell type when designing functional NPs to a specific disease.

[1]This chapter is based on the following publication:

Lima A. C., Ferreira H., Neves N. M. Cellular uptake of nanoparticles in an inflammatory arthritis scenario. *(Submitted).* 2019

VI-1. INTRODUCTION

Different types of nanoparticles (NPs), including polymeric NPs, micelles and liposomes, have been widely used as drug delivery systems with targeted, controlled and site-specific drug delivery in order to enhance drug therapeutic efficacy while reducing adverse side effects [1]. The NPs physicochemical characteristics (e.g. composition, size, shape, hydrophobicity and surface charge and chemistry) affect the interaction with plasma proteins (opsonins) and blood components, the cellular uptake as well as the clearance by macrophages and, consequently, influencing their biodistribution and targeted delivery [2]. Thus, since these carriers are usually aimed to deliver the biomolecule to a specific sub-cellular compartment of the cell, intracellular trafficking and fate of NPs is a vital process for their successful use in therapies [3].

Despite the size of NPs being in the nanometer range, they are normally not able to diffuse readily through the cell membrane [4]. Instead, endocytosis is the major route of cellular uptake of NPs. It involves the generation of new intracellular membrane-enclosed vesicles from the plasma membrane with a concomitant internalization of lipids, proteins and extracellular fluid. This process occurs against the concentration gradient by active transport using energy [5]. It is usually classified into two major categories: phagocytosis and pinocytosis. Phagocytosis is an essential mechanism of the immune system defense, being predominantly used by phagocytes, such as macrophages, neutrophils and monocytes [6]. This pathway begins with the opsonization of the NPs that attach to the cell surface through Fc receptors and complement receptors. This triggers the polymerization of actin membrane protrusions at the site of ingestion and, consequently, engulfing and digesting larger particles and pathogens. After transporting the opsonized particle into the cell, the formed phagosome will undergo degradation by acidification and enzymolysis in the lysosomes. Conversely to phagocytosis, pinocytosis is present in all types of cells and depending on the proteins involved in the pathways, it is classified as clathrin-mediated endocytosis, caveolae-mediated endocytosis, clathrin- and caveolae-independent endocytosis, and micropinocytosis. Clathrin-mediated endocytosis comprises clathrin-coated vesicles formation in the presence of adaptor protein, Epsin, and accessory proteins such as dynamin (GTPase) [7]. The cell fate seems to be associated with the receptor at the cell surface that the NPs attach (e.g. NPs could be released from the endocytosed vesicles or transferred to lysosomes for degradation, which is the most frequently outcome). In caveolae-mediated endocytosis, the NPs binding to the receptors of the plasma membrane induce the formation of flask-shaped vesicles, which results from the interaction with different proteins, mainly caveolin. [8]. The caveolae vesicles are afterwards cut off from the membrane by

dynamin. As the caveolae vesicles fuse with caveosomes or multivesicular bodies (MTV), which will move to the endoplasmic reticulum, cytosol or nucleus, this route avoids lysosomal degradation. Indeed, many pathogens, including viruses and bacteria, select this way to circumvent lysosomal degradation. For the same reason, this pathway is believed to enhance the therapeutic effect of the drugs loaded into the NPs [9]. Clathrin- and caveolae-independent endocytosis occurs in cells that are deprived of clathrin and caveolin, being involved cholesterol-rich microdomains on the plasma membrane, generally referred to as lipid rafts [10]. Although the regulatory mechanisms of these pathways are still unknown, it seems that the cellular fate is recycling endosomes, endocytic compartments (e.g. Golgi complex), or even the directly release into the cytoplasm [11]. Finally, macropinocytosis involves the uptake of large areas of the plasma and, consequently, allows the internalization of big NPs (> 1 μm) [12]. In this pathway, tyrosine kinases activate actin polymerization to form protrusions in the cell membrane. After the encapsulation of the particle, the protrusions fuses once again back with the cell membrane. The fate of macropinosomes will depend on the cell type. Although endocytosis is widely recognized to be the major processes by which NPs enter into cells, there are also other non-endocytic pathways, including passive diffusion, hole formation, direct microinjection, and electroporation [4]. Moreover, recent studies have reported cell-penetrating peptides [13] and membrane fusion between liposomes and cells [14]. Those mechanisms are poorly understood, being the direct cytosolic delivery of NPs payload via non-endocytic pathways an optimal approach to minimize their degradation in the endosomes/lysosomes.

Hence, the pathway of cellular internalization of nanomedicines is a key factor in determining their biomedical functions, biodistribution and toxicity [15]. Indeed, although most of the nanocarriers can enter into cells via endocytosis, generally they are inevitably entrapped in endosomes, which can merge with lysosomes and undergo degradation. In order to design safe and efficient nanomedicines, it is crucial to understand their cellular uptake and intracellular trafficking [16]. However, even though many studies have heightened the variables that impact NPs uptake into cells, including size, shape and surface charge [17], little is known about the effect of cell type and inflammatory environment in this process.

Arthritic diseases, such as osteoarthritis (OA) and rheumatoid arthritis (RA), are multifactorial conditions with several cells and molecules playing an important role [18]. Indeed, the dynamic environment of inflammatory arthritis compromises many cell types including endothelial cells, chondrocytes, synovial like fibroblasts, and inflammatory cells such as macrophages. Under these diseased conditions, the cell phenotype is altered. For instance, endothelial cells in an inflammatory environment become activated and express endothelial cell adhesion molecules (ECAMs), including

vascular cell adhesion molecule (VCAM)-1, E-selectin, P-selectin, and intercellular adhesion molecule (ICAM)-1 [19, 20]. Likewise, activated synoviocytes, rather than unactivated cells, have been reported to have stronger phagocytic capacity during inflammatory conditions [21]. Moreover, depending on the local microenvironment and stimulation profiles, macrophages can be polarized into M1 and M2 phenotype [22]. While M1 macrophages are defined as pro-inflammatory, M2 macrophages are considered immuno-regulatory.

Despite being reported that ''disease specific'' state modifies the NPs cellular uptake [23, 24], our understanding on NPs cellular uptake is rather limited and should increase by not only studying the role of the physicochemical characteristics of the NPs, but also taking into consideration the effects of the disease environment in this process. Moreover, elucidating cellular uptake pathways of a nanomedicine can lead to the improvement of its design, as internalization route is of upmost important for NPs fate into the cell. In order to address some of the fundamental questions of this field, the present study aims to investigate the cellular uptake of different NPs in an inflammatory scenario, using endothelial cells, chondrocytes and macrophages. The NPs formulations include polymeric NPs, micelles and unilamellar liposomes (LUVs). The effect of inflammation on cellular uptake was investigated by culturing the different NPs in normal and inflamed conditions, being the THP-1 cell line polarized to M1 and M2 populations. The uptake of the NPs was also examined in the presence and absence of a series of pharmacological inhibitors of cellular internalization pathways. Therefore, our findings may help researchers in designing NP systems with enhanced targeted delivery to diseased cells.

VI-2. MATERIALS AND METHODS

This section describes the preparation and formulation of the different fluorescent NPs as well as their characterization regarding the size distribution, surface charge and morphology. Also the methods used to assess their internalization level and corresponding pathways, namely by flow cytometry and confocal analyses, are described in detail.

VI-2.1. Materials

Unless otherwise noted, all chemicals were purchased from Sigma-Aldrich (USA) and used as supplied. Chitosan (Ch) with a molecular weight (MW) of 150 kDa and 95% of deacetylation degree (DD)

was purchased from Heppe Medical Chitosan GmbH (Germany). Hyaluronic acid (HA) with a MW of 750 kDa was acquired from Lifecore Biomedical (USA). 1,2-distearoyl-sn-glycero-3-phosphoethanolamineN-[maleimide(polyethyleneglycol)-2000] (ammonium salt) (DSPE-PEG-Mal) was purchased from Avanti Polar Lipids (USA). LabAssay™ Phospholipid was obtained from Wako (Japan). NBD Cholesterol (22-(N-(7-Nitrobenz-2-Oxa-1,3-Diazol-4-yl)Amino)-23,24-Bisnor-5-Cholen-3β-Ol), Roswell Park Memorial Institute (RPMI)-1640 Medium and Fetal Bovine Serum (FBS) were purchased from Thermo Fisher Scientific (USA). Human basic Fibroblast Growth Factor (bFGF), Interferon-γ (IFN-γ), Interleukin (IL)-4 and IL-13 were purchased from Peprotech (UK).

VI-2.2. NPs preparation

The different types of NPs were prepared as previously reported by us. Ch-HA NPs were prepared by polyelectrolyte complexation [25]. Briefly, after dissolving Ch in 1% (v/v) acetic acid and HA in ultrapure water, both solutions were filtered, being the concentration adjusted to 0.25 mg/mL and the pH to 5. The NPs spontaneously formed when the HA solution was added dropwise at 1 mL/min rate to the Ch solution under strong magnetic stirring, being 200 μL of fluorescein isothiocyanate (FITC, 2 mg/mL in ethanol/water, 1:10) added to the Ch solution. Then, the NPs were stabilized adding 50 mM 1-ethyl-3-(3-(dimethylaminopropyl) carbodiimide (EDC) and 200 mM N-hydroxysuccinimide (NHS) in 0.1 M MES buffer (pH 4.7) with 0.9% (w/w) NaCl. Unreacted compounds were removed though centrifugation with ultrapure water (30 min, 4000 rpm at 20 °C with glucose at 2 mg/mL) using Vivaspin 300 kD Filter Units (Fisher Scientific, USA).

Micelles were prepared though the nanoprecipitation method. First, methoxypolyethylene glycol amine-glutathione-palmitic acid (mPEG-GSH-PA) copolymers were synthesized via a two-steps polymerization reaction. Briefly, mPEG (0.01 mmol) reacted with GSH (0.02 mmol) using 50 mM EDC and 200 mM NHS in MES buffer (pH 4.7) with 0.9% (w/w) NaCl for 24 h. After removing unreacted compounds and the water, mPEG-GSH reacted with PA (0.011 mmol) in tetrahydrofuran (THF) using 2-(1H-Benzotriazole-1-yl)-1,1,3,3-tetramethylaminium tetrafluoroborate (TBTU, 0.011 mmol) and triethylamine (TEA, 0.02 mmol) for 24 h. Then, 0.5 mg of FITC was dissolved in the polymer solution, which was added dropwise at 1 mL/min rate to ultra-pure water under strong magnetic stirring during 48 h. Unreacted compounds were also removed though centrifugation with ultrapure water (45 min, 5000 rpm at 20 °C) using Vivaspin 300 kD Filter Units.

LUVs were prepared by the thin-film hydration method, followed by extrusion. Briefly, a lipid film of cholesterol/L-alfa-phosphatidylcholine (EPC)/DSPE-PEG-Mal/NBD-cholesterol at 0.95:0.85:0.15:0.05 (n/n) and α-tocopherol at 1:200 (M/M) was hydrated with HEPES buffer (pH 7.4), and after vigorous vortex multilamellar liposomes (MLVs) were produced. MLVs were then extruded forty three times using an Avanti Mini-Extruder through polycarbonate filters of 0.1 μm pore diameter. LabAssay™ Phospholipid was performed to determine the amount of phosphatidylcholine, according to manufacturer's instructions. The absorbance at 600 nm was acquired using the microplate reader (Synergy HT, BioTek, USA).

VI-2.3. NPs characterization

A Zetasizer Nanoseries ZS equipment (Malvern Instruments, Portugal) was used to determine the particle size and polydispersity index (PDI) by dynamic light scattering (DLS), and the zeta potential was determined by laser Doppler micro-electrophoresis. Ch-HA NPs and micelles measurements were performed at 25.0 °C, being the NPs diluted in ultrapure water (1:20; v/v) and the micelles undiluted. LUVs were measured using a concentration of 500 μM in HEPES buffer at 37.0 °C.

VI-2.4. *In vitro* cellular studies

The degree of internalization of the NPs by the cells and pathways involved were assessed *in vitro*, highlighting its relevance for the therapeutic efficacy of the strategies being developed.

VI-2.4.1. Cell Culture

hACs were isolated from knee cartilage samples that were obtained in knee arthroplasty surgeries obtained through the cooperation agreement between Centro Hospitalar do Alto Ave, Guimarães, Portugal, and the 3B's Research Group, and after informed donor consent. Cells were isolated according to a previously described protocol through enzymatic digestion [26]. hACs cells were cultured in Dulbecco's modified Eagle's medium (DMEM) high glucose (D5671), supplemented with 10% FBS, 10 mM of L-lanyl-L-glutamine, MEM non-essential aminoacids and HEPES buffer, 100 units/mL of penicillin, 100 μg/mL of streptomycin and 10 ng/mL of human bFGF.

Human umbilical vein endothelial (EA.hy926) cell line was maintained in DMEM low glucose (D5523) supplemented with 10% FBS, 100 units/mL of penicillin and 100 μg/mL of streptomycin.

The human monocytic cell line THP-1 was maintained in complete RPMI, containing RPMI-1640 media supplemented with 2 mM of L-glutamine, 100 units/mL of penicillin, 100 μg/mL of streptomycin, 10 mM HEPES buffer and 10% FBS.

All cells were incubated at 37 °C in a humidified 5% CO_2 atmosphere.

VI-2.4.2. Cellular uptake

The cellular uptake of the different type of NPs was evaluated in primary hACs, and EA and THP-1 cell lines by flow cytometry and confocal analyses.

VI-2.4.2.1 *Flow cytometry*

Cells were seeded at a density of 2.5×10^5 cells per well (hACs and EA cell line in 24-well plates and THP-1 cell line in 48-well plates) and incubated at 37 °C in a humidified 5% CO_2 atmosphere for 24 h. For the induction of THP-1 cell differentiation, cells were seeded in cRPMI with 100 nM phorbol 12-myristate-13-acetate (PMA). After 24 h incubation, non-attached cells were removed by aspiration, and the adherent cells were washed three times with cRPMI. Cells were then incubated for an additional 48 h in cRPMI without PMA to ensure reversion of cells to a resting macrophage phenotype. Then, the medium was replaced by medium containing 100 ng/mL lipopolysaccharide (LPS) and 20 ng/mL IFN-γ for the M1 polarization, or 20 ng/mL of IL-4 and IL-13 for the M2 polarization during 120 h, as previously reported [27]. Regarding hACs and EA cell line, cells were culture in normal conditions and also with macrophage conditioned medium containing 500 pg/mL of IL-6 for 24 h to mimic the inflammatory conditions.

To study the effect of incubation time, cells were incubated with the different fluorescent labelled formulations of NPs for 2, 6 and 24 h at 37 °C in a humidified 5% CO_2 atmosphere. Ch-HA NPs and micelles were added at 50 μg/mL and LUVs at 500 mM. After each incubation time, cells were washed twice with PBS in order to remove any cellular debris or non-internalized NPs, and harvested with TripLE express. Afterwards, cells were centrifuged and cell pellets were re-suspended and fixed with 4% formalin in DPBS and kept in the dark at 4 °C (for less than 1 week) [28]. The analyses of the samples were performed in a BD FACSCalibur™ flow cytometer (Biosciences, Belgium), after and before the addition of 0.11% trypan blue during 1 min, in order to quench the fluorescent signal of the NPs adsorbed to the cell surface. This also allows giving an indication of the amount of NPs that were at the NPs' surface [29].

Data were analyzed using Flowing Software 2.5.1. The results were reported as the mean of the percentage of cellular uptake obtained by measuring 20,000 cells and normalized relatively to the cells incubated without NPs.

VI-2.4.2.2 *Confocal analyses*

Cells were seeded as previously described on μ-slides (Ibidi, Germany) at 2.5×10^4 cells per well. After 6 h of seeding of the different formulations of the NPs, cells were fixed with 10% formalin in PBS and stored at 4 °C. Then, cells were permeated with 0.2% (v/v) Triton X-100 for 5 min, nonspecific proteins blocked samples with 3% (w/v) bovine serum albumin (BSA) for 30 min and, then stained with phalloidin (0.25 μg/mL) during 45 min and DAPI (1 μg/mL) during 15 min. Images were acquired using a laser scanning confocal microscopy imaging system (TCS SP8, Leica), using excitation wavelengths of 405 nm (DAPI), 488 nm (FITC) and 561 nm (phalloidin).

VI-2.4.3. Cellular uptake pathways

Flow cytometry was used to study the internalization pathways involved in the cellular uptake of the different NPs formulations. For this assay, after seeding the cells, they were pre-incubated for 30 min at 37 °C in a humidified 5% CO_2 atmosphere with three pharmacological pathway inhibitor solutions: *(i)* 10 μg/mL of chlorpromazine, *(ii)* 1 μg/mL of filipin, or *(iii)* 5 μg/mL of cytochalasin D [29]. Moreover, to study whether the cellular uptake was energy dependent, cells were incubated at 4 ºC for 30 min and then incubated with each NP formulation at 4 ºC. The time of culture was dependent on previous results of the maximum internalization for each cell type and NP formulation. Cells were collected and analyzed by flow cytometric analyses as previously described.

VI-2.5. Statistical analyses

All quantitative data are presented as mean ± standard deviation (SD) of tree independent studies. Statistical analyses were performed using a GraphPad Prism 5.0 software (GraphPad Software, USA). A Shapiro-Wilk normality test was performed to assess data normality. As data do not followed a normal distribution, Mann–Whitney U test was used when two groups were compared (degree of internalization

and percentage at the cell surface) and the Kruskal-Wallis test followed by Dunn's multiple comparison test when more than two groups were compared (cellular uptake pathways).

VI-3. RESULTS

NPs characterization, cellular internalization as well as their pathways are herein described.

VI-3.1. NPs characterization

Ch-HA NPs, micelles and LUVs incorporating a fluorescent dye were characterized in terms of size, PDI and zeta potential (**Table VI-1**). The results are in agreement with previous works. Hence, all the formulations have a size around 115-130 nm and a PDI lower than 0.2, which indicates the homogeneity of the NPs populations. Regarding the zeta potential, Ch-HA NPs have a positive surface charge around +28 mV, while micelles and LUVs present a negative surface charge of around -26 mV.

Table VI-1 – Size distribution and zeta potential of the different NPs formulation

Formulation	Size (nm)	PDI	Zeta potential (mV)
Ch-HA NPs	123.7 ± 1.9	0.102 ± 0.013	28.2 ± 2.8
Micelles	116.2 ± 0.5	0.111 ± 0.020	- 25.2 ± 1.3
LUVs	129.4 ± 2.3	0.121 ± 0.015	- 27.5 ± 1.6

VI-3.2. Cellular internalization

The cellular uptake efficiency of all NP formulations was assessed using flow cytometry and confocal microscopy. Ch-HA NPs, micelles and LUVs were cultured for 2, 6 and 24 h with hACs and EA stimulated or not with macrophage conditioned media, and THP-1 cell line polarized to M1 or M2. The results are reported as the percentage of cellular uptake of the cells treated with the different NPs in respect with the control (cells without NPs), which avoids fluorescence interference that could arise from cells.

Cellular uptake of Ch-HA polymeric NPs (**Figure VI-1-I**) had a different profile depending on the cell type. Indeed, the results show a low percentage of internalization in the hACs and EA cell line (less than

30% after 24 h). Nevertheless, while the stimulation of hACs did not affect the internalization profiles, there is a significant increase of the cellular uptake when the endothelial cells were stimulated with macrophage conditioned media, reaching 93% after 24 h. M1 macrophages were able to internalize more NPs than M2 macrophages, although without significant differences. Taking into consideration the percentage of the NPs at the cell surface (**Figure VI-2-I**), hACs show a high amount of NPs attached to their surface, being around 60% after 24 h. Conversely, there is almost no NPs attached to the surface of endothelial cells. M1 and M2 macrophages present around 20% of NPs attached to their surface. These results were also validated by confocal microscopy (**Figure VI-3**), where the Ch-HA NPs seems to be at the cell surface, with a low uptake degree in hACs and EA cell line, whereas in M1 and M2 macrophages some level of NPs can be observed.

In the case of the micelles, their uptake by the cells showed a similar profile regardless the cell type and the inflammatory environment (**Figure VI-1-II**). Thus, cell uptake was around 20-30% after 2 h, reaching almost 100% after 6 h. Considering the micelles attachment to the cells surface (**Figure VI-2-II**), the results show low percentage for all cell types. Confocal analyses (**Figure VI-3**) also confirms those results, as there is high internalization degree of the micelles for all cell types.

LUVs are rapidly uptaken by all cell types (**Figure VI-1-III**), since there is almost 100% of internalization after 2 h. Thus, there were no LUVs at surface of the cells (**Figure VI-2-III**), except for M1 and M2 macrophages that presented around 5% at their surface. By confocal microscopy (**Figure VI-3**) it is also possible to verify that LUVs have a considerable degree of internalization by the cells. Interestingly, LUVs seem to be located in vesicles around the nucleus.

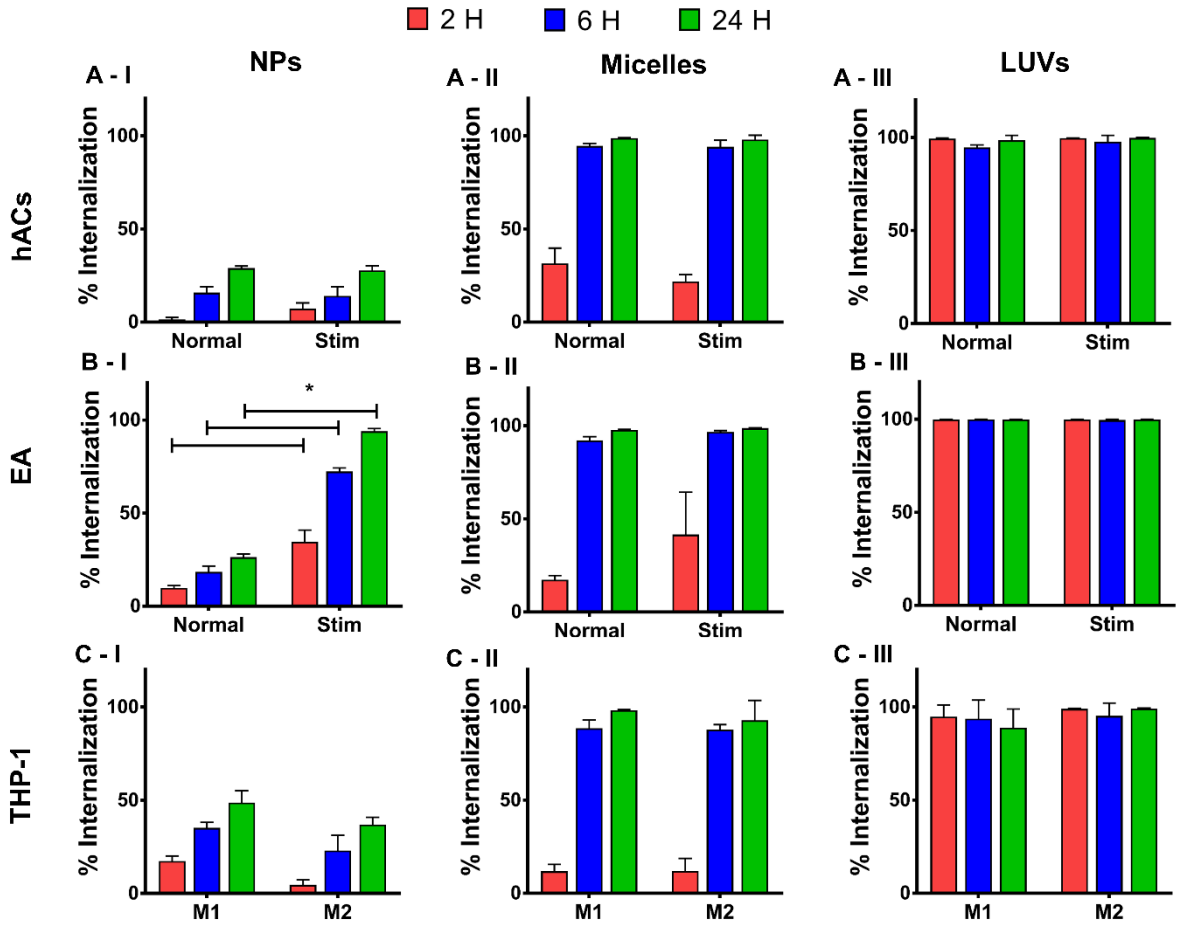

Figure VI-1 – Percentage of cellular internalization of (I) Ch-HA NPs, (II) micelles and (III) LUVs after culturing 2, 6 and 24 h with (A) hACs, (B) EA and (C) THP-1 cell line subjected to different stimulations. Asterisk (*) denotes significant differences ($p < 0.01$).

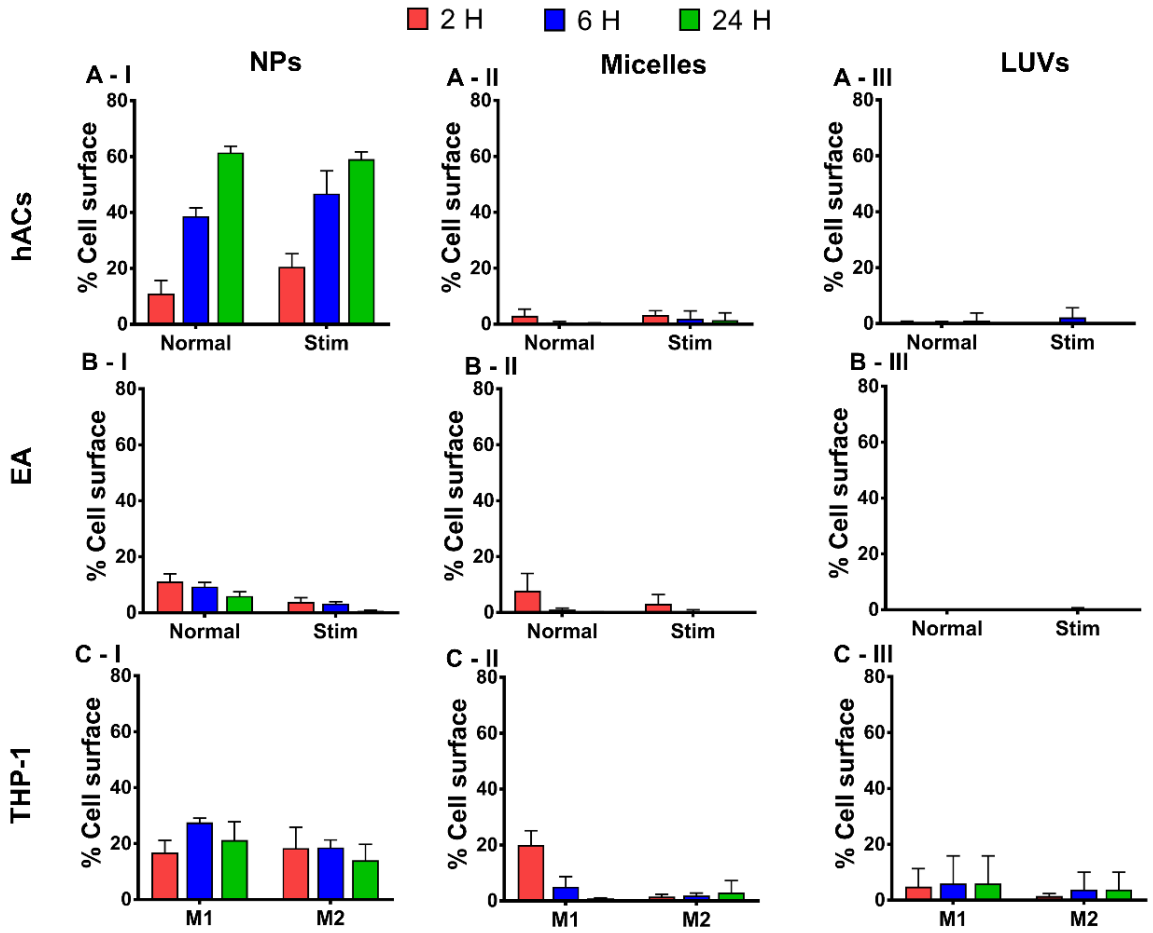

Figure VI-2 – Percentage at the cell surface of (I) Ch-HA NPs, (II) micelles and (III) LUVs after culturing 2, 6 and 24 h with (A) hACs, (B) EA and (C) THP-1 cell line subjected to different stimulations.

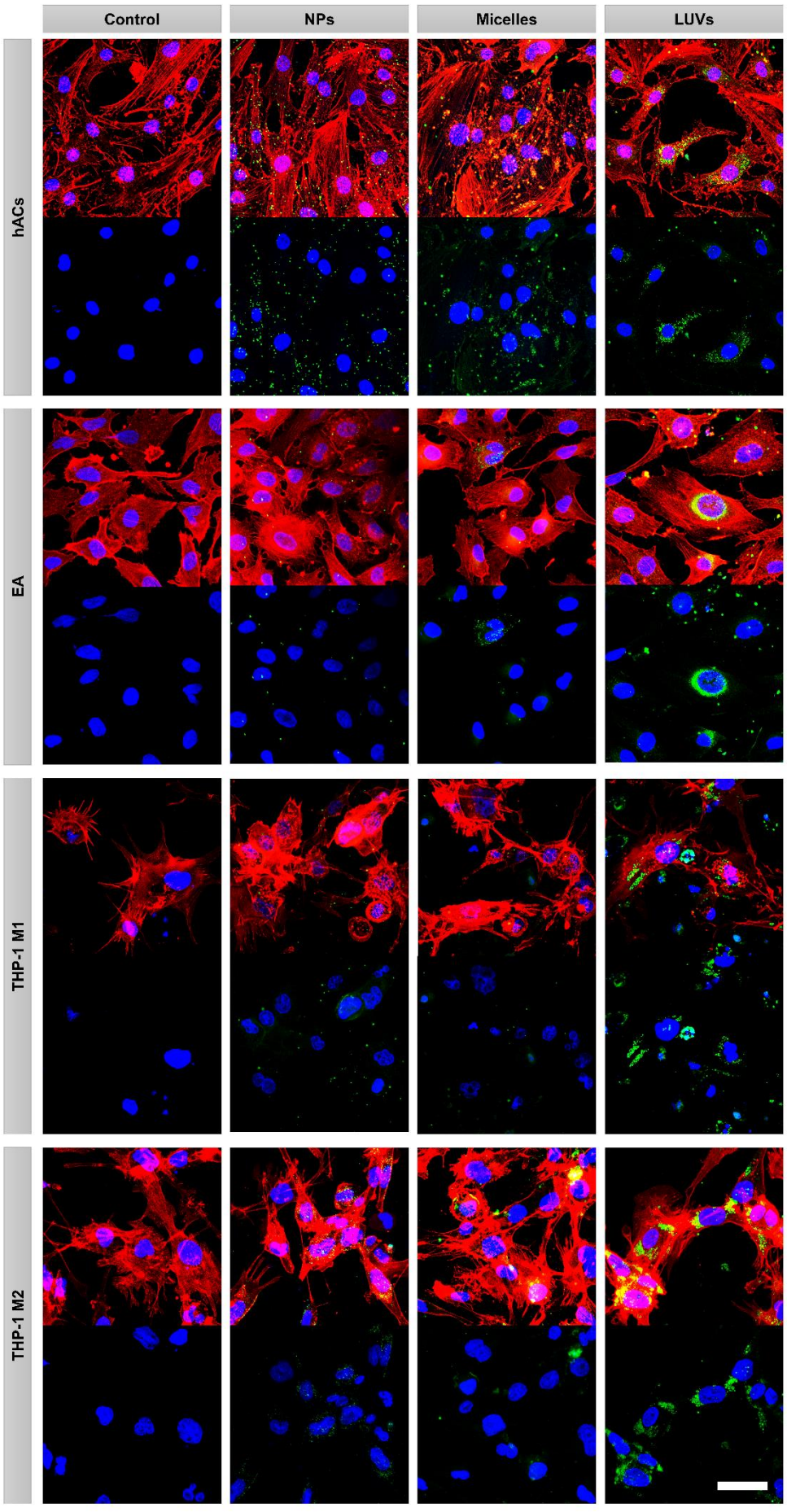
Control
NPs
Micelles
LUVs
hACs
EA
THP-1 M1
THP-1 M2

Figure VI-3 – Confocal microscopy images of the NPs, micelles and LUVs cultured with hACs, EA and THP-1 cell line polarized to M1 and M2, being the nanomedicines formulation green (FITC), nuclei blue (DAPI), and the cytoskeleton red (phalloidin). Scale bar: 50 µm.

VI-3.3. Internalization pathways

Since cellular uptake of nanomedicines can take place via endocytosis or energy-independent non-endocytic pathways, cells were pre-incubated at 4 °C to assess the energy dependence. Moreover, three pharmacological pathway inhibitors were used at 37 °C to evaluate the specific endocytic pathway. Thus, clathrin-mediated endocytosis was inhibited using chlorpromazine, caveolae-mediated endocytosis with filipin, and macropinocytosis/phagocytosis with cytochalasin D [30].

Regarding hACs (**Figure VI-4A**), results show a high inhibitory effect on the uptake of Ch-HA NPs and micelles with lower temperature (4 °C) treatment (± 94% and ± 98%, respectively), suggesting a full active energy-dependent endocytic process. Nevertheless, there is no inhibitory effect with other treatments, which may indicate a clathrin- and caveolae-independent endocytosis uptake for those NPs formulations in chondrocytes. Conversely, the amount of LUVs uptaken by hACs was not affected by none of the treatments under evaluation and, consequently, an energy-independent non-endocytic pathway may be involved.

In the case of the endothelial cell line (**Figure VI-4B**), there is also a high inhibition on the Ch-HA NPs and micelles uptake after treatment with low temperatures (± 94% and ±88 %, respectively), suggesting consequently an energy-dependent endocytic uptake. Further results on the endocytic pathway mechanism study of Ch-HA NPs revealed that the cellular uptake was reduced ± 59% with the inhibition of clathrin-mediated endocytosis, and ±47% with the inhibition of caveolae-mediated endocytosis. Additionally, the inhibition of the macropinocytosis/phagocytosis process only reduced around ± 5% the cellular uptake. Those results suggest that clathrin-mediated endocytosis and caveolae-mediated endocytosis are the main endocytic mechanisms involved in the uptake of Ch-HA NPs by endothelial cells. Considering the polymeric micelles, the results revealed an inhibition in ± 38% after treatment with chlorpromazine and ± 55% after treatment with filipin. Thus, clathrin-mediated and caveolae-mediated endocytosis seems to be the predominant pathway. As with hACs, LUVs uptake by the endothelial cell line was not reduced by none of the treatments under evaluation. Thus, it also seems to be involved an energy-independent non-endocytic pathway.

Cellular uptake by THP-1 polarized both to M1 and M2 macrophages (**Figure VI-4C**) was significantly reduced after lower temperature (4 °C) treatment for all the NPs formulations. Besides being confirmed an energy-dependent endocytic process, different inhibition profiles for each NP were found according to the macrophage polarization. For Ch-HA NPs, M1 macrophages presented ± 58% inhibition for both clathrin-mediated and caveolae-mediated endocytosis, and ± 34% for macropinocytosis/phagocytosis. Cellular uptake in M2 macrophages was inhibited ± 50% with chlorpromazine, whereas filipin and cytochalasin D resulted in an inhibition lower than ± 15%. Thus, while in M1 macrophages clathrin-mediated and caveolae-mediated endocytosis seems to be major pathways, in M2 macrophages the predominant pathway is the clathrin-mediated endocytosis. Considering the micelles, while in M1 macrophages the predominant pathway of cellular internalization seems to be the caveolae-mediated endocytosis (± 76% of reduction by filipin versus ± 39% and ± 20% of reduction by chlorpromazine and cytochalasin D, respectively), in M2 macrophages the clathrin-mediated endocytosis pathway seems to be the predominate role (± 56% of reduction by chlorpromazine versus ± 27% and ± 19% of reduction by filipin and cytochalasin D, respectively). In the case of the LUVs, the results suggest a major role of macropinocytosis/phagocytosis in cellular uptake of M1 and M2 macrophages (around ± 75% of reduction by cytochalasin D).

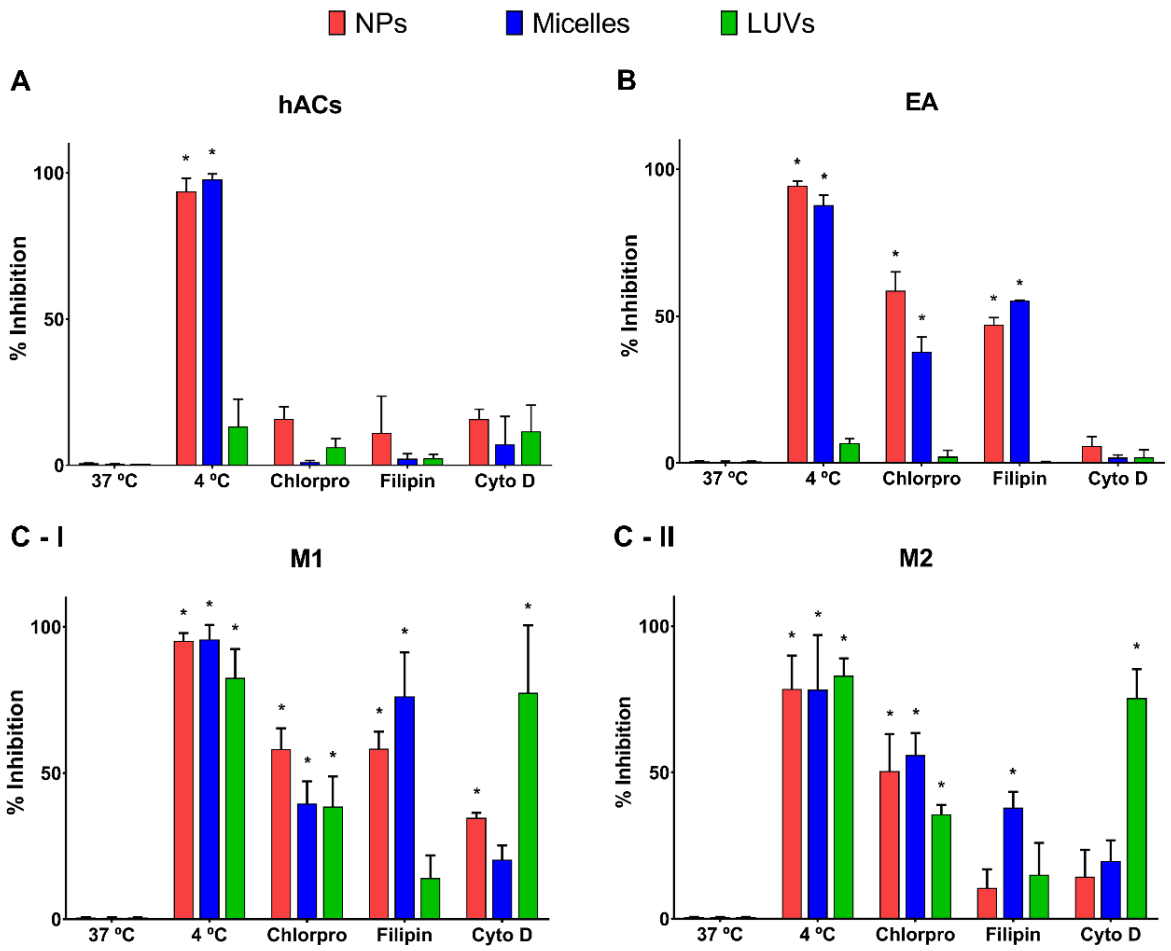

Figure VI-4 – Effect of low temperature and pathway mechanism inhibitors on the uptake of Ch-HA NPs, micelles and LUVs by (A) hACs, (B) EA and (C) THP-1 cell line polarized to (C-I) M1 and (C-2) M2. Asterisk (*) denotes significant differences ($p < 0.01$) in comparison with control of each NPs formulation at 37 °C.

VI-4. DISCUSSION

Nanomedicines are currently at the forefront of cutting-edge research, due to their wide applicability on targeted and controlled delivery of drugs into particular tissues and cells [31]. Even though our knowledge regarding NPs uptake by cells had advanced tremendously in the past years, the differential uptake and internalization pathways concerning the cell type and disease state still needs to be studied. Therefore, the aim of this study was to evaluate the uptake of several NPs systems by chondrocytes, endothelial cells and macrophages, when subjected or not to inflammatory conditions, and concomitantly reveal their internalization pathways.

Both the shape and the size contribute significantly to define the NPs interaction with cells, however the surface charge and chemistry are also considered crucial parameters mediating and influencing those

interactions [17]. In this work, the nanocarriers were designed with similar sizes (110 – 120 nm) and shapes (spherical), being the type of particle, the surface charge and the composition and chemistry the variables under evaluation. Indeed, while Ch-HA solid NPs present a positive surface charge of +28 mV, the micelles and LUVs had a negative surface charge of -25 and -27 mV, respectively. The surface chemistry is dominated by the amine group (NH_2) in the Ch-HA NPs and by PEG chains for both the micelles and the LUVs. Despite having at their surface PEG chains, the chemical composition and end groups was quite different, with the micelles being composed of a mPEG-GSH-PA copolymer (methoxy-functionalized end group) and LUVs had the lipid composition of cholesterol/EPC/DSPE-PEG-Mal (maleimide-functionalized end group). All NPs formulations were previously evaluated regarding their *in vitro* stability and cytocompatibility [25]. Accordingly, the concentration of NPs used in this study was already established as safe. In addition, besides it was already reported the induction of cell death by positively charged NPs, since they can disrupt the integrity of the cell membrane by creating holes [32, 33], Ch-HA NPs did not demonstrated this harmful effect over the cells.

In the present study, the cationic particle had lower cellular uptake degree in comparison with anionic particles in all cell types. While Ch-HA NPs were internalized less than ≈30% in chondrocytes and endothelial cells, and ≈50% in macrophages, polymeric micelles and LUVs displayed ≈95% for all tested cells after 24 h. Although the literature established that the cationic particles have a higher internalization degree, due to their binding to the negatively charged cell surface [15, 34], there are many contradictions related to the complexity of evaluating a single variable of the particle. For instance, the role of zeta potential was evaluated in the cellular uptake of cerium oxide NPs by varying the pH of the solution [35]. Using adenocarcinoma lung cells, the authors reported more efficient uptake of the negatively charged as compared to the positively charged particles, which demonstrated the important role of electrostatic interactions in protein adsorption and cellular uptake of NPs. Therefore, our results highlighted the important role of surface chemistry in NPs internalization by the cells. It was already reported that a slight change in the surface functionality of cationic particles lead to different degrees of cellular internalization [36]. In addition, the end group exposed by the PEG chain deeply influences the cell uptake, along with other factors as PEG density and length [37]. In a previous study, the functionalization of liposomes with maleimide-PEG significantly increased drug-delivery efficiency both *in vitro* and *in vivo* in comparison to the unmodified liposomes [38, 39]. Besides being more rapidly internalized into HeLa, HCC1954, and MDA-MB-468 cells (≥ 2-fold), they presented extended inhibition of tumor growth. Interestingly, Ch-HA NPs have a high degree of cell attachment, especially on chondrocytes. It is worth mentioning that in

many studies the protocol do not allow to quantify the amount of particles attached to the cell surface, which can explain inconsistency of results found in the literature. Moreover, this study was conducted in a monolayer system, where the NPs are rapidly available for cell interaction and internalization, which can explain the high degree of internalization by the cells.

In order to study the role of inflammation in the NPs uptake, chondrocytes and endothelial cells were stimulated with macrophage conditioned media containing 500 pg/mL of IL-6. This concentration is in agreement with the levels found in the synovial fluid of OA and RA patients (119.4 ± 193.2 and 354.7 ± 1851.6 pg/mL of IL-6, respectively) [40]. While hACs after stimulation had no significant differences in the uptake of all NPs formulations, there is a significantly increase on the uptake of Ch-HA NPs by stimulated endothelial cells. Indeed, considering that endothelial cells in an inflammatory environment, for instance, express ECAMs, several NPs were designed with ligands at their surface (e.g. antibodies, peptides) that bind specifically to those targets [19, 20]. Regarding the polarization of THP-1 cell line toward M1 and M2 macrophages, the results did not show significant differences in the cellular uptake for all NP formulations. Likewise, previous studies also displayed very inconsistent results, since while some studies reported higher NP uptake after M2 polarization [41], others found higher phagocytic capacity of M1 macrophages [42]. Additionally, it is also important to understand the physicochemical characteristics that allow a higher retention rate in inflamed joints. In a recent work, a series of liposomes with different particle sizes (70, 100, 200 and 350 nm), surface charges (positive, negative, slight positive and slight negative), PEG chain lengths (1, 2 and 5 kDa), and concentrations (5, 10 and 20% (w/w) of total lipid) were evaluated regarding blood circulation time and accumulation in RA inflamed joints [43]. In a collagen-induced arthritis (CIA) mouse model, the results indicated that liposomes with diameter of 100 nm, a slight negative charge and the 10% incorporation of 5 kDa PEG had longer blood circulation time and inflamed joint targeting in comparison with other liposomal formulations. The encapsulation of Dex into the optimized liposomes improved the antiarthritic efficacy of Dex. Moreover, the authors found an increased cellular uptake by fibroblasts and macrophages in inflamed joints, which can explain the high retention in RA.

The results from the cellular internalization pathways shown that each NP formulation present different uptake mechanism depending on the cell type tested. In summary, Ch-HA NPs were internalized by clathrin- and caveolae-independent endocytosis pathway in chondrocytes, by both clathrin-mediated endocytosis and caveolae-mediated endocytosis in endothelial cells and M1 macrophages, and by clathrin-mediated endocytosis in M2 macrophages. Micelles were internalized by clathrin- and caveolae-

independent endocytosis pathway in chondrocytes and endothelial cells, by clathrin-mediated endocytosis in M2 macrophages and by caveolae-mediated endocytosis in M1 macrophages. LUVs were internalized through an energy-independent non-endocytic pathway in chondrocytes and endothelial cells and by macropinocytosis/phagocytosis in M1 and M2 macrophages. In order to avoid the degradation of the NPs in the lysosomes, NPs should enter in the cells via caveolae-mediated endocytosis or via energy-independent non-endocytic pathway that can be achieved in chondrocytes and endothelial cells by the developed LUVs and in M1 macrophages by the micelles. Polymeric NPs can also circumvent lysosomal degradation in endothelial and M1 macrophages whenever they are uptake by caveolae-mediated endocytosis instead of clathrin- mediated endocytosis. Taking into consideration the cell type, human articular chondrocytes were isolated from diseased knee arthroplasties and, consequently, presenting a cell phenotype associated with arthritic diseases. Indeed, lower expression of caveolin-1 and other proteins was found in osteoarthritic cartilage [44], which can explain the internalization of Ch-HA NPs and micelles by other mechanisms not related with those proteins. Conversely, endothelial cells express high levels of caveolins [45], which was already tested as a target for the specific delivery to those cells [46]. As for M1 and M2 macrophages, previous studies conducted to evaluate the different uptake pathways of each phenotype also provided inconsistent results [47]. As such, NPs interaction with macrophages is also both tissue- and cell-state-specific. Thus, it is not possible to postulate that positively and negatively charged NPs will undergo a specific pathway. In a previous study, maleimide functionalized liposomes also underwent endocytosis and energy-independent transport supposedly via a thiol-mediated transport [39]. These outcomes suggest a high influence of NPs surface chemistry in the cellular uptake and internalization pathways by the cells. Indeed, considering the NPs formulations, many studies reported different cellular pathways internalization depending on the cell type used on the study. Nevertheless, almost all internalization studies are performed in carcinogenic cell lines, especially Hela cells [3], which fail to focus on the connection between the cell origin and the endocytic pathways.

Despite *in vitro* cellular internalization levels and pathways provide important tools in the nanotechnology field, further studies need to be performed to validate and relate those mechanisms with the *in vivo* administration. Moreover, all these results highlight the importance of further investigation regarding the NP–cell interactions that are more complex than currently appreciated. Specifically the role of the cell type and state in the NPs uptake still needs detailed studies to understand and predict the level of interaction with the target cells.

VI-5. CONCLUSIONS

The tuning of the NPs physicochemical properties, such as size, shape and surface properties can modulate their cellular uptake, targeting and intracellular trafficking. The results of the present study demonstrated the important role of surface chemistry for NPs uptake by the cells. Moreover, it was highlighted the complexity and interplay regarding the cell-NPs interaction and, consequently, their mechanisms of cell uptake by the different cell types. Indeed, the same NP was internalized via different pathways in different cell types. For instance, caveolae-mediated endocytosis or via energy-independent non-endocytic pathway, which avoid the degradation of the NPs in the lysosomes, can be achieved in chondrocytes and endothelial cells by the developed LUVs and in M1 macrophages by the micelles. Hence, understanding the mechanism of cellular uptake by each cell type and disease state will provide in the future nanomedicines with efficiently targeted delivery of the biomolecules to a specific sub-cellular compartment of the cell, and consequently, strongly enhanced therapeutic efficacy and reduced off-targeted side-effects.

VI-6. ACKNOWLEDGMENTS

Authors acknowledge the financial support from FCT/MCTES (Portuguese Foundation for Science and Technology/Ministry of Science, Technology and Higher Education) and the FSE/POCH (European Social Fund through the Operational Program of Human Capital), for the PhD scholarship PD/BD/11384/2015 of A. C. Lima (PD/59/2013. Authors would also like to acknowledge FCT for the project PTDC/CTM-BIO/4388/2014 – SPARTAN, and the Northern Portugal Regional Operational Programme (NORTE 2020), under the Portugal 2020 Partnership Agreement, through the European Regional Development Fund (FEDER) (NORTE-01-0145-FEDER-000023-FROnTHERA and NORTE-01-0145-FEDER-000013-PersonalizedNOS). The authors also acknowledge NORTE 2020 Structured Project within the R&D&I Structured Project, co funded by Norte2020 - Programa Operacional Regional do Norte.

VI-7. REFERENCES

1. Farokhzad, O. C. and Langer, R., Impact of nanotechnology on drug delivery. *ACS nano*. **2009**, *3* (1): p. 16-20.

2. Alexis, F., Pridgen, E., Molnar, L. K., *et al.*, Factors affecting the clearance and biodistribution of polymeric nanoparticles. *Mol Pharmaceut*. 2008, *5* (4): p. 505-515.
3. Yameen, B., Choi, W. I., Vilos, C., *et al.*, Insight into nanoparticle cellular uptake and intracellular targeting. *J Control Release*. 2014, *190*: p. 485-499.
4. Behzadi, S., Serpooshan, V., Tao, W., *et al.*, Cellular uptake of nanoparticles: journey inside the cell. *Chem Soc Rev*. 2017, *46* (14): p. 4218-4244.
5. Murugan, K., Choonara, Y. E., Kumar, P., *et al.*, Parameters and characteristics governing cellular internalization and trans-barrier trafficking of nanostructures. *Int J Nanomedicine*. 2015, *10*: p. 2191-206.
6. Swanson, J. A., Shaping cups into phagosomes and macropinosomes. *Nat Rev Mol Cell Bio*. 2008, *9* (8): p. 639-649.
7. Kaksonen, M. and Roux, A., Mechanisms of clathrin-mediated endocytosis. *Nat Rev Mol Cell Bio*. 2018, *19* (5): p. 313-326.
8. Parton, R. G. and Simons, K., The multiple faces of caveolae. *Nat Rev Mol Cell Bio*. 2007, *8* (3): p. 185-194.
9. Rejman, J., Conese, M. and Hoekstra, D., Gene transfer by means of lipo- and polyplexes: role of clathrin and caveolae-mediated endocytosis. *J Liposome Res*. 2006, *16* (3): p. 237-47.
10. Sandvig, K., Pust, S., Skotland, T., *et al.*, Clathrin-independent endocytosis: mechanisms and function. *Curr Opin Cell Biol*. 2011, *23* (4): p. 413-420.
11. Grant, B. D. and Donaldson, J. G., Pathways and mechanisms of endocytic recycling. *Nat Rev Mol Cell Bio*. 2009, *10* (9): p. 597-608.
12. Lim, J. P. and Gleeson, P. A., Macropinocytosis: an endocytic pathway for internalising large gulps. *Immunol Cell Biol*. 2011, *89* (8): p. 836-843.
13. Li, Z. H., Zhang, Y. H., Zhu, D. H., *et al.*, Transporting carriers for intracellular targeting delivery via non-endocytic uptake pathways. *Drug Deliv*. 2017, *24* (2): p. 45-55.
14. Yang, J., Bahreman, A., Daudey, G., *et al.*, Drug Delivery via Cell Membrane Fusion Using Lipopeptide Modified Liposomes. *Acs Central Sci*. 2016, *2* (9): p. 621-630.
15. Foroozandeh, P. and Aziz, A. A., Insight into Cellular Uptake and Intracellular Trafficking of Nanoparticles. *Nanoscale Res Lett*. 2018, *13*.
16. Rees, P., Wills, J. W., Brown, M. R., *et al.*, The origin of heterogeneous nanoparticle uptake by cells. *Nat Commun*. 2019, *10* (1): p. 1-8.
17. Verma, A. and Stellacci, F., Effect of surface properties on nanoparticle-cell interactions. *Small*. 2010, *6* (1): p. 12-21.
18. Pap, T. and Korb-Pap, A., Cartilage damage in osteoarthritis and rheumatoid arthritis-two unequal siblings. *Nat Rev Rheumatol*. 2015, *11* (10): p. 606-615.
19. Burch, E. E., Patil, V. R. S., Camphausen, R. T., *et al.*, The N-terminal peptide of PSGL-1 can mediate adhesion to trauma-activated endothelium via P-selectin in vivo. *Blood*. 2002, *100* (2): p. 531-538.
20. Simion, V., Constantinescu, C. A., Stan, D., *et al.*, P-Selectin Targeted Dexamethasone-Loaded Lipid Nanoemulsions: A Novel Therapy to Reduce Vascular Inflammation. *Mediat Inflamm*. 2016.
21. Bartok, B. and Firestein, G. S., Fibroblast-like synoviocytes: key effector cells in rheumatoid arthritis. *Immunol Rev*. 2010, *233* (1): p. 233-55.
22. Murray, P. J. and Wynn, T. A., Protective and pathogenic functions of macrophage subsets. *Nat Rev Immunol*. 2011, *11* (11): p. 723-737.
23. Brown, S., Pistiner, J., Adjei, I. M., *et al.*, Nanoparticle Properties for Delivery to Cartilage: The Implications of Disease State, Synovial Fluid, and Off-Target Uptake. *Mol Pharmaceut*. 2019, *16* (2): p. 469-479.

24. Serda, R. E., Gu, J., Bhavane, R. C., *et al.*, The association of silicon microparticles with endothelial cells in drug delivery to the vasculature. *Biomaterials*. **2009**, *30* (13): p. 2440-8.
25. Lima, A. C., Cunha, C., Carvalho, A., *et al.*, Interleukin-6 Neutralization by Antibodies Immobilized at the Surface of Polymeric Nanoparticles as a Therapeutic Strategy for Arthritic Diseases. *Acs Appl Mater Inter*. **2018**, *10* (16): p. 13839-13850.
26. da Silva, M. L. A., Costa-Pinto, A. R., Martins, A., *et al.*, Conditioned medium as a strategy for human stem cells chondrogenic differentiation. *J Tissue Eng Regen M*. **2015**, *9* (6): p. 714-723.
27. Binnemars-Postma, K. A., ten Hoopen, H. W. M., Storm, G., *et al.*, Differential uptake of nanoparticles by human M1 and M2 polarized macrophages: protein corona as a critical determinant. *Nanomedicine*. **2016**, *11* (22): p. 2889-2902.
28. dos Santos, T., Varela, J., Lynch, I., *et al.*, Effects of Transport Inhibitors on the Cellular Uptake of Carboxylated Polystyrene Nanoparticles in Different Cell Lines. *Plos One*. **2011**, *6* (9): p. 1-10.
29. Gouveia, V. M., Lopes-de-Araujo, J., Costa Lima, S. A., *et al.*, Hyaluronic acid-conjugated pH-sensitive liposomes for targeted delivery of prednisolone on rheumatoid arthritis therapy. *Nanomedicine*. **2018**, *13* (9): p. 1037-1049.
30. Costa Lima, S. A. and Reis, S., Temperature-responsive polymeric nanospheres containing methotrexate and gold nanoparticles: A multi-drug system for theranostic in rheumatoid arthritis. *Colloids Surf B Biointerfaces*. **2015**, *133*: p. 378-87.
31. Lima, A. C., Ferreira, H., Reis, R. L., *et al.*, Biodegradable polymers: an update on drug delivery in bone and cartilage diseases. *Expert Opin Drug Deliv*. **2019**, *16* (8): p. 795-813.
32. Mecke, A., Majoros, I. J., Patri, A. K., *et al.*, Lipid bilayer disruption by polycationic polymers: the roles of size and chemical functional group. *Langmuir*. **2005**, *21* (23): p. 10348-54.
33. Dawson, K. A., Salvati, A. and Lynch, I., Nanotoxicology: nanoparticles reconstruct lipids. *Nat Nanotechnol*. **2009**, *4* (2): p. 84-5.
34. Huhn, D., Kantner, K., Geidel, C., *et al.*, Polymer-coated nanoparticles interacting with proteins and cells: focusing on the sign of the net charge. *ACS nano*. **2013**, *7* (4): p. 3253-63.
35. Patil, S., Sandberg, A., Heckert, E., *et al.*, Protein adsorption and cellular uptake of cerium oxide nanoparticles as a function of zeta potential. *Biomaterials*. **2007**, *28* (31): p. 4600-4607.
36. Zhu, Z. J., Ghosh, P. S., Miranda, O. R., *et al.*, Multiplexed Screening of Cellular Uptake of Gold Nanoparticles Using Laser Desorption/Ionization Mass Spectrometry. *J Am Chem Soc*. **2008**, *130* (43): p. 14139-14143.
37. Li, Y. and Monteiro-Riviere, N. A., Mechanisms of cell uptake, inflammatory potential and protein corona effects with gold nanoparticles. *Nanomedicine-Uk*. **2016**, *11* (24): p. 3185-3203.
38. Li, T. S. and Takeoka, S., A novel application of maleimide for advanced drug delivery: in vitro and in vivo evaluation of maleimide-modified pH-sensitive liposomes. *Int J Nanomed*. **2013**, *8*: p. 3855-3866.
39. Li, T. S. and Takeoka, S., Enhanced cellular uptake of maleimide-modified liposomes via thiol-mediated transport. *Int J Nanomed*. **2014**, *9*: p. 2849-2861.
40. Kokebie, R., Aggarwal, R., Lidder, S., *et al.*, The role of synovial fluid markers of catabolism and anabolism in osteoarthritis, rheumatoid arthritis and asymptomatic organ donors. *Arthritis Res Ther*. **2011**, *13* (2): p. 1-10.
41. MacParland, S. A., Tsoi, K. M., Ouyang, B., *et al.*, Phenotype Determines Nanoparticle Uptake by Human Macrophages from Liver and Blood. *ACS nano*. **2017**, *11* (3): p. 2428-2443.
42. Qie, Y., Yuan, H., von Roemeling, C. A., *et al.*, Surface modification of nanoparticles enables selective evasion of phagocytic clearance by distinct macrophage phenotypes. *Sci Rep*. **2016**, *6*: p. 26269.

43. Ren, H., He, Y., Liang, J.*, et al.*, Role of Liposome Size, Surface Charge, and PEGylation on Rheumatoid Arthritis Targeting Therapy*. ACS Appl Mater Interfaces*. **2019**, *11* (22): p. 20304-20315.
44. Min, T., Sheng, L. Y., Chao, C.*, et al.*, Correlation between osteopontin and caveolin-1 in the pathogenesis and progression of osteoarthritis*. Exp Ther Med*. **2015**, *9* (6): p. 2059-2064.
45. Schubert, W., Frank, P. G., Razani, B.*, et al.*, Caveolae-deficient endothelial cells show defects in the uptake and transport of albumin in vivo*. J Biol Chem*. **2001**, *276* (52): p. 48619-48622.
46. Voigt, J., Christensen, J. and Shastri, V. P., Differential uptake of nanoparticles by endothelial cells through polyelectrolytes with affinity for caveolae*. P Natl Acad Sci USA*. **2014**, *111* (8): p. 2942-2947.
47. Lunov, O., Syrovets, T., Loos, C.*, et al.*, Differential uptake of functionalized polystyrene nanoparticles by human macrophages and a monocytic cell line*. ACS nano*. **2011**, *5* (3): p. 1657-69.

SECTION 5

IN VIVO STUDIES

Chapter VII

Nanoparticle-mediated neutralization of IL-6 and TNF-α for osteoarthritis treatment

Chapter VII

Nanoparticle-mediated neutralization of IL-6 and TNF-α for osteoarthritis treatment[1]

ABSTRACT

Osteoarthritis (OA), a progressive degenerative joint disease, affects millions of people worldwide. Biological agents are promising treatments for OA, as pro-inflammatory cytokines play an important role in synovial inflammation and cartilage destruction. In this work, anti-IL-6 and anti-TNF-α antibodies were immobilized at the surface of polymeric nanoparticles (NPs) to selectively capture and neutralize those cytokines. Our system intends to extend and increase the antibodies therapeutic efficacy, owing to the protection from degradation that the NPs provide, and to avoid systemic side effects through intra-articular administration. Biological properties as well as their synergistic effects were confirmed *in vitro* using a co-culture model of inflammation. The *in vivo* therapeutic effect was assessed in a carrageenan-induced inflammatory arthritis model of OA by measuring different clinical parameters, nociceptive behavior and histological analyses. Biofunctionalized NPs exhibited a safe profile, a prolonged action and a stronger efficacy than the soluble antibodies. Hence, as this strategy is able to increase the therapeutic efficacy of the currently available treatments, it presents good perspectives to revolutionize OA treatment.

[1]This chapter is based on the following publication:

Lima A. C., Amorim D., Laranjeira I., Almeida A., Reis R. L., Ferreira H., Pinto-Ribeiro F., Neves N. M. Nanoparticle-mediated neutralization of IL-6 and TNF-α for osteoarthritis treatment. *(Submitted)*. 2019.

VII-1. INTRODUCTION

Osteoarthritis (OA), the most common form of arthritis, is a painful and disabling disease that affects millions of people worldwide [1, 2]. Although its etiology is largely unknown, several risk factors have been identified, such as joint injury, obesity, aging and heredity [3]. Moreover, it is well-established that the imbalance between the matrix-producing and matrix-degrading properties of cartilage-resident chondrocytes has a major role in the pathogenesis of this disease [4]. The release of degradative enzymes from chondrocytes initiates a cascade of events that leads to the breakdown of collagen and other extracellular matrix (ECM) components. At this stage, synovial macrophages become activated, releasing pro-inflammatory cytokines, including tumor necrosis factor-α (TNF-α) and interleukins (IL), which enhance cartilage degradation, promoting a cycle of cartilage damage and disease progression [5].

Current treatments consist in pain management and joint replacement for an end-stage OA. Therefore, this disease not only significantly impacts the patients' quality of life, but also increases comorbidities and mortality. Indeed, OA represents a serious burden to both patients and society [1], being one of the largest unmet medical needs in the field of rheumatology.

Due to the major role of pro-inflammatory cytokines in the development and progression of OA, their targeting constitute a promising therapeutic strategy [6]. Indeed, biologic agents demonstrated outstanding clinical efficacy and tolerable safety profiles in some rheumatic inflammatory diseases. An example is rheumatoid arthritis (RA), for which there are several antibodies (Abs) in clinical use, including the anti-TNF-α Abs infliximab and adalimumab, and the IL-6 receptor (IL-6R)-targeting Abs tocilizumab [7]. Despite no disease-modifying drugs are available for OA [8], similar therapeutic effects are expected, due to the presence of high concentrations of IL-6 and TNF-α in the plasma and synovial fluid [9, 10]. However, even though some clinical trials reported promising results, others failed to demonstrate a significant clinical improvement [11, 12]. Limitations of Abs-based therapies are related to the short half-life that decreases their therapeutic efficacy and severe systemic side effects, such as increased risk of infection, malignancy or administration reactions [13]. Indeed, considering the ubiquitous expression of cytokines in the body, Abs systemically injected can and frequently interfere with other biological mechanisms [2]. Hence, novel therapeutic strategies are needed to improve their efficacy and safety profile.

Intra-articular (IA) administration is considered one of the most effective routes to treat joint diseases, since it offers many advantages, such as the direct targeting, high local drug concentration, lower drug dose and avoidance of systemic side effects [14]. Therefore, IA therapy can not only reduce the costs of

treatments, but also improve the drugs therapeutic index. IA injections of hyaluronic acid (HA) and corticosteroids, for instance, are currently broadly used for OA management [15]. However, IA administration can lead to some disability and pain when multiple injections are required and due to the highly vascularized synovial membrane that efficiently filters most solutes and drugs in the synovial space, the drug efficiency is limited. Thus, the development of IA drug delivery systems to provide a local and sustained drug release is a crucial step for a successful OA treatment.

Nanomedicine is a rising field aiming to address the limitations of conventional therapies [16]. Indeed, nanoparticle (NP) formulations are been engineered to increase the therapeutic efficacy and reduce adverse effects of drugs [17]. Several types of IA delivery systems, such as microparticles, NPs, liposomes and hydrogels are being investigated for the treatment of OA [14]. Polymeric NPs have attracted considerable interest due to their properties, particularly the biodegradability and potential biocompatibility [18]. Natural polymers, chitosan (Ch) and HA, were used in this work. The non-cytotoxicity, high stability and availability of Ch makes it an attractive biodegradable polymer for biomedical applications [19]. In turn, HA is a natural component of the ECM of articular cartilage and synovial fluid, playing an important role in the ECM function. Moreover, HA of high molecular weight (MW) displays anti-inflammatory and immune-suppressive properties [20].

In this work, anti-IL-6 and anti-TNF-α Abs were immobilized at the surface of Ch-HA NPs to increase their therapeutic effect after IA administration (**Figure VII-1**). In OA, as in inflammatory diseases in general, the combinatory effect of several pro-inflammatory cytokines play an important role in its pathogenesis, which can explain the difficulty to prevent the damaging events using only one interfering Ab. Thus, the developed system can have synergistic effects on OA by simultaneously targeting IL-6 and TNF-α. After polymeric NPs production, the maximum immobilization capacity for each Ab at their surface was assessed. The *in vitro* validation of the biofunctionalized NPs was evaluated using a co-culture system of human articular chondrocytes (hACs) and activated macrophages. Finally, we assessed the therapeutic efficacy of the biofunctionalized NPs as an IA drug delivery system in a carrageenan-induced arthritis rat model and demonstrated its feasibility in future clinical applications.

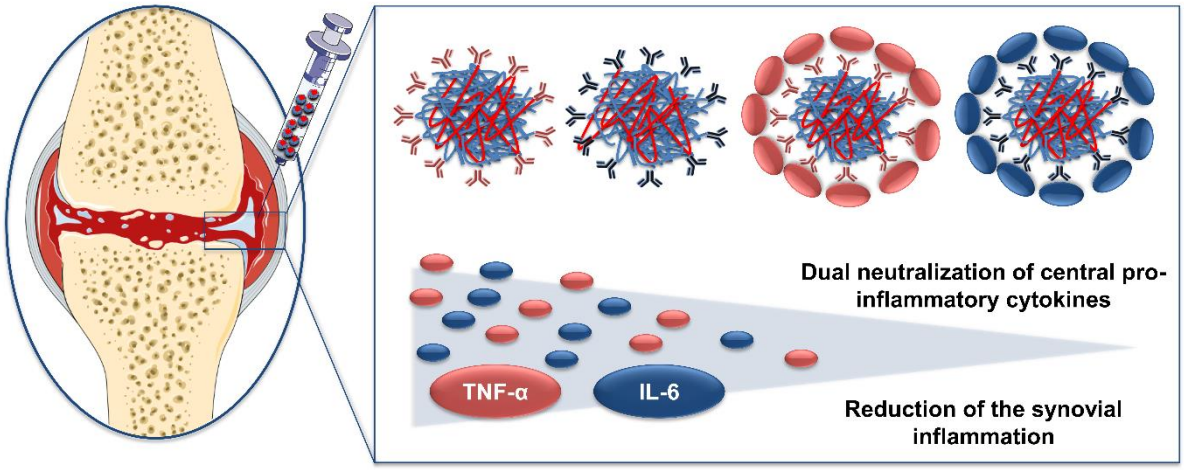

Figure VII-1 – Schematic illustration of the biofunctionalized NPs role in osteoarthritis treatment. After intra-articular administration, the dual neutralization of central pro-inflammatory cytokines tumor necrosis factor-α (TNF-α) and interleukin-6 (IL-6) will promote the reduction of the synovial inflammation and, consequently, osteoarthritis symptoms.

VII-2. MATERIALS AND METHODS

This section describes the polymeric NPs preparation and biofunctionalization. It also presents the *in vitro* and *in vivo* effects of the biofunctionalized NPs assessed in relevant models of inflammatory arthritis, in a co-culture model of chondrocytes and macrophages and in a carrageenan-induced inflammatory arthritis model of OA, respectively.

VII-2.1. Materials

Ch with a MW of 150 kDa and 95% of deacetylation degree was purchased from Heppe Medical Chitosan GmbH (Germany). HA with a MW of 750 kDa was acquired from Lifecore Biomedical (USA). Mouse monoclonal anti-IL-6 Abs and rabbit polyclonal anti-TNF-α Abs were purchased from Abcam (UK). Alexa Fluor® 594 donkey anti-mouse, Alexa Fluor® 594 donkey anti-rabbit, Alexa Fluor® 488 donkey anti-rabbit, Roswell Park Memorial Institute (RPMI)-1640 media and fetal bovine serum (FBS) were purchased from Thermo Fisher Scientific (USA). Human IL-6 and TNF-α Standard ABTS ELISA development kits and human fibroblast growth factor (bFGF) were acquired from Peprotech (USA). All other reagents were purchased from Sigma-Aldrich (USA).

VII-2.2. NPs preparation and biofunctionalization

Ch-HA NPs were prepared as previously described [21]. Briefly, Ch was dissolved in 1% (v/v) acetic acid and HA in ultrapure water. After filtration through a 0.22 μm pore membrane, the pH of both polymers was adjusted to 5 and the concentration to 0.25 mg/mL. Then, HA solution was added dropwise at 1 mL/min rate to the Ch solution under strong magnetic stirring. To produce biofunctionalized NPs with anti-TNF-α Abs or with anti-IL-6 Abs, the Abs were activated with a solution of 50 mM EDC and 200 mM NHS in 0.1 M MES buffer (pH 4.7) with 0.9% (w/w) NaCl for 15 min. Then they were incubated with NPs overnight at 4 °C. To remove unreacted compounds, the NPs were centrifuged twice with ultrapure water (30 min, 4000 rpm at 20 °C with glucose at 2 mg/mL) using Vivaspin 300 kD Filter Units (Fisher Scientific, USA).

To determine the maximum immobilization capacity at NPs surface, different concentrations of each Abs were used (from 0 to 20 μg/mL). After remove unbound primary Abs, the biofunctionalized NPs were incubated with the secondary Abs for 1 h at room temperature (RT). Alexa Fluor® 594 donkey anti-mouse was used for the anti-IL-6 Abs and Alexa Fluor® 594 Donkey Anti-Rabbit was used for the anti-TNF-α Abs. The fluorescence of unbound secondary Abs was determined by the analysis of the supernatant after centrifugation (45 min, 4000 rpm, 25 °C) using an excitation wavelength of 590/20 nm and an emission wavelength of 645/40 nm in a microplate reader (Synergy HT, BioTek, USA). The concentration of the primary Abs immobilized at the NPs surface can be related with the difference between the incubated initial amount and supernatant amount of the unbound secondary Abs.

VII-2.3. NPs characterization

NPs size distribution, surface charge and morphology were assessed as described in the following sub-sections.

VII-2.3.1. Size distribution and zeta potential measurements

Using a Zetasizer Nanoseries ZS equipment (Malvern Instruments, Portugal), the dynamic light scattering (DLS) was used to assess the size and polydispersity index (PDI) and the laser Doppler micro-electrophoresis was used to determine the zeta potential of the biofunctionalized NPs diluted in ultra-pure water (1:20; v/v).

VII-2.3.2. NPs morphology

Morphological analyses of the biofunctionalized NPs were performed by atomic force microscopy (AFM). Diluted NPs (1:20; v/v) were air-dried into the surface of a glass slide. A MultiMode STM microscope controlled by a NanoScope III from Digital Instruments system was used for AFM measurements, using a tapping mode at a frequency of 1 Hz.

VII-2.4. Biological assays

A co-culture model of human chondrocytes and macrophages was used to assess the biologic effects of the biofunctionalized NPs.

VII-2.4.1. Isolation and Cell Culture

Knee cartilage samples collected from arthroplasties surgeries biopsies were used to isolate hACs. Samples were obtained through the cooperation agreement between Centro Hospitalar do Alto Ave, Guimarães, Portugal, and I3Bs – Research Institute on Biomaterials, Biodegradables and Biomimetics, and after informed donor consent. Cells were isolated by enzymatic digestion, as previously described [22]. hACs cells were cultured in Dulbecco's modified Eagle's medium (DMEM), supplemented with 10% FBS, 10 mM HEPES buffer, 10 mM L-lanyl-L-glutamine, 10 mM MEM nonessential amino acids, 100 units/mL of penicillin, 100 μg/mL of streptomycin and 10 ng/mL of human bFGF, and incubated at 37 °C in a humidified 5% CO_2 atmosphere.

The human monocytic cell line THP-1 was maintained in complete RPMI, containing RPMI-1640 media supplemented with 2 mM of L-glutamine, 100 units/mL of penicillin, 100 μg/mL of streptomycin, 10 mM HEPES buffer and 10% FBS.

VII-2.4.2. Co-culture of hACs with macrophages

For the induction of THP-1 cell differentiation, cells were seeded 2.5×10^5 cells per well in cRPMI with 100 nM phorbol 12-myristate-13-acetate (PMA) in 24-well cell culture inserts (pore size: 1 μm). After incubation during 24 h, non-attached cells were removed by aspiration, and the adherent cells were

washed three times with cRPMI. To ensure reversion of cells to a resting macrophage phenotype, cells were incubated for an additional 48 h in cRPMI without PMA.

For hACs seeding, cells at a concentration of 5×10^4 cells per well were added to 24-well plates. After 24 h of incubation, the co-culture system was established by transferring the inserts to the hACs culture.

VII-2.4.3. Biological effects of the biofunctionalized NPs

Resting M0 macrophages were activated to the M1 phenotype by adding 100 ng/mL of lipopolysaccharide (LPS). Monoculture systems were used as controls. After 2 h of stimulation, different conditions were tested: *(i)* no treatment, *(ii)* treatment with anti-TNF-α Abs, *(iii)* treatment with anti-IL-6 Abs, *(iv)* treatment with anti-TNF-α and anti-IL-6 Abs, *(v)* treatment with biofunctionalized NPs with anti-TNF-α Abs, *(vi)* treatment with biofunctionalized NPs with anti-IL-6 Abs, and (7) treatment with biofunctionalized NPs with anti-TNF-α and anti-IL-6 Abs. The Abs were administered at 1 μg/mL.

After 1, 3, 7 and 14 days, samples were collected and evaluated regarding cell viability, proliferation and morphology, as described. The amount of IL-6 and TNF-α in the media was assessed by ELISA. During the time of experiment 300 μL of fresh media was added each 3 days, but no media was removed to keep the NPs in contact with the cells.

VII-2.4.3.1 *Cell viability*

Alamar blue (AB) reagent (Bio-Rad, USA) was used to assess the metabolic activity of cells, following the manufacturer's instructions. Samples were incubated 4 h with medium containing 10% AB. The fluorescence was measured in a microplate reader (Synergy HT, BioTek, USA), using an excitation wavelength of 528 nm and an emission wavelength of 590 nm.

VII-2.4.3.2 *DNA quantification*

A fluorimetric dsDNA quantification kit (Quant-iT™, PicoGreen®, Molecular Probes, Invitrogen, USA) was used to assess cell proliferation, following the manufacturer's instructions. The fluorescence was measured in a microplate reader (Synergy HT, BioTek, USA), using an excitation wavelength of 485 nm and an emission wavelength of 528 nm, being the DNA concentration of the samples inferred from the standard curve.

VII-2.4.3.3 *SEM analyses*

SEM was used to analyze the hACs morphology. After fixation with 2.5% glutaraldehyde, samples were dehydrated using increasing concentrations of ethanol (10%, 20%, 40%, 60%, 80%, 90%, 95%, and 100%). In order to evaluate the samples by High-Resolution Field Emission Scanning Electron Microscope (Auriga Compact, ZEISS), they were sputter-coated (EMACE600, LEICA) with a thin layer (8–12 nm) of palladium. Microphotographs were recorded at 5 kV.

VII-2.4.4. Cytokines quantification

IL-6 and TNF-α cytokines were quantified using human sandwich ELISAs Kit that were performed according to the manufacturer procedure. ABTS liquid substrate was added to each well and the color development was monitored in a microplate (Synergy HT, BioTek, USA) at 405 nm, with a wavelength correction set at 650 nm. Cytokines concentration was inferred from the standard curve.

VII-2.5. *In Vivo* Studies

The experimental protocol was approved by the Institutional Ethical Commission (SECVS 109/2016) and followed the European Community Council Directive 86/609/EEC and 2010/63/EU concerning the use of animals for scientific purposes. Efforts were always made to minimize the number of animals used per experiment or test and their potential suffering.

VII-2.5.1. Animal use and care

Wistar rats (n=32, 8 weeks old) were housed in pairs in a limited-access rodent facility, with food and water available *ad libitum*. The temperature was maintained at 22.0 ± 0.5 °C with a 12/12 h light/dark cycle (starting at 8:00 a.m.). General health parameters were surveyed twice per week by the resident veterinary and the animals' weight was recorded every week throughout the experimental period. On the day of the experiments, animals were left in the experimental room for one hour in order to get acquainted with the surroundings.

VII-2.5.2. Induction of arthritis

The induction of arthritis was performed as described in detail elsewhere [23]. Briefly, a 3% solution of carrageenan was dissolved in sterile saline solution (0.9% NaCl) and injected into the synovial cavity of the right knee joint at a volume of 0.1 mL. Control animals (SHAM) were injected with 0.1 mL saline in the synovial cavity of the right knee joint.

VII-2.5.3. Behavioral assessment and clinical parameters

Behavioral and clinical parameters were assessed to analyze the edema and nociception of the animals through different parameters.

VII-2.5.3.1 *Evaluation of the knee perimeter*

Joint perimeter was assessed as an indirect indicator of the development of an inflammatory state with edema. Knee perimeters of both hind paws were measured using a paper strip with a ruler.

VII-2.5.3.2 *Flexion/extension test*

Mechanical allodynia was evaluated by the flexion/extension test, in which animals were submitted to five consecutive flexion/extension movements in both knees. The number of vocalization during each flexion/extension movement was registered.

VII-2.5.3.3 *Pressure application measurement*

A classical approach to measure mechanical hyperalgesia is the application of noxious pressure to the primary site of injury [24]. The pressure application measurement (PAM) applies a force range of 0–1500 g and allows an accurate behavioral quantification of the mechanical hypersensitivity in rodents with chronic inflammatory joint pain [25]. PAM method was used as previously described [26]. Briefly, with the animal securely held, an increasing force was gradually applied across the joint until a behavioral response was observed (paw-withdrawal, freezing of whisker movement, wriggling or vocalization) with a cut-off of 5 s. Limb withdrawal threshold (LWT) was recorded as the peak force (in grams force - gf)

applied immediately prior to the behavioral response. LWT was measured twice in both paws at 1 min intervals. The mean LWTs were calculated per animal.

VII-2.5.3.4 *Footprint area*

The animals performed the catwalk gait analyses and the footprint area of both feet was measured using the Image J software.

VII-2.5.4. Experimental design

In vivo studies were divided in two main experiments: *(i)* assessment of NPs biocompatibility after IA delivery and their therapeutic potential, and *(ii)* evaluation of the NPs therapeutic efficacy and its comparison with the injection of both free Abs. Both experiments used a carrageenan-induced inflammatory arthritis model of OA.

In the first experiment, three days after the arthritis induction through an IA injection of carrageenan into the right knee joint of adult male and female Wistar rats, the development of arthritis was verified as previously described (time point 0) and the animals were treated with NPs or NPs+Abs. The control (SHAM) animals were injected with saline during the induction and then treated with the NPs. At the end of the behavioral session, after 4 days of treatment, animals were sacrificed with a lethal dose of pentobarbital and the knee joints were removed for further histological analyses.

In the second *in vivo* experiment, arthritis induction (after 3 days of the carrageenan injection) in male Wistar rats was assessed as previously described (time point 0), and four groups were tested: *(i)* saline, *(ii)* NPs, *(iii)* Abs and *(iv)* NPs+Abs. At time points 4 and 10, the disease progression was assessed, and in the last time point the animals were sacrificed as described and the joints removed for subsequent histological analyses.

VII-2.5.5. Histological analyses

Rats were sacrificed 4 or 10 days after treatment administration, in the first and second experiment, respectively. The joints were removed, fixed with 10% (v/v) of formalin, decalcified in Biodec R (BioOptica, Italy) until all the mineral part of the bone was removed. Then, samples were transferred to histological cassettes, processed and embedded in paraffin. Sagittal sections (5 μm) were cut through the knee joint

using a manual rotary microtome (Micron Technology, USA) and stained with hematoxylin and eosin (H&E, Thermo Scientific, USA) following a routine protocol. Briefly, sections were deparaffinized with xylene, rehydrated in ethanol and stained with Gill hematoxylin and alcoholic eosin. Afterwards, the sections were dehydrated and mounted with resinous mounting medium. The histological sections were analyzed under Leica DM750 microscope. For immunohistochemistry (IHC) analyses, after deparaffinization in xylene and rehydration, the tissue sections were subjected to heat-induced antigen-retrieval with sodium citrate buffer (10 mM sodium citrate, 0.05% (v/v) tween 20 (Bio-Rad, USA), pH 6) for 20 min at 98 °C. To block nonspecific antigen binding, sections were incubated for 30 min with 3 % (w/v) BSA. Sections were incubated with the mouse anti-IL-6 Abs and rabbit anti-TNF-α Abs at 4 °C overnight. Then, sections were incubated with the secondary Abs Alexa Fluor 488 or 594 for 2 h at RT. After removing unbound secondary Abs, the sections were mounted using aqueous mounting medium. For negative controls, the incubation step for primary Abs was replaced with Abs diluent solution alone (data not shown). The samples were examined using a confocal laser scanning microscope (TCS SP8, Leica).

VII-2.6. Statistical Analyses

GraphPad software was used to perform statistical analyses. Normality was analyzed using the Shapiro-Wilk test. Since data did not follow a normal distribution, results were analyzed using the Kruskal-Wallis test with Dunn's Multiple Comparison post-test. Significance was set to $*p<0.05$, $**p<0.01$; $***p<0.001$. Results are presented as mean ± Standard deviation (SD).

VII-3. RESULTS

Biofunctionalized NPs characterization, *in vitro* biological effects as well as *in vivo* studies were performed to validate their activity in inflammatory arthritis.

VII-3.1. Biofunctionalization and characterization of Ch-HA NPs

After Ch-HA NPs preparation, anti-TNF-α Abs or anti-IL-6 Abs were covalently immobilized at their surface using the carbodiimide chemistry. The maximum immobilization was 11.85 μg/mL for anti-TNF-α Abs and 10.81 μg/mL for anti-IL-6 Abs using an initial concentration of 15 μg/mL (**Figure VII-2A**).

Biofunctionalized NPs displayed 132.05 ± 2.58 nm of diameter, 0.12 ± 0.01 of PDI and +20.07 ± 2.10 mV of zeta potential, keeping their stability for at least 6 months (size increased less than 10%). AFM analyses revealed the spherical shape of the biofunctionalized NPs, as shown in **Figure VII-2B**. Moreover, the NPs size was around 130 – 140 nm, confirming the DLS measurements.

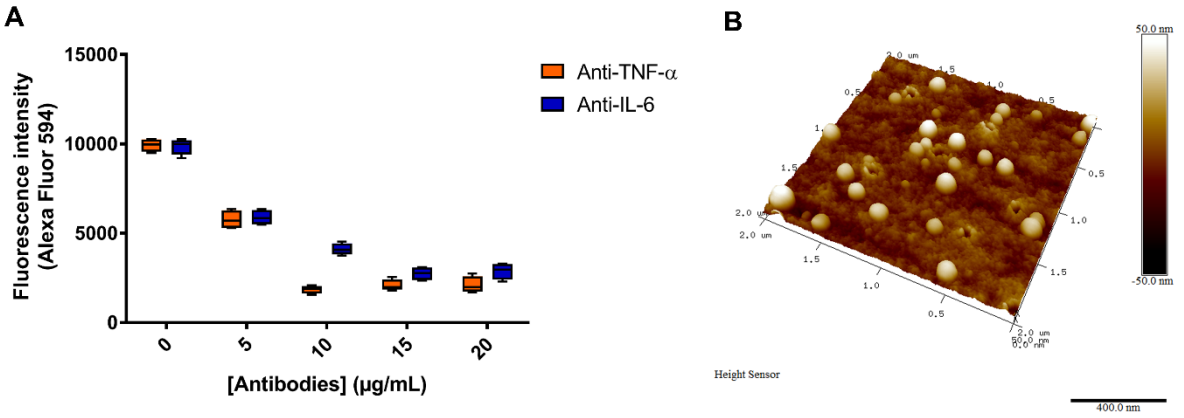

Figure VII-2 – (A) Maximum immobilization capacity at the surface of polymeric NPs of anti-TNF-α Abs or anti-IL-6 Abs. (B) AFM micrographs of the biofunctionalized NPs with anti-IL-6 and anti-TNF-α Abs. Scale bar: 400 nm.

VII-3.2. Biological Assays

To assess the biological performance of the Abs immobilized at the NPs' surface, a co-culture model was used. The co-culture of hACs with M1 simulated macrophages significantly decreased the cell viability and DNA concentration comparatively to the control (**Figures VII-3A** and **B**). Alternatively, the treatment with biofunctionalized NPs with anti-IL-6 Abs and biofunctionalized NPs with anti-TNF-α and anti-IL-6 Abs (NPs-IL6 and NPs-TNF+IL6) increased the cell viability and proliferation in comparison to No treat group. Moreover, no significant differences were observed when compared to the control of hACs (**Figures VII-3A** and **B**). The biofunctionalized NPs with TNF-α Abs were not able to prevent the reduction of the cell viability. Remarkably, the dual targeting of the biofuntionalized NPs with anti-TNF-α and anti-IL-6 Abs had the highest effect in the cell viability. Furthermore, the dual treatment with the soluble Abs (TNF+IL6) was only able to prevent the nefarious effects of the macrophage stimulation in hACs at the first time point (Day 1; **Figures VII-3A** and **B**). These results were corroborated by the cell morphology analyses (**Figure VII-4**). Indeed, after 14 days of co-culture, a low density and altered morphology with shrinkage of hACs were observed. The addition of biofunctionalized NPs with anti-TNF-α and anti-IL-6 Abs (NPs-TNF+IL6) significantly prevented these features and in a higher extension than soluble Abs.

Regarding the amount of unbound IL-6 and TNF-α in the medium (**Figures VII-3C** and **D**, respectively), the results showed that the co-culture of hACs and activated macrophages had a huge impact on those cytokines production. For IL-6 cytokines, both hACs and LPS stimulated THP-1 produce around 10 ng/mL. After the establishment of the co-culture system, the IL-6 amount increased to a maximum ≈ 2 μg/mL. This huge production of IL-6 cytokine corroborates the susceptibility to inflammation of hACs isolated from osteoarthritic patients. The treatment with the biofunctionalized NPs containing anti-IL-6 Abs reduced more the IL-6 amount in the medium than the soluble Abs. Moreover, since these reduction was significantly higher for biofunctionalized NPs with anti-IL-6 and anti-TNF-α Abs (**Figure VII-3C**), it was confirmed the synergistic effect of the dual targeting and the value of the proposed approach. For TNF-α cytokines (**Figure VII-3D**), whereas hACs without any stimulus do not produce this cytokine, activated M1 macrophages produce around 1.2 ng/mL after 1 day and reduced to 0.1 ng/mL after 14 days. In this case, both soluble and immobilized Abs were able to effectively reduce the amount of this cytokine in the medium. Nevertheless, dual targeting with biofunctionalized NPs had a significant reduction of the TNF-α quantity at all time points when compared to no treatment group. Therefore, the overall results confirmed the initial hypothesis that NPs can prolong Abs half-life and efficacy as well as the synergistic effect of the dual capture and neutralization of IL-6 and TNF-α cytokines.

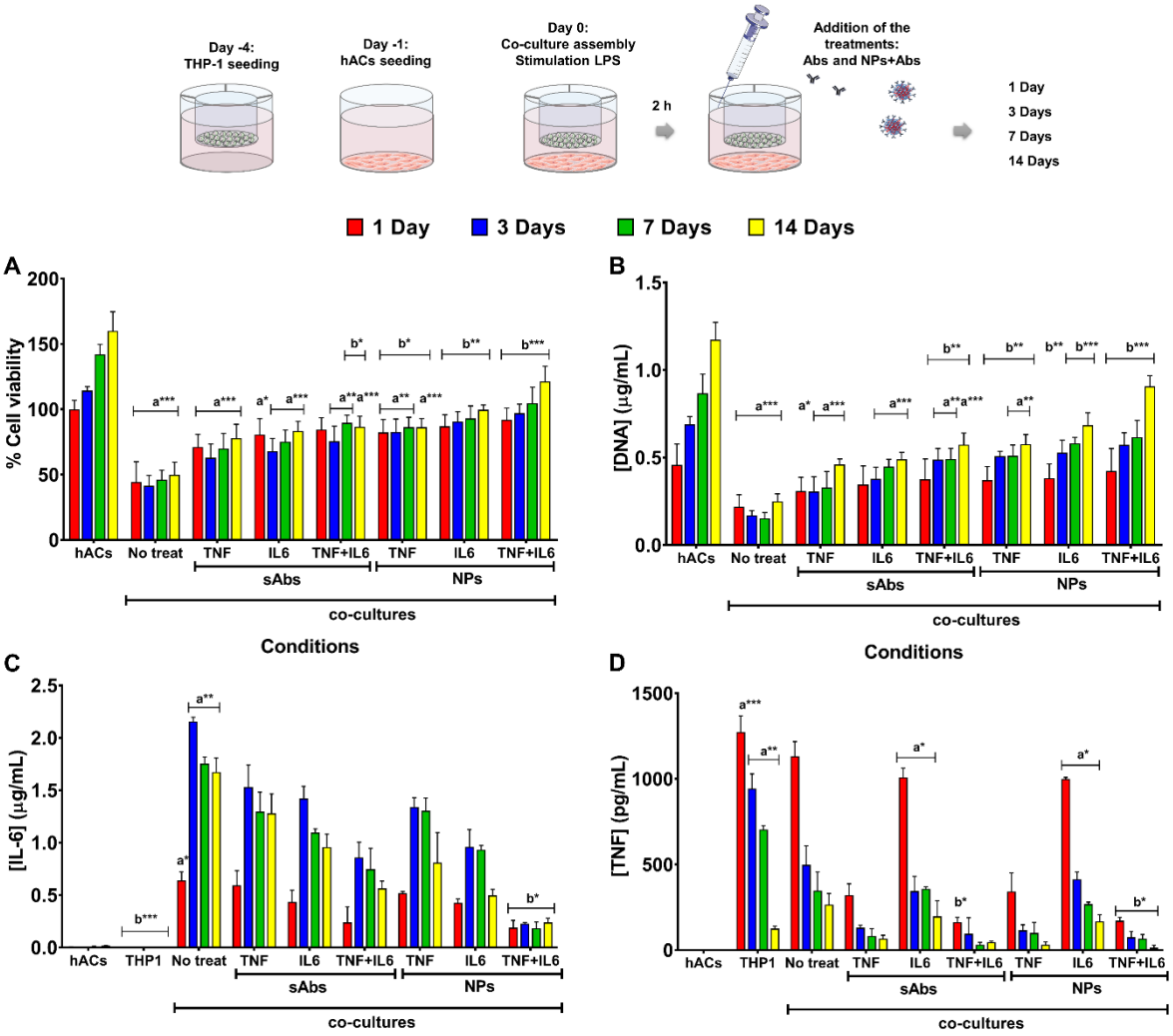

Figure VII-3 – Biochemical performance of hACs co-cultured with activated M1 macrophages: *(i)* no treatment (No treat), *(ii)* treatment with soluble anti-TNF-α Abs (TNF), *(iii)* treatment with soluble anti-IL-6 Abs (IL6), *(iv)* treatment with soluble anti-TNF-α and anti-IL-6 Abs (TNF+IL6), *(v)* treatment with biofunctionalized NPs with anti-TNF-α Abs (NPs-TNF), *(vi)* treatment with biofunctionalized NPs with anti-IL-6 Abs (NPs-IL6), and *(vii)* treatment with NPs biofunctionalized with anti-TNF-α and anti-IL-6 Abs (NPs-TNF+IL6). The samples were analyzed regarding (A) cell viability, (B) cell proliferation, (C) IL-6 concentration, and (D) TNF-α concentration. hACs and/or activated THP-1 cultured alone were used as controls (Ctr). Letter "a" denotes significant difference compared to the hACs group, and "b" denotes significant difference compared to No treat group, being *p<0.05, **p<0.01, ***p<0.001.

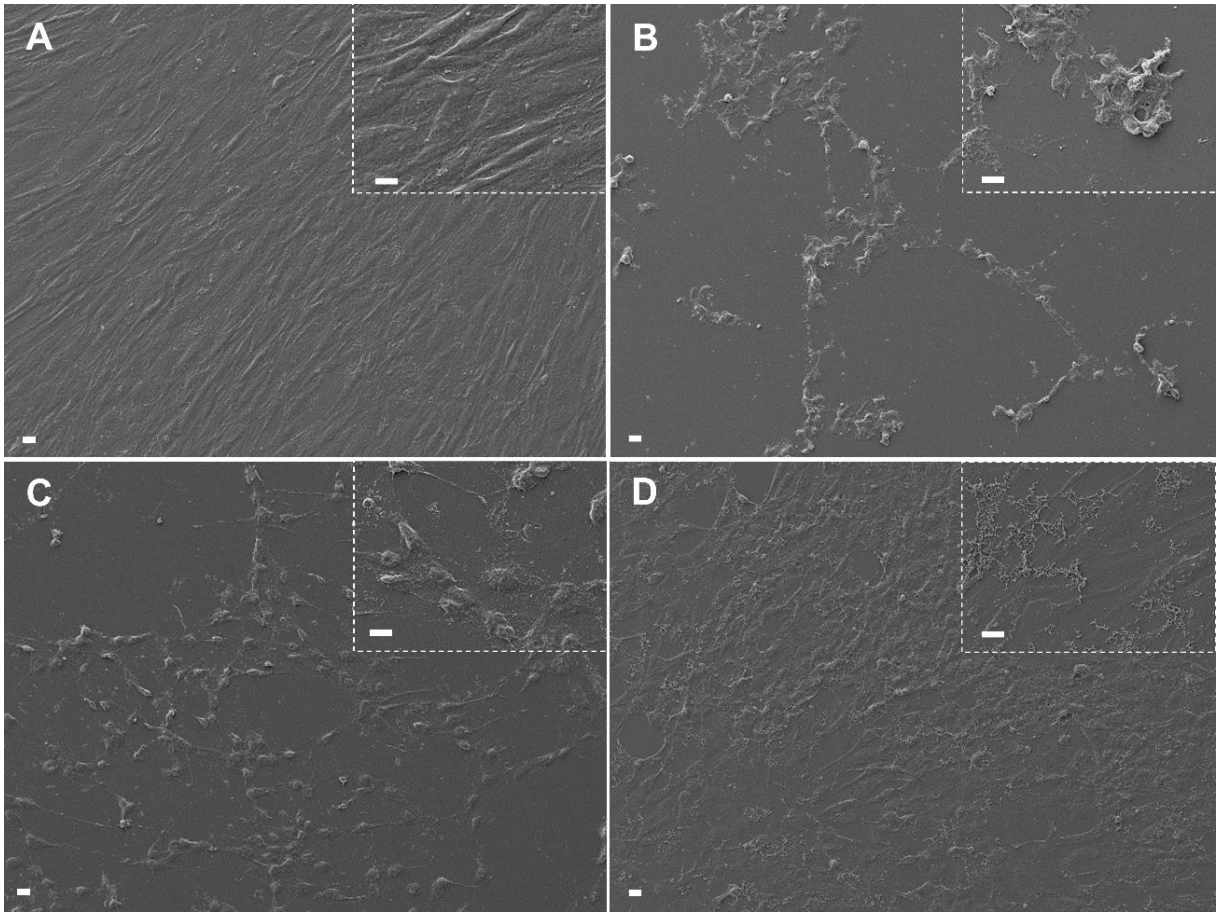

Figure VII-4 – SEM micrographs of hACs co-cultured with activated M1 macrophages after 14 days. (A) Control (hACs cultured alone), (B) THP-1 stimulation without treatment, (C) THP-1 stimulation and addition of free soluble anti-TNF-α and anti-IL-6 Abs, and (D) THP-1 stimulation and addition of biofunctionalized NPs with anti-TNF-α and anti-IL-6 Abs. Scale bars: 10 μm.

VII-3.3. *In vivo* studies

Two different *in vivo* experiments were performed to: *(i)* assess the NPs biocompatibility after IA delivery and the therapeutic potential of the biofunctionalized NPs, and *(ii)* evaluate the therapeutic efficacy of the biofunctionalized NPs and compare with the injection of the free Abs.

VII-3.3.1. NPs biocompatibility

To investigate the NPs biocompatibility after IA delivery and the potential therapeutic efficacy of the biofunctionalized NPs, an inflammatory arthritis rat model was used (**Figure VII-5**) – Experiment 1. Clinical and behavior parameters were assessed regarding the edema (increased number of knee perimeter

represent high edema), mechanical allodynia (increased number of vocalization represent high mechanical allodynia) and mechanical hyperalgesia (reduced values of LWT represent high mechanical hyperalgesia).

The IA delivery of NPs into control animals (SHAM) showed no differences in all the analyses over time (**Figure VII-5**). Thus, NPs have no harmful effects in the nociceptive behavior. Histological analyses also showed almost no inflammatory cells in the synovial membrane (**Figure VII-6**). As in the SHAM group, the presence of a few inflammatory cells can be a result of the IA injections that triggers a small inflammatory reaction. Consequently, these results demonstrated the biocompatibility of the produced NPs when injected IA.

Regarding the assessment of the therapeutic effect of the biofunctionalized NPs, paw perimeter did not show any differences among experimental groups (**Figure VII-5A**). By contrast, NPs+Abs animals decreased the number of vocalizations while increasing LWT when compared to NPs animals (**Figures VII-5B** and **C**). Indeed, on the on post-treatment day 4, NPs+Abs group display a significant decrease in the number of vocalizations when compared to NPs animals. Histological analyses showed a concomitant reduction in the number of inflammatory cells in the synovial membrane of the NPs+Abs group when compared to the NPs group (**Figure VII-6**). Therefore, these *in vivo* results suggest biofunctionalized NPs are able to reduce inflammation and pain.

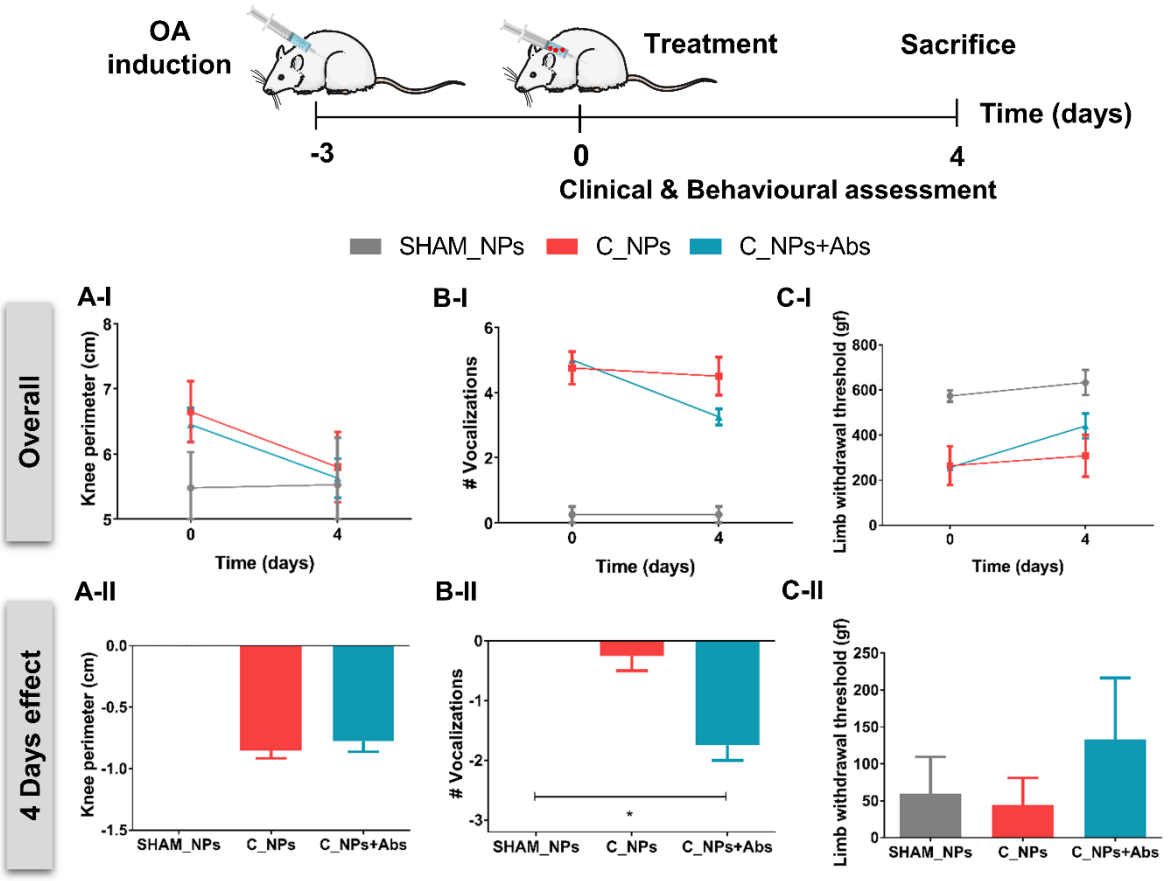

Figure VII-5 – Clinical and behavioral assessment of the effects of treatment with NPs and biofunctionalized NPs (NPs+Abs) on Carrageenan (C)-induced experimental arthritis of the rat's right knee joints. The experimental plan of Experiment 1 is presented. (A) Knee perimeter (cm). (B) Flexion/extension test (#vocalizations). (C) PAM (Limb withdrawal threshold - gf). (I) Overall measurements, and (II) 4 days effect. Significance was set to (*) $p<0.05$.

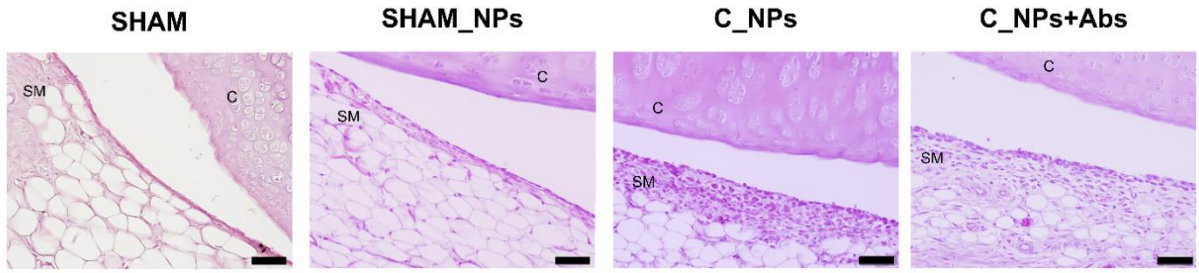

Figure VII-6 – Histopathological analyses of the effect of treatment with NPs and biofunctionalized NPs (NPs+Abs) on Carrageenan (C)-induced experimental arthritis of the rat's right knee joints in the Experiment 1. (SHAM group was injected with saline. Sections were stained with Hematoxylin/Eosin; C, cartilage; SM, synovial membrane). Scale bars: 50 μm.

VII-3.3.2. Therapeutic effects of the biofunctionalized NPs

To evaluate the therapeutic efficacy of the biofunctionalized NPs in comparison to the soluble biological agents, the inflammatory carrageenan-induced arthritis rat model was used as previously referred – Experiment 2.

The clinical and behavior parameters assessed were development of edema, mechanical allodynia, mechanical hyperalgesia, and gait (reduced values of footprint area represent high nociceptive behavior). Considering the edema (**Figure VII-7A**), the results show no statistically significant differences between groups. Overall, the knee perimeter decreases throughout time in all groups (≈6.8 cm to 6.0 cm). In the flexion/extension test (**Figure VII-7B**), the number of vocalizations is almost the same for the time point 0 and decreased in the time point 4, but no significant differences were found between groups (number of vocalizations of 1.60 ± 1.14 SAL, 1.40 ± 1.67 NPs, 1.60 ± 1.82 Abs and 0.25 ± 0.50 NPs+Abs). At the time point 10, the number of vocalizations in the NPs+Abs group decreased to 0, being significantly smaller than those of the SAL and NPs groups (p = 0.0118 and 0.0396, respectively; number of vocalizations of 3.4 ± 0.55 SAL and 3.2 ± 0.84 NPs). Despite no significant differences, the decrease in the number of vocalizations after treatment with NPs+Abs group was higher than the one obtained after treatment with the soluble Abs alone. Moreover, the absence of vocalization of the animals treated with the NPs+Abs is also found in healthy animals. Therefore, the mechanical allodynia reduced in the animals treated with the biofunctionalized NPs. In the PAM test (**Figure VII-7C**), the LWT values were identical for all groups at the time point 0. However, a greater increase in LWT was observed in the NPs+Abs group when compared to the SAL group, mainly until day 4 (p = 0.0128; LWT of 353.29 ± 159.27 SAL, 436.01 ± 108.77 NPs, 386.76 ± 98.05 Abs and 650.66 ± 107.63 NPs+Abs). Similarly, at the time point 10, the NPs+Abs group displayed the highest value of LWT, although not statistically different (LWT of 446.08 ± 131.78 SAL, 415.64 ± 151.97 NPs, 432.10 ± 25.14 Abs and 655.03 ± 194.58 NPs+Abs). Healthy animals display a LWT of 655.58 ± 97.07, which is in alignment with the values obtained with the biofunctionalized NPs. This increase in LWT indicates a reduction of mechanical hyperalgesia and, consequently, a lower susceptibility to the induction of nociception was obtained for the NPs+Abs group. Regarding the analyses of gait (**Figure VII-7D**), the footprint area significantly increased 4 and 10 days after treatment with biofunctionalized NPs in comparison with SAL (p = 0.0025 and 0.0078, respectively). The same effect was not observed in the Abs group. Thus, the clinical and behavioral assessment demonstrate the benefits of the capture and inactivation of both pro-inflammatory cytokines by the

biofunctionalized NPs, when injected IA. Moreover, those benefits where higher than the injection of the soluble Abs, suggesting a prolonged action associated to their immobilization.

The histological analyses (**Figure VII-8**) corroborate the reduction of inflammation provided by the Abs treatment, mainly if they are immobilized at NPs surface. In comparison to the control group (healthy joints), the Sal group was characterized by marked immune cells infiltration in the synovium and fibrosis and the Abs group by some decrease in the cellular infiltration and fibrosis while the NPs+Abs group was able to significantly reduce these parameters. Importantly, the synovial membrane structure was mostly preserved after the treatment with biofunctionalized NPs. Moreover, the IHC analyses (**Figure VII-8**) of the IL-6 and TNF-α cytokines present in the synovium tissue also corroborated the higher efficacy of the biofunctionalized NPs than with the soluble Abs. Indeed, in the saline group a high expression of both cytokines can be observed, which was reduced with treatment with Abs and NPs+Abs. Interestingly, the IL-6 was inactivated in a higher extension than TNF-α in both treatments (Abs and NPs+Abs).

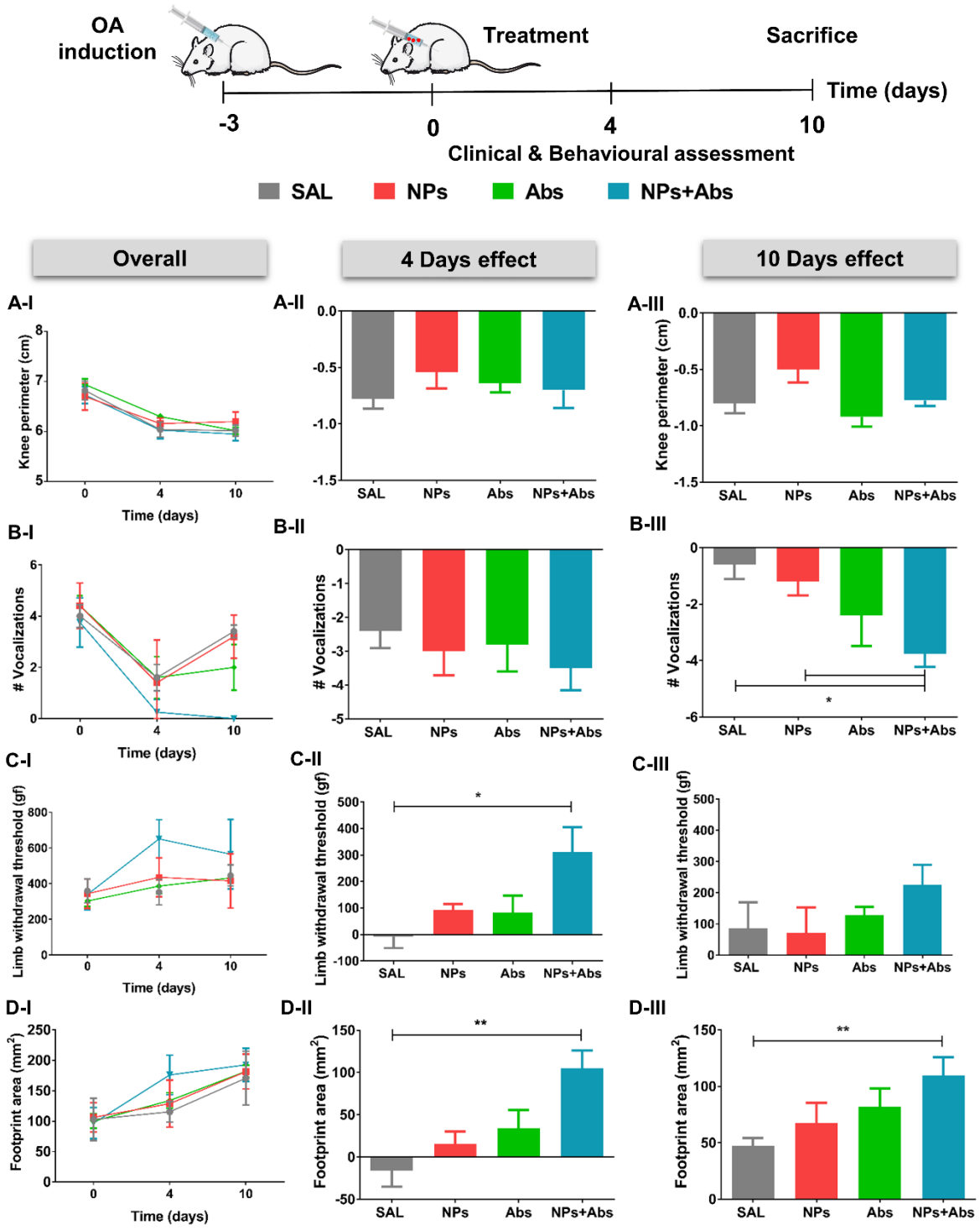

Figure VII-7 – Clinical and behavioral assessment of the effects of treatment with NPs, soluble antibodies (Abs) and biofunctionalized NPs (NPs+Abs) on a carrageenan-induced arthritis rat model in Experiment 2. (A) Knee perimeter (cm). (B) Flexion/extension test (#vocalizations). (C) PAM (Limb withdrawal threshold - gf). (D) Catwalk gait (footprint area - mm²). (I) Overall measurements, (II) 4 days effect, and (III) 10 days effect. Significance was set to (*) $p<0.05$ and (**) $p<0.01$.

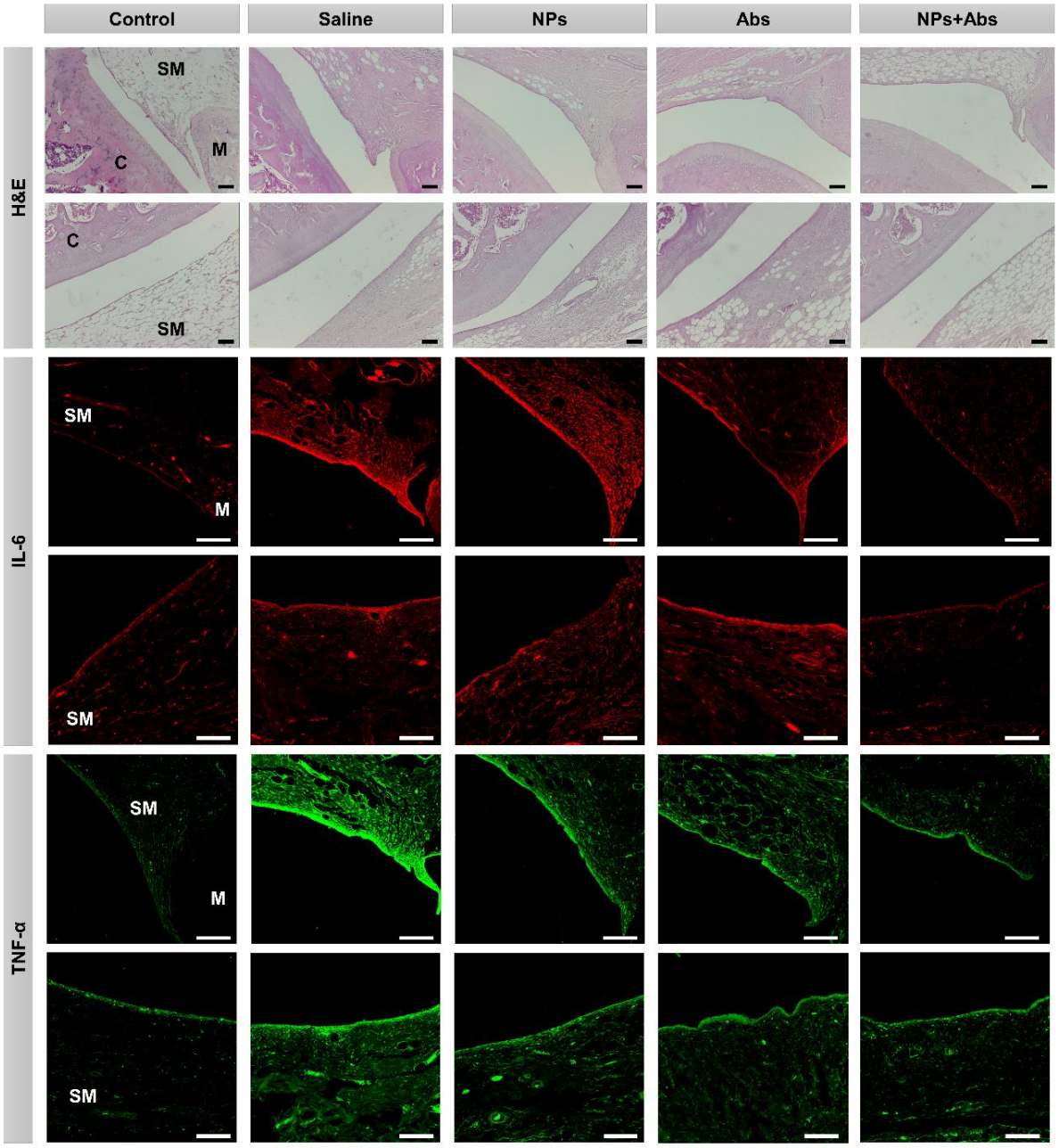

Figure VII-8 – Representative histopathological (Hematoxylin and Eosin -H&E- staining) and immunohistochemistry (IHC) staining of IL-6 and TNF-α cytokines after 10 days of treatment with saline, NPs, soluble antibodies (Abs) and biofunctionalized NPs (NPs+Abs) on a carrageenan-induced arthritis rat model in the Experiment 2. (Controls correspond to healthy joints; C, cartilage; SM, synovial membrane; M, meniscus). Scale bars: 100 μm.

VII-4. DISCUSSION

OA is a complex disease that involves a synergistic action of several mediators and/or an upregulation of different receptors. Therefore, the dual targeting may improve the therapeutic efficacy of

Abs due to the blockade of different pathological mediators and pathways [27]. Indeed, many fusion Abs are been designed to treat arthritic diseases, including IL-6 and TNF-α fusion protein [28] and IL-17A and TNF-α fusion protein [29]. Beyond its higher effectiveness, the dual targeting can overcome drug resistance caused by cytokine redundancy [30]. Therefore, the aim of this work was to study the therapeutic effects of biofunctionalized NPs in OA by capturing and neutralizing two central pro-inflammatory cytokines, namely IL-6 and TNF-α. The IA injection of developed NPs can lead to a reduction of the systemic side effects. Moreover, the immobilization of the Abs at the surface can protect them from degradation, prolonging their half-life and increasing their efficacy [31, 32]. In a previous study [21], the cytocompatibility in contact with hACs and human macrophages as well as the capacity to capture and neutralize IL-6 by biofunctionalized NPs with anti-IL-6 Abs were clearly demonstrated *in vitro*. Thus, in this study the polyelectrolyte complexation of the same polysaccharides were used to prepare biodegradable polymeric NPs, as previously described [21]. Then, the maximum immobilization of each Ab was determined, being 11.85 μg/mL for anti-TNF-α Abs and 10.81 μg/mL for anti-IL-6 Abs using an initial concentration of 15 μg/mL. After this point, the values reached a plateau and no more Abs were able to bind to the NPs' surface. In addition, the biofunctionalization of the NPs did not affect their properties.

Since inflammation plays a pivotal role in the pathological processes of OA, human chondrocytes were co-cultured with activated M1 macrophages and whether the biofunctionalized NPs could avoid the harmful impact of inflammation in those cells was investigated. Indeed, *in vitro* models could play a vital role not only to advance research into the etiological mechanisms, but also to help in the design and assessment of the efficacy of potential treatments. An *in vitro* inflammation model of osteoarthritic chondrocytes and macrophages transwell co-culture system was used as it closely resembles the permeable synovial joint [33]. Considering the polarization of the macrophages into pro-inflammatory phenotype (M1) and anti-inflammatory phenotype (M2) [34], in this study they were stimulated to the inflammatory M1 phenotype using LPS. Therefore, high levels of TNF-α, IL-1, IL-6, IL-12, IL-23 and reactive oxygen species will be produced. The induction of inflammation in the co-culture system was confirmed by the higher amounts of IL-6 and TNF-α cytokines in the medium in comparison to hACs cultured alone. IL-6 production in the co-culture system was much higher than TNF-α (≈2 μg/mL and ≈1.2 ng/mL, respectively). These outcomes are also found in the plasma and synovial fluid of OA patients [10]. The co-culture of hACs with M1 macrophages led to a higher reduction of hACs viability and proliferation and significant changes in their morphology. The treatment with the biofunctionalized NPs was able to prevent more effectively those harmful effects than the free Abs. Indeed, the quantification of

the amount of free IL-6 and TNF-α in the medium clearly demonstrated that the Abs successfully capture those cytokines, being the biofunctionalized NPs able to reduce significantly more IL-6 and TNF-α than the soluble Abs. Importantly, they were able to maintain those effects even after 14 days of culture. Thus, this strategy could increase the Abs half-life and efficacy in the inflamed joints. Moreover, those effects were higher when both cytokines were inhibited, confirming the synergistic effects of the simultaneous blockage of IL-6 and TNF-α. Since TNF-α is responsible for the increased synthesis of other cytokines, especially IL-6 [35, 36], its inhibition could reduce IL-6 expression.

In vivo studies were performed using a carrageenan-induced arthritis rat model to validate if the biofunctionalized NPs are compatible and to evaluate their therapeutic efficacy after IA administration. In the first experiment, the compatibility of the biofunctionalized NPs was clearly demonstrated, as no harmful effects were detected. Moreover, biofunctionalized NPs were able to reduce inflammation and pain, indicating their potential therapeutic efficacy. In the second experiment, this innovative approach was able to reduce the mechanical allodynia and hyperalgesia associated with this inflammatory model. Thus, the capture and inactivation of both pro-inflammatory cytokines by the biofunctionalized NPs demonstrated their clinical and behavioral beneficial therapeutic effect.

In normal joints, the synovium comprises a continuous surface layer of cells, intima (20 to 40 μm thickness in cross section), and the underlying tissue, subintima (up to 5 mm in thickness), which can be fibrous, areolar or adipose depending on its structure and content [37]. Histopathological assessment of the control group (healthy joints) showed a thin intima and an adipose-like sub-intima. After arthritis induction and treatment with saline, the synovial membrane presented a marked fibrosis and high infiltration of immune cells in the synovium was observed. Outstandingly, the microscopic images showed that NPs+Abs reduced more the infiltration of immune cells than the Abs group. In addition, the IHC analyses confirmed the reduction of IL-6 and TNF-α amount by the Abs immobilized at the NPs surface. Since this effect was higher than the obtained for soluble Abs, the initial hypothesis that the primary Abs immobilized at the NPs' surface protect the Abs from degradation, prolonging their effects, was also demonstrated. Hence, the IA injection of this advanced therapy can be a viable and effective strategy to increase the Abs efficacy and to avoid associated systemic side effects.

VII-5. CONCLUSION

To the best of our knowledge, we are the first to develop biofunctionalized NPs to simultaneously target IL-6 and TNF-α, the most important cytokines involved in arthritic disease. Our findings suggest the inhibition of those cytokines in inflamed joints may have a therapeutic benefit in OA. Indeed, the capture and neutralization of IL-6 and TNF-α by the biofunctionalized NPs effectively reduced the inflammatory scenario *in vitro* and *in vivo*. They were able to reduce the harmful effects on the hACs provided by inflammatory macrophages and also ameliorated inflammatory arthritis more efficiently than soluble Abs. By increasing the therapeutic action of the Abs and avoiding the systemic side effects, this innovative strategy will be able to increase the therapeutic efficacy of the currently available treatments. Thus, the developed biofunctionalized NPs provide a promising strategy for the local and sustained treatment of OA and other arthritic conditions.

VII-6. ACKNOWLEDGEMENTS

Authors acknowledge the financial support from FCT/MCTES (Portuguese Foundation for Science and Technology/Ministry of Science, Technology and Higher Education) and the FSE/POCH (European Social Fund through the Operational Program of Human Capital), for the PhD scholarship PD/BD/11384/2015 of A. C. Lima (PD/59/2013). Authors would also like to acknowledge FCT for the project PTDC/CTM-BIO/4388/2014 – SPARTAN, the Northern Portugal Regional Operational Programme (NORTE 2020), under the Portugal 2020 Partnership Agreement, through the European Regional Development Fund (FEDER) (NORTE-01-0145-FEDER-000023-FROnTHERA), and the NORTE 2020 Structured Project within the R&D&I Structured Project, co funded by Norte2020 - Programa Operacional Regional do Norte.

VII-7. REFERENCES

1. Cross, M., Smith, E., Hoy, D.*, et al.*, The global burden of hip and knee osteoarthritis: estimates from the Global Burden of Disease 2010 study*. Ann Rheum Dis*. **2014**, *73* (7): p. 1323-30.
2. Glyn-Jones, S., Palmer, A. J., Agricola, R.*, et al.*, Osteoarthritis*. Lancet*. **2015**, *386* (9991): p. 376-87.
3. Chen, D., Shen, J., Zhao, W.*, et al.*, Osteoarthritis: toward a comprehensive understanding of pathological mechanism*. Bone Res*. **2017**, *5*: p. 1-13.

4. Pap, T. and Korb-Pap, A., Cartilage damage in osteoarthritis and rheumatoid arthritis-two unequal siblings. *Nat Rev Rheumatol*. 2015, *11* (10): p. 606-15.
5. Calich, A. L. G., Domiciano, D. S. and Fuller, R., Osteoarthritis: can anti-cytokine therapy play a role in treatment? *Clin Rheumatol*. 2010, *29* (5): p. 451-5.
6. Zheng, S., Hunter, D. J., Xu, J., *et al.*, Monoclonal antibodies for the treatment of osteoarthritis. *Expert Opin Biol Ther*. 2016, *16* (12): p. 1529-40.
7. Tanaka, T., Hishitani, Y. and Ogata, A., Monoclonal antibodies in rheumatoid arthritis: comparative effectiveness of tocilizumab with tumor necrosis factor inhibitors. *Biologics*. 2014, *8*: p. 141-53.
8. Mathiessen, A. and Conaghan, P. G., Synovitis in osteoarthritis: current understanding with therapeutic implications. *Arthritis Res Ther*. 2017, *19* (18): p. 1-9.
9. Larsson, S., Englund, M., Struglics, A., *et al.*, Interleukin-6 and tumor necrosis factor alpha in synovial fluid are associated with progression of radiographic knee osteoarthritis in subjects with previous meniscectomy. *Osteoarthritis Cartilage*. 2015, *23* (11): p. 1906-14.
10. Mabey, T., Honsawek, S., Tanavalee, A., *et al.*, Plasma and synovial fluid inflammatory cytokine profiles in primary knee osteoarthritis. *Biomarkers*. 2016, *21* (7): p. 639-44.
11. Grunke, M. and Schulze-Koops, H., Successful treatment of inflammatory knee osteoarthritis with tumour necrosis factor blockade. *Ann Rheum Dis*. 2006, *65* (4): p. 555-6.
12. Chevalier, X., Ravaud, P., Maheu, E., *et al.*, A Randomized, Multicentre, Double Blind, Placebo-Controlled Trial of Anti Tnf Alpha (Adalimumab) in Refractory Hand Osteoarthritis. The Dora Study. *Osteoarthr Cartilage*. 2013, *21*: p. S146.
13. Woodrick, R. S. and Ruderman, E. M., Safety of biologic therapy in rheumatoid arthritis. *Nat Rev Rheumatol*. 2011, *7* (11): p. 639-52.
14. Kang, M. L. and Im, G. I., Drug delivery systems for intra-articular treatment of osteoarthritis. *Expert Opin Drug Deliv*. 2014, *11* (2): p. 269-82.
15. Ayhan, E., Kesmezacar, H. and Akgun, I., Intraarticular injections (corticosteroid, hyaluronic acid, platelet rich plasma) for the knee osteoarthritis. *World J Orthop*. 2014, *5* (3): p. 351-61.
16. Ferrari, M., Onuoha, S. C. and Pitzalis, C., Trojan horses and guided missiles: targeted therapies in the war on arthritis. *Nat Rev Rheumatol*. 2015, *11* (6): p. 328-37.
17. Zhang, R. X., Li, J., Zhang, T., *et al.*, Importance of integrating nanotechnology with pharmacology and physiology for innovative drug delivery and therapy - an illustration with firsthand examples. *Acta Pharmacol Sin*. 2018, *39* (5): p. 825-44.
18. Banik, B. L., Fattahi, P. and Brown, J. L., Polymeric nanoparticles: the future of nanomedicine. *Wires Nanomed Nanobi*. 2016, *8* (2): p. 271-99.
19. Ferreira, H., Martins, A., da Silva, M. L. A., *et al.*, The functionalization of natural polymer-coated gold nanoparticles to carry bFGF to promote tissue regeneration. *J Mater Chem B*. 2018, *6* (14): p. 2104-15.
20. Campo, G. M., Avenoso, A., Nastasi, G., *et al.*, Hyaluronan reduces inflammation in experimental arthritis by modulating TLR-2 and TLR-4 cartilage expression. *Biochim Biophys Acta*. 2011, *1812* (9): p. 1170-81.
21. Lima, A. C., Cunha, C., Carvalho, A., *et al.*, Interleukin-6 Neutralization by Antibodies Immobilized at the Surface of Polymeric Nanoparticles as a Therapeutic Strategy for Arthritic Diseases. *Acs Appl Mater Inter*. 2018, *10* (16): p. 13839-50.
22. da Silva, M. L. A., Costa-Pinto, A. R., Martins, A., *et al.*, Conditioned medium as a strategy for human stem cells chondrogenic differentiation. *J Tissue Eng Regen M*. 2015, *9* (6): p. 714-23.
23. Radhakrishnan, R., Moore, S. A. and Sluka, K. A., Unilateral carrageenan injection into muscle or joint induces chronic bilateral hyperalgesia in rats. *Pain*. 2003, *104* (3): p. 567-77.

24. Randall, L. O. and Selitto, J. J., A method for measurement of analgesic activity on inflamed tissue. *Arch Int Pharmacodyn Ther*. **1957**, *111* (4): p. 409-19.
25. Leite-Almeida, H., Almeida-Torres, L., Mesquita, A. R., *et al.*, The impact of age on emotional and cognitive behaviours triggered by experimental neuropathy in rats. *Pain*. **2009**, *144* (1-2): p. 57-65.
26. Amorim, D., David-Pereira, A., Pertovaara, A., *et al.*, Amitriptyline reverses hyperalgesia and improves associated mood-like disorders in a model of experimental monoarthritis. *Behav Brain Res*. **2014**, *265*: p. 12-21.
27. Kontermann, R. E., Dual targeting strategies with bispecific antibodies. *mAbs*. **2012**, *4* (2): p. 182-97.
28. Kim, Y., Yi, H., Jung, H., *et al.*, A Dual Target-directed Agent against Interleukin-6 Receptor and Tumor Necrosis Factor alpha ameliorates experimental arthritis. *Sci Rep*. **2016**, *6*: p. 1-12.
29. Liu, Z., Song, L., Wang, Y., *et al.*, A novel fusion protein attenuates collagen-induced arthritis by targeting interleukin 17A and tumor necrosis factor alpha. *Int J Pharm*. **2018**, *547* (1-2): p. 72-82.
30. Evans, C. H., Kraus, V. B. and Setton, L. A., Progress in intra-articular therapy. *Nat Rev Rheumatol*. **2014**, *10* (1): p. 11-22.
31. Arruebo, M., Valladares, M. and Gonzalez-Fernandez, A., Antibody-Conjugated Nanoparticles for Biomedical Applications. *J Nanomater*. **2009**: p. 3103-27.
32. Bacelo, E., Alves da Silva, M., Cunha, C., *et al.*, Biofunctional Nanofibrous Substrate for Local TNF-Capturing as a Strategy to Control Inflammation in Arthritic Joints. *Nanomaterials*. **2019**, *9* (4): p. 1-16.
33. Bauer, C., Niculescu-Morzsa, E., Jeyakumar, V., *et al.*, Chondroprotective effect of high-molecular-weight hyaluronic acid on osteoarthritic chondrocytes in a co-cultivation inflammation model with M1 macrophages. *J Inflamm (Lond)*. **2016**, *13* (31): p. 1-9.
34. Rana, A. K., Li, Y., Dang, Q., *et al.*, Monocytes in rheumatoid arthritis: Circulating precursors of macrophages and osteoclasts and, their heterogeneity and plasticity role in RA pathogenesis. *Int Immunopharmacol*. **2018**, *65*: p. 348-59.
35. Guerne, P. A., Carson, D. A. and Lotz, M., IL-6 production by human articular chondrocytes. Modulation of its synthesis by cytokines, growth factors, and hormones in vitro. *J Immunol*. **1990**, *144* (2): p. 499-505.
36. Wojdasiewicz, P., Poniatowski, L. A. and Szukiewicz, D., The role of inflammatory and anti-inflammatory cytokines in the pathogenesis of osteoarthritis. *Mediators Inflamm*. **2014**, *2014*: p. 561459-67.
37. Smith, M. D., The normal synovium. *Open Rheumatol J*. **2011**, *5*: p. 100-6.

SECTION 6

GENERAL CONCLUSIONS

Chapter VIII

General conclusions and future perspectives

Chapter VIII

General conclusions and future perspectives

VIII-1. GENERAL CONCLUSIONS

The increasing burden of arthritic diseases makes their effective treatment an unmet clinical need. Despite the breakthroughs in the field of drug discovery, current treatments still present low efficiency and severe side effects. To overcome these limitations, different strategies of drug delivery have been widely investigated. One of the most promising strategies to treat arthritic diseases comprises the design of NPs with tunable properties to extend the therapeutic index of current therapeutic agents. Indeed, their unique properties enable to reduce the dose and frequency of the administration and, consequently, the systemic side effects of the drug. Therefore, an appropriate delivery system can give a new hope to overcome the limitations of the current treatments.

The major goal of the work developed under the scope of the present thesis was to develop and validate *in vitro* and *in vivo* novel strategies to treat arthritic conditions. Thus, taking into consideration the nature of the drugs to be incorporated and the mechanisms that will control its therapeutic action and/or release in the inflammatory environment, different nanomedicine systems were developed in **Section 3**. The nanocarriers herein proposed and studied are aimed to match the main drawbacks of current treatments and overcome them. In **Chapter III**, biodegradable polymeric NPs were successfully developed from natural origin polysaccharides and biofunctionalized with anti-IL-6 Abs. Since the biological agents have limited efficacy, due to their short half-life and unspecific tissue targeting, their immobilization at the NPs surface will protect, extend and enhance the therapeutic efficacy after its local administration in the affected joint. Biological studies led to the conclusion that a concentration of 50 μg/mL of Ch-HA NPs was ideal for IA administration, since it was demonstrated their cytocompatibility in contact with chondrocytes and macrophages. Moreover, when the chondrocytes are stimulated with macrophage conditioned medium, the biofunctionalized NPs show the beneficial role of the capture and neutralization of IL-6, exhibiting a prolonged action and stronger efficacy than the free Ab. As the local therapy in OA may offer particular advantages over systemic therapy, the findings of this work may lead to important implications in the treatment of this debilitating condition. In RA, the systemic therapy is

generally more indicated and appropriated. For that, in **Chapter IV** liposomes encapsulating AuNPs with long-circulation times were functionalized with anti-IL-23 Abs at their surface. The aim of this work was also to enhance the therapeutic efficacy of the immobilized Abs, while reducing their adverse side effects, due to the accumulation of the nanocarrier in the inflammatory sites via the EPR effect. Biological studies demonstrated their cytocompatibility when cultured with chondrocytes, macrophages and endothelial cells within a concentration of 2 mM. Importantly, PBMCs of healthy donors and RA patients that were activated though Th17 differentiation presented an efficient reduction of the IL-17A production, after the treatment with biofunctionalized liposomes. Moreover, the therapeutic effect is potentiated by the synergistic effects of IL-23 level reduction and vitamin E and AuNPs anti-oxidant activity. Thus, the results validate the biofunctionalized liposomes as a promising treatment for RA. **Chapter V** describes the development of enzymatic- and redox-responsive polymeric micelles for targeted and controlled drug delivery in inflammatory arthritic conditions. The inadequate pharmacokinetics of GCs, with low drug bioavailability and off-targeted biodistribution profile, is a major limitation of their therapeutic efficacy and safety. Thus, polymeric micelles were designed to increase the therapeutic index of the drug and reduce the severe side effects. To establish a sensitive system, the thiol groups of the GSH were oxidized intermolecularly to retain the drug inside the micelles, providing a barrier against its blood dilution. After accumulation at the inflammatory site via the EPR effect, the drug will undergo a quick release triggered by both redox and GR activity. After demonstrating their cytocompatibility in contact with human endothelial cells, chondrocytes and macrophages until the concentration of 50 μg/mL, a co-culture system was used to show the beneficial role of encapsulating the drug into the micelles. Indeed, Dex encapsulated into the polymeric micelles, in the presence of GR and redox media, exhibited higher efficacy than the free drug. Importantly, as they were able to reduce the negative effects of Dex in normal cells, this strategy may provide important outcomes in arthritis treatment. Overall results from **Section 3** highlight the importance of designing nanocarriers considering specifically their application. Hence, the positively charged NPs will enhance their retention in the joint cavity after IA administration, whereas the PEG chains of both micelles and liposomes will enhance the blood circulation time after systemic administration. Moreover, while Ch-HA NPs and LUVs reduce the inflammatory scenario by the capture and inactivation of key pro-inflammatory cytokines through Abs linked at their surface, polymeric micelles release in-situ (arthritic inflammation) the drug though the break of S-S bonds in the presence of GR and high intracellular concentrations of GSH. Importantly, all the developed formulations avoid the harmful effects of the drugs in normal cells, which will severely limit their side effects after administration.

Despite the vital role of NPs internalization process by the cells, which determines their activity, biodistribution and toxicity, our understanding on NPs cellular uptake is rather limited. **Section 4** aims to provide evidence by not only studying the role of the physicochemical characteristics of the NPs, but also taking into consideration the effects of the disease environment in this process. Accordingly, the goal of the **Chapter VI** was to assess the internalization and pathways used for different NPs previously developed (polymeric NPs, LUVs and micelles) in a normal and inflammatory scenario by different cells, namely endothelial cells, chondrocytes and macrophages. The results shown the important role of surface chemistry in NPs internalization by the cells. Despite some studies established a higher internalization degree of cationic particles, in the present work the results shown the opposite. Moreover, it was highlighted the complexity and interplay regarding the cell-NPs interaction and, consequently, their mechanisms of cell uptake by the different cell types. Indeed, each NP had a similar uptake level regardless the cell type, but the same NP exploited different cellular pathways depending on the cell type. As internalization route is of utmost importance for the NPs fate into the cell, it is crucial to understand their pathways of cellular uptake and intracellular trafficking. Indeed, in order to avoid the degradation of the NPs in the lysosomes, NPs should enter in the cells via specific pathways. For instance, caveolae-mediated endocytosis or via energy-independent non-endocytic pathway, which avoid the degradation of the NPs in the lysosomes, can be achieved in chondrocytes and endothelial cells by the developed LUVs and in M1 macrophages by the micelles. As such, we can conclude that the micelles will provide an intracellular delivery of the inflammatory drug to the target cells (M1 macrophages). Hence, understanding the mechanism of cellular uptake by each cell type and disease state will provide in the future nanomedicines with efficiently targeted delivery of the biomolecules to a specific sub-cellular compartment of the cell and, consequently, enhanced therapeutic efficacy.

Section 5 provides the *in vivo* evaluation of the safety and therapeutic efficacy of the biofunctionalized Ch-HA NPs immobilizing anti-TNF-α and anti-IL-6 Abs at their surface. The synergistic effects of neutralizing two key pro-inflammatory cytokines were confirmed in **Chapter VII** though their *in vitro* investigation using a co-culture model of inflammation and *in vivo* using an experimental carrageenan-induced arthritis rat model. *In vitro* studies demonstrated a higher inhibition of the harmful effects on the chondrocytes provided by inflammatory macrophages after the treatment with biofunctionalized NPs in comparison with soluble Abs. Moreover, those effects were higher when both cytokines were inhibited, confirming the synergistic effects of the simultaneous blockage of IL-6 and TNF-α. After IA administration, biofunctionalized NPs demonstrated a safe profile and stronger efficacy on reducing arthritic symptoms

and synovial inflammation than soluble Abs. Hence, by increasing the therapeutic action of the biological agents and avoiding the systemic side effects, this innovative strategy will be able to increase the therapeutic efficacy of the currently available treatments, being a promising strategy for the local and sustained treatment of OA.

Despite the value of the overall results presented in this thesis being very promising in terms of its translational potential, many more questions can be formulated than those that were answered in this thesis. Indeed, although a higher retention in the joint is expected after the IA injection of the Ch-HA NPs, they can still be leaked from the joint or to be engulfed by the macrophages before providing their therapeutic effect. Consequently, their biodistribution profile after administration is an important issue that needs further research. Moreover, while IA injections favor the therapeutic efficacy of the drugs, the administration reactions can reduce their use. Regarding the LUVs and the micelles, the accumulation into the inflamed joint via EPR effect may not be sufficient, as they could be removed from the blood stream, accumulating in the liver and spleen. Since many nanocarriers are using targeting molecules to enhance their accumulation in the joint, this limitation can be overpass though the covalent linking of those ligands to the surface of the developed NPs. Moreover, their biodistribution after administration also needs to be exploited, since this feature greatly influences the drug off-target effects. In fact, the value of all the developed NPs deeply relies on the effective reduction of the drugs side effects, which was herein only shown in *in vitro* relevant models of arthritis. Hence, these and other critical questions need to be addressed in the future before the present technologies can be tested in patients.

As general conclusion, the nanomedicines developed in this thesis were able to improve the drugs therapeutic index by simultaneously: *(i)* promote the targeted delivery to the inflammatory environment of arthritic conditions through local administration or EPR effect, *(ii)* enhance the biomolecules therapeutic effects by protecting from degradation or providing sustained and controlled release, and *(iii)* reduce the undesirable side effects of the therapeutic agents.

VIII-2. FUTURE PERSPECTIVES

This thesis aimed at combining several multidisciplinary fields, including nanotechnology, materials science and cell biology, in order to improve the current drugs therapeutic index in arthritic conditions. In the last decade, NPs design has gained much attention as it holds the potential of contributing for more effective treatments. Despite the impressive scientific effort achieved to this date, none of the

technological developments has led to the "ideal NP". Indeed, to be able to develop new outstanding alternatives, designing novel nanomedicines should take into consideration the increased knowledge about the pathophysiology of these diseases, biomarkers and targets. A deeper understanding of the biological phenomena that contribute to the limited success of current treatments will provide the insights needed to overcome them.

From a practical point of view, there are many different possibilities of complementing and deepening the developed work. For instance, the liposomes and micelles formulations developed in the **Chapter IV** and **V** should be tested in relevant models of arthritis. In the case of the biofunctionalized NPs (**Chapters III and VII**), further studies aiming at understanding their biodistribution profiles *in vivo*, validating its safety profile, and also evaluating their role in OA by avoiding the cartilage degradation. Considering the **Chapter VI,** further studies also relies on validating the *in vitro* results using *in vivo* experiments of NPs tracking. Moreover, it will be also interesting to assess the NPs internalization in primary macrophages of healthy and arthritic patients, since the cell state is a critical parameter for the NPs uptake. Therefore, all those experiments are planned to take place in a near future. Indeed, we aim to explore not only their safety and efficacy, but also understand the NPs biodistribution after administration.

With the knowledge generated with this work, it is expected that the proposed NPs will have an important impact in arthritic field. Incontestably, if the *in vivo* studies validate the promising results obtained so far, further steps including clinical trials will be conducted to move forward those therapies into the clinic.